THE AUTOMATED LOADING AND DETECTION OF BRACHYTHERAPY ELEMENTS USING NON-MECHANICAL INTERACTION FOR USE IN PROSTATE CANCER TREATMENT

By

Jason Andrew Proffitt

A Thesis
Submitted to the
Faculty of the Graduate School
of
Western Carolina University
in Partial Fulfillment of the
Requirements for the Degree
of
Master of Science in Technology

Committee:

_____Director

_____

_____

_____Dean of the Graduate School

Date: _____

Spring 2011
Western Carolina University
Cullowhee, North Carolina

THE AUTOMATED LOADING AND DETECTION OF BRACHYTHERAPY ELEMENTS USING NON-MECHANICAL INTERACTION FOR USE IN PROSTATE CANCER TREATMENT

A thesis presented to the faculty of the Graduate School of
Western Carolina University in partial fulfillment of the
requirements for the degree of Master of Science in Technology.

By

Jason Andrew Proffitt

Director: Dr. Aaron K. Ball
Professor of Engineering Technology
Kimmel School Department of Engineering Technology

Committee Members: Dr. Phillip A. Sanger, Engineering Technology
Dr. Chip W. Ferguson, Engineering Technology

June 2011

Acknowledgements

I would like to thank my thesis director, Dr. Aaron Ball, and my committee members, Dr. Phillip Sanger and Dr. Chip Ferguson, for their continued help and advice with the completing of this work and throughout my career as an undergraduate and then graduate student at WCU. You have all given to me lessons in both engineering and life that I will always take with me wherever I go. In particular, I would like to thank Dr. Ball for his support and guidance. You have helped me and my fellow students far more than you can realize. You said that “good students make good professors”, but you prove the reverse is also true. A great professor will also make good students.

I would also like to thank the SHANDS cancer treatment facility at the University of Florida in Gainesville. The SHANDS staff members express the proverbial front line in the treatment and research of cancer treatments, and have been extremely helpful in my work. In particular, I would like to express my heartfelt thanks to Mr. Richard Helmig and Mr. Thomas Mitchell, without whom this work would have never been completed thanks to their respective knowledge bases in medical devices, brachytherapy, and cancer treatment. Thank you for giving me your time and support.

I also wish to convey thanks to my family, my parents, Michael and Valencia Proffitt, and my twin brother Matt Proffitt. And to the rest of my family, all of whom have never stopped encouraging me to perform at my best no matter the obstacles. I would like to thank all the faculty, students, and staff of the Kimmel School’s department of Engineering and Technology. And finally, I would like to thank my fellow graduate students, especially Chris Rhoads, Tyler Bennett, AJ Punch, and of course again Matt Proffitt. With whom I have shared both highs and lows with.

It is through all of your support that I was able to keep going until the end.

TABLE OF CONTENTS

LIST OF TABLES

LIST OF FIGURES

ABSTRACT

THE AUTOMATED LOADING AND DETECTION OF BRACHYTHERAPY ELEMENTS USING NON-MECHANICAL INTERACTION FOR USE IN PROSTATE CANCER TREATMENT

Jason Andrew Proffitt, M.S.T.

Western Carolina University (July 2011)

Director: Dr. Aaron K. Ball

Within the recent resurgence of brachytherapy as treatment for prostate cancer, many new devices have been conceived in the preparation of surgical brachytherapy equipment. Specifically, this work encompasses the automated preparation of pre-loaded surgical brachytherapy applicators or"needles" through the loading of radioactive seed elements and benign spacer elements. While traditionally a manual operation, current device methodology in this application revolves around semi-automatic mechanical interaction within the element loading procedure. Mechanical interaction can subject elements to damage; specifically seed elements due to thin metallic construct. Damage to elements within a loading system can result in failure of the performed brachytherapy treatment causing potential harm to the patient. Hesitancy in acceptance of these mechanical separation element loading devices can be attributed to the failure nature of these devices. This work seeks to solve the current issue of element damage through non-interaction while offering improvement through full automation of the loading procedure.

CHAPTER 1: INTRODUCTION

The following work presents effort performed and related to the development of a non-mechanical brachytherapy element loading device for improving prostate cancer treatment. The device constructed for this work relies on the principles of both vacuum and air pressure to move various element types into a specialized needle applicator based on a pre determined dosimetry plan. The following Chapter I serves to introduce the work and briefly describe the purpose, problem, objectives, hypothesis, significance, and associated delimitations. Found at the end of this chapter, are general terms related to this work.

1.1 Purpose of Work

Cancer is a major health concern for both the United States populous and those around the world. According to the American Cancer Society, in the year 2009 one in four deaths were related to cancer (Jemal et. al. 2009). More specifically, prostate cancer accounted for an estimated 192,280 new cases in US males for 2009 (Jemal et al. 2009). These new cases resulted in the largest percent of organ-based cancer in US males. Various medical procedures exist for combating such cancerous growth within the human body. Medical procedures used to treat cancer locations, such as the prostate, commonly include invasive surgical methods or the exposure of the cancerous area to radioactivity. According to Naitoh, Zeiner, and Dekernion (1998) the current methods of invasive surgery and beam-based radiation have been used extensively throughout the medical community for a number of years to prevent and remove cancerous cells from within the human body (Naitoh, Zeiner, and Dekernion, 1998). In contrast, a third option for cancer treatment, entitled brachytherapy, has been steadily gaining acceptance within the sphere

of cancer treatment (Naitoh, Zeiner, and Dekernion, 1998). Brachytherapy is a medical procedure in which radioactive material is surgically placed within the human body, using hypodermic needle application, for the localized destruction of cancerous cells. By simply placing the radioactive material in close proximity to the cancerous location, the cancer is steadily diminished over time (Naitoh, Zeiner, and Dekernion, 1998).This radiology technique of brachytherapy provides an alternative treatment for prostate cancer over invasive surgery or larger more expensive beam-based treatments, which according to Wirth and Hakenberg (1999) subject neighboring tissues to secondary radiation dosages that can cause tissue damage to neighboring organs (Wirth and Hakenberg, 1999). Based upon interviews of current and retired medical professionals from the cancer treatment facility of the University of Florida's SHANDS medical center, the radioactive and non radioactive, or seeds and spacers, used within the brachytherapy process have traditionally been hand loaded into specialized hypodermic needles based on a physician's dosimetry, or radioactivity placement, treatment plan (Helmig, Mitchell, and Lu, personal communication, March 2010). Accurate placement of the radioactive seeds is crucial to impart the correct dosage of radioactivity to the correct tissue. Accuracy within the brachytherapy process currently suffers due to the long lead times between the initial scanning of the cancerous area and the brachytherapy surgical treatment itself (Helmig, Mitchell, and Lu, personal communication, March 2010).

Many cancerous locations, such as the prostate, commonly shift position within the human body over time (Crook, Raymond, Salhani, Yang, and Esche, 1995). This natural movement is then complicated by the lithotomy position patients must assume for both the initial scanning of the prostate gland and then reassume for the actual

brachytherapy procedure (Mitchell, personal communication, Jan. 2011). The time delay and unrepeatable circumstances found between the initial scan and the actual brachytherapy treatment translates to a higher probability of the cancerous area moving within the body or moving in relation to the proscribed treatment based on initial scanned position. Movement or change of any kind in the prostate brachytherapy procedure causes inaccuracy within the radioactive material placement causing the radioactive seeds to miss target locations and be placed in otherwise healthy tissues (Helmig, personal communication, May 2010). The inaccuracy in the radioactive seeds placement can be improved with the immediate on-site loading of brachytherapy needles through an automated process. Automation in the prostate brachytherapy seed and spacer loading process could possibly eliminate, or reduce, the time delay currently present when performing the procedure and lead to improvements in prostate cancer treatment.

1.2 Problem Statement

From current background research, a fully automated brachytherapy element loading system incorporating no mechanical interaction or human manipulation has not been constructed or documented before the development of this work. Currently, the uses of vacuum based designs have only been seen in an assistant role and not in that of the actual brachytherapy element loading process. This work seeks to design, build, and test a system that loads brachytherapy seeds and spacers based entirely on non-mechanical interaction with the selected elements. In this attempt at non-mechanical loading, the choice of the researcher has been to focus on the use of vacuum and air pressures to perform the set task of element loading to the currently used single application needles. The decision to base the constructed system on the premise of control through vacuum

pressure was first introduced through initial unpublished experimentation by Richard Helmig at the SHANDS cancer treatment facility (Helmig, personal communication, May 2010). These initial experimentations have been continued and refined to form this work. To complete the task of automating a non-mechanical brachytherapy element loading system, various steps were required; each of which will be further detailed in Chapter III of this work. The first of these was a pilot test to explore the feasibility of the attempted design. In this pilot test, design decisions were explored, tested, and observed. Validation on the small-scale pilot testing allowed for design of the overall device to commence. Three-dimensional (3D) parametric models were created using computer aided design (CAD) software to virtually simulate the finial prototyped device. Following the completion of the 3D CAD model, building of the device was performed using computer numerical control (CNC) machining practices. CNC machining allowed for various complex geometries to be achieved in the building of the final device. Testing of the device was performed with respect to characterization of detection sensors within the device and overall reliability of the system to follow a randomized dosimetry plan. Results from these tests are further described within Chapter IV of this work.

1.3 Objectives

Introduction to overall device.

For the current work, an automated system was designed and constructed for the purpose of loading and detecting both radioactive and non radioactive seeds within the prostate brachytherapy process. The automated brachytherapy seed loading system was designed and constructed for the purpose of minimizing the measured time between the initial scanning the cancerous area and brachytherapy treatment process. The automated

brachytherapy seed loader utilized both positive and vacuum pressures assisted with vibration to non-mechanically interact and direct the placement of brachytherapy seeds. Through having no mechanical loading method, the brachytherapy seed loading system cannot damage brachytherapy seeds during the loading process. Verification and detection of seeds locations within the brachytherapy seed loading device is provided through the use of electronic sensors and a programmed logic control. The brachytherapy seed loading system was controlled through the use of a computer based interface. This computer controlling interface was independent of the cancerous location scan and required the input of radioactive seed positioning data normally generated in the current dosimetry process. In this process, the computer interface loads elements to achieve this prescribed sequence.

Implementation of testing fixtures.

The brachytherapy seed loading system was first tested through the use of various miniature testing apparatuses (MTA) to verify design choices and usability within the overall system before construction of the main system was undertaken. Within this work, the use of these MTAs has been referred to as a pilot test. MTAs varied in functionality, allowing for observation and experimentation of problem areas that could have arisen within the complete system. Data and observations from the MTAs were collected throughout the design development process. Subsequently, a finalized completed brachytherapy seed loading system integrated the results gathered from miniature testing rigs to improve overall design functionality. All facets of the completed brachytherapy seed loading system were then tested using manual control to ensure the feasibility of the device. As the brachytherapy seed loading system functioned as intended with manual-

based control, the loading system was then attached to a computer to allow for programmable execution of the control system. The brachytherapy seed loader was successfully controlled via computer interface in such a way to ensure the exact loading of brachytherapy seeds through the programmed automation of various air pressure inputs within the system. Electrically-based light sensors within the overall brachytherapy seed loading system provided the outputs necessary for the detection of seeds at various stages within the device.

1.4 Statement of Hypotheses

The main hypothesis presented in this work regards the feasibility of developing an automated non-mechanical contact brachytherapy element loading system. As current applied methodologies for placing or selecting brachytherapy elements within applicator systems all rely on mechanical interaction or manual dexterity, the construction and testing of such a system would create a new area of knowledge within this realm of medical devices. Within this work the process is described of proving or disproving this main hypothesis through the experimentation, design, construction, testing, and characterizing of an automated non-mechanical interaction brachytherapy element loading system. In this main hypothesis, the constructed system should load both seed and spacer elements automatically into a selected brachytherapy needle based on a randomly generated dosimetry plan while having no mechanical contact with the elements. The constructed system should also detect the presence of a loading error within the process and alert medical clinicians.

Should this main hypothesis show plausible results, that such a system can perform the set task, a secondary hypothesis states the constructed automated non-

mechanical interaction brachytherapy element loading system should perform reliably under normal indoor conditions. In this secondary hypothesis, the constructed system should not jam, or cease to function properly, over a set of trial runs inferring that an element loading system based on non-mechanical interaction is feasible for product implementation. For the purpose of current work, the brachytherapy seed loading system should be able to cycle one thousand samples, regardless of element type and material, without any type of system failure occurring. Any and all failures have been accounted for and studied to prevent future errors within the system.

Data regarding the evaluation and testing of these hypotheses have been presented in both raw and adjusted formats included within Chapter IV of this work. Changes to the finalized design of the brachytherapy material loading system due to testing of small scale testing fixtures have been explained in detail within Chapter V of this work. Testing of the constructed brachytherapy material loading system has provided a concrete basis in which to demonstrate proof of concept for automating the loading of brachytherapy materials to the general medical population with a focus on the specialized medical community of LDR brachytherapy.

1.5 Significance of Work

The initial suggestion of an automated brachytherapy seed loading system based on the concept of vacuum pressures was first proposed for development and research by Richard Helmig of SHANDS Hospital at the University of Florida (Helmig, personal communication, May 2010). Richard Helmig, the chief scientific instrument maker and designer at SHANDS Hospital, saw the need for an automated brachytherapy seed loading system due to his personal experiences within the field of medical devices and

that of brachytherapy prostate treatments. Traditionally, the use of negative air pressures, or vacuum, for the loading of radioactive and non radioactive brachytherapy seeds have been used extensively in the manual hand-loading of seeds for years in the form of stylist devices as shown in *figure 1.1*. In the manual hand-loading process, brachytherapy seeds are simply deposited into a guided template or directly into the brachytherapy needles.

Figure 1.1: Vacuum apparatus commonly used in the hand loading process of brachytherapy seeds. Correct Products, Aug.2008 <http://www.correctproducts.com>

However, the idea of automated brachytherapy seed loading using the premise of a vacuum pressure system had not been developed prior to this current work. Conversely, all current brachytherapy seed loading devices rely mostly on the concept of direct

mechanical or manual separation and placement. Common failure of these mechanical separation and placement designs, along with long load times found in traditional manual methods, have prompted the desire for a new non invasive separation and loading methods (Helmig, personal communication, May 2010). Following the proposed project of a negative air pressure-based seed loading system during the summer of 2009, research was initiated on the topic of designing, testing, and constructing a proper negative air pressure-based brachytherapy seed loader.

For research within the field of prostate brachytherapy, the construction and testing of an automated system with the ability to load brachytherapy needles with both radioactive and non radioactive seeds within a sterile operating room environment was conducted. This automated brachytherapy seed loading system has the ability to fill a wide variety of treatment plans requested from medical physician through the loading of both radioactive seeds and non radioactive "spacer" seeds. The combination of non-radioactive spacers within the treatment plan serves to properly align the radioactive material with the desired implant location. The required patent treatment plan is delivered to the brachytherapy seed loading system through an electronic computer-based format currently in use within the medical practice or through the use of a manual user interface. The current work provided a benefit to brachytherapy cancer treatment by furthering the knowledge and information regarding loading of brachytherapy materials.

1.6 Delimitations of Work

In the world of prostate brachytherapy treatments, the study of dosimetry is vital in determining the proper amount of radioactivity to impart on cancerous regions (Wirth and Hakenberg, 1999). Through the process of dosimetry, placement of radioactive

brachytherapy seeds is determined and a treatment plan, or map of radioactive and non-radioactive materials, is then formulated. While the process of dosimetry provides the location of both radioactive and non-radioactive brachytherapy seeds, this was not the focus of the current work. Information produced by the dosimetry process was simply fed into the constructed brachytherapy seed loading system using the current established processes. The brachytherapy seed loading system has been constructed only to automate the existing process of hand-loading brachytherapy seeds into existing specially designed needles using non-mechanical means. The brachytherapy seed loading system does not have the capability to automatically administer the actual brachytherapy treatment by inserting loaded needles into the prostate gland as can be seen in some current experimental prostate brachytherapy devices (Zhang et. al. 2006). This work does not pertain in any facet to the actual surgical brachytherapy treatment. Physical indication of the status of each needle and its contents are displayed using programming logic to all operating room staff to ensure accuracy. It has been left to the actual attending surgeon to correctly place the filled brachytherapy needle from the constructed brachytherapy seed loading system. However; as manual insertion is still the norm within most current medical practices (Helmig, personal communication, Aug. 2009), the constructed brachytherapy seed loading system delivers filled brachytherapy needles to the administering surgeon during the brachytherapy treatment process. Additionally, physical identification of brachytherapy seeds based upon radioactivity does not pertain to this work as the detection of seed type within the constructed brachytherapy seed loading system has been based solely upon logic.

1.7 Introduction to Chapters

The following chapters will detail all research conducted in regards to the current thesis topic and the development of an automated negative air pressure-based brachytherapy seed loading device. Chapter II discusses various background information and previous works to better comprehend the sphere of knowledge encompassing prostate brachytherapy, automated design, radiology, and mechanical design. Chapter III includes information regarding design work, testing methodologies, and constructed automated system. Chapter III includes all design testing fixtures and the overall constructed brachytherapy seed loading system. Chapter IV focuses on any and all results gathered throughout the current work. Results from all testing systems will consist of analysis on both design and statistical performance criteria involving all aspects of the constructed brachytherapy seed loading system. Conclusions made by the researcher and any opinions of medical clinicians and related personnel are provided in Chapter V. Chapter V of this work also includes needed work and direction for any potential future iterations of the current work. A bibliography of cited works will be provided at this end of this document.

1.8 Definition of Key Terms

Air Pressure – a force of positive pressure applied within this work to push or move selected brachytherapy elements through the constructed system. Primarily employed as an assist to the force of gravity or to prevent friction bonding.

Brachytherapy – radiotherapy in which the source of radiation is placed (as by implantation) in or close to the area being treated. (Used interchangeably within this work for LDR brachytherapy). Brachytherapy. (n.d.). In Merriam-Webster's

online dictionary (11th ed.). Retrieved from http://www.merriam-webster.com/dictionary/brachytherapy

Seed Element– a singular cylindrical metallic capsule containing radioactive material for use within a brachytherapy treatment. Seeds have been simulated in this work through the use of a “dummy” or training seed containing a non-radioactive payload.

Spacer element – can consist of either a singular cylindrical metallic capsule containing no radioactive materials or an extruded piece of biodegradable polymer or suture material for use within brachytherapy treatment to align radioactive seed elements.

Capture Area – area within the constructed device in which vacuum pressure is applied to halt elements as they travel.

Cancer – a malignant tumor of potentially unlimited growth that expands locally by invasion and systemically by metastasis. Cancer. (n.d.). In Merriam-Webster’s online dictionary (11th ed.). Retrieved from http://www.merriam-webster.com/dictionary/cancer

DAQ – a data acquisition device used within the work to control all aspects of the constructed device such as: solenoid activation and sensor data.

Directional Control Valve (DCV) – normally operated pressurized air valve as related to the constructed system. Cycling of these valves on and off through solenoid connections serves to allow and disallow air flow through the pneumatic section of the device.

Dosimetry – the measurement of radiation dosage (as X-Rays). (Referred to within this work primarily within the constraints of patterning brachytherapy elements).

Dosimetry. (n.d.). In Merriam-Webster's online dictionary (11th ed.). Retrieved from http://www.merriam-webster.com/dictionary/dosimetry

Hand-Off – term used within this work to describe the action of moving only a single element from one capture area to another keeping trailing elements in a stationary position.

Jam – the act of one or more brachytherapy elements impeding travel of sequential elements as they traveled through the constructed system. Seen as a critical failure within regular operation of the device.

Hopper – reservoirs within the constructed system that contain elements not yet cycled through the device.

Light Gate Sensor – a dually constructed sensor consisting of a high intensity LED and photoelectric resistor separated by distance and fitted within specially constructed housings to send a shaped beam of light. Dependent on the material between the sensor sections, the resistance across the photoelectric resistor varies.

Lithotomy Position – a supine position in which the hips and knees are fully flexed with the legs spread apart and raised and the feet resting in straps.

Lithotomy Position. (n.d.). In The American Heritage Stedman's Medical Dictionary. Retrieved from http://www.dictionary.reference.com/browse/lithotomy_position

Piloted Directional Control Valve – referred to within this work as a "piloted valve", this component allows for control of vacuum to the system based on input from an associated pneumatic DCV. This secondary valve component was required due to the requirement of positive air pressure for normal DCV operation.

Prostate Gland – a firm partly muscular partly glandular body that is situated about the base of mammalian male urethra and that secretes an alkaline viscid fluid which is a major constituent of the semen.

Prostate Gland. (n.d.). In Merriam-Webster's online dictionary (11th ed.). Retrieved from http://www.merriam-webster.com/dictionary/prostate+gland

Radioactivity – the property possessed by some elements (as uranium) or isotopes (as carbon 14) of spontaneously emitting energetic particles (as electrons or alpha particles) by the disintegration of their atomic nuclei.

Radioactivity. (n.d.). In Merriam-Webster's online dictionary (11th ed.). Retrieved from http://www.merriam-webster.com/dictionary/radioactivity

Radiology – a branch of medicine concerned with the use of radiant energy (as X-rays) or radioactive material in the diagnosis and treatment of disease. Radiology. (n.d.). In Merriam-Webster's online dictionary (11th ed.). Retrieved From http://www.merriam-webster.com/dictionary/radiology

Rapid Prototyping – the use of various methods and equipment in a process of producing physical components through additive layer-by-layer construction based on predefined three-dimensional geometries.

Solenoid – an electrical component employed in the control of pneumatic DCVs within the constructed system. The DAQ device controls activation and deactivation of these electrical components with the use of steady state relays.

Solid State Relays –optically isolated solid state relay switches that allow for isolation of various power supplies from one another. Within the constructed system these relays serve to isolate 5 volts (v) signals sent from the DAQ from 24 volts required for solenoid activations.

Vacuum Pressure – a force of negative pressure, or suction, applied within this work to capture and manipulated brachytherapy elements as they travel through the constructed system.

CHAPTER 2: LITERATURE REVIEW

In the following Chapter II, the realm of prostate brachytherapy as it relates to the work performed will be defined. Beginning from a large scale, the scope of the background related to this work will be defined to the current LDR prostate brachytherapy practices. Previous research that has culminated in the ability to perform the current work will be presented dating to the discovery of modern radiology to the use of today's practices of element implantation. Applied methodologies of currently utilized medical devices within this cancer treatment process will also be explored.

2.1 Background

In the world of cancer treatment, invasive surgery was first thought to be the only defense against cancerous tumors within the human body by simply removing the problem area. However with the discovery of x-ray radiation in 1895 by Wilhelm Roentgen, a new field of knowledge, radiology, was born (Glasser, 1931). With the initial discovery of radiation by Roentgen others began to experiment within the field of radiology finding various uses for this new science. There is discrepancy in the first treatment of patients using x-ray radiation and a Chicago medical student, Emile Grubbé, is widely considered to be the first to use such methods (Orton, 1995). Yet, due to not immediately documenting and reporting his findings, Grubbé's claim cannot be fully verified. The first documented example of radiology with the purpose of medical practice was documented the year after Roentgen's x-ray discovery in 1896 with a German physician Voight. As with Grubbé, Voight's first attempts to use radiation in the fight against cancer were conducted using various x-ray tubes placed in proximity to the cancerous locations (Glasser 1933). Although extremely crude in nature, this radiation

source proximity approach used by Voight is the same logic applied to the current methodology of brachytherapy.

From the first discovery of radiation by Roentgen, the study and understanding of radiology has improved. New and more exact methods of delivering radiation to cancer locations have been conceived. During this expansion of radiology, the practice of brachytherapy was introduced along with other fields of study including proton therapy, photon therapy, and electron therapy. With the introduction of modern radiation based treatments to fight against the spread of cancer in the human body, invasive surgical procedures have now become a policy of last resort in most clinical settings when it is thought that the cancer has progressed beyond the target organ (Helmig, Mitchell, and Lu, personal communication, March 2010). Of the current radiation-based cancer treatments, external beam radiation therapy (EBRT) treatments have become the mainstay method of treatment due to the noninvasive nature in which the procedure is performed (Bostwick (Ed.), 2005). The use of EBRT does not require the large scale physical damage of surrounding tissue needed for exploratory surgery and thus lessens the bodily strain on already weak patents who could otherwise not tolerate the extensive surgery recovery time. However, the advantages associated with EBRT are gained at a price over more traditional invasive surgeries. Due to the nature of EBRT, exact accuracy can become unattainable due to bodily scatter, patient movement, and various other issues within the treatment process (Helmig, Mitchell, and Lu, personal communication, March 2010). Another negative issue relating to the use of EBRT for cancer treatment lies in the damage commonly suffered by neighboring tissues during treatments (Bostwick (Ed.), 2005). In many cases, unintentional radiation damage to non-targeted

healthy cells can result in various complications due to healthy cell damage. Specifically, a major concern in prostate cancer treatments is the attempt to limit cell damage to neighboring organs such as the bladder, the urethra and the rectum (Wirth and Hakenberg, 1999). It is from the undesired effects of EBRT with respect to prostate cancer treatment that brachytherapy based treatment on such areas has received a high amount of attention within the recent decades. Brachytherapy prostate treatment offers a "middle-ground" of sorts when comparing surgery options and EBRT. Brachytherapy treatment involves the use of surgical methods to place radioactive material within the targeted area, or cancerous region, of the prostate. The impact prostate brachytherapy has to the patient is minimal when compared to invasive surgeries if the procedure is performed correctly (Wallner (Ed.). 2008). Damage suffered to the cancer patient from the initial brachytherapy procedure is similar to that of multiple applications of a common injection syringe. Injuries suffered by the patient from the brachytherapy procedure typically heal in a fraction of the time allotted for more traditional surgical procedures as the brachytherapy process can be treated as an outpatient procedure with typically less than day of treatment (Helmig, Mitchell, and Lu, personal communication, March 2010). The brachytherapy process employs the use of radiation in the destruction of cancerous cells as can also be found with EBRT. Once the radioactive brachytherapy seeds have been positioned in proximity to the cancerous region, radiation from the implants destroys the cancerous tissues it has been placed next to (Naitoh, Zeiner, and Dekernion, 1998).

2.2 Brachytherapy History

The word brachytherapy stems from the Greek word “brachy” meaning short. The term brachy refers the low travel distance of radiation associated with the implanted radioactive brachytherapy seeds (Simon and Laing, 2008). The radiation from these implanted seeds travel only a short distance into their surrounding tissues. A typical brachytherapy seeds can be seen in *figure 2.1*. Because of the low travel distance of the radiation from the brachytherapy seeds, accuracy is paramount when placing these seeds within the human body (Simon and Laing, 2008). Without a high degree of placement, the eradiation from the radioactive material housed within the seeds will not reach the target location. Inaccuracy in brachytherapy seed placement can also cause damage to healthy cells while allowing unwanted tissues to remain unharmed (Potters et.al. 2005).

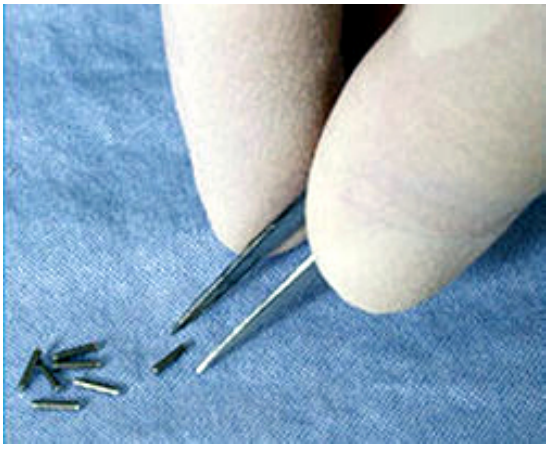

Figure 2.1: Typical brachytherapy seeds. Emory Healthcare Interstitial Radiation or Seeds (Brachytherapy), May, 2010 <www.emoryhealthcare.org>

Modern brachytherapy as we know it today can trace lineage to Pasteau and Degrais’s 1911 experiments in introducing radium isotopes with a transurethral catheter to treat cancer in patients (Pasteau and Degrais, 1913). Results from these early

experiments by Pasteau and Degrais's were promising, yet they did not show enough satisfactory results to continue along these lines of research. As time progressed from Pasteau and Degrais's first attempt, the use of implanted radioactive material to fight against cancerous growth was again attempted using radioactive gold isotopes in the 1930's (Flocks, Kerr, Elkins, and Culp, 1952). It was during the 1930's that radioactive gold isotopes became far easier to obtain and use for medical purposes. However, this second attempt at radioactive implantation by Flocks was performed before the widespread introduction of ultrasound. Without the use of ultrasound, the accurate placement of seeds within the body still proved a challenge (Ash, Bottomley, and Carey, 1998). The study and practice of placing radioactive materials within the body to destroy cancer cells was once more experimented with during the 1970's using traditional surgery to accurately place seeds within the patient's body at the Memorial Hospital in New York (Whitmore, Hilaris, and Grabstald, 1972) (Aronowitz, 2002). While the New York's Memorial Hospital operations were successful in the accurate placement of the radioactive seeds; however, the surgical techniques practiced at the time lacked the ability to keep the implanted seeds in the correct location within the target organ. Namely, the operations at New York's Memorial Hospital were performed using traditional exploratory surgical practices. The placement of the radioactive seed using the traditional surgical methods allowed for movement and dislocation of seeds from their intended position through migration along surgical incisions (Whitmore, Hilaris, and Grabstald, 1972). Seeds implanted using traditional surgical procedures within the target organ were also found to commonly group together within the organ resulting in "hot

spots” and “cold spots” of radioactivity, neither of which is a desirable result due to ending variance from the original prescribed radiation dosage.

Only in the eras of the 1990’s and 2000’s have the current methodologies of brachytherapy as described in this work been applied and practiced using specially designed equipment and methods. Of these newly introduced practices, the current prostate brachytherapy process owes much of its accuracy to the introduction of transrectal ultrasound (TRUS) in 1981 (Holm and Gammelgaard, 1981). The technique of TRUS enables the real-time viewing of the prostate gland using ultrasonic waves through the use of a probe inserted into the anal cavity. Images generated by devices, such as the TRUS, are typically displayed as two dimensional grid images. A number of companies manufacture TRUS devices for use in prostate brachytherapy. An example of a TRUS device, photographed at the University of Florida’s SHANDS Medical Center, can be seen in *figure 2.2.*

Figure 2.2: Example of transrectal ultrasound (TRUS) device used within the prostate brachytherapy process. SHANDS UF Hospital (2010). Photograph by J. Tyler Bennett (2010).

The introduction of quicker and more widespread computer usage within the last few decades has also allowed for a quicker and more accurate dosimetry process (Wirth and Hakenberg, 1999). In the dosimetry process, the radiation dosage is calculated for the individual patient and radioactive sources are placed in accordance. The use of and availability of specialized equipment in the preparation, loading, and delivering of the brachytherapy seeds has greatly increased the accuracy and effectiveness of process of prostate brachytherapy (Ellis, 2002).

2.3 Current Applied Methodologies

Current types of brachytherapy.

Within the practice of modern brachytherapy, two differing treatment methods exist. These different methods of brachytherapy are typically referred to respectively as permanent implant brachytherapy and removable implant brachytherapy. The methods of

permanent and removable implant brachytherapy treatments differ in many aspects, most notably the radiation levels associated with both. The radiation levels used in typical removable implant brachytherapy procedures are High Dose Rate implants (HDR), while permanent implant brachytherapy procedures use Low Dose Rate implants (LDR). These procedures have been titled as such to represent the general radiation exposure to the patient's target area during treatment (Ash, Bottomley, and Carey, 1998).

Removable implant brachytherapy.

Removable implant brachytherpay typically uses the radioactive isotope iridium-192 (Ir^{192}) (Bostwick (Ed.), 2005). In the basic practice of removable implant brachytherapy at the SHANDS Hospital at the University of Florida, treatments of multiple strands are placed in the patient's body using surgical methods (Helmig, personal communication, Aug. 2009). These stranded materials can be commonly preloaded with a number of radioactive and non-radioactive sources to correspond to the patient's cancerous area according to a dosimetry plan. However, these strands can also be eradiated from a secondary source once surgically placed. Commonly, the placement procedure of these strands involves the use of limited invasive surgical methods when compared to surgical removal of the cancerous region (Helmig, personal communication, Aug. 2009).

In most applications radioactive material placed in this manner is HDR and the strands are kept within the patient's body only for a limited time period. Typically, this time period that removable implant brachytherapy are placed within the patient's body ranges around forty-eight hours according to SHANDS Hospital at the University of Florida (Helmig, personal communication, Aug. 2009). After the calculated time limit for

the removable brachytherapy strands have been reached, these HDR strands are then removed from the patient. The removal of these HDR strands is required due to the dangers associated with long term exposure to high-dose levels of radiation. The removal of these strands takes place in not in an additional surgical procedure, but in the patient's room (Mitchell, personal communication, Jan. 2011). Once the radioactive material has been removed, the patient is allowed to recover.

However, according to the American Cancer Society some advancement for the usage of HDR in prostate applications has evolved to become more specialized and less evasive (Bostwick (Ed.), 2005). In this application of HDR to the prostate, specialized needles are inserted into the prostate. The act of removing the specialized needles from the prostate allows a type of catheter to be deposited. Multiple catheters are attached to a computerized mechanism. This HDR computerized machine delivers radioactive seeds through the implanted catheters to the patient's prostate based on a treatment plan. In this prostate-based HDR procedure, the procedure is allowed to be spaced out over a set length of time longer than traditional strand implantation of HDR as previously described (Bostwick (Ed.), 2005).

Permanent implant brachytherapy.

Differing from removable implant brachytherapy, permanent implant brachytherapy materials consist of much lower radiation levels. Typically radioactive iodine (I^{125}) or palladium (Pd^{103}) materials are used (Bostwick (Ed.), 2005). These radioactive materials do not have the prolonged exposure risk associated with HDR brachytherapy. Rather, these materials decay overtime becoming benign and emitting little to no radiation after a period of time. Because of the relative low dosage of radiation

emitted by these materials and the relatively quick decay over time, these materials are commonly left within the patient's body. This allows for only one surgical procedure. Additionally, this singular surgery can be minimized through the use of depositors. These depositors traditionally take the form of a modified hypodermic needle with a plunger attachment as can be seen in *figure 2.3*. Typically low-dose brachytherapy procedures take less time and require less recovery time for the patient. The automated loading system described within this work has been conceived for use with permanently implanted LDR brachytherapy materials.

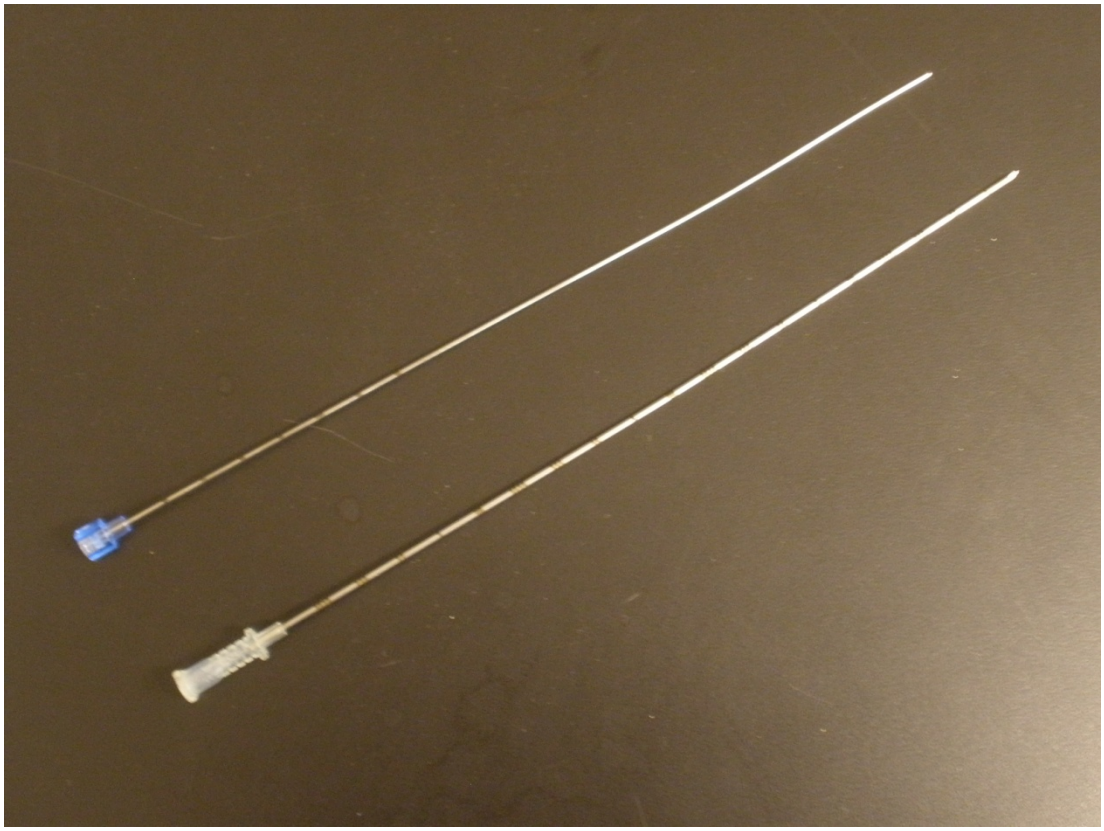

Figure 2.3: Photograph of specialized needles used in traditional permanent implantation LDR procedures provided by SHANDS Hospital.

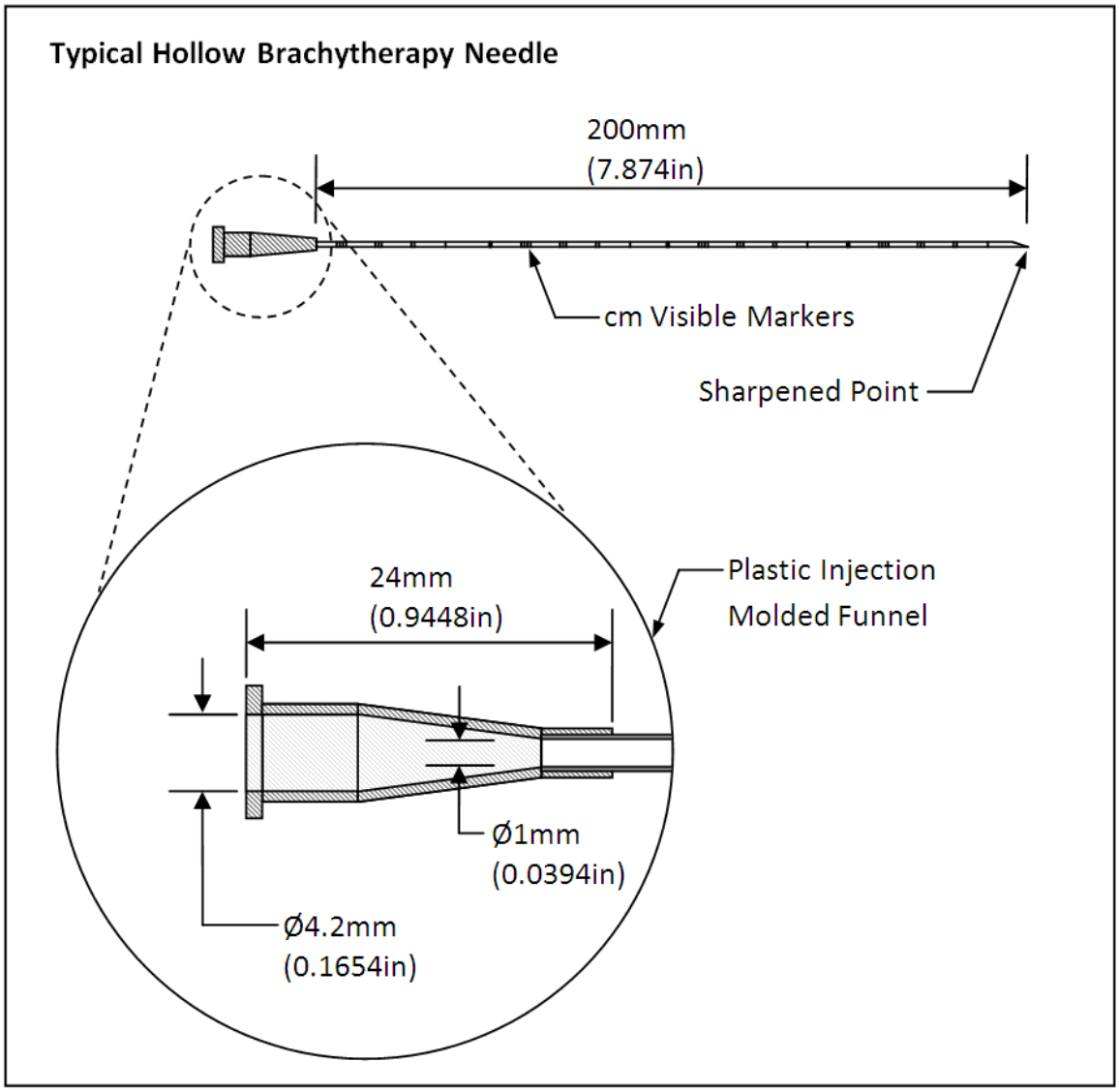

Figure 2.4: Diagram detailing construction of typical permanent implant brachytherapy needles.

Permanent implant LDR brachytherapy seeds.

The current practice of prostate brachytherapy involves the use of small metallic containers filled with radioactive and non radioactive materials called “seeds”. Only seeds consisting materials of Iodine^{125} (I^{125}) and Palladium^{103} (Pd^{103}) have been included as this work regards only permanent implant LDR brachytherapy seeds. According to the

American Association of Physicists in Medicine, both of these seed types are comparable to that of one another through having similar photon energies (Yu et. al., 1999).

According to the text, Prostate Brachytherapy Made Complicated; seeds consisting of I^{125} have become the most popular choice for permanent implant brachytherapy procedures due to its large half-life of sixty days (Wallner (Ed.), 2008). The sixty day half-life allows for non-immediate usage. Seeds consisting of I^{125} are produced from the element Xenon^{124} (Xe^{124}) via a nuclear reactor. Once produced, the I^{125} decays over time into the element Tellurium^{125} (Te^{125}). In this decaying state, the created I^{125} material releases photons with an average energy of 29 killoelectronvolts (keV) of energy. Silver was first used in this production of the I^{125} allowing the radioactive element to be absorbed onto the silver material. However, tungsten is now also used in this process resulting in two methods of creating the I^{125} radioactive material for use in LDR brachytherapy treatment. Radioactive I^{125} material is then enclosed within a titanium capsule using precision welding (Yu et al., 1999). As the ends of the "capsule-like" I125 brachytherapy seed are welded shut, the resulting seed is a rounded cylindrical shape. The typical construction of an I^{125} brachytherapy seed can be seen in *figure 2.5*.

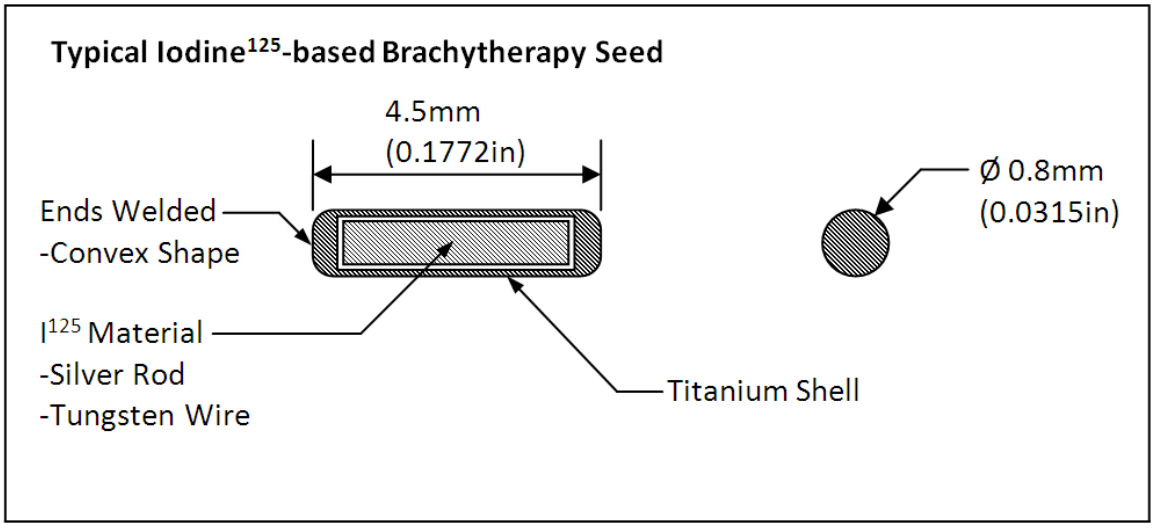

Figure 2.5: Diagram detailing construction of typical seed containing radioactive payload of Iodine125 for permanent implant LDR brachytherapy. Adapted from "Prostate Brachytherapy Made Complicated 3rd Ed.," by Wallner (Ed.), 2008, 6.6. Copyright 2008 by SmartMedicine Press.

The second most popular choice of radioactive seed isotope for use in permanent implant brachytherapy is Pd^{103}. Isotope Pd^{103} can be created through two methods. As with the more popular isotope I^{125}, Pd^{103} can be produced in a nuclear reactor. Production of Pd^{103} using a nuclear reactor was accomplished through forcing Pd^{102} to absorb an additional neutron. Over time though, production by nuclear reactor has decreased and currently Pd^{103} is produced through a cyclotron. Pd^{103} production using a cyclotron is accomplished through bombarding rhodinium material with protons. The radioactive isotope Pd^{103} decays into the element Rhodium^{103} (Rh^{103}) after using the cyclotron production method. In this decay of Pd^{103} into Rh^{103} energy is released on an average of 21 keV. Typically, the radioactive Pd^{103} material is plated on radiolucent graphite rods (Wallner (Ed.), 2008). In the construction of the Pd^{103} based seeds, the plated graphite rods are placed at either side of a lead x-ray marker comprising the center payload of the seed. As in the construction of the I^{125} seeds, the Pd^{103} seeds are sealed within an outer

titanium shell. The Pd^{103} seeds are typically constructed with "cupped" or concave ends, differentiating them from other seed types to avoid confusion (Yu et al., 1999). The typical construction of a Pd^{103} brachytherapy seed can be seen in *figure 2.6*.

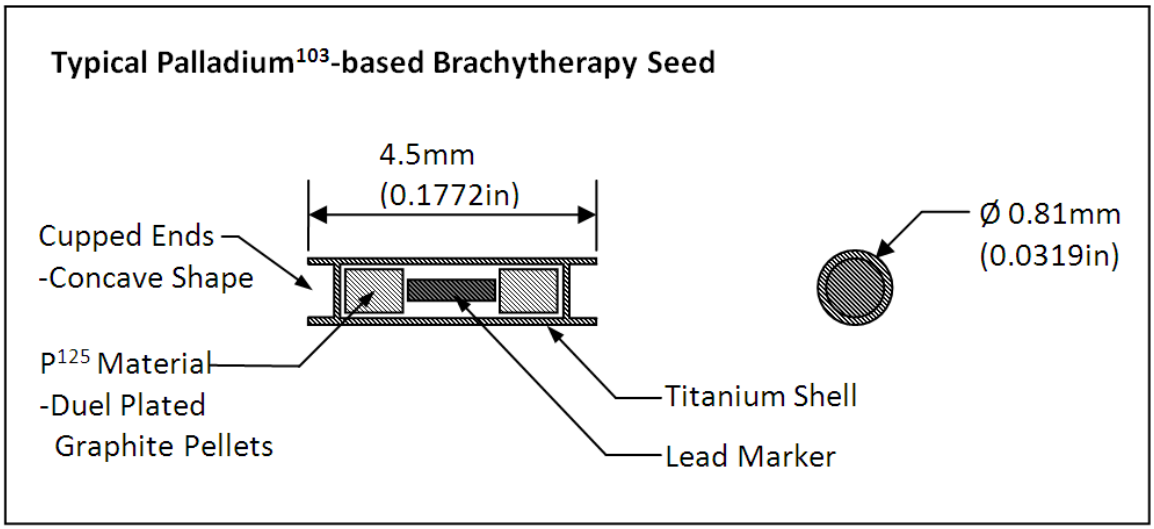

Figure 2.6: Diagram detailing construction of typical seed containing radioactive payload of Palladium103 for permanent implant LDR brachytherapy. Adapted from "Prostate Brachytherapy Made Complicated 3rd Ed.," by Wallner (Ed.), 2008, 6.9. Copyright 2008 by *S*martMedicine Press.

Due to the hazardous nature of handling radioactive materials, this work was performed with I125 seeds that had fully decayed. These fully decayed I125 seed elements, referred to within this work as dummy seeds, were supplied by SHANDS hospital. The size, shape, weight, texture, and manufacturing construction consisting of a small cylindrical container sealed with a precision weld were an exact metric to that of a live or radioactive element. These dummy seeds were used in all experimentation and research found in Chapter 3 and Chapter 4 of this work. The construction and physical dimensions of the dummy seeds can be seen in *figure 2.7* while a photograph of the elements can be seen in *figure 2.8*.

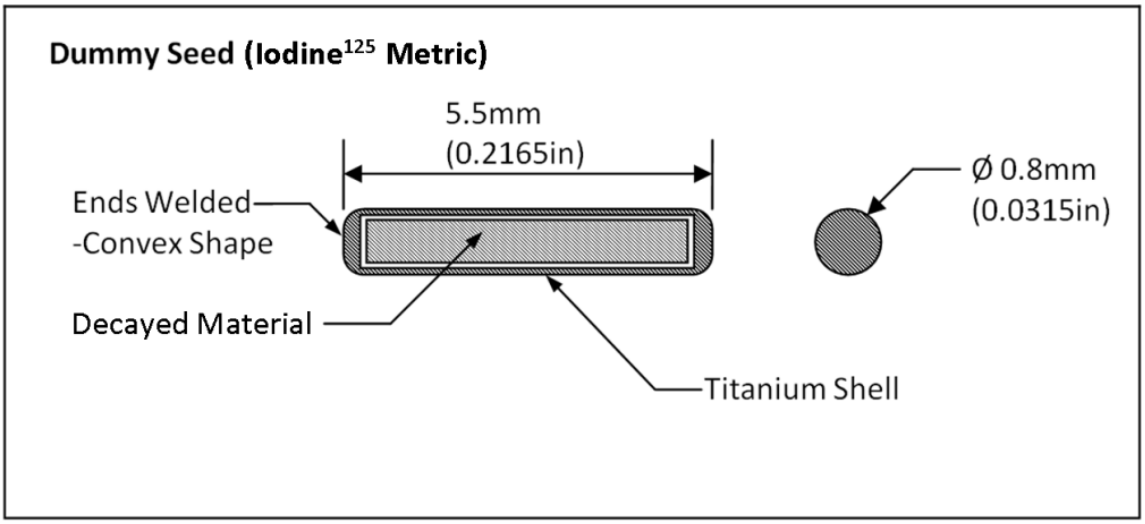

Figure 2.7: Diagram detailing construction of disposable collagen proxy seeds used with this work to approximate traditional I125 permanent implant seeds. Material provided by SHANDS hospital.

Figure 2.8: Photograph of typical brachytherapy source seeds used in permanent implant LDR procedures.

Spacer seeds.

Elements used in the brachytherapy treatments not containing any radioactive materials used to properly position the seed elements are commonly called “spacers” within the medical industry (Helmig, personal communication, Aug. 2009). Spacer seeds can be produced in much the same fashion as their radioactive seed counterparts in the form of metallic casings with benign payloads, as has been described in the previous section within this work on seeds. However, the use of these metallic spacers is not in common practice within the brachytherapy industry. Suture materials such as “catgut”, a natural animal fiber that is absorbable by the human body, are the most common in brachytherapy procedures (Lucas (Ed.), 2005). At the present time, suture material technology has advanced with the introduction of synthetic materials and the use of vicryl and Poly-P-Doxanon-Suture (PDS) have become the industry standard (Hammer, Hawliczek, Kärcher, and Riccabona, 1989). Other biodegradable synthetic materials such as polyglycolic acid (PGA) polylactic acid (PLLA) are also in industry usage for the role of spacer (http://www.cpmedical.com). These various materials provide a few advantages over metallic spacers as they are able degrade within the human body whereas the non radioactive metallic spacers will not. Synthetic spacers made from materials such as PDS show further advantages over more traditional suture materials such as catgut as they resist swelling due to the presence of liquids (Hammer, Hawliczek, Kärcher, and Riccabona, 1989). Spacer seeds are produced using an extrusion process (Helmig, personal communication, Aug. 2009). Through this manufacturing process, cost per spacer is reduced dramatically over precision welded metallic spacer seeds. The production of traditional suture materials for brachytherapy applications can show edge

deformation as seen in *figure 2.9* (Hammer, Hawliczek, Kärcher, and Riccabona, 1989). This edge deformation will be further discussed in Chapters III and IV of this work as this phenomenon was observed during experimentations.

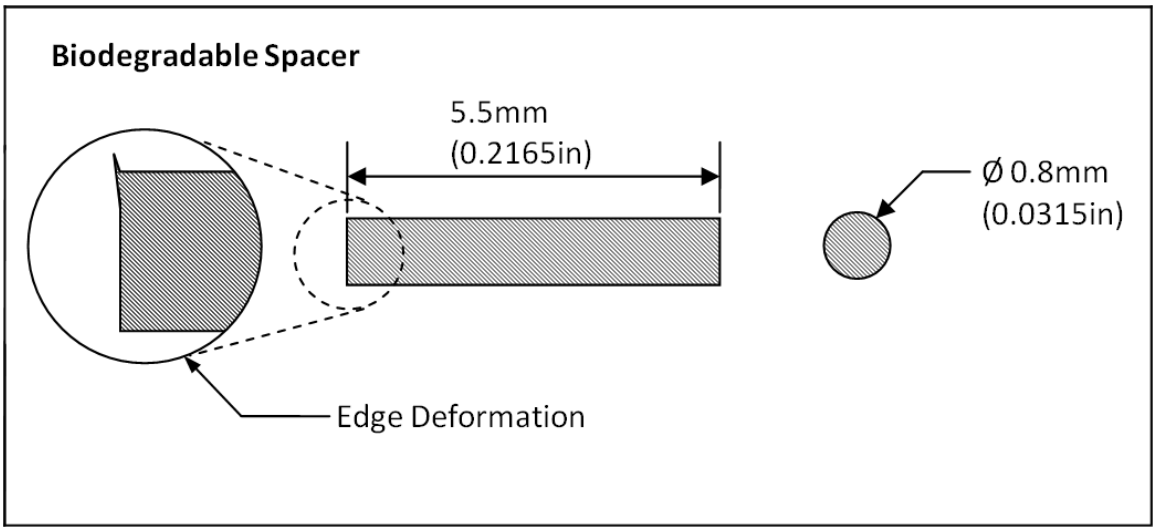

Figure 2.9: Diagram detailing biodegradable spacer elements. Diagram based on CP Medical, Inc product: Bio Spacer 910™

No matter the material or construction used, spacer seeds perform a much needed alignment action within the brachytherapy procedure. As the brachytherapy needle exits from the patient body, a cylindrical wound is created in the shape of the exiting needle. It is within this cylindrical wound that the brachytherapy seeds are dropped, or deposited, within the patient (Wallner (Ed.), 2008). Seeds positioned in such a manor without the use of spacer seeds inherently move according to the needle exit path (Helmig, Mitchell, and Lu, personal communication, March 2010). If placed without spacer seeds, the radioactive seeds would migrate along the needle exit path relative to the original placement, thus decreasing the effective treatment of the cancerous area. This seed migration phenomenon often results in “hot spots” of radioactivity within the patient

(Ash, Bottomley, and Carey, 1998). These hot spots are formed when multiple seeds migrate toward one another forming a cluster of radioactive material in an unintentional location. With the spacer seeds in position, the needle exit wound is filled allowing reduced movement of the radioactive seeds. With the radioactive material fixed into a designated location, the correct dosage of radiation is transferred to the selected tissues. Various spacer seeds can be seen in *figure 2.10.*

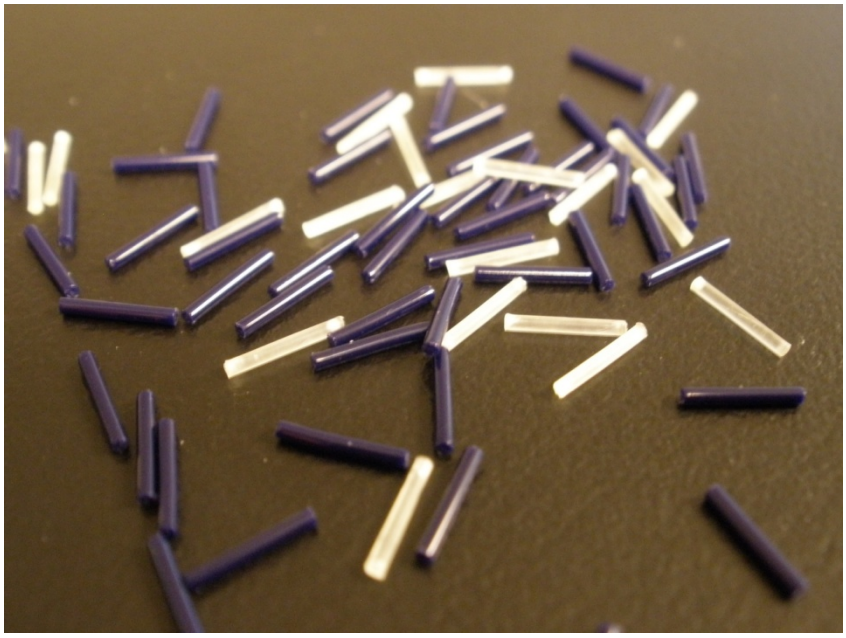

Figure 2.10: Photograph of various spacer seeds used in permanent implant LDR procedures. Spacer supplied by SHANDS hospital.

Current practice.

During the process of prostate brachytherapy, the first step performed is an initial scan of the prostate gland as illustrated in *figure 2.11.* The initial scan is referred to within the industry as a "volume study" (Helmig, Mitchell, and Lu, personal communication, March 2010) (Dicker (Ed.), 2005). The volume studies vary throughout

the medical industry, but commonly consist of an x-ray, TRUS, CT, or MRI scan performed from various angles centered on the cancerous location (Ellis, 2002). Any of these techniques has the ability to develop a three dimensional image of the patient's prostate allowing for a treatment plan to be developed through dosimetry although TRUS is typically used as it has been found to be at least as effective as CT (Wallner et. al. 1999). Typically, a volume study on the prostate gland is performed a week or so prior to the actual brachytherapy procedure (Wallner (Ed.), 2008).This allows time to prepare and load the brachytherapy needles with the required patterns of seeds and spacers.

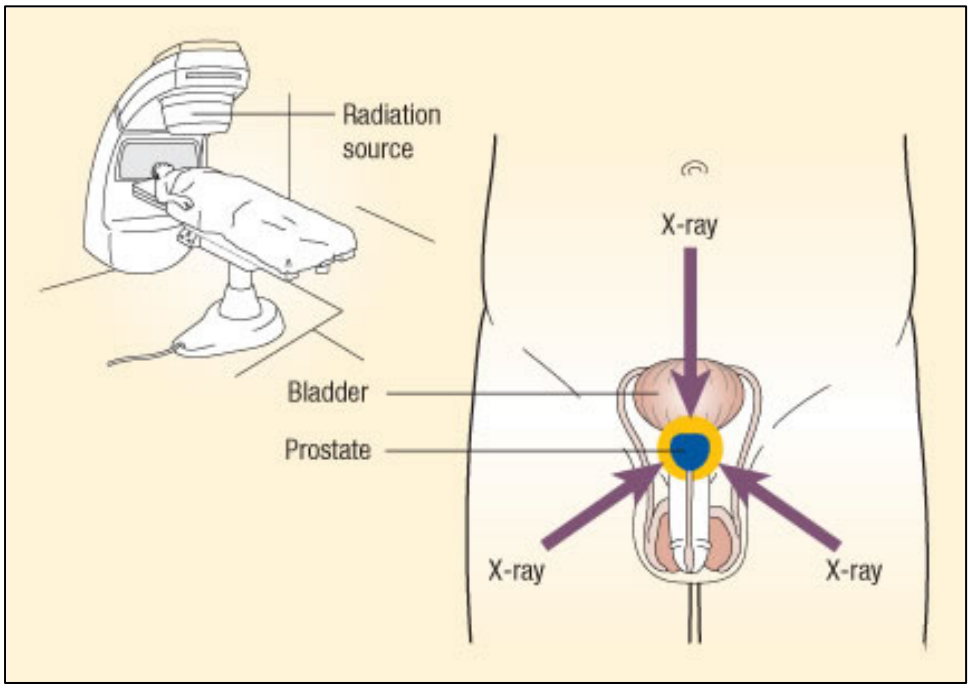

Figure 2.11: General illustration of the x-ray method in which the initial scan of the prostate is performed. Prostate UK (2010). Radiotherapy. Retrieved from: http://www.prostateuk.org/prca/prcatreatinradio.htm

During both a TRUS scan of the prostate and the actual brachytherapy treatment, the patient is positioned in the lithotomy position on an examining table (Mitchell,

personal communication, Jan. 2011). The lithotomy position uses stirrups to position the patient's femurs in a vertical plane (Dicker (Ed.), 2005). Positioning the patient in this manner allows for medical clinicians to access the patient's lower abdomen. The lithotomy position is a commonly found practice during medical examinations and procedures, such as pregnancy. Once positioned properly in the lithotomy position, the TRUS probe is inserted into the anal cavity and incremented by a set distance (commonly five millimeters) along the location of the prostate to form a three dimensional volume study of the cancerous region (Ellis, 2002). Studies have shown that incrementing the TRUS probe between three and five millimeters would allow for most target areas to be sufficiently scanned (Davis et al., 1999). Traditionally the volume study is performed manually by a medical professional manipulating the TRUS probe through the anal cavity and capturing satisfactory still images. The resulting volume study results in a stack of images representing the shape of the prostate gland (Helmig, Mitchell, and Lu, personal communication, March 2010). An example of one of these single images created during the volume study can be seen in *figure 2.12.*

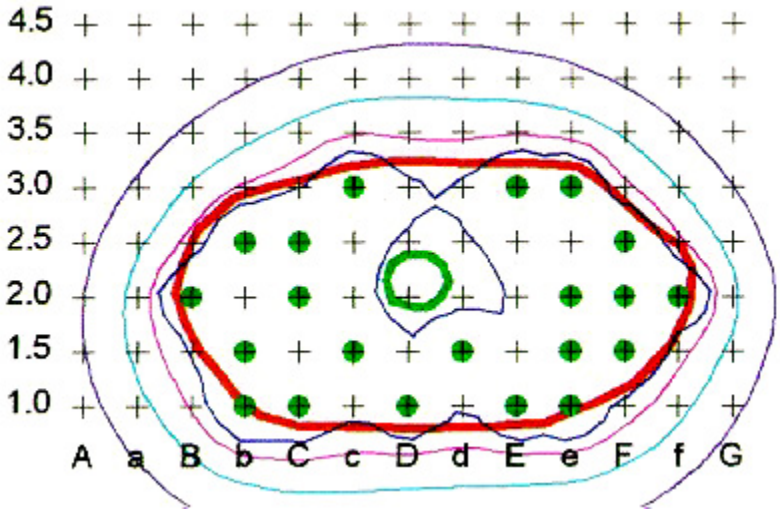

Figure 2.12: Example image of prostate gland resulting from volume study (2011). Dosimetry plan. Retrieved from: http://www.emedicine.medscape.com/article/453349-media

Various methods for interpreting the volume study of the prostate are in usage in the medical community. Once the dosimetry has been performed based on the performed volume study, the selected diagnosis is created that corresponds to an appropriate pattern in which the radioactive brachytherapy seeds and non-radioactive brachytherapy spacers should be placed to impart the greatest effect on the selected cancerous region. This dosimetry plan can then be contracted to an external entity to manual fill the specialty needles with the correct patterns of seeds as depicted in *figure 2.13*. The process of manually filling the brachytherapy seeds within the needles can also take place within the cancer facility in a prepared clean room by a specially trained individual. However, this is rarely performed on site due to large setup times associated with room and instrument stylization along with the inherent chance of radiation contamination within the cancer facility (Mitchell, personal communication, Jan. 2011).

Figure 2.13: Medical technician hand loading Brachytherapy seeds behind a protective shield. Australasian Brachytherapy Group (2008). Frequently Asked Question. Retrieved from: http://www.abg.org.au/General/BrachytherapyFAQs.asp

The process of filling brachytherapy seeds within the needles commonly involves the use of specialized employees in the hand loading of each individual needle. The current brachytherapy seed loading procedure is a time consuming process exposing medical technicians to a small secondary dose of radiation. According to Tom Mitchell, a retired medical professional, each individual needle takes around one to two minutes to manually fill (Mitchell, personal communication, Jan. 2011). The use of human personnel in the task of loading brachytherapy seeds can also introduce the chance of human error within the overall seed loading process. Human workers, no matter the specialized training, are prone to mistakes and require precise dexterity and time to manually load needles with the correct seed orientation. The loading of an incorrect dosage within the

overall brachytherapy procedure reduces the effectiveness of the entire procedure (Wallner (Ed.), 2008).

If the brachytherapy needles are preloaded offsite, the units are transported to the cancer treatment operating room according to the proscribed dosimetric prescription created from the volume study. Transportation, especially from an outside needle loading source, compounds the time required from the initial patient volume study until the brachytherapy procedure is performed. Differing from the original volume study, in which the patient is awake and aware, the patient is given a local anesthetic (Dicker (Ed.), 2005) or is placed under general anesthesia during the prostate brachytherapy procedure. In preparing for the prostate brachytherapy procedure, the patient is again situated in the lithotomy position with stirrups. The medical clinician then attempts to align the patient's body to match the orientation of the original volume study (Mitchell, personal communication, Jan. 2011). Patient alignment in this manner can become difficult as the position of the pelvis and legs directly impact the position of the prostate gland. In most procedures, the TRUS system is again deployed in the same manner as with the volume study to assist the medical clinician in the realignment process. The TRUS system allows the medical clinician to observe the prostate in real-time to assist with alignment to the volume study. Once the prostate has been aligned to the clinician's satisfaction, the prostate brachytherapy procedure can begin. To allow for proper insertion of the preloaded brachytherapy needles into the prostate, a grid-like template to be positioned above the anal cavity as can be seen in *figures 2.14 and 2.15.*

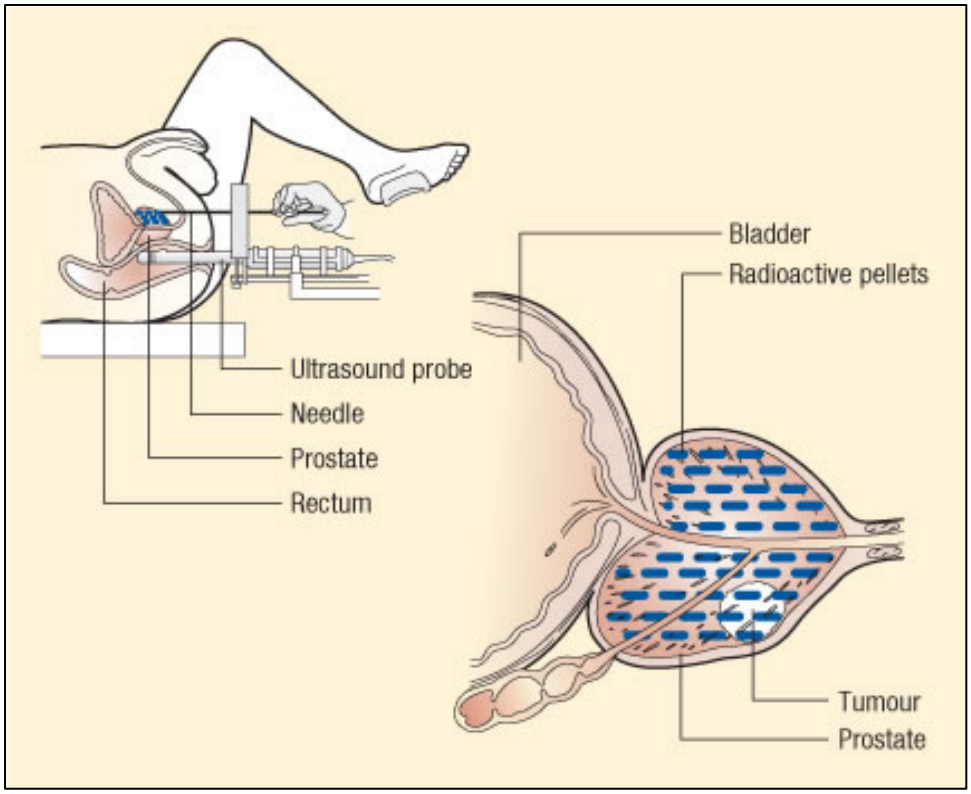

Figure 2.14: General illustration of the surgical placement of Brachytherapy seeds within the prostate. Prostate UK (2010). Radiotherapy. Retrieved from: http://www.prostateuk.org/prca/prcatreatinradio.htm

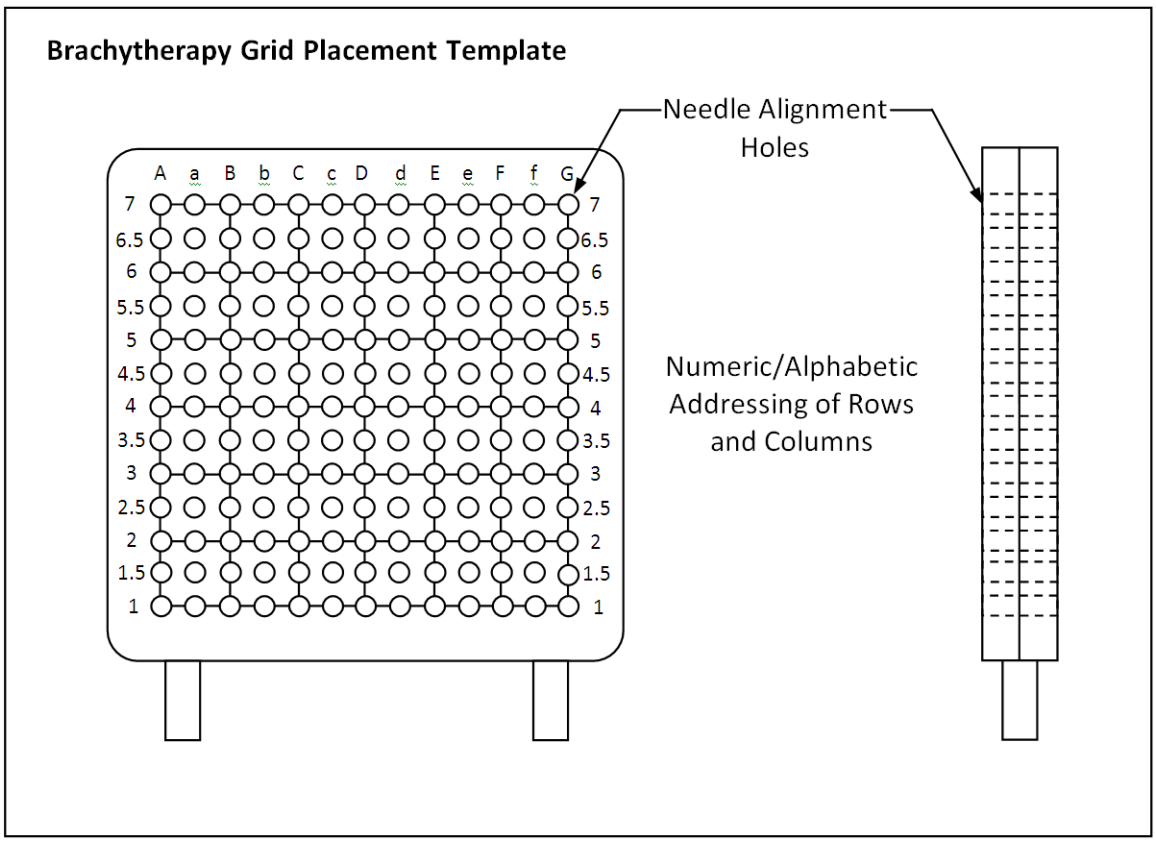

Figure 2.15: Diagram of the grid template used to position the Brachytherapy needles in relation to the treatment area. Diagram based on information and illustrations from: IZI Medical Products (2010). Radiation Therapy. Retrieved from: http://izimed.com/radiation_therapy.shtml

The positioning of the TRUS system also serves to impair most prostate gland movements during the operation. Following the dosimetric volume study, the preloaded brachytherapy needles are inserted according to the positioned template grid. Filled brachytherapy needles enter the prostate gland to a determined depth based on the dosimetric volume study. During the retraction of the brachytherapy needles from the patient's body, the needle is slid over a small plunger positioned behind the internally loaded seeds and spacers. *Figure 2.16* illustrates the current method of permanent brachytherapy seed and spacer depositing within the patient.

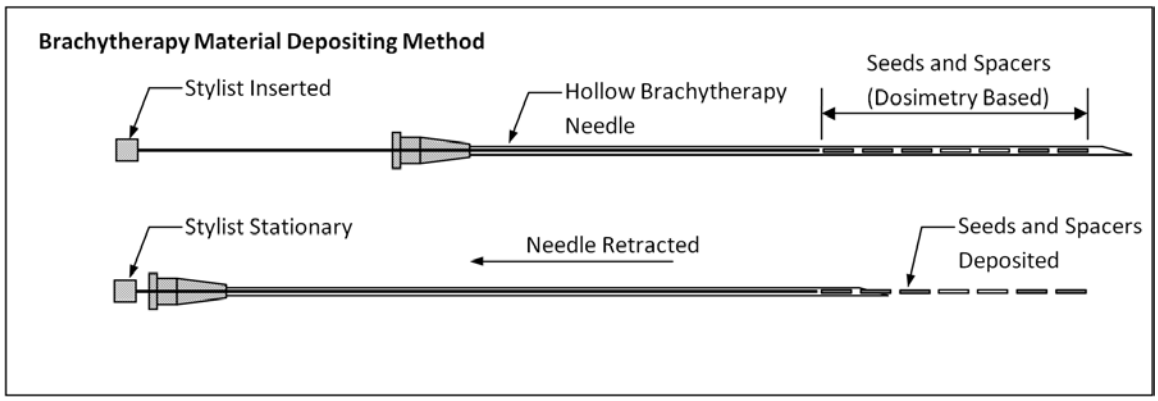

Figure 2.16: Diagram of the current method of depositing both seed and spacer units with the use of modified hypodermic needling devices. Adapted from "Prostate Brachytherapy Made Complicated 3rd Ed.," by Wallner (Ed.), 2008, 6.17. Copyright 2008 by *S*martMedicine Press.

As the hollow needle is retracted, seeds and spacer are kept stationary due to the position of the plunger. The action of the plunger deposits the seeds and spacers along the needle entry path within the prostate allowing the needle to be removed (Wallner (Ed.), 2008). The resulting depositing of seeds and spacers can be seen in *figure 2.17*.

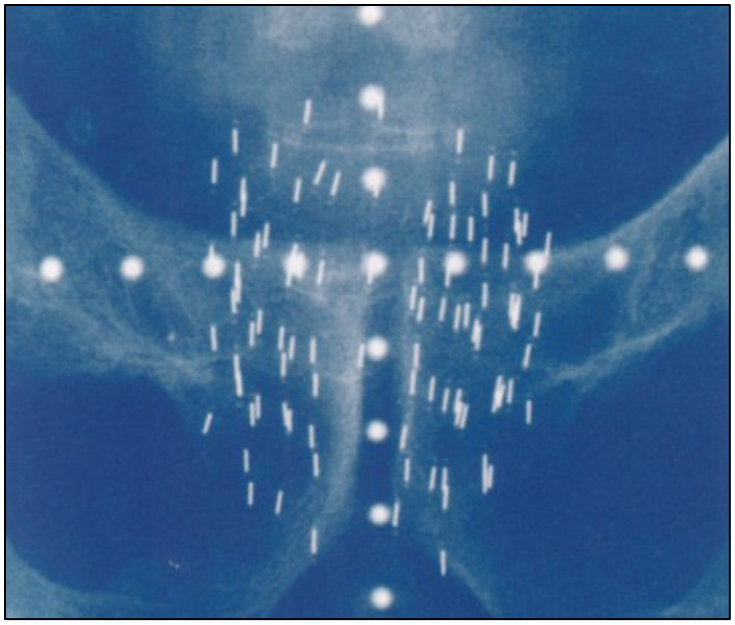

Figure 2.17: Resulting location of Brachytherapy seeds placed within the prostate. Prostate UK (2010). Radiotherapy. Retrieved from: http://www.prostateuk.org/prca/prcatreatinradio.htm

Prostate movement.

While modern prostate brachytherapy strives for highly accurate placement of radioactive material, precision location is complicated by the normal movement of some target cancerous locations within the body and the procedure itself. Specifically, the prostate gland can show a great amount of movement and shape change over time (Beard et. al. 1993). Prostate movement occurs due to various factors. Two of the largest causes of prostate movement are the proximity location of the prostate gland to the bladder and colon (Schild, Casale, and Bellefontaine, 1993). During the course of normal bodily functions, both the bladder and colon fill with bodily waste. The natural actions of the bladder and colon organs position the prostate accordingly within the body. Voiding these organs causes a shift in the location of the prostate. However, in this voided state a relaxation of the pelvic floor is observed (Cook et. al. 1995). A relaxation of the pelvic

floor may cause a sagging effect in the prostate. It is due to this observed sag in the pelvic floor that most brachytherapy procedures are performed with both the colon and bladder filled.

Because of prostate motion over time, current prostate brachytherapy may suffer inaccuracy and complications. Existing research using fiducial markers has shown the prostate to migrate position normally within the body over time further decreasing accuracy when related to time (Cook et. al. 1995). From these factors of prostate movement, it can be concluded that once any amount of time has passed after an initial scan of the prostate, a fixed point of location cannot be exactly reproduced in a future setting. Combined with natural movements, the practice of realigning the patient according to the previously preformed volume study can result in an inaccuracy in brachytherapy seed and spacer placement. As various conditions affect the shape and location of the prostate, it is seen as an ideal course of action to administer the prostate brachytherapy treatment immediately to the patient after the initial scan has been completed, rather than using the traditional method of waiting on the dosimetric diagnosis to be filled and performing the brachytherapy procedure at a later date (Helmig, personal communication, Sept. 2009). The immediate action of seed placement following the initial scanning and dosimetric analysis should allow surgeons the highest degree of accuracy in the prostate brachytherapy process as the shape and position of the prostate gland would be relatively unchanged. More importantly, this immediate loading and placement scenario should allow for an improved impact on the cancerous regions while sparing surrounding tissues thus improving the prostate brachytherapy procedure.

2.4 Current Approaches and Methodologies

Pre-loaded needles.

The loading of brachytherapy seeds within the specially designed hypodermic needles has seen many varied approaches over the years. The current prostate brachytherapy methodology relies on the design of specialty needles in which brachytherapy seeds and spacers are aligned into according to a planed dosimetry proscription that can be seen in *figure 2.18* (Mercereau and Jacobs, 1999). This needling system has been generally adopted by the University of Florida's SHANDS medical center within their permanent implant brachytherapy practices (Helmig, personal communication, Sept. 2010). A survey of current clinical practices in the late 1990's found this method of depositing brachytherapy source materials in around forty-six percent of facilities in the United States (Prestidge, 1998).

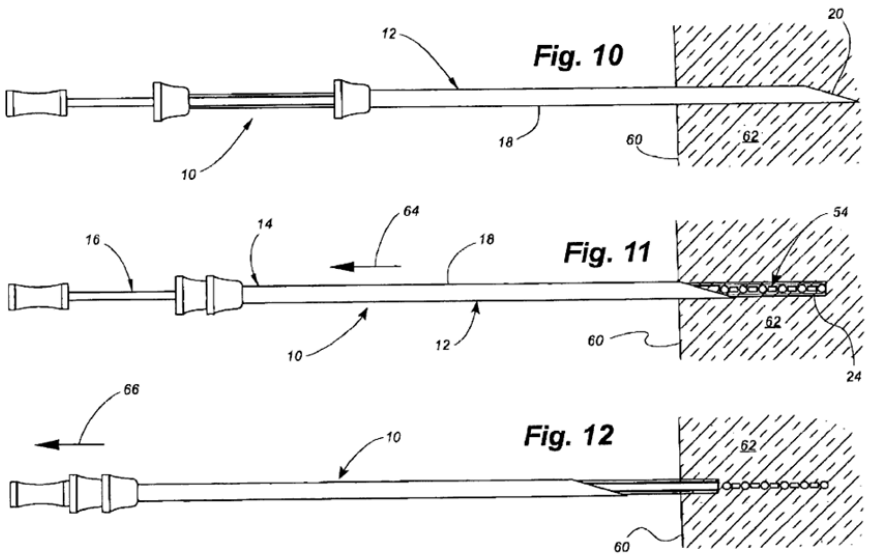

Figure 2.18: Patented design of pre-loaded brachytherapy seed and spacer depositor. Mercereau and Jacobs (1999). *U.S. Patent No. 6,450,937 B1.* Washington, DC: U.S. Patent and Trademark Office.

Commonly found in conjunction with the depositing action of the plunger and stylist brachytherapy needling approach shown in *figure 2.18* is the disposable grid template in *figure 2.19* (Whitmore, Barzell, and Wilson, 2000). The disposable grid template allows for relatively proper positioning of the brachytherapy needling apparatuses as they are injected into the patient's body during normal prostate brachytherapy treatment. Each needling apparatus is filled regarding the bodily positing according to the disposable grid template and the dosimetry plan. Typically this template is positioned within two centimeters of the patient's skin (Wallner (Ed.), 2008).

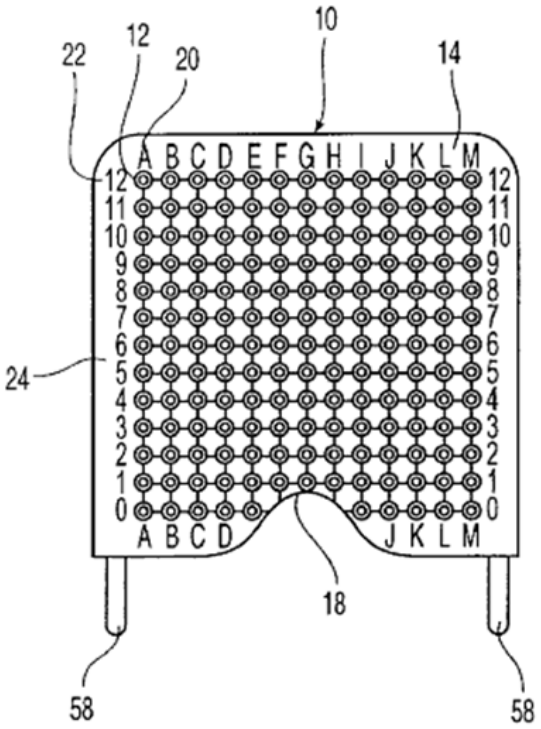

Figure 2.19: Patented design of current brachytherapy disposable grid template. Whitmore, Barzell, and Wilson (2000). *U.S. Patent No. 6,036,632.* Washington, DC: U.S. Patent and Trademark Office.

The Mick® applicator system.

According to Prestidge in 1998, around sixty percent of the medical clinicians practicing LDR prostate brachytherapy in the United States used the Mick® Applicator System (Prestidge, 1998). The Mick® Applicator has been in use within the brachytherapy field since 1972 and has become the standard for automated loading of brachytherapy source materials (Wallner (Ed.), 2008).

Figure 2.20: Currently produced brachytherapy applicator with ability to manually load seeds with aid of hopper attachment. Mick Radio-Nuclear Instruments, Inc. (2009). Mick® 200- TPV Applicator Kit Instructions for Use. Retrieved from: http://www.micknuclear.com/

Seen in the above *figure 2.20*, the Mick® Applicator's design is similar to that of the pre-loaded brachytherapy needles in that both employ a hollow needle and stylist in the depositing of seeds and spacers within the prostate (Mick and Zabrouski, 1999). However the Mick® Applicator utilizes a duel magazine system, in which, seed and spacer elements can be loaded into the hollow needle body. The preloaded hopper design allows those using the Mick® Applicator to manually load seeds and spacers during the actual procedure should a change in the prostate be observed (Wallner (Ed.), 2008). In

the recent past, jamming of the Mick® Applicator has not been uncommon, but can be easily corrected during the LDR brachytherapy treatment process. Jams within early Mick® Applicator devices tended to focus on the spacer elements (DeGinder and Mistry, 1978)

Automated and conceptual systems.

Multiple patents and intellectual properties exist concerning the automated loading of brachytherapy seeds and spacer materials for use in permanent implant brachytherapy (Ellard, 2003) (Green, 2004) (Shi, 2000) (Kan, 1999). Brachytherapy material loading design approaches range from conceptual theory to that of a marketed product. However, none of these design methodologies have replaced the reliability and accuracy of the simple hand loading of the brachytherapy seeds and spacers individually by hand, be it either on or offsite to the cancer treatment facility (Helmig, personal communication, Sept. 2009). Of the current brachytherapy seed loading designs, automated mechanical methods of separation and loading through the use of preloaded cartridges, as in the Mick® Applicator, are the most common (Green, 2004). At the time of this publication, no marketed product uses a fully automated non-invasive type of separation and loading when dealing with brachytherapy seed and spacer orientation and placement according to a preset dosometric pattern. All current products use either a human interface or direct mechanical interface with the brachytherapy seeds and spacers. Due to the current mechanical interface between loading system and material, this provides an area of improvement over the current market methodology. Mechanical parts entail the use of moving parts within a constructed design, parts that can damage or deform materials (Helmig, personal communication, Sept. 2010). A United States

patented design illustrating loading of brachytherapy seed and spacers can be seen in *figure 2.21* (Green, 2004).

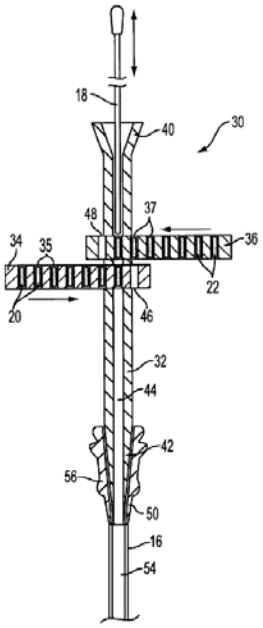

Figure 2.21: Patented design for a manual cartridge-based brachytherapy seed and spacer loading device. Green (2004). *U.S. Patent No. 2004/0162458 A1*. Washington, DC: U.S. Patent and Trademark Office.

The design illustrated in *figure 2.16* represents a common design approach when tackling the issue of automated loading of brachytherapy material. This design provides a direct method of insertion of both brachytherapy seeds and spacer elements into the brachytherapy needle by simply placing the seeds and spacers in the path of the existing plunger. Providing the plunger is depressed, the positioned seed or spacer is forced into the body of the needle. Two positioned cartridges provide the device the ability to quickly position a new seed or spacer when the plunger is depressed. Various patented systems have been designed around this plunger insertion method, including the Mick® Applicator (Wallner (Ed.), 2008). Other related intellectual properties involve the use of magazines or preloaded material loading mechanisms (Kala, Bossi, and Cutrer, 2003)

(White and Carr, 2005). This method requires both radioactive seeds and spacers be preloaded within the cartridge-like housings before the scheduled LDR brachytherapy process. In preloading the seeds and spacers, surgeons using the device in the brachytherapy procedure must either pre load multiple cartridges or halt the procedure to load more into the used cartridges. According to an interview with medical professionals, the act of loading the seed or spacer from a cartridge to the actual working device can risk jamming the device by physically deforming the shape of the source material (Helmig, Mitchell, and Lu, personal communication, March 2010). Once altered, the seed or spacer may prove challenging to maneuver within the brachytherapy needle or applicator resulting in a jam. A jam of an automated seed and spacer delivery system could cause catastrophe if employed in an on demand loading procedure.

Aside from the popular design choice of pre-loaded magazine feeding methods, most other related brachytherapy material loading designs are based on assisted manual loading. *Figure 2.22,* shows a United States patented design based upon a gravity feeding action in which brachytherapy seeds and spacers are manually loaded into the underlying brachytherapy needles through human manipulation with an additional stylist (Ellard, 2003). While this design initially uses the non-mechanical interface of gravity to theoretically feed both seeds and spacers into a working environment; a human component is then needed to maneuver individual materials into the awaiting needle. This design shares much with various other intellectual properties in the methodology of simply adding to the industry standard vacuum assisted stylist as discussed in Chapter I.

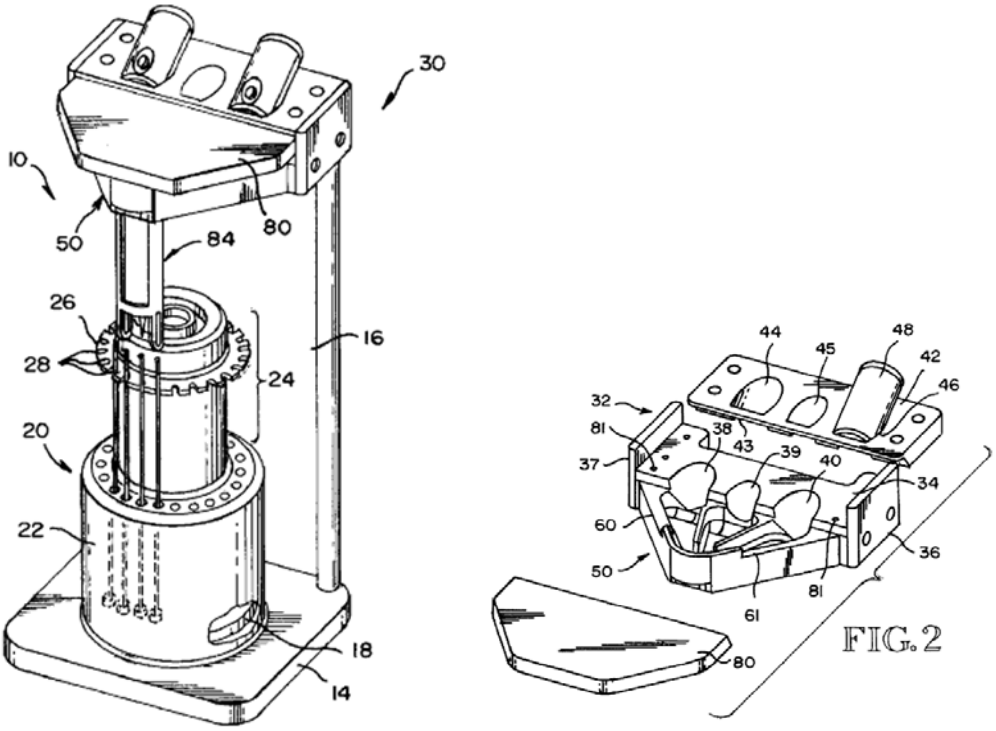

Figure 2.22: Patented design for a manual funnel feeding action brachytherapy seed and spacer loading device. Ellard (2003). *U.S. Patent No. 6,582,354 B2.* Washington, DC: U.S. Patent and Trademark Office.

These systems in development that utilize vacuum-based design features in the loading of brachytherapy seeds are again as numerous as mechanical magazine feeding approaches. These vacuum based devices show promising characteristics, yet as with their mechanical interaction based counterparts, they lack certain factors needed for real-time loading during a medical brachytherapy procedure. In *figure 2.23*, the device shown uses a vacuum force to transfer seeds from a reservoir section to the main work environment (Shi, 2000). The system is unique in the fact that the stylist has been elongated from the normal configuration to allow for multiple seeds and spacers to be gathered within the stylist before manually deposited into the awaiting brachytherapy

needle. While this system employees a vacuum system, the hand loading of brachytherapy needles still requires the use of a human operator.

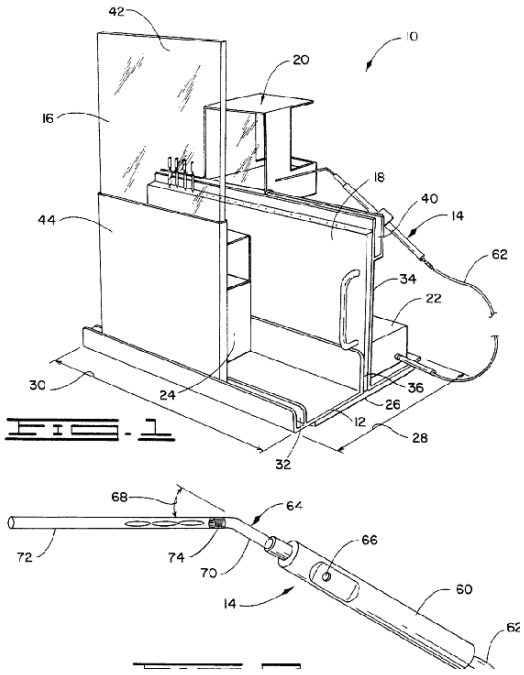

Figure 2.23: Patented design for a vacuum assisted loading station for brachytherapy needles. Shi (2000). *U.S. Patent No. 6,113,529.* Washington, DC: U.S. Patent and Trademark Office.

The intellectual property illustrated in *figure 2.24* shows another use of vacuum force in the manual loading of brachytherapy seeds comparable to the approach shown in *figure 2.15*. The system uses relatively the same process as the current manual hand loading approach with the use of a vacuum based hand tool. An improvement over the more traditional hand loading approach can be noted in the sealed enclosure of the system. Sealing the enclosure provides a level of protection to those loading the brachytherapy seeds. However, this design is far from efficient as manual dexterity is required to nimbly maneuver seeds into the awaiting needle. This process, as with others

human-based operator systems, does not provide the speed necessary to adequately provide service to surgeons during the brachytherapy process.

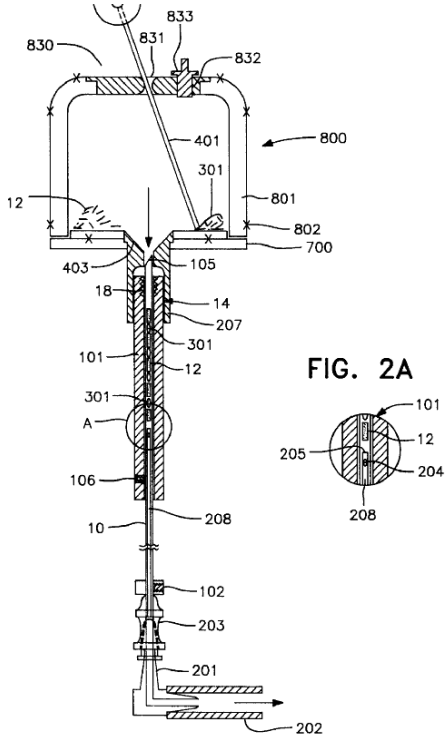

Figure 2.24: Patented design for an enclosed vacuum assisted loading station for brachytherapy needles. Kan (1999). *U.S. Patent No. 5,906,574.* Washington, DC: U.S. Patent and Trademark Office.

CHAPTER 3: METHODOLOGY

The following, Chapter III Methodology, includes work performed in the conceptualization, implementation, and characterization of the constructed non-mechanical brachytherapy element loading system. Within this chapter, the initial design constraints, performed pilot study, and fabrication appear earliest. This has been sectioned to give the reader perspective on the actual statistical testing performed regarding the reliability and characterization testing performed on the completed device. Outcomes and observations from tests described within this chapter will be further explained in the subsequent Chapter IV Results.

3.1 Experimental Design

The goal of this research was to create and test an automated system for the loading of brachytherapy elements intended for use within a cancer treatment facility utilizing no mechanical interaction with elements. In this application, the device needed the ability to interpret a set dosimetry plan, execute the plan through the loading of elements to the dosimetry pattern, and discern if the task was accomplished successfully. To tackle these set conditions, various steps were required. The first of these steps was the visualization of a design concept. The applied conceptual approach of the researcher to this process can be seen in *figure 3.1.*

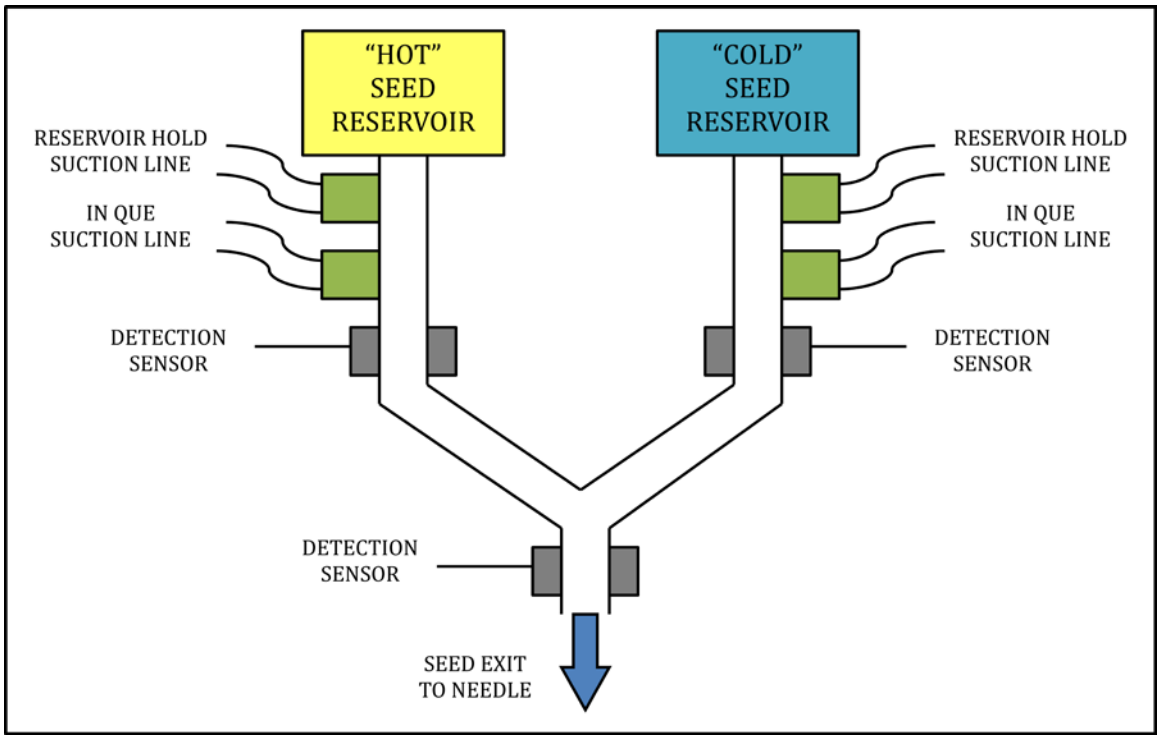

Figure 3.1: Proposed negative air pressure control method for dual loading of automated system.

The initial proposed device operation consisted of two removable element reservoirs, a vacuum pressure based seed depositing section, a rotary needle carrousel, and computer based control system. This system would be able to provide immediate loading of both radioactive and non radioactive seeds based on electronic-based output from the clinical diagnosis created from the dosimetric volume study. The chosen method of data export from the volume study would then be imported into the system. The rapid loading action of the proposed device will, in theory, eliminate any prostate movement associated with time increasing the accuracy of the prostate brachytherapy procedure. The method of interfacing with the loading elements using only air pressures has been chosen within this design for various reasons. The first reason of using air pressures for loading the brachytherapy elements has been the tendency of system failure in previous

mechanically driven brachytherapy loading systems (Helmig, personal communication, August 2009). Talks with medical professionals at the SHANDS University of Florida cancer treatment facility have revealed the current mechanical brachytherapy loading systems show tendency to jam or damage brachytherapy seeds and spacers during automated deployment. Additionally, the use of mechanical seed loading systems could introduce lubricants and other factors in the operating room environment. An air pressure based system provides a non-mechanical interaction method of controlling the seeds within the system. Air pressure based devices are commonly used throughout various medical practices and find easy acceptance into a hospital-like setting. The proposed device utilizes this air pressure feature by allowing brachytherapy elements from the reservoirs into the needle using various negative pressures. Brachytherapy elements exiting from the dual reservoirs are to be held in place by the first air pressure stations. These lines have been placed to allow only one element at a time to be positioned in the "in que" pressure position. Varying this "in que" position will allow the system to deposit a single element into the positioned brachytherapy needle. Detection sensors are to be placed accordingly along the brachytherapy element travel lines to allow the system to register and verify the loading sequence of the seeds from both the radioactive "hot" seed reservoir and the non radioactive "cold" seed reservoir. The computer based logic system will then use these inputs to determine the resulting seed configuration in the positioned brachytherapy needle. Once a needle has been filled per the required diagnosis by the proposed system, a carousel section will position the filled needle to allow for access by the operator. Positioning the needle in such a manor will also show the operators the condition of the needle in question by displaying an indication of the radioactive and non

radioactive seed positions within the needle. This is needed to insure the correct needle will be used. After placing this filled needle in position, an empty needle will need to be fed into position under the loading section of the device. Interchanging the filled needle with the empty needle will allow for filling during the implantation of the previously needle into the patient. Both speed and accuracy of this device will be tested to determine feasibility and reliability of the system in a clinical setting. The proposed design will be tested by passing both brachytherapy seeds and spacers through the system based on a preset randomized dosage pattern. The resulting values of the randomized dosage pattern and actual loading configuration will then be compared. Differences in speed and accuracy will be analyzed. It is the hope that the testing from this work will form a reliability background for this device. The results from this research will advance the overall knowledge in brachytherapy implementation and medical device implementation within the sphere of prostate brachytherapy.

3.2 Equipment and Materials Used

In this work brachytherapy elements were supplied by SHANDS hospital. Included within these materials were dummy seeds along with two spacer element types, one violet one white. Inspection of these elements under magnification revealed various shape differences attributed to manufacturing processes. Under magnification a number of dummy seed elements were noted to posses irregularities in the welded ends. These irregularities tended to form ends that were misaligned to the seed body in construction. As stated in Chapter II of this work, the spacer elements tended to show an edge deformation or “burr” located on the top and bottom faces deemed consistent that of an extrusion manufacturing process (Hammer, Hawliczek, Kärcher, and Riccabona, 1989).

Under magnification it was determined that both types of spacer elements received from SHANDS hospital did posses such edge deformation. Compared, it was determined that of the two provided spacer types, the violet spacer elements possessed less drastic edge deformation. From this initial visual observation, violet spacers were chosen as the more preferred option due to the detrimental effects of any element deformation on the loading of elements within the conceptual design. All three element types were tested throughout this work.

3.2 Pilot Study: Miniature Test Apparatuses

To account for features and design decisions present in the final iteration brachytherapy seed loading system, a pilot study was first conducted were concepts were first tested through the use of various Miniature Testing Apparatuses (MTA). MTAs were machined pieces constructed to represent conditions present in the final constructed device. A formative approach was taken in regards to the use of MTAs within this work, as these MTAs were tested to verify design choices and usability within the overall system before construction of the main device was undertaken. The MTAs varied in functionality, allowing for observation and experimentation of problem areas that could have arose within the overall complete system. Observational data from the MTA rigs were collected throughout the design development process. Subsequently, the finalized completed brachytherapy seed loading system was the combined genesis of results gathered from the pilot study MTA rigs to improve overall design functionality. In the use of MTAs, no automated systems were utilized. Rather, controls of various features were controlled by the researcher to simulate an automated process.

Within the construction and implementation of these MTAs the following steps were employed:

1. Potential Problem Area Identified
2. Probable Factors Impacting Element Travel in Problem Area Identified
3. Conceptual Designs Created
4. 3D Parametric Models Created
5. CNC Subtractive Machining Performed
6. Assembly of MTA
7. Testing and Observations

All MTAs were constructed from a polymer material – methyl methacrylate, also known as acrylic. The design decision to use acrylic material for MTA fabrication was due mainly to the material's optical clarity and ease of machining. Within the testing and troubleshooting of both the finalized loading system and MTAs, it was deemed vital by the researcher to allow for visual inspection of element travel and possible jams within the system. In a clinical atmosphere, the use of acrylic would also allow for surgeons to immediately determine the location of a problem within the system should one occur. CNC machining was performed utilizing tooling and equipment at Western Carolina University (WCU), as seen in *figure 3.2*.

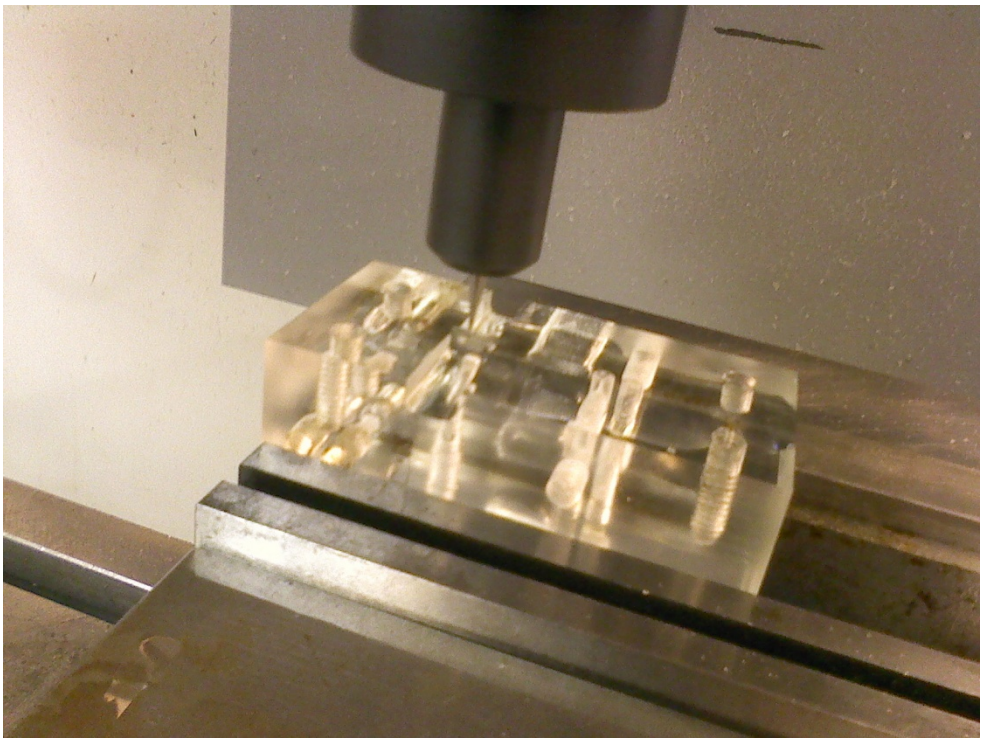

Figure 3.2: Photograph of subtractive CNC machining practices employed in manufacturing of all MTAs within this work.

MTA: initial two-part testing.

The purpose of pilot study MTAs were to observe the characteristics of brachytherapy seed and spacer travel through a machined groove in the selected acrylic material. Geometry of the machined travel channel was varied throughout initial tests to determine the optimum characteristics to impart into the final constructed system. Using basic tooling, channels in the shape of a square, half circle, and full circle were machined into blocks of acrylic seen in *figure 3.3*. All designs consisted of fastening two acrylic blocks together to form the desired channel geometry as shown in *figure 3.4.*

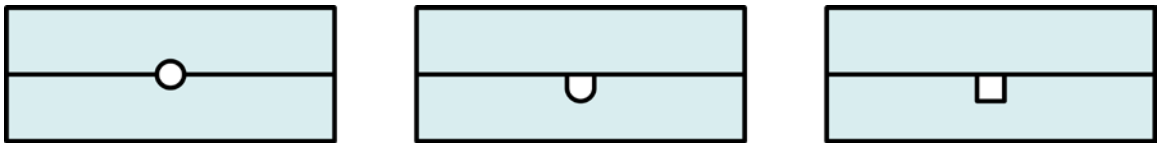

Figure 3.3: Diagrams of intended geometry in initial MTAs. Full circle geometry channel (left) half circle geometry (center) and square geometry (right).

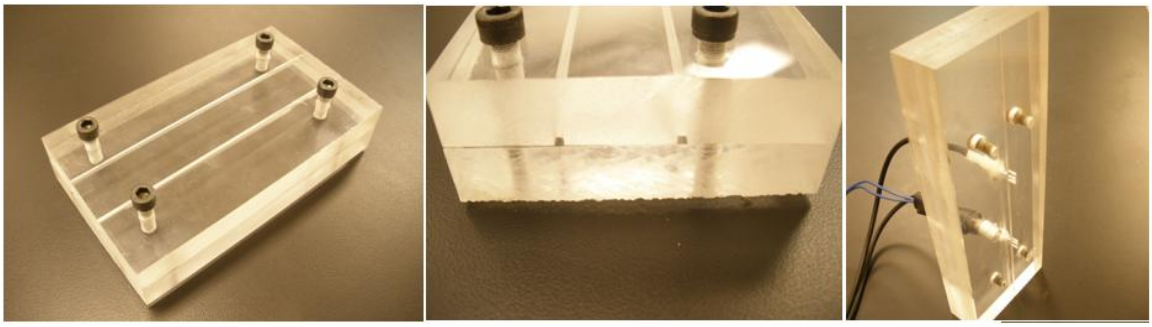

Figure 3.4: Photographs of initial two-part testing apparatuses. Square and half circle geometry channels (left and center) with full circle geometry channel (right).

These initial MTAs were machined as two sections due to the general physical tooling constraint. Factory polished edge was left intact were possible to impart the best possible finish and lessen geometry variation. Within these MTAs, it was attempted to pass seed and spacer elements through the various geometry channels and observe the impact the various geometries would have on element travel. This initial testing was performed with no intention of collecting numerical data. Rather, only initial observation data was gathered. As the geometry aspect was the main focus of these initial MTAs, external factors such as vibration and air pressure were not employed until later dates within this work. Observations from these tests found potentially the largest issues with the intended loading design, the factor of friction and apparent bonding of elements to the channel walls by the elements. As elements attempted to begin travel through the MTAs

from a stationary or static position, Coulomb's theory of dry friction could have been applied as follows.

$$F \leq F_{max} = \mu_s N \tag{3.1}$$

Where under static conditions, F is the force exerted upon an object based on the mass and area of the object and F_{max} is the maximum amount of force possible before static equilibrium is broken and the object in question experiences movement. μ_s denotes the coefficient of static friction expressed between the two contacting materials. In the context of this work, μ_s is related to acrylic and titanium materials. Finally, N represents the normal force applied to the object. However, due to multiple factors both accounted and unaccounted for in the travel of elements through machined acrylic channels, it was deemed impractical by the researcher to attempt measurements and subsequent friction calculations within this work. Seen below is a preliminary list of possible factors associated with element friction within the constructed MTAs.

- Geometry of Machined Channel
- Material Finish within Channel
- Angle of Element Decent within Channel
- Weight of Element
- Surface Area of Element
- Point(s) of Seed to Channel Contact

This bonding due to friction of the machined acrylic surfaces proved to be troublesome when attempting to move elements through the channels using the forces of

vibration and gravity. Particularly, channels machined with circular geometries, such as the MTAs with full and half circle geometries, allowed for the highest amount of surface area contact to the machined acrylic surface. Specifically, jams within the machined channels were commonly observed during initial trial runs and very few elements were successfully passed through the MTAs. Polishing of the machined channels proved to elevate this issue somewhat, but did not remove this issue satisfactorily. Acrylic surface finish on non-machined surfaces was found to have the least friction bond reaction on element travel.

Additional testing observations found using these initial MTAs were found when vacuum was applied to create a “capture area”. In this capture area, it was attempted to bring elements to a stationary position through application of vacuum pressure. Once the element in question arrived at the capture area, the vacuum pressure would overcome the force of gravity propelling the element down the machined channel. This capture area would allow for elements to be dropped into the system at will providing a non-mechanical form of interaction. To create the capture area, vacuum lines were machined into the acrylic blocks to connect with the machined channels. In this, upon activation of the vacuum line the falling seed or spacer would be pulled against the side wall of the machined channel and captured at the vacuum line location. Observations from these tests showed a tendency of the seed or spacer to be captured at the desired location at great regularity within the MTAs should the seed or spacer be pulled against a circular geometry of the milled channel such as the full or half circle geometries. Elements travelling through machined channel with square geometry tended to bypass the capture area location and continue travel out of the MTA. This phenomenon was attributed to the

circular geometry allowing for a better seal between the element and the vacuum line machined into the channel.

MTA: initial one-part testing.

Focusing only on the capturing of a seed or spacer using vacuum pressure, these MTAs were machined from single pieces of material. Common tooling and machinist practices were employed in the machining processes as well. Channels for element travel used drilling operations in the machining of the MTAs. As such, only fully circular drilled channels were feasible considering the miniature size of the seed and spacer elements as seen in *figure 3.5.*

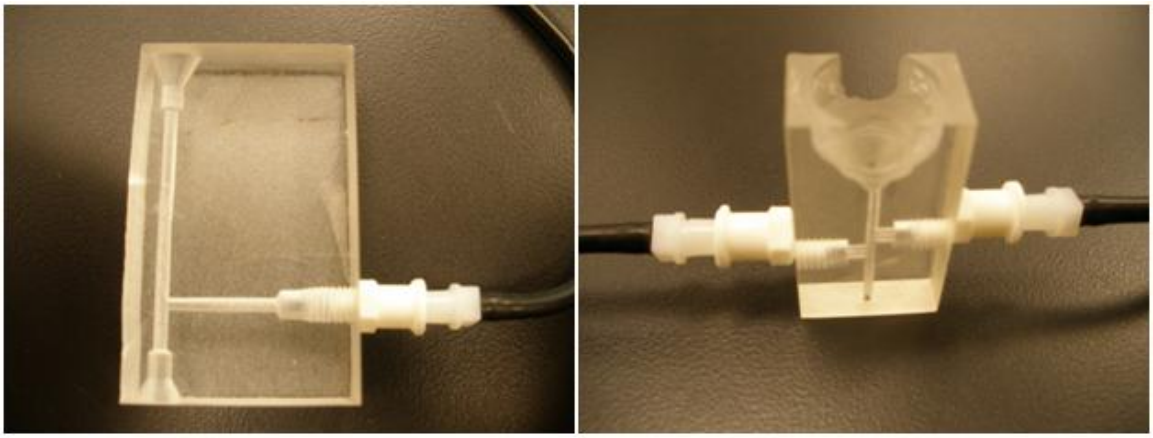

Figure 3.5: Photographs of initial one-part testing apparatuses. Single-in vacuum line (left) triple-inlet vacuum line (right).

As with the previous MTAs, no numerical results were gathered while only observational results were noted. The first version of the single-piece MTA was machined with a singular capture area inlet connected to the drilled channel. During the free fall of the seed or spacer, the activated vacuum line presented no observed problems in capturing the selected element. However, the vacuum line inlet into the drilled channel

proved to be too large and elements were observed migrating into the vacuum line rather than continuing normal travel out of the MTA through the drilled channel. In addition to the vacuum line size, the drilling machine cycle used to fabricate the drilled channel resulted in a much poorer surface finish than was attained during machining of the initial two-part MTAs. The resulting poor surface finish proved problematic in seed and spacer travel and resulted in irregular passage through the initial one-part MTA. Jamming of the elements within the apparatus was common. Spacer elements were especially prone to jam within the MTA due to their sharp edges and edge deformation created from their own mass manufacturing process.

In an attempt to remedy the surface finish problem and explore additional capture line designs, an additional MTA was machined using a single block of acrylic. In this MTA, two capture areas were included within the design in the attempt to release single elements out of the system when presented with a stacked amount of elements. The vacuum inlets to the capture areas were separated from one single line into the drilled channel into three lines to prevent migration into the vacuum lines. These capture areas were positioned in a staggered formation to allow a "hand-off" of a single element from the first to the second capture area preventing all others stacked behind the selected element from entering the remainder of the system as seen in *figure 3.6*.

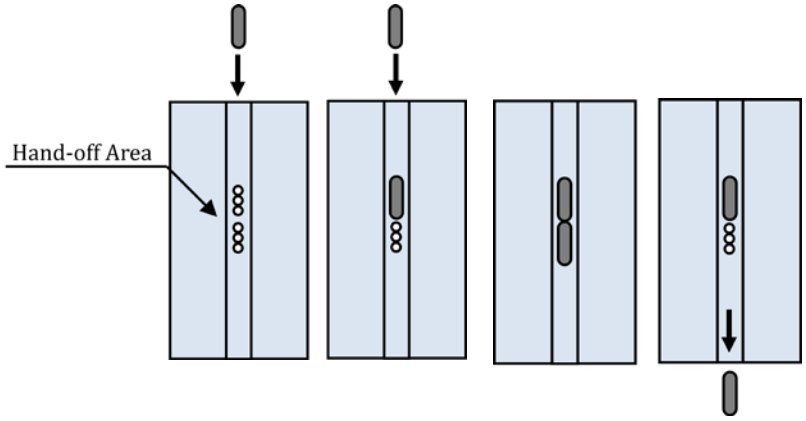

Figure 3.6: Illustration of sequential actions in "hand-off" method.

Surface finish of the drilled channel was improved with a variation in machining process and application of lubricant. The improvement in surface finish found on this new MTA was observed to be still unsatisfactory when compared to observation results from previously explored two-part MTA designs. Jamming of elements was still observed during testing of this MTA. However, it was found that testing of the "hand-off" positioning of the capture areas showed promise within this MTA. Elements were successfully passed from the first to second capture area without incident when passing single elements through the system. This observation changed however with the addition of multiple elements within the system. It was observed that when multiple elements were loaded into the MTA, the leading element was captured at the first capture area and held all others behind it stationary. As both vacuum lines were activated on either capture area, once the first capture area's vacuum was disconnected, all elements shifted down the drilled channel until the leading element was captured by the second capture area. After the capture of the leading element by the second capture area, the previously deactivated vacuum line was reactivated in an attempt to separate the trailing elements

from the leading element. In this position, the leading element was captured by the second capture area while the second element in line was captured by the first capture area preventing all sequential trailing elements stationary. Upon deactivation of the second vacuum line, it was hoped that the leading element would exit the MTA using the force of gravity while all other elements would be kept stationary by the first capture area. Observations from this cycling of vacuum lines showed the leading element not exiting the system upon completion of the actions as intended and deactivation of the second vacuum line. Rather, the leading element was observed to either be kept in place through neighboring vacuum pressure from the first capture area, or in some cases was even pulled back into position with the first capture area forcing all trailing elements to move upwards.

MTA: "hand off" testing.

Attempting to explore the phenomenon observed in the second one-piece MTA of leading element failure to exit the system in the "hand off" design, an additional MTA was constructed. In this design, a two-piece construction was employed as results of previous surface finish observations made of more favorable results in two-piece construction than one-piece construction using common machining practices. Two capture areas were machined to allow for the previously described "hand off" motion to occur within the MTA. These capture areas employed the previously explored triple vacuum line per area to prevent element migration into the vacuum lines. The geometry of the semi circle was chosen for the testing apparatus as during observations of the initial two-piece MTAs, this design allowed for greatest seal in capture areas due to circular geometry.

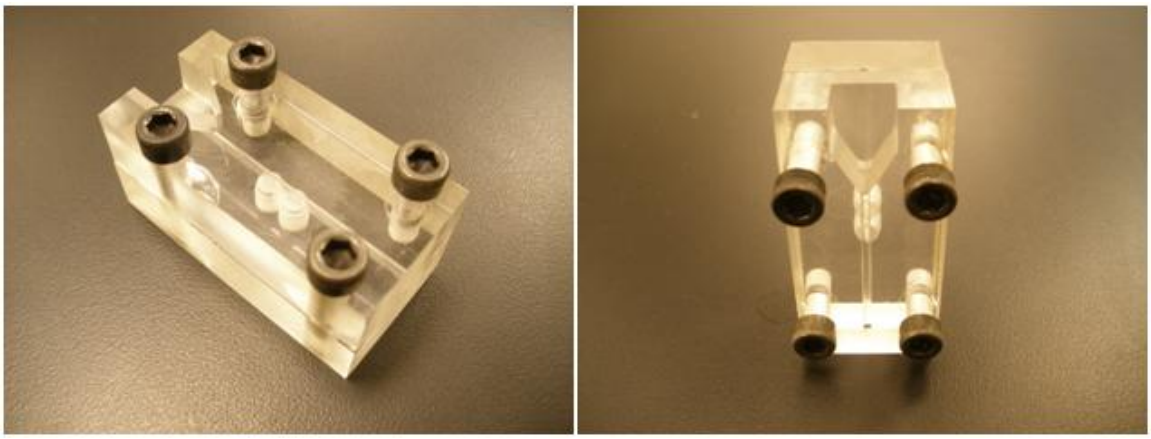

Figure 3.7: Photographs of two-piece testing apparatus employing "hand-off" method.

In the testing of this MTA, it was observed that the neighboring vacuum lines again prevented the initial element from exiting the system due to neighboring vacuum pressure. As with the previously explored single-piece MTA "hand off" design, the initial element was either fixed in place around the second capture area or pulled back into line of the initial capture area displacing the trailing elements. No successful testing of multiple seeds and/or spacers from this apparatus was observed, however the passing of single elements through the MTA proved an observed repeatable success.

MTA: vent, angle, and vibration application.

To account for the observed neighboring vacuum pressure recapturing a released element found in the previously constructed MTAs, a vent was added to the design between the capture areas. This vent was positioned between the first and second vacuum lines to allow for neighboring vacuum pressures to be only relevant to elements positioned directly adjacent to the vacuum line inlets. In this configuration, the vent would disallow vacuum pressure from the first capture area from reaching elements released from the second capture area. Additional features placed in this MTA were the inclusion of both a small vibration motor and variable angle adjustment gauge.

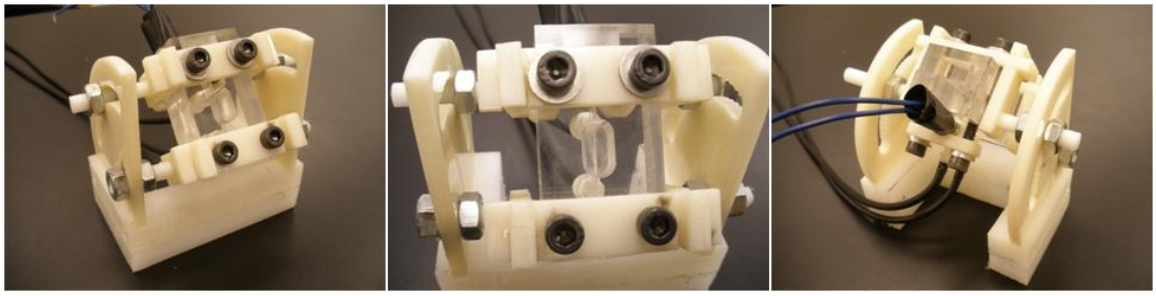

Figure 3.8: Photographs of two-piece testing apparatus including vent, angle, and vibration.

Observations from this MTA proved promising as seed and spacer elements were successfully transferred between the two capture areas with the initial element not impacted by neighboring vacuum pressures. Elements were observed to be successfully passed through the system using this design. It was in this testing apparatus that the design intent of the “hand-off” method was finally realized. However, within this MTA it was found that elements tended to overlap each other when stacked within the milled channel. In this overlapping, the seed and spacer elements were found to stop travel and form a jam in which the system could no longer load elements into the system properly. The MTA was observed to only pass one element at any interval successfully due to a design error in channel width. Additional observations found relating to the “hand-off” method was the tendency of elements to be recaptured by the second capture area providing the element had not exited the system. This was accounted to the machined vent placement on the area between the capture areas alone. Other observations from MTA testing of angle variation and vibration illustrated a large role of gravity in the current design. As angle was decreased, the impact of gravity was observed to less on the elements and thus speed of element travel through the milled channel was drastically

reduced. However, as the angle of element decent was increase the opposite effect of gravity was observed as speed of the elements was increased. This was a favorable observation, but in this some elements traveled too quickly and were not captured by vacuum pressure. Vibration was observed to assist the travel of the elements at lower angles through prevention of friction bonding with the milled section of the channel.

MTA: refined capture area.

Building off of the observations from the previously constructed MTA, the design of the capture area was further explored. In this MTA, the capture sections were placed at increased distance from one another to limit neighboring vacuum pressure interference. To counteract the issue of recapture by the second capture area upon release, the machined vent was extended to cover the capture areas entirely. Vibration location was also moved in an attempt to provide a larger impact to the element travel through the system and decrease the tendency of elements to not release from the capture areas once vacuum was disengaged. In this, the vibration motor was positioned between the two capture sections to impart the greatest effect on the MTA. The milled channel was also reduced in an attempt to prevent elements from overlapping one another jamming the system. Addressing the observed result of inadequate vacuum pressure at high travel angle, the previously implemented design feature of three machined inlets per vacuum line was changed to a shaped groove just under the size of the elements.

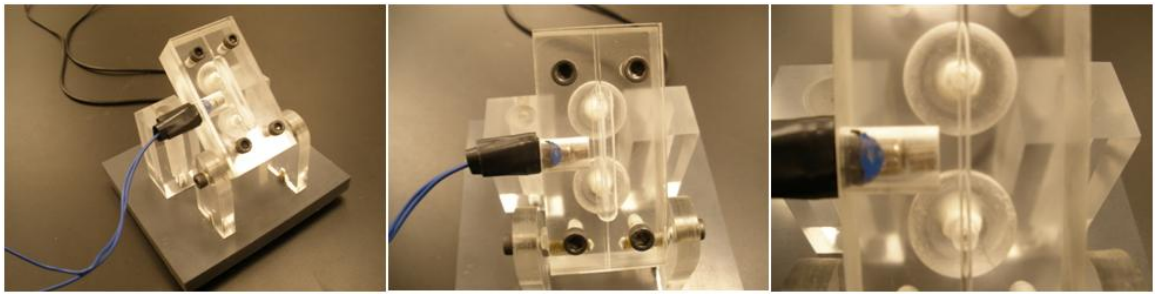

Figure 3.9: Photographs of refined two-piece testing apparatus including vent, angle, and vibration.

Observations from passing elements through this refined “hand-off” MTA proved majorly unsuccessful as the changes implemented into this MTA showed detrimental improvement compared to the previous MTA on most all issues addressed. Due to the increase in distance between the capture areas, elements were forced to free fall between vacuum lines. This produces a tendency for elements to stop mid travel between the capture areas. The new placement of the vibration motor at this location was thought to alleviate the issue somewhat. However, elements continued to jam at this problem area. The previous issue of element recapture by the second capture area was found to be completely resolved with the extension of the machined vent. Within the observed testing of this MTA, one of the only positive changes found was in the vacuum line inlet design. As the design change replaced the previously implemented three line inlet with a higher volume single profiled inlet, vacuum pressure was increased and the system was able to capture elements at higher angles of decent. Finally, due to the decrease in the machined channel width, seed elements were no longer observed overlapping one another. Overlapping with elements was still observed with spacer elements and was further reduced during design and manufacturing of the following MTA.

MTA: “light gate” and positive air addition testing.

All MTAs until this point in the pilot testing have relied solely on the premise of force applied by gravity to feed the elements downward. This was observed as an ineffective weak link in the overall system design. Reliance upon the force of gravity subjected the system to long wait times between capture areas and element exit from the system while allowing elements to friction bond with the machined channel. In an attempt to gain more repeatability and reliability from the system, the concept of positive air pressure was introduced into this final MTA. The initial thought behind this addition was to provide an assist to the unsatisfactory force of gravity on element travel through the system. Two air inlets were machined into the MTA to interact with the central machined channel between the first and second capture areas or “hand-off” section. Positioning the air inlets at this point nullified the observed reactions of both recapture by a previous vacuum line and element jams at the point of vacuum line deactivation. Air inlets were placed at 45° intersection with the central machined channel to direct air pressure downwards into the system and prevent interaction above the selected area. Two air inlets were machined into the MTA to determine optimum placement for the final constructed device. As the design change of the capture areas in the previous MTA was undesirable, they were reset back to original locations.

A unique addition to this MTA was the introduction of a “light gate” sensor, a diagram of which can be seen in *figure 3.10*. This constructed sensor contained duel housings separated by distance from one another. Mounted within one of these housings, a high intensity LED was used to project a beam of light roughly the same shape as a brachytherapy element across the distance between the fixed position housings. Within

the remaining housing, a photoelectric resistor was mounted in line with the high intensity LED. This second housing was also shaped to allow the projected beam of light to shine on the mounted photoelectric resistor. The shaped inlet of this second housing was also roughly in the same shape as that of a brachytherapy element, but was increased to allow for scattering of light to the photoelectric resistor. This light gate sensor was placed to allow the machined channel to rest between the duel housings. In this application, the light detected by the photoelectric resistor would change depending on the object between the housings. This change in light present was directly parallel to the resistance value measured on the photoelectric resistor imparting to the system a method to identify various elements. This light gate was added to the MTA along with an additional vacuum line to allow for a third capture section at the sensor itself. By capturing an element at this location, the light gate would be able to determine element type based on photoelectric resistor shadow.

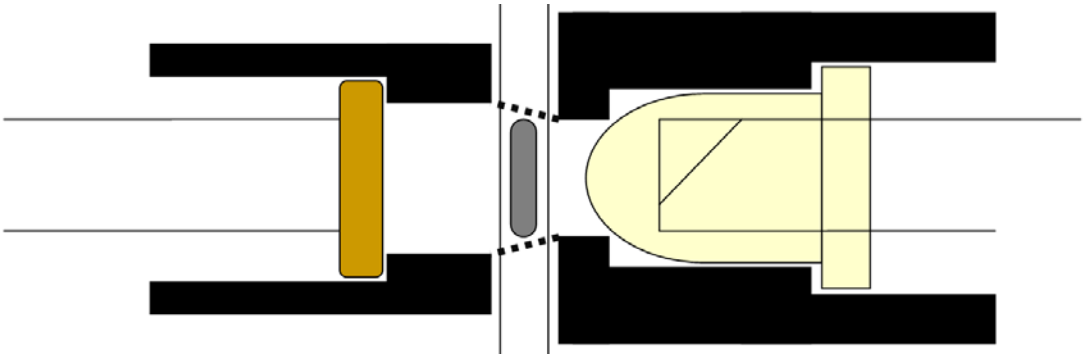

Figure 3.10: Generalized illustration of “light gate” functionality. Photoelectric resistor (left) and high intensity LED (right) work in conjunction to detect the presence and type of material passed between them.

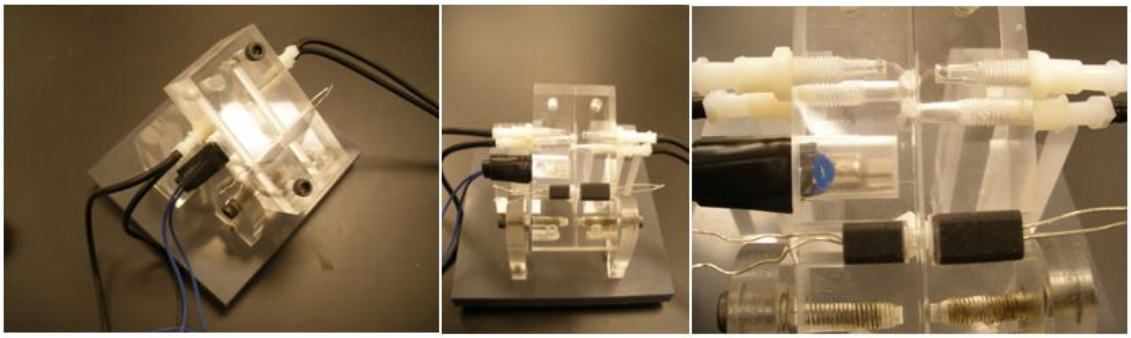

Figure 3.11: Photographs of two-piece testing apparatus including "light gate" sensors and positive air pressure design additions.

In this constructed fashion, elements were observed to successfully pass between all capture areas as intended. Inclusion of air pressure within the design served to eliminate the recapture of the elements by the initial vacuum line and achieved the desired "hand-off" from the hopper to the remainder of the system. Speed of the element travel through the machined channel was also improved as elements no longer relied solely on the force of gravity to exit the system. This air assist to gravity was also observed to reduce the impact of both vibration and angle of element decent in the system. With the introduction of the light gate sensor into the MTA, observations were also made as to changes in measured resistance generated by the sensor due to presence of various elements. Resistance in this instance was measured as an association to voltage employing Ohm's law within this basic electrical circuit. Ohm's law states $I = V/R$, where I represents current, or amperage, flowing through the constructed circuit and V symbolizes voltage with R corresponding to resistance. In this fashion, any variation in resistance due to change in light would correspond to a measurable change in voltage within the circuit. A high amount of success was found with this sensor as a discernable

difference was ascertained in the element type through resulting resistance of the light gate sensor based on shadow present.

Overlapping of elements through normal operation had been observed in all MTAs in some facet until this unit. It was found that should an overlap of elements occur within operation, it would require complete disconnection of the duel connected machined acrylic pieces to clear the jammed area. This condition was seen by the researcher to be catastrophic if occurring during a normal LDR brachytherapy treatment. Due to a change in channel width however, elements were no longer observed to jam by overlapping within this MTA. The finalized diameter of the machined channel was set to 0.05” following this observation. Other jam conditions in normal operation of this final MTA were uncommon, but present. Within this MTA it was observed that any jammed seed element due to the relationship with channel friction was quickly solved through the application of higher air pressures to the system. Spacer elements had a higher tendency to jam due to channel friction within the system. This observation was mostly attributed to the manufacturing processes of each element resulting in a non-rounded shape of the spacer elements in comparison to the seed element circular ends. When observed under the condition of a jam due to friction, spacer elements required higher air pressure assistance to be moved.

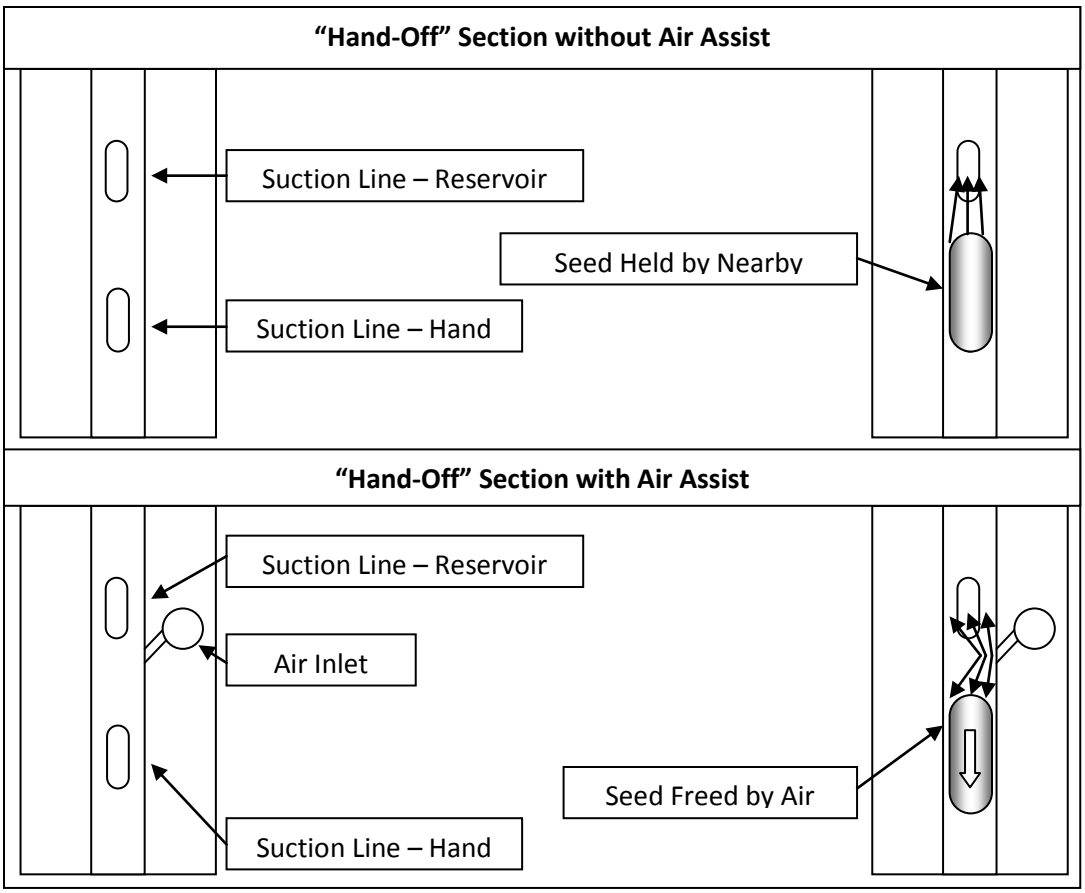

Figure 3.12: Illustration of addition of air inlet in "hand-off" section of device.

Additional testing on this MTA concerning the speed and reliability of element travel, especially concerning the lighter spacer elements, was also explored. To reduce possible impact of friction applied to the elements during travel, the orientation of the two-plate design was flipped. In this change, the machined channel was placed above the vent as seen in *figure 3.13* allowing the traveling elements to impact the flat surface of the channel.

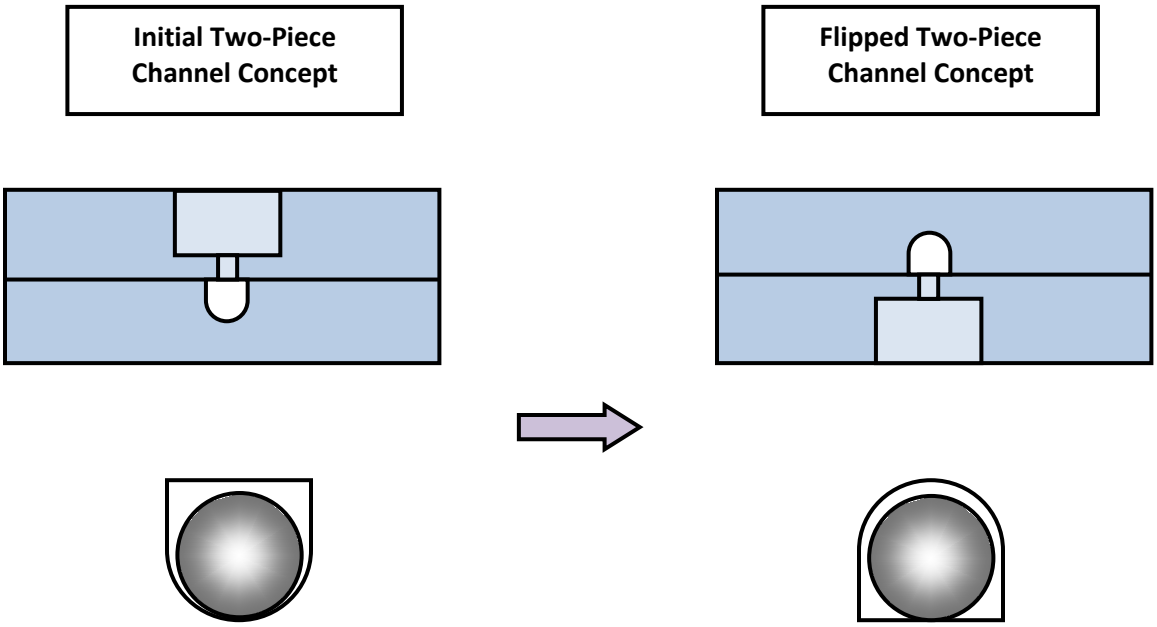

Figure 3.13: Illustration of two-plate design with plate orientation flipped to reduce friction during element travel.

In this new orientation, vacuum lines were reoriented as well causing captured elements to be vacuumed to the curved channel roof. As the curved geometry tended to give a better vacuum seal during element capture, this effect was deemed by the researcher to be satisfactory as element capture was seemingly unaffected by this orientation change. This flip also allowed for elements to drop or "seat" into the machined vent area during the performed pilot testing; however, this difference in element behavior was seen as negligible as no jams were observed. As this MTA showed the ability to repeat the loading of seed and spacer elements with consistence over fifty trial runs, trial data was collected, the design was accepted, and work began on the final designed system.

3.3 Design of Overall Device

After validation of the concept of non-contact separation and capture of brachytherapy elements was observed within the pilot tests, work then began on full scale implementation of the concept. Positive design features explored within the pilot test were kept and scaled into a full scale non-mechanical brachytherapy element loading system. As the pilot testing explored the separation and detection within the individual element type lines, the full scale system was designed around this vital preliminary tested area as seen in *figure 3.14.*

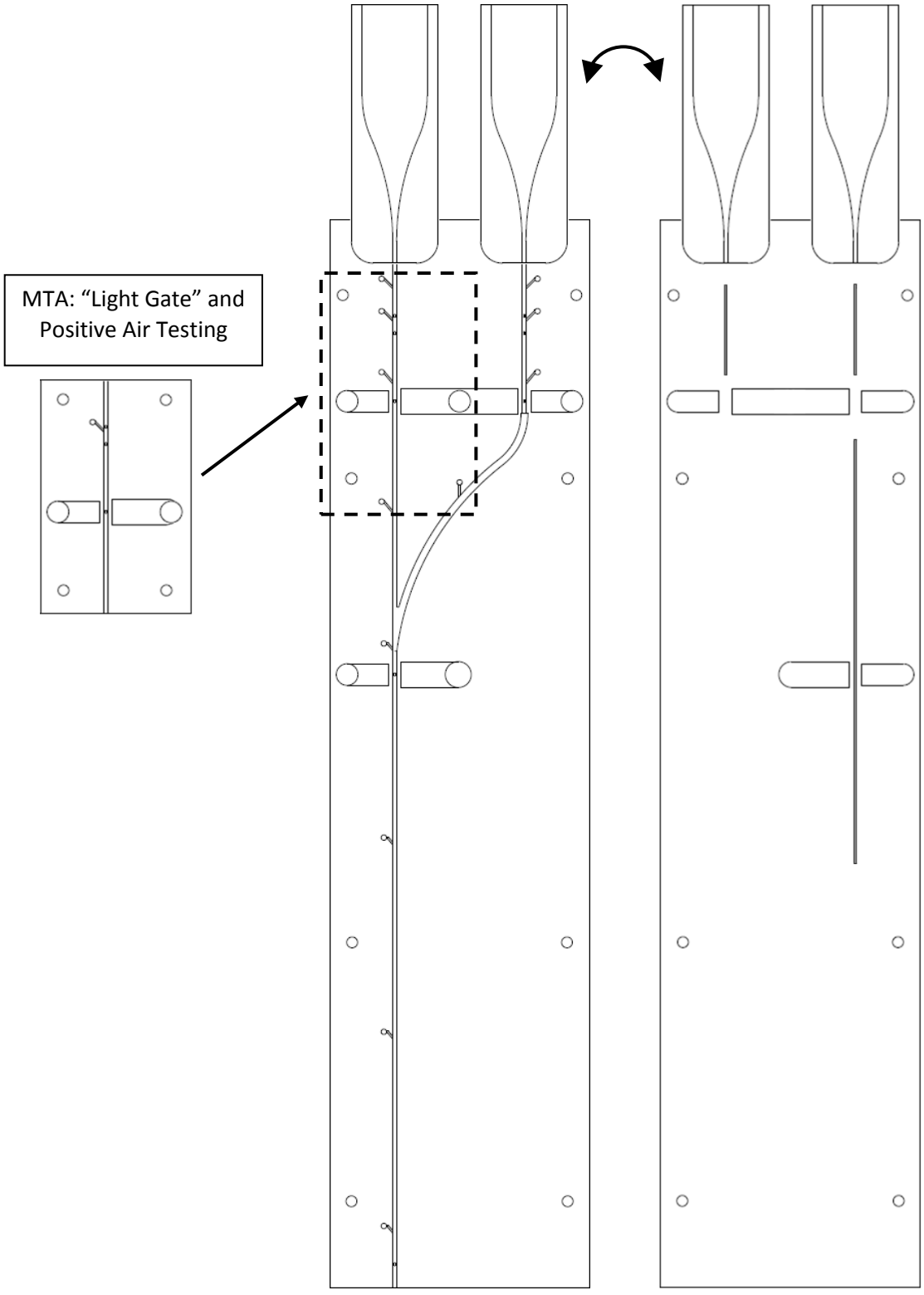

Figure 3.14: Illustration of MTA (left) pilot study impact to final two-piece full scale implementation including main section (center) and vented lid (right).

Within the full scale system, duel hoppers provided a reservoir of two element types to be fed into a central working environment or “main body” of the device. As in the pilot tests, two machined acrylic pieces were attached together to form this main body. Channels for element travel were machined into the first acrylic plate of the main body of the device along with air and vacuum pressure attachments at various locations to provide non-contact manipulation of elements. This plate has been referred to within this work as the “main section” of the main body as a majority of actions performed within the element loading sequence was dependent on geometries found within this section. Selection and movement of elements within this main body were designed to occur through the activation and deactivation of vacuum and air lines situated at critical points of the main section plate. Vents, as seen in the MTA pilot testing, were also included to provide separation of air and vacuum pressure effects within the system. Went features were included in an attempt to reduce the impact of unwanted pressure effects on neighboring sections within the main body. The geometries of these vents along with various other features were included on the second acrylic plate of the main body. This second plate has been referred to within this work as the “vented lid” due to its secondary functionality and primary purpose. Connection points mirrored on both acrylic plates in the main body provided attachment points in which fasteners were used to connect the plates forming a singular body. This main body piece governed the critical operation of element selection and detection within the system as a whole. A detailed diagram of the main section plates can be seen in *figures 3.15 and 3.16.*

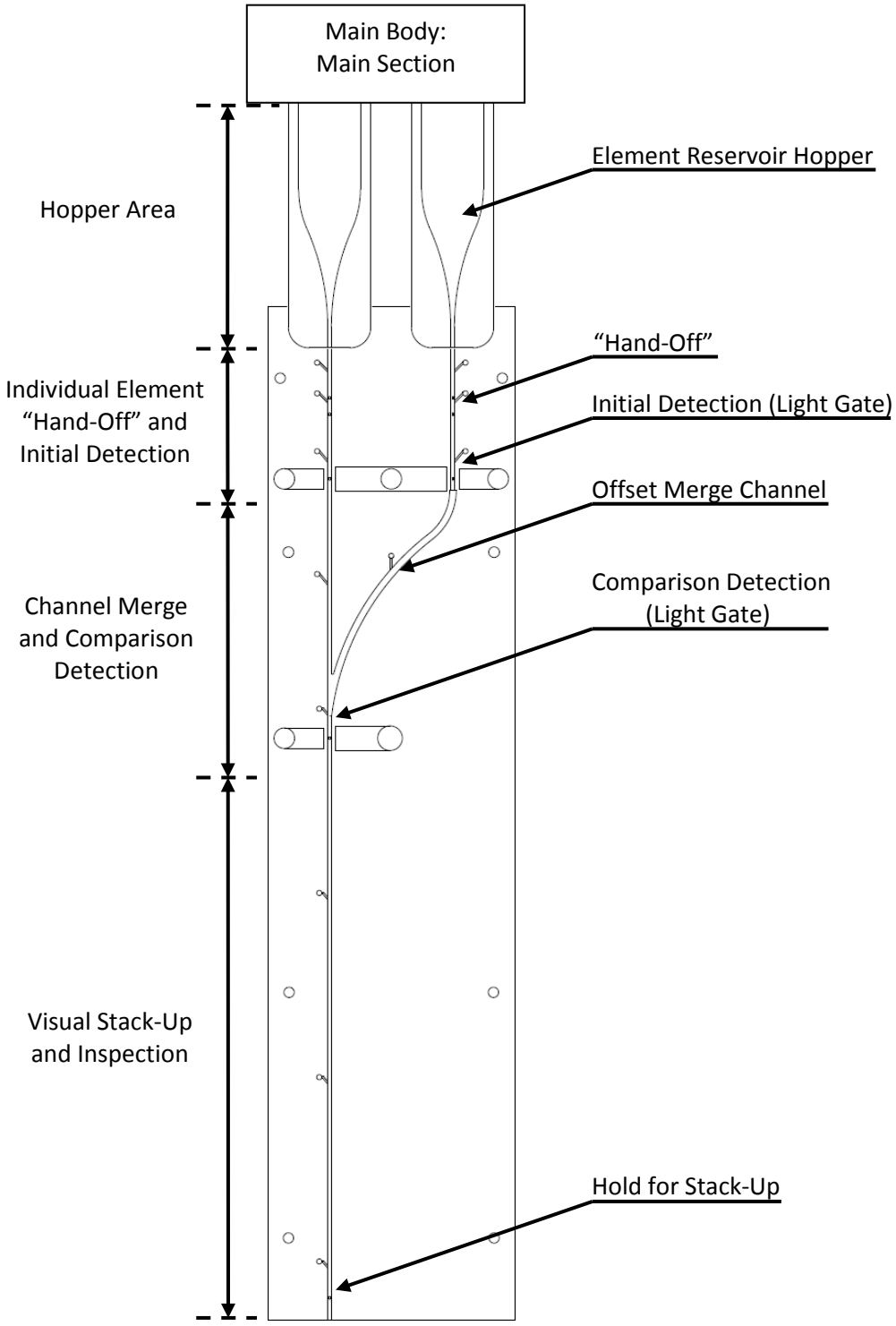

Figure 3.15: Diagram of first acrylic plate in device main body: main section.

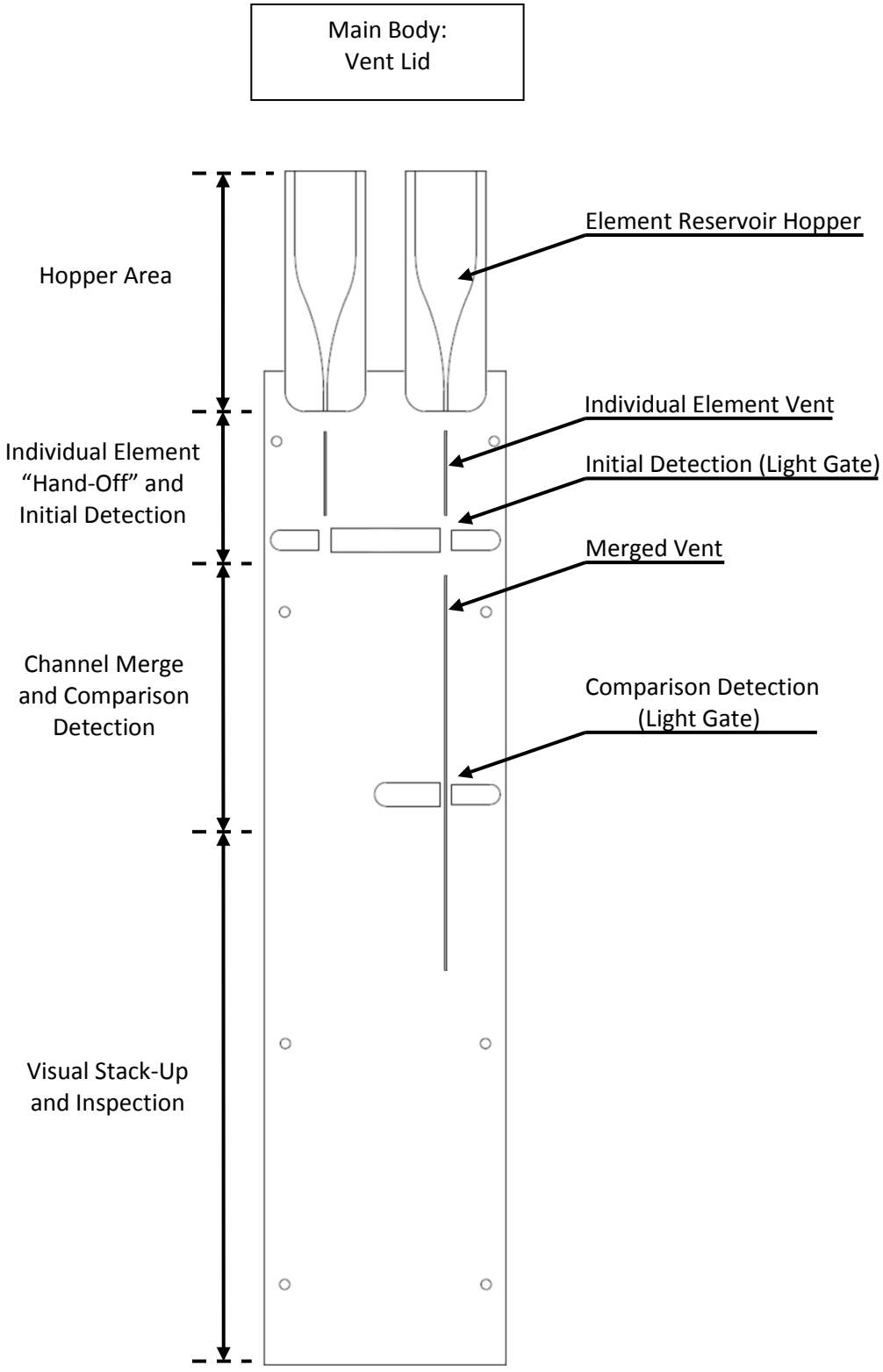

Figure 3.16: Diagram of second acrylic plate in device main body: vent lid.

As in the design of all MTAs, the full scale non-mechanical brachytherapy element loading system was first designed in a virtual 3D environment to allow for complex geometries to be properly defined and detailed for following CNC machining and rapid prototyping (RP) processes. A 3D parametric model of the main section piece of the main body can be seen in *figure 3.17*. This 3D model of the main section has been color coded to represent element travel (red), vacuum lines (green), air lines (blue), and light gates (yellow).

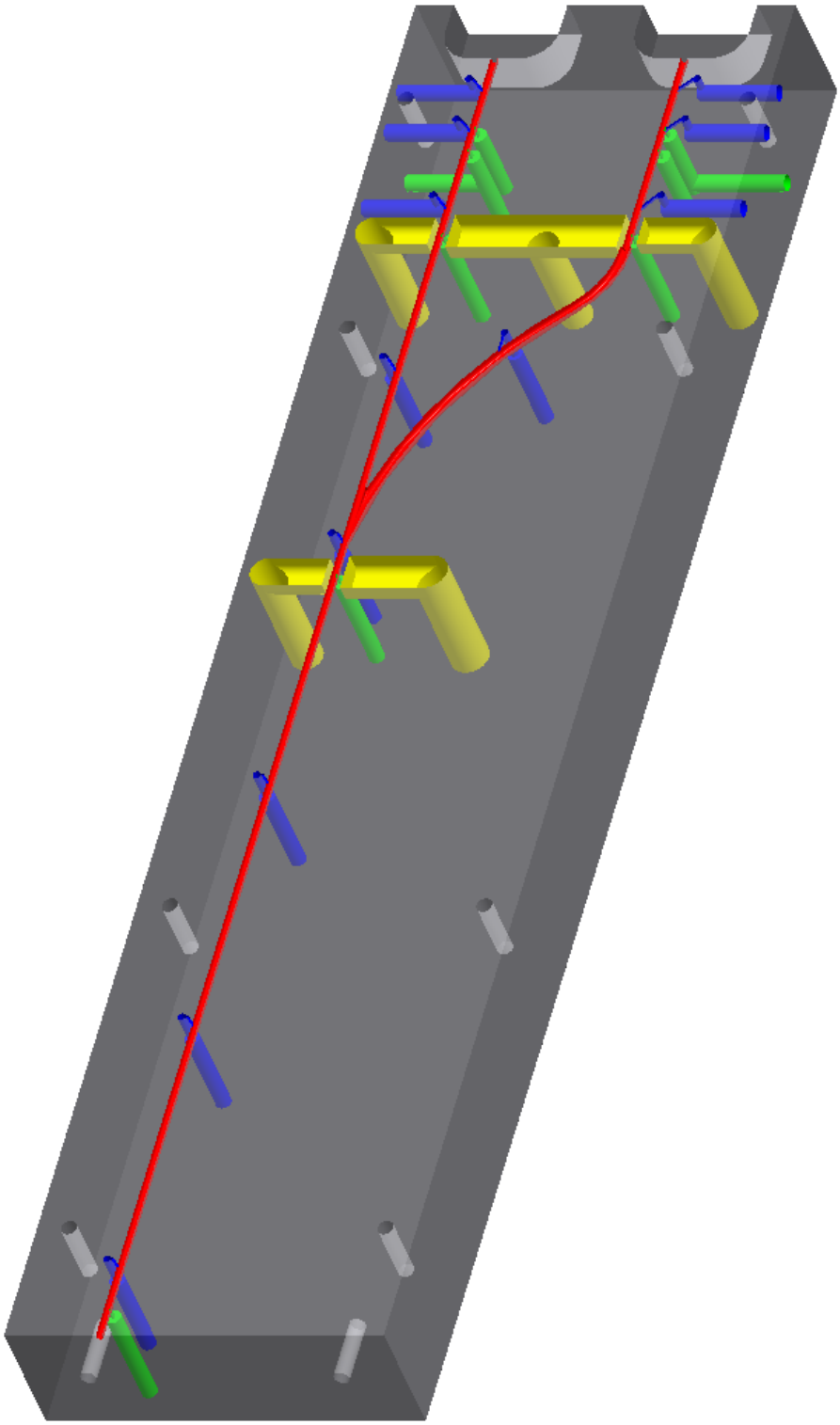

Figure 3.17: Original 3D parametric model of finalized two part construction main body: main section. Applied color code dependent on feature purpose.

Within the main section of the main body, the previously MTA explored “hand-off” method was employed within this finalized design to restrict elements fed from the duel hoppers to that of a single element into the main body of the system. This single element input from each line of the “hand-off” sections within the device was controlled through the use of vacuum and air pressures intersecting the element channels. Following this initial “hand-off” section of the main body, the single released element traveled to the next area of the main body which included the previously MTA explored light gate sensor. Two of these light gates were placed in parallel to monitor the independent lines from each element hopper. As a single element was released from the “hand-off” section, the element would then be captured by vacuum and inspected by the light gate before being allowed to continue travel. Inspection in this manner concerned voltage loss and was recorded. Following this inspection, the independent element channels were connected into a central or main element channel. As the spacer elements showed a higher chance of jamming within the MTAs during the pilot testing due to sharper edges, the design of the seed element channel was changed to allow for connection into the spacer element channel, removing the allowance of spacers to travel through curved channels. This was a design choice by the researcher made to minimize the possibility of a jam. A change of geometries in this duel to single line transition was required due the cylindrical shape of the seed elements and was allowable due to the restriction placed by the previous “hand-off” area of a single seed traveling through this area of the system. Directly in line after this merger of seed channel and spacer channel, a third and final light gate was placed. In this final light gate area, the traveling elements were captured and inspected a second time within the system. This secondary light gate inspection

allowed for a comparison to be performed by an automated control system to discern if the correct element type, previously called by the automated programming, had been successfully delivered. Should an argument occur between the two recorded light gate readings of a single element traveling through the system, the first measurement being at either of the single channels and the second being at the merged channel, the element would be ideally independently removed from the system before being loaded into the needle. However within the current design, any incorrect element would be loaded into the attached needle and the automated control program would notify the operator of the abnormality. Within the designed system after the secondary inspection light gate, the element is then released traveling to the exit of the main body. At the exit of the main body of the system, a last vacuum hold was applied to prevent elements from entering into the attached needle. By this action, elements were stacked on top of each other within the main body as the automated control program loaded the subsequent desired element pattern from the two element hoppers. As the loaded elements were held in this position above the needle, the human operator could visually inspect the loaded dosage of elements before they were deposited into the needle. Once satisfied, the human operator then released the stacked elements loading the needle for the brachytherapy procedure. During the initial design phase, additional features were added, such as a user interface panel with LED display allowing for manual selection of element pattern for loading and an area to unload seeds if needed. The original 3D assembly model designed for the element loading system can be seen in *figure 3.18.*

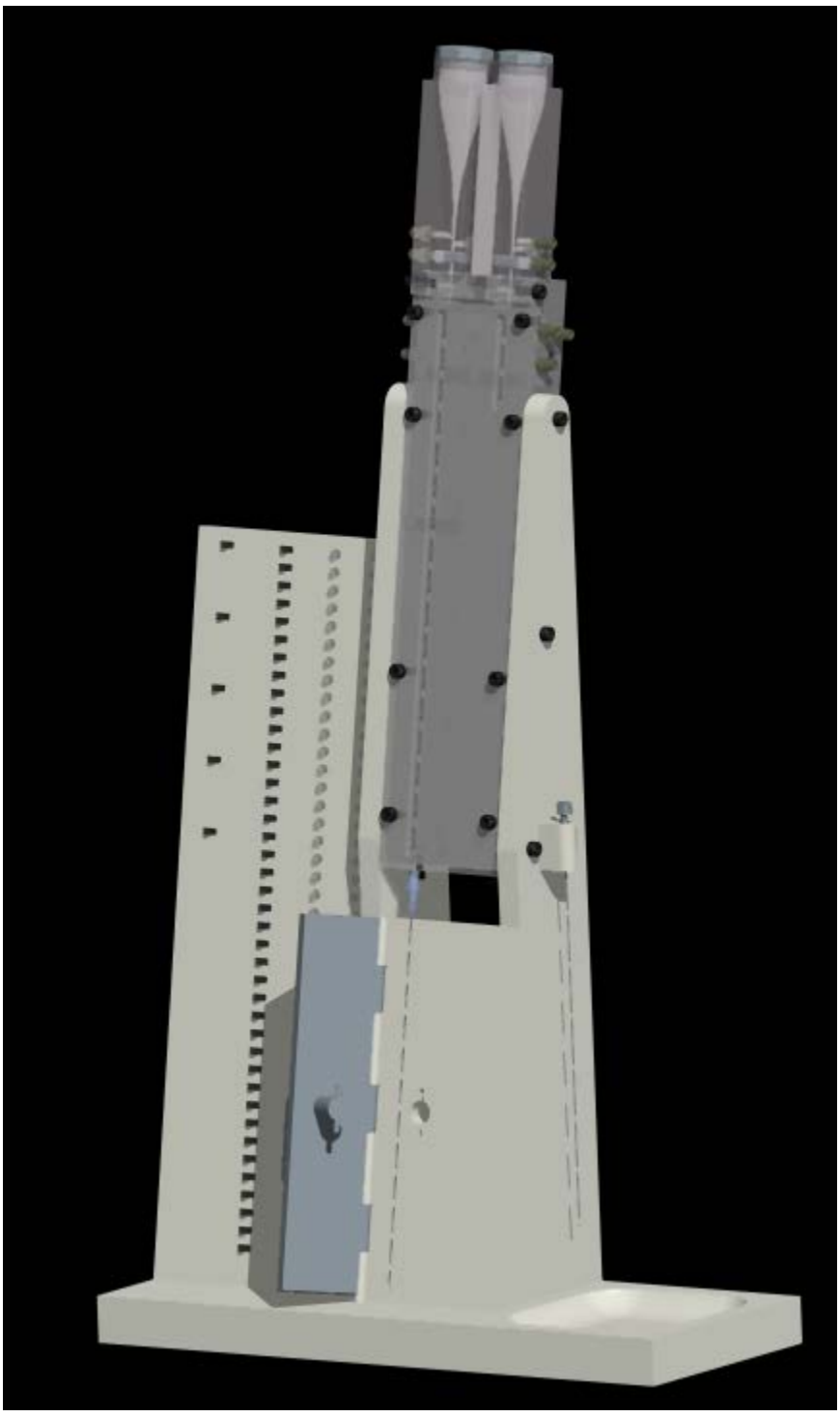

Figure 3.18: Original 3D parametric assembly model of non-mechanical brachytherapy element loading device (shown with original main body pieces orientation).

.

3.4 Fabrication and Assembly of Device

Due to pilot testing that found complex geometries necessary in the non-mechanical loading of brachytherapy elements, various CNC machining and RP processes were utilized in the fabrication of the final designed device. Equipment and processes were limited to that within WCU. Due to the physical and time restraints of fabricating tangible components, design details were changed to allow for such CNC machining and RP procedures within the time frame of this work. In these design changes to the originally conceived 3D parametric models, components deemed by the researcher to be non-critical to successful device operation were simplified in nature of design or removed entirely from the device. Of these changes to occur during the fabrication process, the following areas of the device were simplified: hopper sections and needle exit section. While the following areas were removed due to aforementioned constraints and non-critical functions: physical user input area and manual unload area.

Hopper area fabrication.

The original conceived design for the hopper area, seen in *figure 3.19*, utilized a funnel shape with a resulting geometry to that of a single brachytherapy element. This conceived funnel shape would allow the end user to simply pour loose elements into the hopper section rather than rely on magazines or other such pre-loaded components common to mechanical based loading systems. This original design would have required additional vacuum line connections for intended operation. In this intended design, duel vacuum lines for each hopper would have allowed for the removal of the hopper sections from the device while still containing loose elements. This concept was simplified due to both component and time restraints.

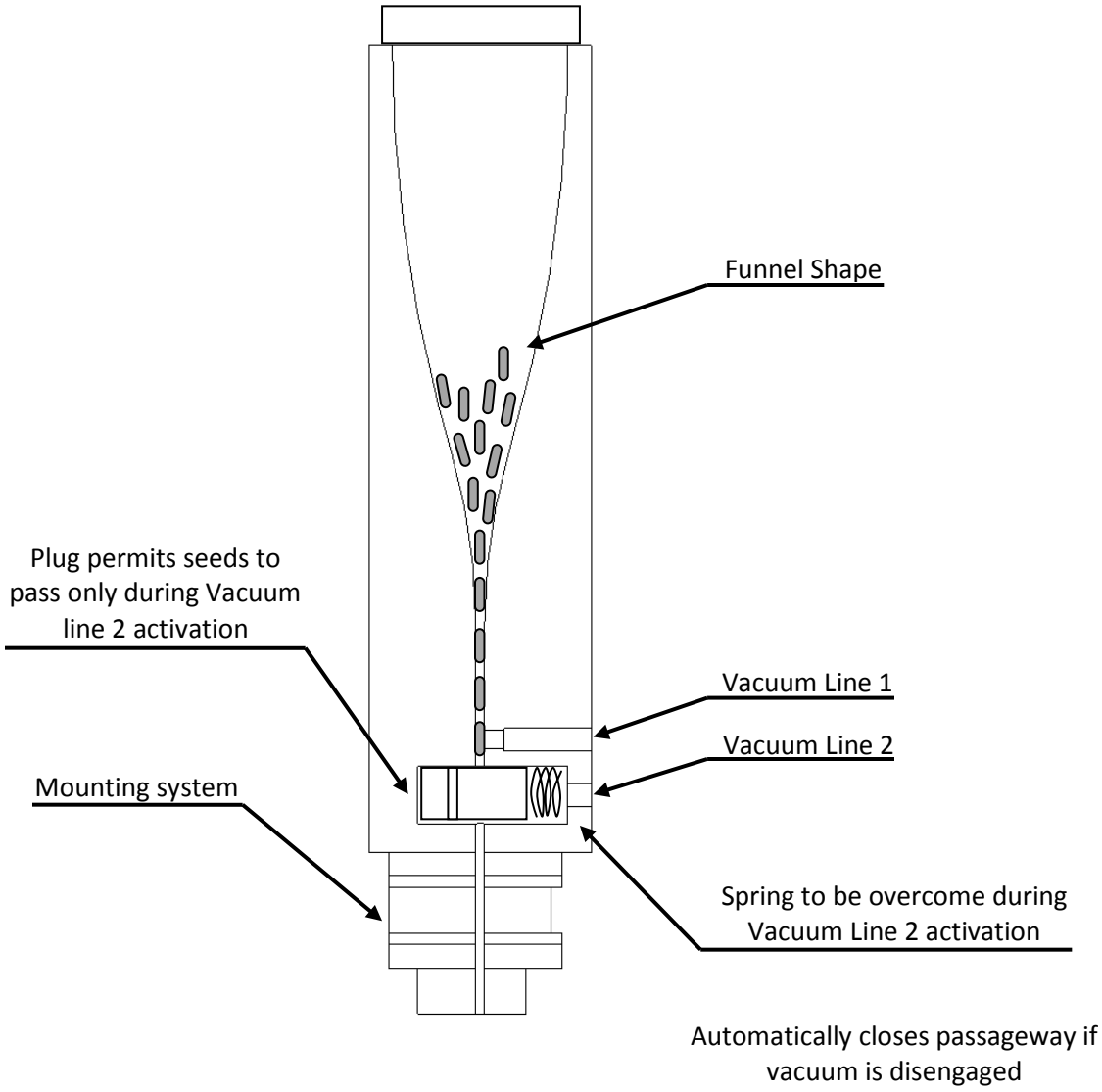

Figure 3.19: Original funnel-based hoper concept utilizing multiple vacuum line inlets to allow for removal from device.

Application of this original hopper concept within the full scale constructed system would have reduced the possible vacuum pressure available for more critical design features involving element selection within the main body of the device. An additional concern with this original hopper design concept was the introduction of a moving part within the device. While having no movement during normal element

loading operations, any moving part within the device could still subject elements to damage. These negative design points were deemed by the researcher to be possible points of failure and simplified for actual fabrication and implementation in to the full scale device. The design was simplified keeping the basic funnel shape and were redesigned using 3D modeling software and machined using 3D CNC machining to achieve the desired geometry shape. As elements were predicted to become jammed during the reduction of the hopper's funnel diameter to that of the single element, an air line was added to the simplified design. In this application, the air line was toggled between on and off states pulsing air upwards clearing any potential jams at this problem area. This design would allow elements to feed into the main body from the hoppers via gravity until a jam would occur, at which the air line would be pulsed freeing the jam by forcing the elements back into the hopper. Should this design have failed to function properly within the final full scale device, straight pre-stacked hoppers were also manufactured as a backup option (see Appendix A – Reference Photographs). These pre-stacked hoppers would have been undesirable due to the manual hand loading process required before loading into the automated device, but would allow for device testing should the more complex funnel geometry hoppers fail in desired operation. The process of design and fabrication of these simplified funnel hoppers is illustrated in *figure 3.20* while the finished part can be seen in *figure 3.21*. The set sequence using the process of initial conceptual design, 3D parametric model, and CNC machining process or RP was utilized through the fabrication of all components.

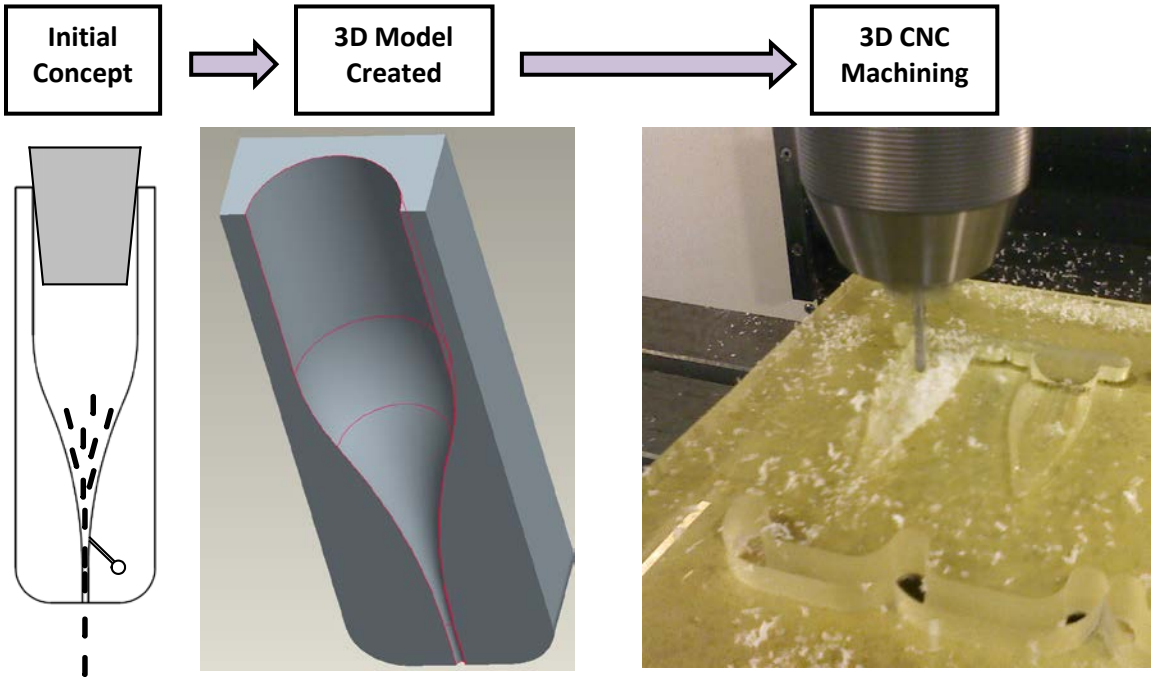

Figure 3.20: Process of manufacturing simplified funnel-based hoppers for final fabrication and implementation into full device.

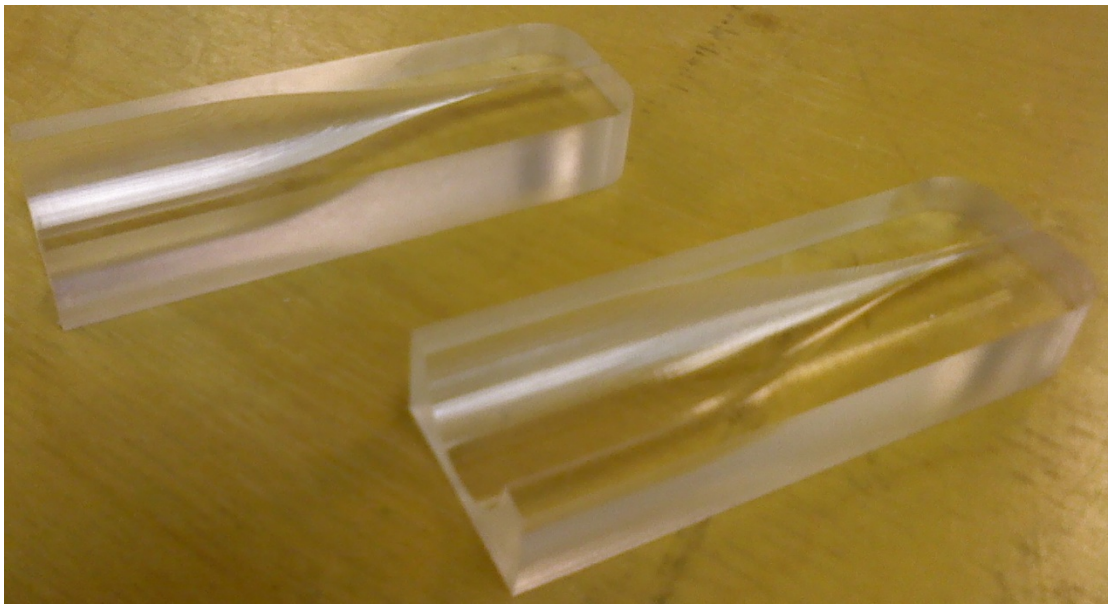

Figure 3.21: Two piece construction simplified hopper sections before attachment.

Needle connection area fabrication.

In the original conceptual device design, this area of the device contained multiple moving and locking components to secure the brachytherapy needle during element loading. This multipart design was deemed by the researcher far too complex in nature to be manufactured within the time frame of this study. To reduce the inherent complexity of this section, the original design was entirely scrapped and replaced with a simple attachment plate to the main body of the device. In this application, a brachytherapy needle would simply thread onto the device using a preexisting tread pattern on current preloaded needles provided by SHANDS hospital. This direct attachment to the main body of the device allowed for a secure connection disallowing the possibility of elements exiting the system prematurely. As this newly designed needle attachment plate required complex geometry in manufacturing a reverse thread pattern based on the current needle design, thus CNC subtraction machining was not sufficient. To produce the needle attachment plate, additive RP was utilized within WCU to manufacture the needle attachment plate. Both 3D model and physical RP part of the needle attachment plate can be seen in *figure 3.22.*

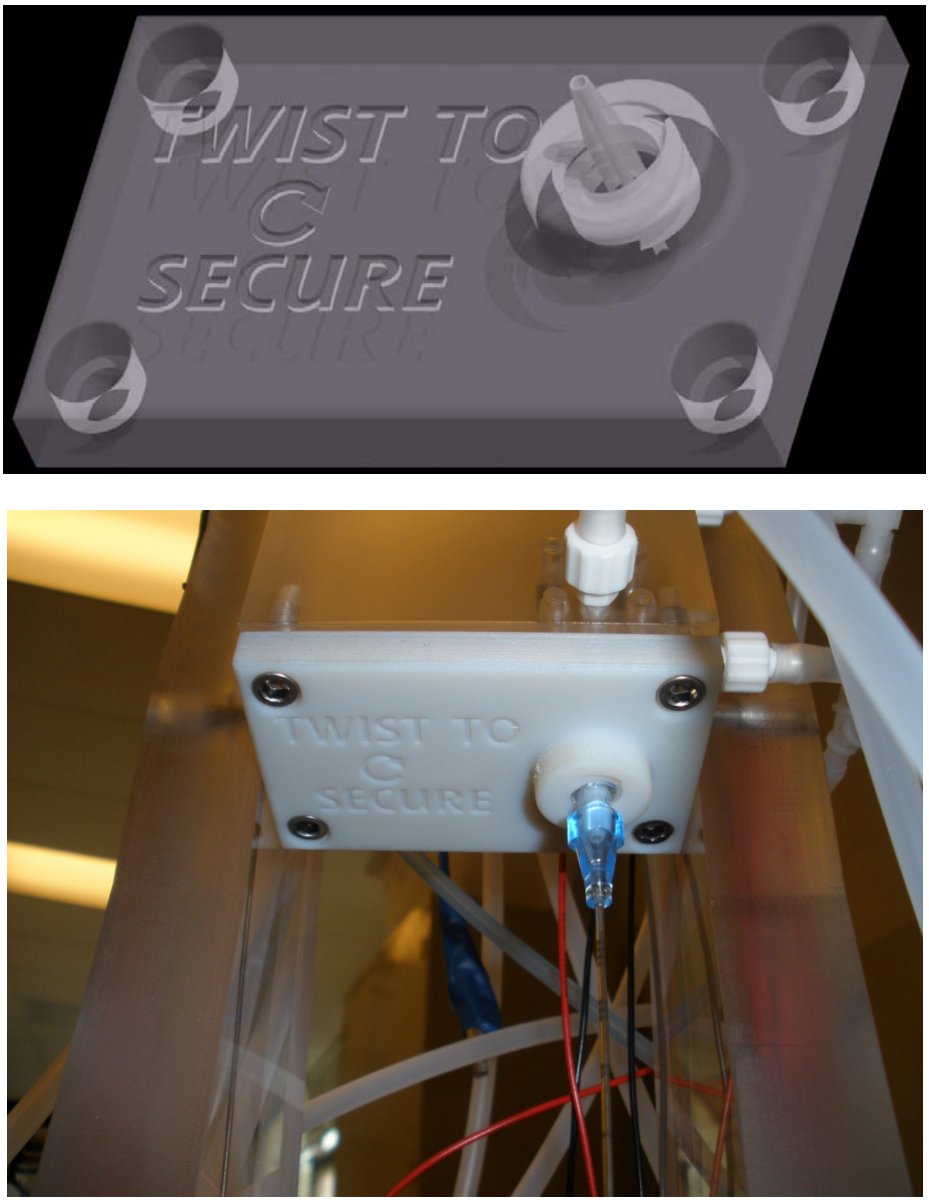

Figure 3.22: Needle connection plate, 3D model (top) and physical rapid prototyped part (bottom), allowed for connection of the brachytherapy needle to the main body of the loading device.

Main system fabrication.

The main body of the device, including the main section and vent lid, were constructed in the same manner as all MTAs during the pilot study of this work; however, on a much larger scale using subtractive machining processes limited to those within

WCU. Design changes in this section of the device were minimal during the manufacturing process as production and manufacturing techniques were previously established through MTA pilot testing. Upon completion of the CNC subtractive machining processes on the critical main body pieces, less critical components such as fixture components were manufactured as seen in *figure 3.23.* These less critical components included vertical supports, the device base, and various component housings.

Figure 3.23: CNC subtractive machining performed to manufacture vertical supports used in final constructed device.

Upon the completion of all manufacturing processes, the overall acrylic device, including both the main body and secondary fixture components, was assembled according to the created 3D assembly models. In *figure 3.24* the original fully assembled

device can be seen upon completion of all manufacturing processes and initial polishing processes.

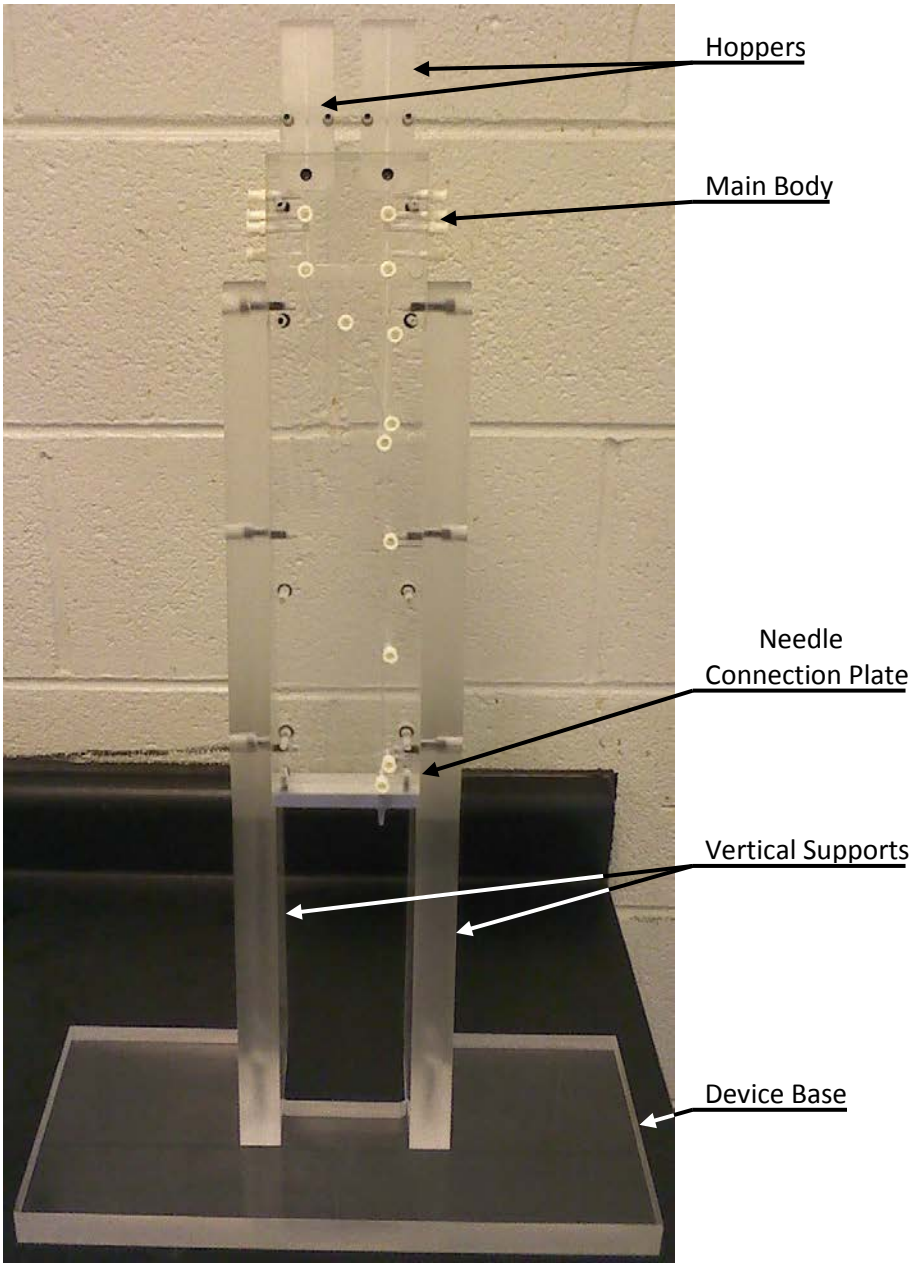

Figure 3.24: Original fully assembled non-mechanical brachytherapy element loading device (shown with early straight line hoppers and needle connection plate).

3.5 Control and Testing Stand

To provide the necessary electrical power, vacuum pressure, and air pressure to the main body pieces; a control and testing stand was fabricated. This stand allowed for the control of inputs to the device and measurement of outputs from the device through multiple means. Automated control and light gate measurement functions of the system were performed employing a National Instruments (NI) data acquisition device (DAQ) and associated Laboratory Virtual Instrumentation Engineering Workbench (LabVIEW™) software package discussed later within this section. A generalized diagram of this control and testing stand, including location and configuration, can be seen in *figure 3.25*.

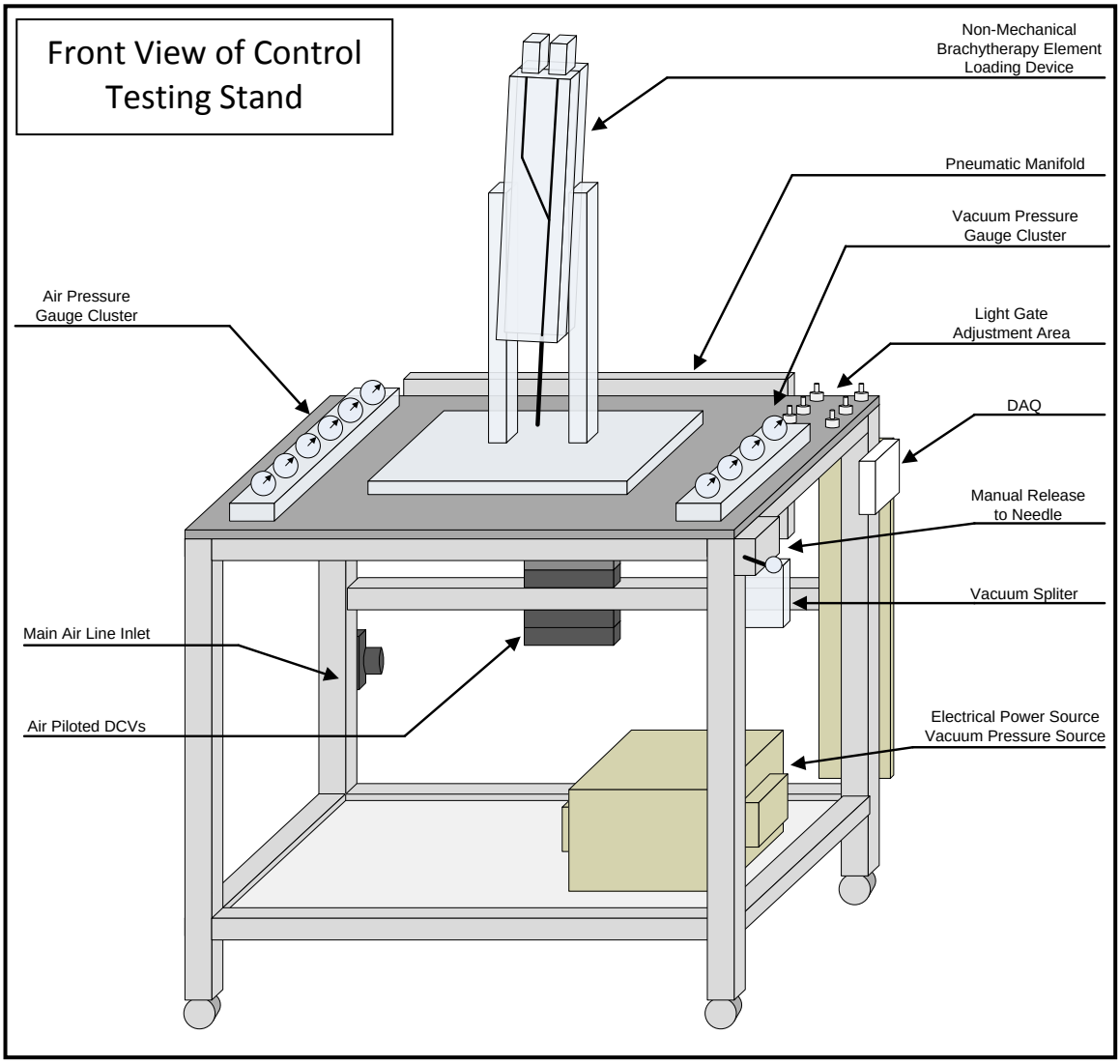

Figure 3.25: Front view diagram of constructed control and testing stand implemented in this work (air lines, vacuum lines, and electrical connections not shown).

While the Ni DAQ allowed for the electrical measurement of light gates, analog gates were utilized for measurement of both air and vacuum pressures. Regardless of measurement method, all inputs and outputs were controlled and measured independently. The control and testing stand was used throughout this work to provide measurable conditions to and from the attached machined acrylic brachytherapy element

loading device. The following *table 3.1* contains all measured inputs and outputs found on the testing stand.

Table 3.1

Measurable System Inputs and Outputs on Constructed Testing Stand

Input / Output	Governing Component(s)	Label	Measurement	Unit	Amount
Input	Pressure Reducing Valve Cluster	Positive Air Pressure	lbs per in^2	psi	x6
Input	Adjustable Atmospheric Vent	Negative Vacuum Pressure	inches per mercury	in.Hg	x4
Input	Potentiometer Cluster	Light Gate Normal Loss	voltage loss	-v	x3
Output	Photoelectric Resistors	Light Gate Operational Loss	voltage loss	-v	x3

Automated Control System.

For the task of automated system control, NI LabVIEW™ software was used in tandem with a NI USB-6008 DAQ. The use of a DAQ device within this work allowed for both the collection of data from light gate circuits and the sending of activations/deactivations to pneumatic components within the system using the LabVIEW™ software as a control. In this application, the DAQ device was configured with twelve digital output channels to control pneumatic components and three analog inputs to read light gates. Digital outputs controlling pneumatic components were utilized

for automated control over vacuum and air lines controlling element manipulation, while the analog inputs were utilized for automated measurement voltage loss across light gates allowing for element detection. A wiring diagram of the DAQ device and its connection to associated components can be seen in Appendix B (System Schematics). Within the LabVIEW™ software a Virtual Instrument (VI) was created and linked to the DAQ channels to allow for user control the system. The constructed VI allowed for a visual representation of the working system through both inputs and outputs along with a user interface allotting both automated and manual controls. User interface within the system included the loading of a dosimetry pattern; including individual needle pattern and length, along with manual activation of the individual solenoids should elements need to be individually loaded. To allow for needles to be removed and replaced once filled utilizing the needle connection plate and threaded connection, the automated program was set to cease the loading process and wait on a manual start signal once the replacement had been performed. Once the empty needle had been properly secured, the user pressed the manual activation button within the VI and the automated loading sequence was restarted by the user. A screenshot from the automated loading VI can be seen in *figure 3.26*.

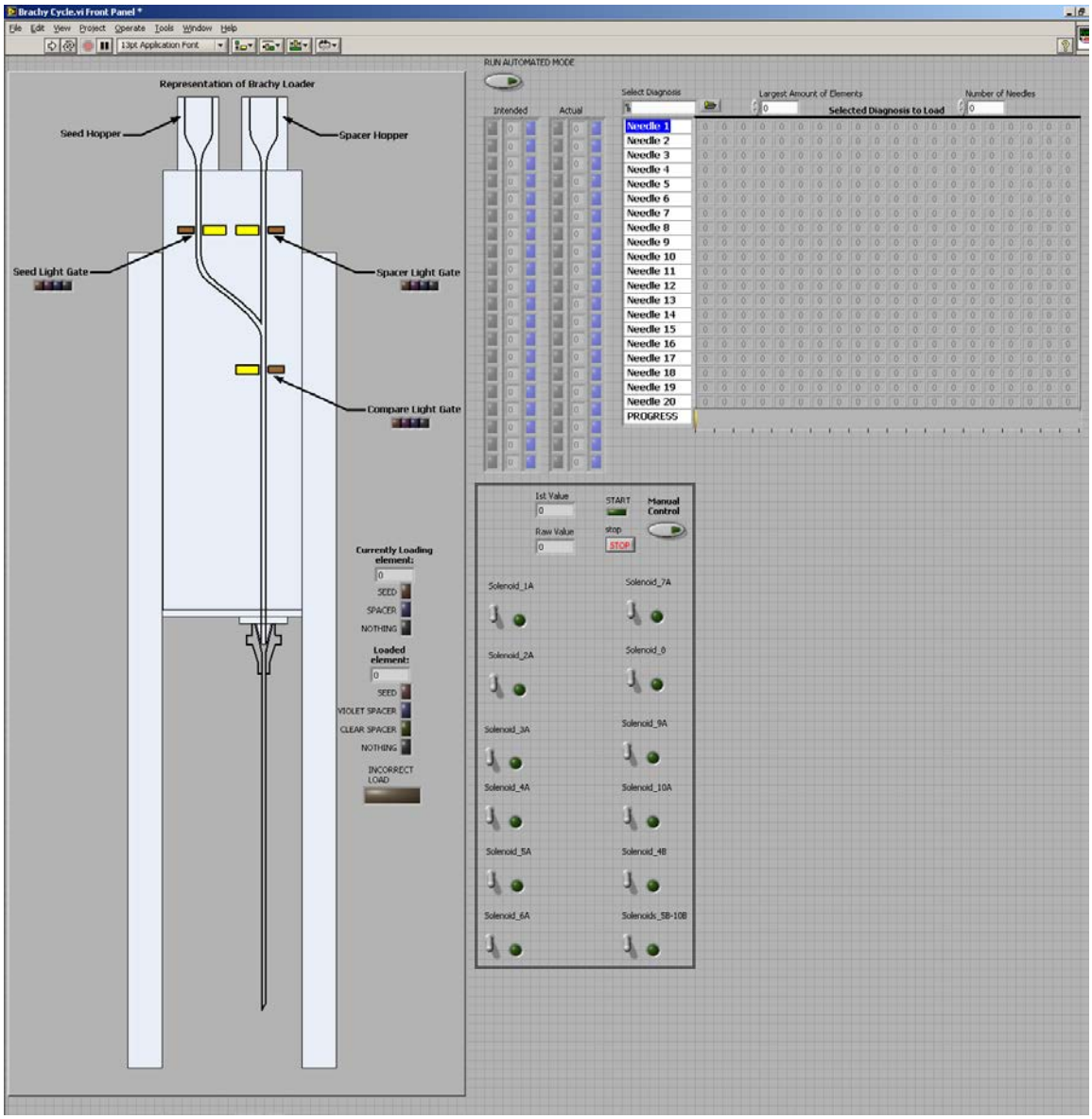

Figure 3.26: Front panel screenshot of automated loading VI constructed in National Instrument's LabVIEW software package.

Within the control environment for the VI program there existed various commands and features available to the end user. A visual representation of the main body of the loading device can be seen on the right side of *figure 3.26.* Within this section of the VI, the end user was also able to observe the conditions of each light gate as it related to the current element load interpreted by the automated program. Within this

visual representation area, there also exists an incorrect load detection to alert the user if the device has failed to load the intended element to the needle as desired. In the lower mid area of the VI in *figure 3.26* there exists a manual control area to enable the manual operation of all pneumatic solenoid valves found on the device. This manual control area allowed for the user to cycle any problem areas within the device and load individual elements outside the automated dosimetry pattern. In the upper mid area of the VI in *figure 3.26* there exists the automated dosimetry loading area. This automated loading area allowed for the user to select a predefined dosimetry pattern and load this set pattern of seed and spacer elements within the provided VI. Once loaded, the VI interpreted the predefined dosimetry pattern and displayed the overall pattern within the table located in the upper right section of the VI. Within this dosimetry pattern display the following coding was used to specify element presence and type: 0 = no element, 1 = seed element, and 2 = spacer element. Taking from this overall table, the current needle selected by the VI to fill is also displayed in detail through numerical and visual means in the upper mid section of the VI.

Within normal operation of the system, the following actions were performed for full operation:

1. Power was activated engaging all vacuum lines and electrical components on the device.
2. Element types were poured into their respective funnel shaped hoppers.
3. A brachytherapy needle was attached to the base of the device using a threaded connection.

4. A predefined dosimetry plan including random element pattern and random needle sequence was loaded into the computer-based VI.
5. The VI was then activated relying on interface with the DAQ device to both send and receive signals from the device to the computer.
    a) The VI then determined the appropriate element type in which to load based on the loaded dosimetry plan.
    b) Hoppers sections were then pulsed with air to clear obstructions into the main body of the device caused by funnel shaped design.
    c) Elements from both hopper sections then entered the main body in a single file fashion causing a stacking effect.
    d) Stacked elements were then held stationary at the second vacuum line allowing for the second element in line to be positioned at the first vacuum line on both individual element channels.
    e) The first vacuum lines were then activated on both element channels capturing the second elements in each stack.
    f) Based on the element type previously called by the automated program, one of the second vacuum lines was then released. This action allowed only the desired element type to proceed while keeping the opposing element stationary.
    g) The released element then travelled to the corresponding light gate area and was subsequently captured.

h) At this time, readings on all three light gates within the system were gathered. This data allowed the VI to determine both the location of the element within the device as well as element type.

i) Upon successful capture of data from the light gates, the element was then released from the light gate area.

j) Travelling further within the device, the individual element channels were then combined to form a single channel. Directly after this junction, a final light gate area caught the element for a secondary inspection.

k) As with the initial light gate area data was collected on all light gate areas. This second data set was then compared with respect to previous light gate value, threshold values for element type, and logical progression through the device based on location within the VI.

l) The element was then released from the second light gate area and sent to the exit area of the device.

m) Elements exiting the device were then held with vacuum and allowed to stack in series with one another. This action allowed for visual inspection of the dosimetry plan before the elements were deposited into the awaiting needle.

n) Upon the successful loading of the first single element, the VI then repeated the necessary steps to fill the remaining elements using the same procedure.

o) Once all elements had been successfully loaded, the VI then prompted the user to replace the filled needle with an empty one. Should an error have

occurred during the loading process, the VI would have alerted the user to dispose of the incorrectly loaded needle and the loading sequence would then been repeated.

6. Providing the automated loading sequence had been completed correctly, the user then released the loaded element stack into the needle by disengaging a vacuum line via a manual release lever.
7. The user then changed the loaded needle out for an empty one.
8. Finally, the user then signaled the VI to continue the automated dosimetry loading sequence.

Pneumatics and vacuum systems.

A pneumatics system was utilized within the testing stand to allow for control of both positive air and negative vacuum pressures within the main body. A schematic of the testing stand pneumatics can be found in Appendix B (System Schematics). A Festo™ pneumatics manifold was selected for this capacity consisting of a central air inlet, seated directional control valves (DCVs), and exhausts. A pressure relief valve was positioned between the Festo™ pneumatics manifold and a pressurized air source to limit the system to around 70 pounds per square inch (psi) working pressure. In total, ten DVCs were seated on the pneumatics manifold. These DVCs consisted of an inlet to the Festo™ manifold to provide pressurized air, electronic solenoid controls, and two exiting ports. As the intent within the constructed system was to provide an on/off condition for all pneumatic controls, all DVCs were restricted to a single exit port by capping the secondary port. All DVCs within this system were operated through attached electrical solenoid valves. Orientation and position of these valves can be seen in *figure 3.27.*

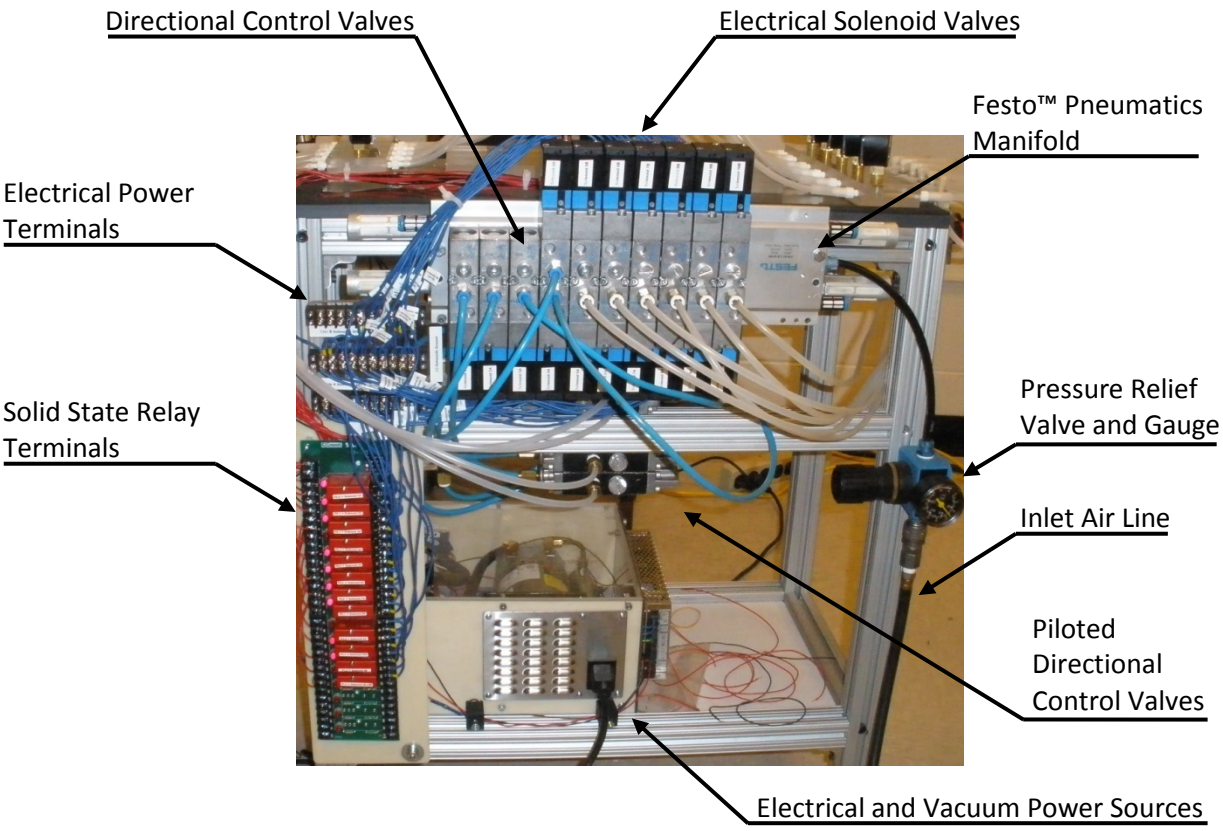

Figure 3.27: Rear mounted Festo™ pneumatics system utilized within normal operations on testing stand.

Activations of these electrical solenoid valves were controlled through the automated LabVIEW™ program and the connected NI DAQ device. Solenoids within this system required 24 volts direct current (DC) power to activate. As signals sent from the DAQ were limited to 5 volts DC, these signals required an increase to 24 volts DC to activate the DCV solenoid valves. This increase in electrical power from 5 volts DC to 24 volts DC was accomplished through the use of isolated steady state relays allowing the smaller 5 volts DC DAQ signals to activate corresponding 24 volt signals to the specified solenoid valves. The 24 volts DC required to activate the solenoid valves was supplied by a dedicated 24V DC power supply found on the base of the testing stand and jumped to

the isolated steady state relays. Vacuum pressures to the system were supplied by a central vacuum pump, which was also located at the base of the testing stand. The central vacuum pump generated a constant 23-22 inches of mercury (inHg) vacuum pressure to the system. To provide vacuum to multiple lines, central vacuum pressure was divided into five possible outlets through a machined acrylic manifold. This machined acrylic manifold split the source vacuum, which allowed for a minimum of around 4 inHg possible vacuum pressure when all lines were activated (not accounting for pressure loss through connection lines). Due to the nature of the pneumatic DCVs activated by the DAQ, positive air pressure was required for proper activation. This was problematic when dealing with vacuum pressures as the vacuum lines could not be attached to the DCVs in the same manner as the positive air lines. To resolve this DCV activation issue, four additional air-piloted DCVs were utilized to allow control over four of the five vacuum lines. These air-piloted DCVs were set in series with four of the aforementioned DCVs located on the Festo™ manifold and can also be seen in *figure 3.28*. In this application, DCVs mounted on the Festo™ manifold were able to in turn control the piloted DCVs (which did not have the positive air requirement). The remaining six DCVs controlled the positive air pressures throughout the system and were connected to individual flow reducing valves. These flow reducing valves enabled individual control of the allowable air to each air line. Regardless of vacuum or air, each line was then connected to an analog gage to enable observation of input pressures to the main body. In normal operations of this testing stand, input values relating to positive air pressure and light gate normal loss were preset to assumed values. These assumed input values were derived from initial testing and experimentation of the full scale system.

Electrical Power.

Multiple electrical components within the control and testing stand needed set power requirements for proper operations. These components were as follows:

- Vacuum Motor 120V AC
- Vacuum Motor Fan 120V AC
- Pneumatic DCV Solenoids 24V DC
- Vibration Motors 5V DC

To provide these various components within the control and testing stand with required power, three sources were utilized. As seen in the general wiring diagram located in Appendix B (System Schematics), a line of 120 volts alternating current (AC) was supplied from a normal 120 volts AC grounded wall outlet to the electrical and vacuum supply housing. The inlet line of 120 volts AC source was controlled via an on/off switch to the remainder of the system serving as a master power switch. Provided the switch was set in the on position, the 120 volts AC power was supplied to both the vacuum motor and vacuum motor fan cooling fan. The 120 volts AC power was also supplied to both a 24 volts DC power supply and a 5 volts DC power supply. These two DC power supplies provided electrical power to the remainder of the system such as the pneumatic solenoid valves and vibration motors.

3.5 Original Fixture Testing and Rework

Following the completion and assembly of the acrylic main body pieces, the control and testing stand, and the automated LabVIEW™ program; the researcher attempted to operate the system as intended by loading brachytherapy elements into each hopper section. However, the system failed to successfully operate as intended. In this

initial assembly, the system was only able to load from the seed element hopper. No successful element loads were recorded from the spacer hopper. This issue was then compounded by the tendency of elements to not be captured by the third light gate area for the intended element comparison. Observed results from this initial assembly were inconsistent to those found during the pilot testing and were deemed unsatisfactory. Under further inspection, it was determined that a vibration during the subtractive machining process had resulted in a variation in material thickness within the acrylic main body pieces. Due to this vibration, the machined channel in which the elements traveled varied in depth. Accuracy in the machining depth of the element channels was vital to proper functioning of the overall system. In channel areas too deeply machined such as that around the comparison light gate area, elements were observed to overlap one another. Channel areas too lightly machined, such as that around the spacer hopper and spacer “hand-off” area, were observed to constrict elements disallowing the passage of any element. Both of these conditions resulted in jamming within the system preventing any subsequent elements from successfully passing through. Additional jamming within the original main body pieces was also discovered due to the initial ventilation design. During travel through the system, elements tended to “seat” themselves in the vent area of the lid section. While this was an expected observation previously noted during the pilot testing, elements were observed to overlap one another at vent areas due to the variance of channel depth throughout the main body pieces. Attempts were made to rework the original machined main body pieces to account for the vibration error and achieve the desired tolerances. However, due to initial design tolerance tightness and loss of pressures through the reworked pieces due to the

additional machining processes, no success was achieved using the reworked main body pieces.

After the unsuccessful testing and unsuccessful reworking of the original acrylic main body pieces, it was deemed necessary by the researcher that proper working of the system could only be achieved through the machining of additional main body pieces. In this facet, the original vent design was altered in an attempt to remove any possible impact on element travel. To accomplish this removal of element impact, vents were redesigned venting out of the seam between the two main body pieces rather than through the vented lid. An illustration of this change can be seen in *figure 3.28*.

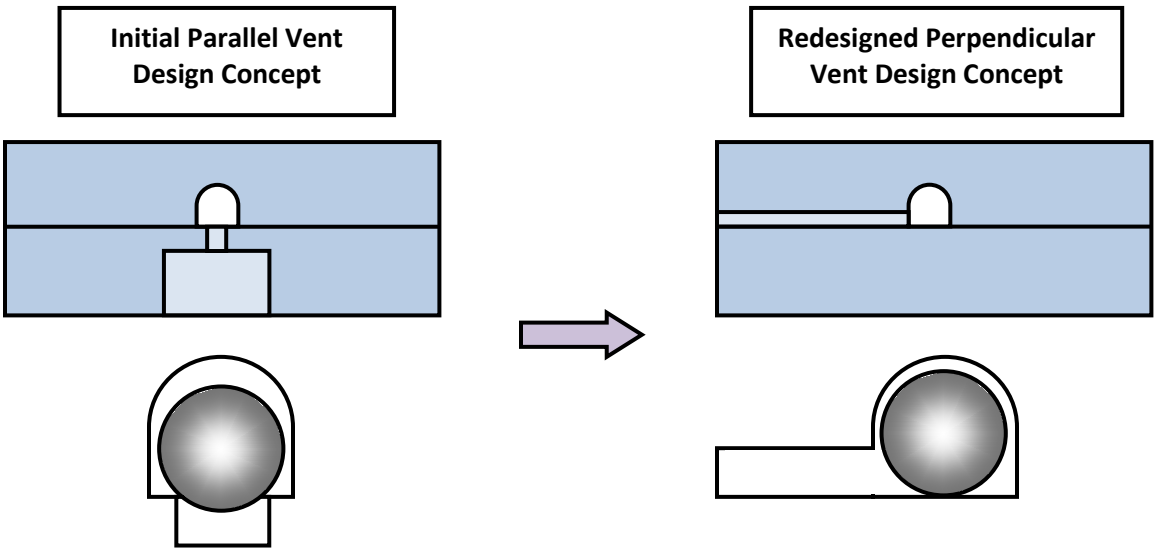

Figure 3.28: Illustration of vent design change to remove "seating" effect on element travel.

The vent design change was translated to the main section piece as can be seen in *figure 2.29*. As with the previous main section design found in *figure 3.16*, this 3D model of the redesigned main section has been color coded to represent element travel (red),

vacuum lines (green), air lines (blue), and light gates (yellow) with the addition of the redesigned vents (purple).

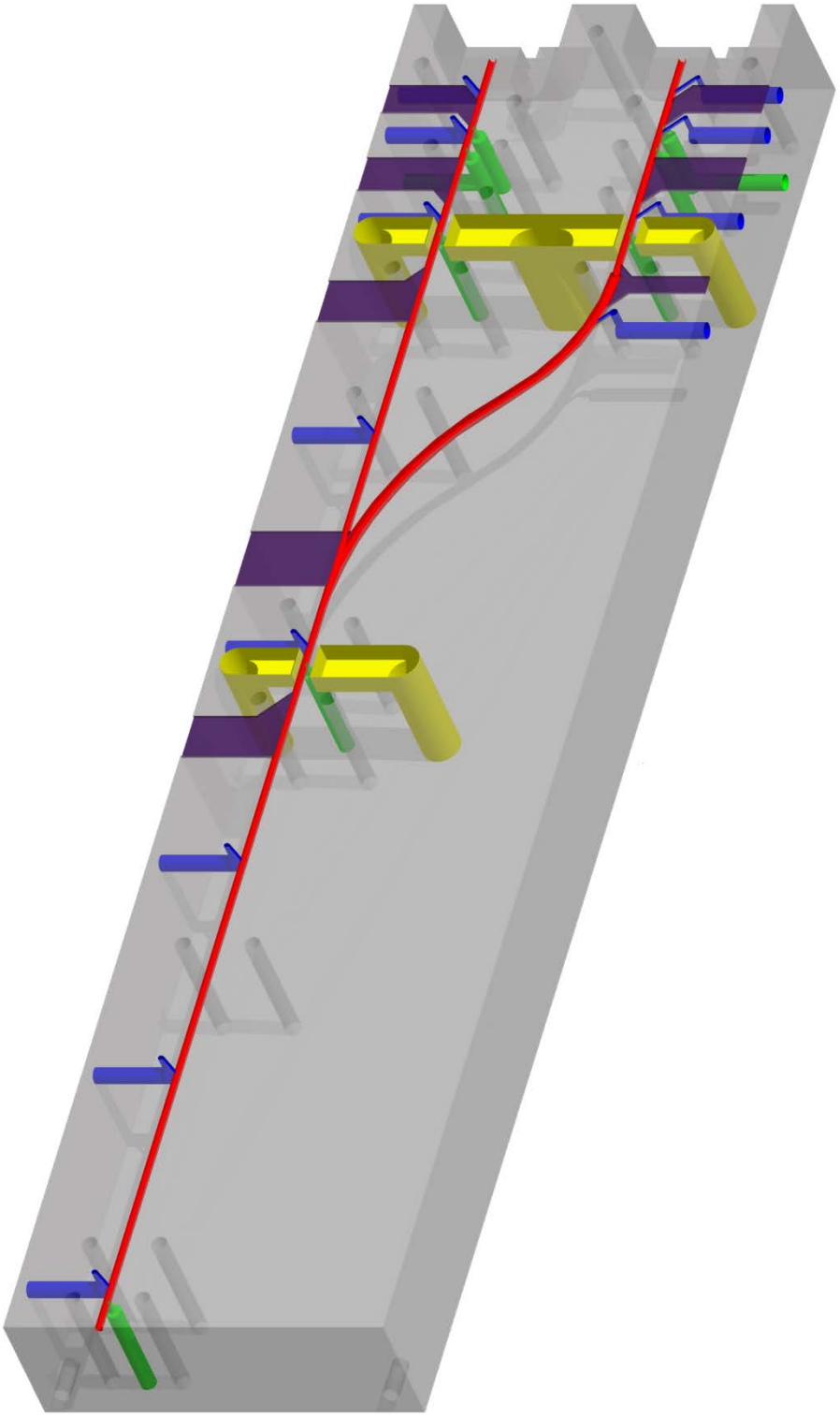

Figure 3.29: Redesigned 3D parametric model of finalized two part construction main body: main section. Applied color code dependent on feature purpose.

The second main body pieces were then attached to the overall system and tested to ensure proper functioning. Through producing new main body pieces, proper tolerances were achieved to design specifications and elements were observed to pass properly through the device without any apparent jamming. The completed system can be seen in *figure 3.30* with all components connected.

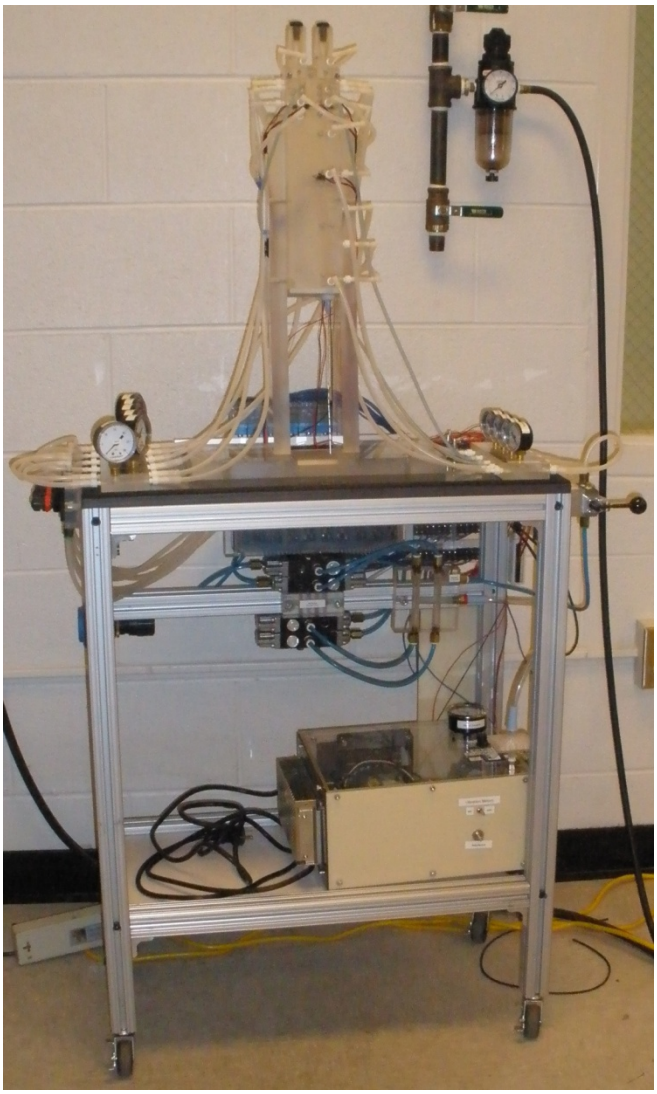

Figure 3.30: Photo of fully assembled non-mechanical brachytherapy loading device. Includes all reworked components.

3.6 Performed Data Collection

To verify the validity of the design of the constructed non-mechanical element loading system, initial testing was performed to determine if the system could properly load and detect elements based on a preset dosimetry pattern supplied by an outside source. Data collection was performed based on recorded light gate measurements of voltage loss and visual verification of correct system operations during the automated loading process. All light gate measurements were taken with respect to the two measurements taken by the automated system during the loading of a single element. In this method, measurements were recorded of all three light gates twice during the loading of a single element in an attempt to show variations in voltage losses in relation to element travel. It was anticipated that by recording data from all light gates multiple times within a single load, an element capture would be discernable based off of the recorded values. One measurement of all light gates was taken when an element, regardless of type, was called by the automated program and captured at either element light gate area. This first light gate measurement was referred to as “condition 1” within this work. In this condition 1, either of the two initial detection light gates positioned in parallel on the individual element channels was susceptible to display an element captured via a low voltage loss reading, while the opposing initial detection light gate and the comparison light gate should show no element capture and relatively high voltage loss. Following this condition 1, a second “condition 2” was also employed to provide basis for both a logic and comparison detection of element travel. In this condition2, the comparison light gate should display an element captured via a low voltage loss reading, while the initial element light gates should show no element capture and high voltage

loss. Using the principles of both basic logic and recorded value comparison of the voltage loss between the two conditions, an association would be possible as to the loaded element type giving the system a method of self checking. An illustration of these conditions and the associated intended element placement can be seen in *figure 3.31, figure 3.32,* and *figure 3.33.*

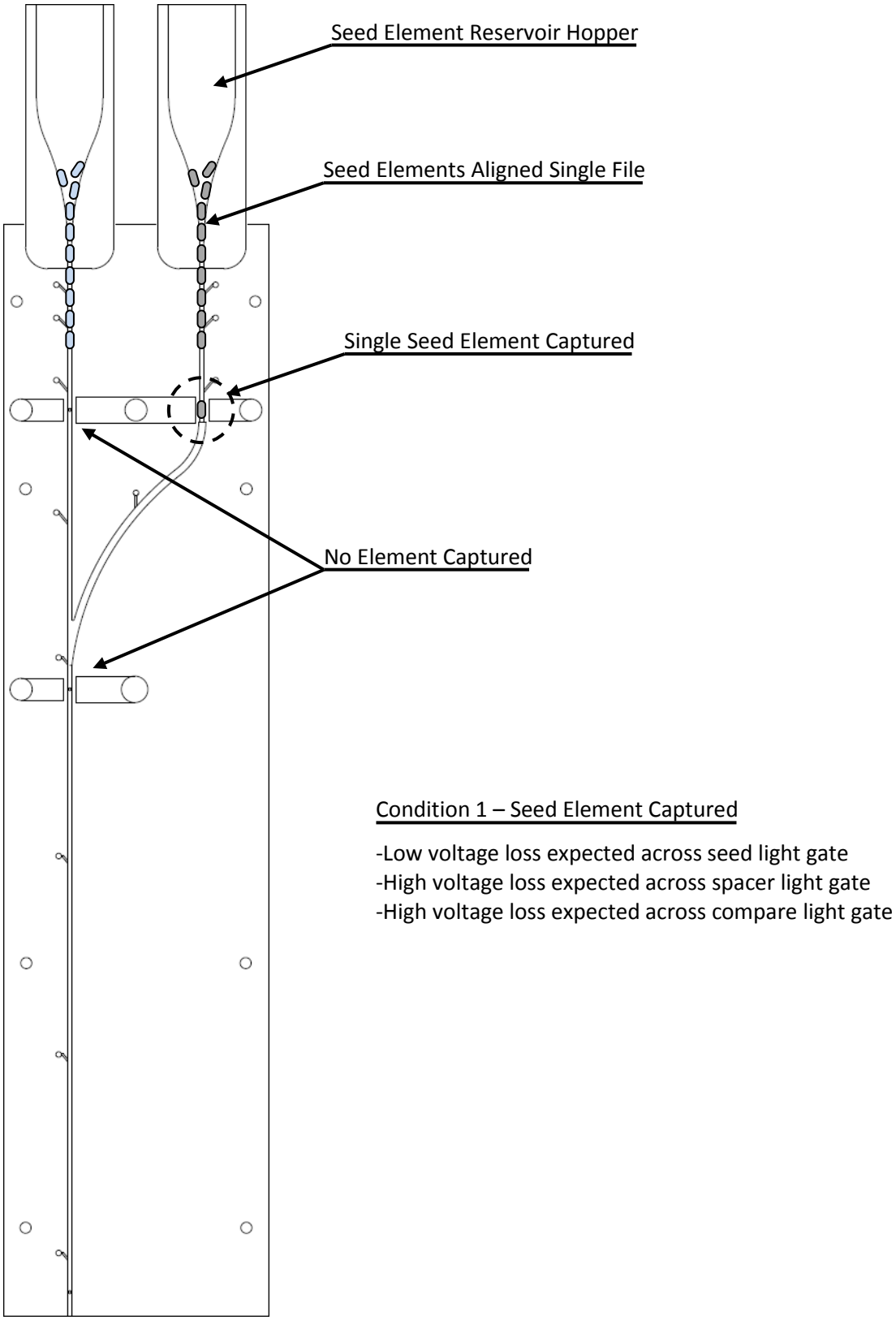

Figure 3.31: Illustration of Condition 1 data collection where element has been called from seed hopper and captured on the corresponding seed light gate area.

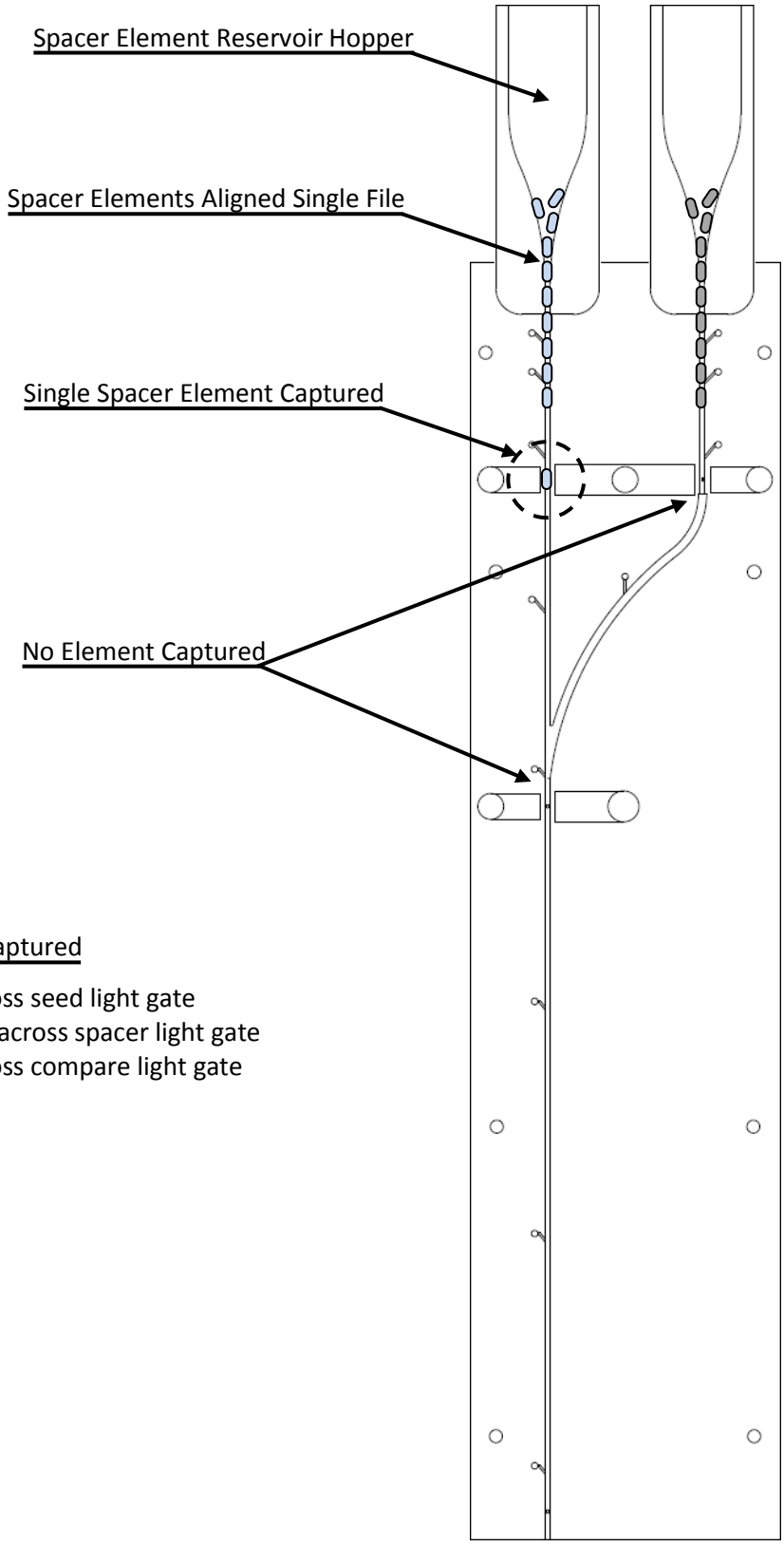

Condition 1 – Spacer Element Captured

-High voltage loss expected across seed light gate
-Medium voltage loss expected across spacer light gate
-High voltage loss expected across compare light gate

Figure 3.32: Illustration of Condition 1 data collection where element has been called from spacer hopper and captured on the corresponding spacer light gate area.

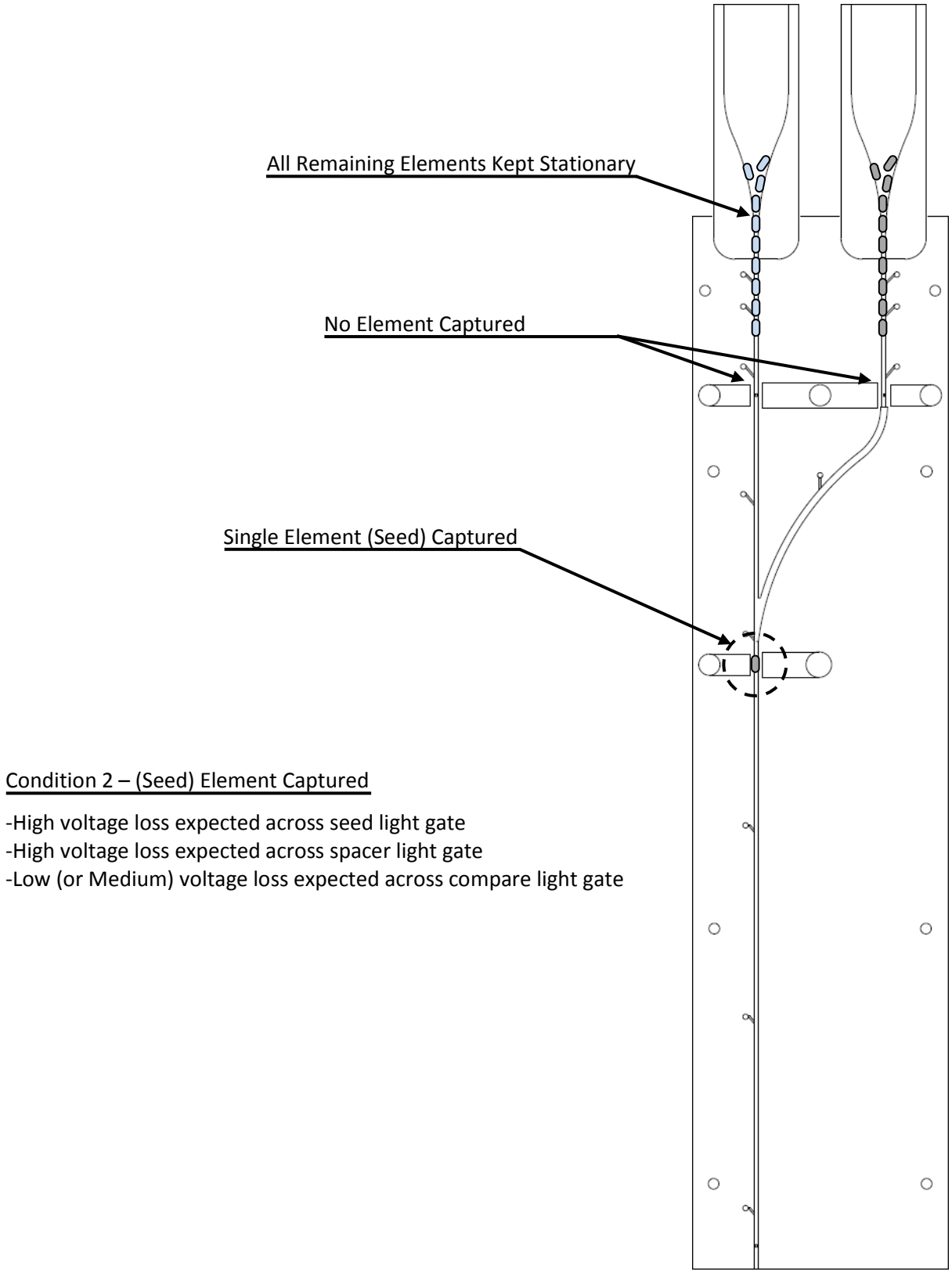

Figure 3.33: Illustration of Condition 2 data collection where element has been called (from seed hopper) and captured on the corresponding spacer light gate area.

Data sets collected based on voltage losses across light gates were separated based on individual trials and consisted of both condition 1 and condition 2 values. This separation was performed due to changes, both intentional and unintentional, found between trial runs of the constructed system. Intentional changes performed between these trials concerned the following factors: speed of actions, individual vacuum pressures, and individual air pressures. Notably, changes of individual vacuum pressures, air pressures, and normal voltage loss across light gates were performed in an attempt to provide a "best case scenario" in the loading of elements. Unintentional changes between trial runs of the system could have included, but were not limited to, changes in: temperature, humidity, light, and other known and unknown environmental factors.

3.7 Interpretation and Statistical Testing of Collected Data

The main focus of the performed statistical testing within this work was to determine if the light gate method of detection was feasible within the application of detecting element presence within the constructed system.

General statistical analysis.

Once recorded, data sets were subject to interpretation using general statistical formulas. These formulas were utilized to generate common values such as: mean (μ), standard deviations (σ), range (R), and sample size (n) for each individual data set. These common statistical values allowed for general interpretation and comparisons of the data sets.

Normal distribution interpretations.

As many data sets consisted of low sample numbers, normal distribution curves were generated from each light gate under each condition for each trial. In this use of

normal distribution curves were generated for each light gate under each condition. The use of normal distribution curves allowed the collected data sets to represent larger populations and their relationships to one another. To accomplish this task, compiled data sets were first subjected to the removal of errors from the data sets. In this removal of errors, skewness of the statistical results based on the data sets would be limited. However, attention has been paid to both the cause and result of these errors discussed later within this work in Chapter IV. The remaining data points were then subjected to interpretation into normal curves based on $\pm 3\sigma$. Data sets interpreted in this way would represent 95% of probable values based on the collected data. To interpret the collected data to that of $\pm 3\sigma$, μ and σ were referenced from each data set. In the calculations to acquire the normal distribution curves, a "rescale" value (r) was generated based on a scale of numbers ranging from -3 to 3 representing the desired $\pm 3\sigma$ range (x) along with the μ and σ of the individual data set. These rescaled values were calculated using the following formula:

$$r = \mu + (x * \sigma) \tag{3.1}$$

Calculated in this manner, rescaled values allowed for individual ranges to be applied to each data set. In essence, these rescaled values served to constrain the normal distribution curves within a specified range of values based on the recorded samples. This gave a corresponding scale of rescaled values for the desired $\pm 3\sigma$ range.
These rescaled values were then calculated according to the normal distribution equation with respect to probability density:

$$f(r;\mu,\sigma^2)=\frac{1}{\sqrt{2\pi\sigma^2}}e^{-(r-\mu)^2/(2\sigma^2)} \quad (3.2)$$

In these calculations, each rescaled value was assigned a probability based on the overall data set. Through graphing the rescaled values along the x axis and the normal distribution values along the y axis, a normal distribution curve for each of the data sets was achieved. In calculating the rescaled values through the normal distribution equation, a normal distribution value for each of the rescaled values could be achieved. The overall purpose of such calculations was to determine the probability of the rescaled value falling within the normal distribution curve according to the collected data. This interpretation allowed for a generalized graphical view of the rescaled ±3σ data set to the normal distribution data sets as they related to each other in the form on a multiple line graph. While this method of interpretation aided in the visual determination of separation between the data sets, it should not be taken as an absolute certainty in illustrating a proper exclusion between the recorded data sets. Rather, graphs calculated from the data sets in this manner should only be used as visual aids as the overarching population could conform to a non-normal distribution of values

Two-sample t tests.

Differing from the normal distribution graphical interpretation previously described, statistical testing using two-sample t tests were also performed on paired data sets according to light gate. Utilizing data sets with errors removed, two-sample t tests were used to determine if means of two paired data sets were statistically different from one another (NIST Engineering Statistics Handbook, 2010). This type of statistical test

was employed to determine if the mean of values recorded when an element was present at a light gate to the mean of those recorded when an element was not at a light gate were statistically different from one another. It was assumed that depending on the presence of an element, the means of the associated data sets would show or not show a difference in means. In this application, should a light gate observe an element at condition 1 while not observing an element at condition 2, the two-sample t test would show a statistical difference in means. The null hypothesis (H0) of these statistical tests were the following: where a data set with an element present (μ1) compared to a data set with an element present (μ2) would return no statistical difference.

$$H_0: \mu_{\text{Light Gate Condition 1}} = \mu_{\text{Light Gate Condition 2}}$$

The alternative hypothesis (Ha) stated that a data set with an element present (μ1) compared to a data set with an element not present (μ2) would return a statistical difference. Within the normal operations of the constructed device, this statistical non-difference of means would only be possible on one of the element light gates during a load from the opposing element light gate.

$$H_a: \mu_{\text{Light Gate Condition 1}} \neq \mu_{\text{Light Gate Condition 2}}$$

In these statistical comparisons, only data sets from individual light gates were evaluated against one another due to minuet preset voltage and manufacturing differences inherent between each light gate. Even with the attempt of the researcher to adjust the

voltage losses across all light gates to one another, it should be noted that errors could have been introduced if comparisons across light gates were made.

Using the two-sample t test, resulting p values were calculated from each light gate condition. These p-values related to statistical significance of a difference between the selected mean values. P-values from the two-sample t tests were compared to an alpha (α) value representing the confidence level within the statistical test. Within this work, α was selected at 0.05 or 95%. The α value of 0.05 translated to a 95% confidence that the selected mean values differed from one another.

$$p > \alpha : \ \mu_{\text{Light Gate Condition 1}} \neq \mu_{\text{Light Gate Condition 2}} \tag{3.3}$$

In this facet, should the p-value for any light gate comparison using the two-sample t test fall below that of 0.05, the means of the light gates would have been statistically different from condition 1 to condition 2 showing an element captured at one of the two conditions. Inferences based on voltage losses were then used to determine the condition in which the element capture occurred.

CHAPTER 4: RESULTS

In the following Chapter IV Results, all results from both the performed pilot test and the full scale initial testing of the completed non-mechanical brachytherapy element loading system as they pertain to this work have been presented. Results within this chapter consist of observations, raw data sets, interpreted data sets with general statistical values, calculated normal distribution curves, and performed statistical two-sample t tests. Each of these result sections has been detailed along with the presented results. It should be noted that results within this chapter are constant only to the current constructed system.

4.1 Observed Design Features

Pilot test.

The following details accepted and rejected features discovered within the pilot testing prior to the final device fabrication and assembly.

Pilot Testing Design Results

- Circular geometry allowed for greatest vacuum seal were needed.
- Flat geometry allowed for smoothest travel through system.
- Semi-circular geometry in element channels allowed for both vacuum seal and smooth travel.
- Two-piece construction allowed for proper machining of complex geometries.
- Hand-off method successful in application of introducing single element into system while holding remainder.

- Atmospheric venting of element channels required to isolate vacuum and air pressures.
- Light gate method of element detection showed positive results in initial application.
- Addition of positive air allowed for higher level of element control during travel through system.
- Vibration motor application appeared to have negligible impact on element travel.
- Orientation of semi-circular channel to allow for circular top and flat bottom found to have best results on element travel and capture.
- Vent design found to have minimal impact on element travel, “seating” elements within the vents.

Full scale system testing.

The following details accepted and rejected features discovered within the full scale system fabrication and assembly.

- Funnel type hopper successful in orientation and introduction of loose elements into main system in “stacked” orientation.
- Pilot tested features successful in introducing single element from either hopper into system on demand.
- Needle attachment section able to secure brachytherapy needle to automated system, utilizing existing threads.
- Automated program able to fill dosimetry pattern based on sequential control of vacuum and air lines.

- Originally machined acrylic main body pieces unsuitable due to machining error.
- Atmospheric vent design modified from parallel to perpendicular orientation to remove interaction with element travel.
- Secondary machined acrylic main body pieces successful in utilization within system meeting design intent.
- Data successfully gathered from light gates and recorded for data analysis.

Additionally, during the experimentation with the full scale device, it was found that spacer elements utilized in pilot testing had degraded to a point of non-usability and tended to break apart when manipulated using either manual or automated means. This observation of spacer degradation was attributed to exposure of the biodegradable spacer material to normal atmospheric conditions during pilot testing. It is believed that this caused the spacer material to undergo a degradation process. Due to this unsatisfactory spacer element degradation, only seed elements were utilized in the initial device testing and were poured into both hopper sections simulated the loading of two element types. Observations from normal working of the system found that seed elements were readily loaded from each hopper of the device. No jams or catastrophic failures of the device resulting in disassembly were recorded during all performed tests. However, failures to load proper elements were observed. Those element loading failures have been detailed within the following section.

4.2 Raw Light Gate Data

The following raw data represents values gathered from all trials executed using the automated non-mechanical element loading device. These trials were gathered under

four trials including: the loading of single type elements, the loading of both element types using a small-scale randomized dosimetry program, the loading of both element types using a large-scale randomized dosimetry program, and finally a higher sequence speed using single element loading. These trials are exploratory in nature and were thought to express a general representation of the systems functions.

Single element type trials.

The following *table 4.1* and *table 4.2* represent the raw data collected from trial runs concerning the automated loading of elements from a single hopper. In these trials, seed elements were loaded into only one of the two hoppers and the automated control system was programmed to request only elements from the selected area. *Table 4.1* shows data collected through voltage loss across all light gates at the previously discussed two conditions using the automated system to load seed elements from only the seed element hopper with seed elements. Errors within the loading process have been highlighted to show improper loads.

Table 4.1

Raw Voltage Loss Data Concerning Single Line Loading Trials Utilizing Seed Elements and Seed Channel

	Condition 1			Condition 2		
Run	Light Gate Seed	Light Gate Spacer	Light Gate Compare	Light Gate Seed	Light Gate Spacer	Light Gate Compare
1	-1.333	-1.346	-1.349	-1.35	-1.35	-1.312
2	-1.318	-1.348	-1.345	-1.347	-1.347	-1.311
3	-1.318	-1.348	-1.347	-1.351	-1.349	-1.314
4	-1.321	-1.349	-1.346	-1.35	-1.346	-1.313
5	-1.317	-1.347	-1.345	-1.349	-1.348	-1.347
6	-1.318	-1.348	-1.346	-1.349	-1.348	-1.311
7	-1.317	-1.349	-1.346	-1.348	-1.345	-1.315

8	-1.319	-1.348	-1.346	-1.35	-1.349	-1.312
9	-1.321	-1.348	-1.348	-1.348	-1.35	-1.313
10	-1.318	-1.348	-1.347	-1.347	-1.345	-1.313
11	-1.321	-1.347	-1.347	-1.35	-1.346	-1.312
12	-1.321	-1.348	-1.346	-1.35	-1.348	-1.33
13	-1.317	-1.348	-1.345	-1.35	-1.348	-1.312
14	-1.319	-1.347	-1.346	-1.349	-1.347	-1.312
15	-1.321	-1.348	-1.345	-1.35	-1.348	-1.31
16	-1.317	-1.346	-1.345	-1.349	-1.349	-1.315
17	-1.32	-1.346	-1.348	-1.35	-1.346	-1.315
18	-1.316	-1.348	-1.347	-1.349	-1.347	-1.31
19	-1.316	-1.346	-1.345	-1.349	-1.347	-1.311
20	-1.319	-1.347	-1.346	-1.348	-1.348	-1.31
21	-1.316	-1.346	-1.345	-1.349	-1.344	-1.328
22	-1.321	-1.345	-1.345	-1.348	-1.346	-1.31
23	-1.317	-1.345	-1.347	-1.349	-1.346	-1.31
24	-1.35	-1.349	-1.347	-1.35	-1.35	-1.346

Note. Trials with unsatisfactory results or errors have been highlighted above.

The following lists explanations for data omission of the highlighted values in *table 4.1*.

Run 1 – Values not properly updated within automated program.

Run 5 – Air pressures within system too high causing seed element to bypass comparison light gate.

Run 24 – Only one seed element left within system. Last element recaptured by previous vacuum line within presence of trailing elements.

Table 4.2 shows data collected through voltage loss across all light gates at the previously discussed two conditions using the automated system to load seed elements from only the spacer element hopper loaded with seed elements. Errors within the loading process have been highlighted to show improper loads.

Table 4.2

Raw Voltage Loss Data Concerning Single Line Loading Trials Utilizing Seed Elements and Spacer Channel

Run	Condition 1			Condition 2		
	Light Gate Seed	Light Gate Spacer	Light Gate Compare	Light Gate Seed	Light Gate Spacer	Light Gate Compare
1	-1.35	-1.35	-1.349	-1.349	-1.35	-1.347
2	-1.35	-1.32	-1.346	-1.35	-1.349	-1.29
3	-1.35	-1.321	-1.349	-1.35	-1.346	-1.33
4	-1.35	-1.321	-1.346	-1.353	-1.349	-1.321
5	-1.349	-1.323	-1.346	-1.35	-1.347	-1.33
6	-1.35	-1.32	-1.348	-1.351	-1.347	-1.33
7	-1.35	-1.321	-1.345	-1.35	-1.348	-1.319
8	-1.35	-1.323	-1.345	-1.35	-1.35	-1.326
9	-1.349	-1.321	-1.344	-1.35	-1.348	-1.321
10	-1.35	-1.324	-1.345	-1.35	-1.349	-1.32
11	-1.35	-1.32	-1.345	-1.349	-1.349	-1.315
12	-1.349	-1.32	-1.345	-1.351	-1.35	-1.328
13	-1.35	-1.32	-1.345	-1.35	-1.349	-1.327
14	-1.351	-1.317	-1.341	-1.348	-1.347	-1.342
15	-1.348	-1.317	-1.345	-1.349	-1.35	-1.327
16	-1.35	-1.32	-1.344	-1.348	-1.348	-1.313
17	-1.35	-1.318	-1.343	-1.352	-1.346	-1.327
18	-1.349	-1.319	-1.343	-1.35	-1.348	-1.344
19	-1.349	-1.316	-1.345	-1.35	-1.316	-1.344
20	-1.35	-1.312	-1.345	-1.35	-1.348	-1.312
21	-1.349	-1.314	-1.344	-1.349	-1.348	-1.312

Note. Trials with unsatisfactory results or errors have been highlighted above.

The following lists explanations for data omission of the highlighted values in *table 4.2.*

Run 1 – Values not properly updated within automated program.

Run 14 – Air pressures within system too high causing seed element to bypass comparison light gate.

Run 18 – Air pressures within system too high causing seed element to bypass comparison light gate.

Run 21 – Only one seed element left within system. Last element recaptured by previous vacuum line within presence of trailing elements.

Small random dosimetry trial runs.

The following *table 4.3* represents the raw data collected from trial runs concerning the automated loading of elements from a randomized dosimetry plan. This random dosimetry plan consisted of five needles with a random number of elements between ten and twenty. In these trials, seed elements were loaded into both of the two hoppers and the automated control system was programmed to call elements based on the random dosimetry plan. *Table 4.3* shows raw data collected through voltage loss across all light gates at the previously discussed two conditions using the automated system to load seed elements. Errors within the loading process have been highlighted to show improper loads.

Table 4.3

Raw Voltage Loss Data Concerning Small Scale Randomized Dosimetry Pattern Utilizing Seed Elements and Both Seed and Spacer Channels

				Condition 1			Condition 2		
Run	Needle	#	Type	Gate Seed	Gate Spacer	Gate Comp.	Gate Seed	Gate Spacer	Gate Comp.
1	1	1	Seed	-1.314	-1.349	-1.347	-1.349	-1.347	-1.31
2	1	2	Seed	-1.318	-1.348	-1.346	-1.349	-1.346	-1.32
3	1	3	Spacer	-1.35	-1.316	-1.346	-1.348	-1.346	-1.327
4	1	4	Spacer	-1.35	-1.319	-1.345	-1.35	-1.347	-1.312
5	1	5	Spacer	-1.349	-1.316	-1.347	-1.351	-1.348	-1.347
6	1	6	Spacer	-1.35	-1.317	-1.346	-1.349	-1.346	-1.348
7	1	7	Spacer	-1.35	-1.316	-1.346	-1.35	-1.349	-1.312
8	1	8	Spacer	-1.347	-1.316	-1.344	-1.349	-1.347	-1.321

9	1	9	Spacer	-1.349	-1.32	-1.347	-1.352	-1.347	-1.315
10	1	10	Spacer	-1.349	-1.346	-1.347	-1.349	-1.346	-1.345
11	1	11	Seed	-1.319	-1.35	-1.346	-1.348	-1.35	-1.315
12	2	1	Spacer	-1.349	-1.318	-1.345	-1.349	-1.346	-1.329
13	2	2	Seed	-1.319	-1.347	-1.345	-1.348	-1.346	-1.346
14	2	3	Spacer	-1.349	-1.316	-1.345	-1.349	-1.345	-1.33
15	2	4	Seed	-1.317	-1.346	-1.346	-1.349	-1.347	-1.315
16	2	5	Spacer	-1.348	-1.316	-1.344	-1.348	-1.346	-1.324
17	2	6	Spacer	-1.349	-1.319	-1.346	-1.349	-1.348	-1.324
18	2	7	Seed	-1.322	-1.347	-1.344	-1.35	-1.346	-1.329
19	2	8	Spacer	-1.35	-1.319	-1.347	-1.349	-1.346	-1.314
20	2	9	Seed	-1.318	-1.349	-1.346	-1.348	-1.345	-1.31
21	2	10	Seed	-1.319	-1.348	-1.345	-1.35	-1.347	-1.31
22	2	11	Seed	-1.318	-1.345	-1.347	-1.349	-1.345	-1.311
23	3	1	Seed	-1.319	-1.349	-1.345	-1.349	-1.347	-1.308
24	3	2	Seed	-1.315	-1.346	-1.346	-1.348	-1.344	-1.327
25	3	3	Seed	-1.319	-1.348	-1.345	-1.35	-1.345	-1.316
26	3	4	Spacer	-1.348	-1.316	-1.346	-1.349	-1.346	-1.326
27	3	5	Seed	-1.316	-1.347	-1.345	-1.35	-1.344	-1.321
28	3	6	Seed	-1.316	-1.346	-1.345	-1.35	-1.346	-1.314
29	3	7	Seed	-1.321	-1.347	-1.345	-1.349	-1.345	-1.31
30	3	8	Spacer	-1.35	-1.314	-1.344	-1.349	-1.346	-1.328
31	3	9	Seed	-1.317	-1.348	-1.346	-1.348	-1.346	-1.325
32	3	10	Seed	-1.321	-1.346	-1.346	-1.35	-1.347	-1.324
33	3	11	Seed	-1.321	-1.346	-1.345	-1.35	-1.344	-1.346
34	4	1	Seed	-1.317	-1.346	-1.344	-1.35	-1.345	-1.327
35	4	2	Spacer	-1.35	-1.319	-1.346	-1.349	-1.345	-1.345
36	4	3	Seed	-1.316	-1.345	-1.345	-1.35	-1.346	-1.314
37	4	4	Seed	-1.319	-1.35	-1.345	-1.349	-1.346	-1.322
38	4	5	Spacer	-1.35	-1.316	-1.344	-1.349	-1.346	-1.293
39	4	6	Seed	-1.318	-1.346	-1.346	-1.349	-1.346	-1.312
40	4	7	Spacer	-1.35	-1.317	-1.344	-1.351	-1.348	-1.327
41	4	8	Seed	-1.319	-1.345	-1.344	-1.347	-1.347	-1.314
42	4	9	Spacer	-1.35	-1.317	-1.345	-1.349	-1.344	-1.345
43	4	10	Spacer	-1.348	-1.318	-1.345	-1.349	-1.347	-1.315
44	4	11	Seed	-1.321	-1.347	-1.346	-1.348	-1.347	-1.325
45	4	12	Seed	-1.321	-1.346	-1.345	-1.348	-1.345	-1.31
46	5	1	Spacer	-1.35	-1.316	-1.345	-1.349	-1.346	-1.323
47	5	2	Spacer	-1.35	-1.319	-1.345	-1.35	-1.35	-1.314
48	5	3	Spacer	-1.349	-1.314	-1.346	-1.347	-1.349	-1.316
49	5	4	Seed	-1.318	-1.346	-1.345	-1.346	-1.345	-1.318
50	5	5	Spacer	-1.348	-1.318	-1.345	-1.353	-1.345	-1.316
51	5	6	Spacer	-1.349	-1.322	-1.344	-1.35	-1.345	-1.312
52	5	7	Spacer	-1.348	-1.316	-1.345	-1.349	-1.345	-1.324
53	5	8	Seed	-1.326	-1.347	-1.344	-1.349	-1.345	-1.327

54	5	9	Spacer	-1.35	-1.317	-1.347	-1.35	-1.345	-1.31
55	5	10	Seed	-1.318	-1.344	-1.346	-1.35	-1.344	-1.31
56	5	11	Spacer	-1.348	-1.317	-1.344	-1.349	-1.345	-1.312
57	5	12	Spacer	-1.348	-1.315	-1.346	-1.348	-1.347	-1.329

Note. Trials with unsatisfactory results or errors have been highlighted above.

The following lists explanations for data omission of the highlighted values in *table 4.3.*

Run 5 – Air pressures within system too high causing seed element to bypass comparison light gate.

Run 6 – Air pressures within system too high causing seed element to bypass comparison light gate.

Run 10 – System failed to load from spacer line due to error in automated program timing.

Run 13 – Air pressures within system too high causing seed element to bypass comparison light gate.

Run 33 – Air pressures within system too high causing seed element to bypass comparison light gate.

Run 35 – Air pressures within system too high causing seed element to bypass comparison light gate.

Run 38 – “Double load” observed. Two elements from single line entered into system when specific element was called by automated program.

Run 42 – Air pressures within system too high causing seed element to bypass comparison light gate.

Large random dosimetry trials.

The following *table 4.4* represents the raw data collected from trial runs concerning the automated loading of elements from a randomized dosimetry plan. This random dosimetry plan consisted of five needles with a random number of elements between ten and twenty. In these trials, seed elements were loaded into both of the two hoppers and the automated control system was programmed to call elements based on the random dosimetry plan. *Table 4.4* shows raw data collected through voltage loss across all light gates at the previously discussed two conditions using the automated system to load seed elements. Errors within the loading process have been highlighted to show improper loads.

Table 4.4

Raw Voltage Loss Data Concerning Large Scale Randomized Dosimetry Pattern Utilizing Seed Elements and Both Seed and Spacer Channels

				Condition 1			Condition 2		
Run	Needle	#	Type	Gate Seed	Gate Spacer	Gate Comp.	Gate Seed	Gate Spacer	Gate Comp.
1	1	1	Seed	-1.326	-1.35	-1.35	-1.349	-1.35	-1.311
2	1	2	Spacer	-1.349	-1.325	-1.35	-1.348	-1.351	-1.334
3	1	3	Seed	-1.317	-1.35	-1.35	-1.348	-1.351	-1.33
4	1	4	Seed	-1.32	-1.35	-1.351	-1.349	-1.35	-1.333
5	1	5	Seed	-1.321	-1.35	-1.35	-1.35	-1.35	-1.32
6	1	6	Seed	-1.317	-1.353	-1.35	-1.349	-1.35	-1.33
7	1	7	Spacer	-1.348	-1.32	-1.35	-1.349	-1.35	-1.305
8	1	8	Seed	-1.319	-1.35	-1.349	-1.349	-1.35	-1.329
9	1	9	Seed	-1.315	-1.35	-1.349	-1.348	-1.353	-1.316
10	1	10	Seed	-1.318	-1.351	-1.35	-1.35	-1.35	-1.317
11	2	1	Seed	-1.318	-1.349	-1.349	-1.348	-1.35	-1.325
12	2	2	Spacer	-1.348	-1.32	-1.35	-1.349	-1.351	-1.315
13	2	3	Seed	-1.316	-1.35	-1.351	-1.348	-1.352	-1.328
14	2	4	Spacer	-1.349	-1.323	-1.35	-1.35	-1.35	-1.33

15	2	5	Seed	-1.316	-1.349	-1.35	-1.349	-1.35	-1.33
16	2	6	Spacer	-1.349	-1.326	-1.349	-1.349	-1.35	-1.33
17	2	7	Seed	-1.325	-1.352	-1.35	-1.347	-1.351	-1.314
18	2	8	Spacer	-1.35	-1.319	-1.351	-1.349	-1.349	-1.32
19	2	9	Spacer	-1.349	-1.319	-1.35	-1.348	-1.351	-1.326
20	2	10	Spacer	-1.349	-1.322	-1.35	-1.349	-1.35	-1.322
21	2	11	Seed	-1.319	-1.35	-1.35	-1.35	-1.35	-1.324
22	3	1	Spacer	-1.348	-1.321	-1.35	-1.348	-1.35	-1.33
23	3	2	Seed	-1.316	-1.35	-1.35	-1.349	-1.35	-1.35
24	3	3	Seed	-1.319	-1.35	-1.349	-1.347	-1.35	-1.33
25	3	4	Spacer	-1.35	-1.325	-1.349	-1.348	-1.35	-1.35
26	3	5	Seed	-1.32	-1.35	-1.35	-1.349	-1.351	-1.32
27	3	6	Seed	-1.316	-1.35	-1.35	-1.349	-1.35	-1.33
28	3	7	Seed	-1.32	-1.35	-1.349	-1.35	-1.35	-1.32
29	3	8	Seed	-1.316	-1.35	-1.35	-1.35	-1.351	-1.331
30	3	9	Seed	-1.315	-1.35	-1.349	-1.349	-1.35	-1.33
31	3	10	Seed	-1.318	-1.35	-1.349	-1.349	-1.348	-1.323
32	3	11	Seed	-1.315	-1.351	-1.35	-1.347	-1.35	-1.315
33	4	1	Seed	-1.32	-1.35	-1.35	-1.348	-1.35	-1.316
34	4	2	Seed	-1.35	-1.35	-1.35	-1.349	-1.35	-1.35
35	4	3	Seed	-1.322	-1.353	-1.35	-1.349	-1.35	-1.314
36	4	4	Seed	-1.318	-1.349	-1.35	-1.35	-1.351	-1.319
37	4	5	seed	-1.321	-1.35	-1.35	-1.347	-1.35	-1.333
38	4	6	Spacer	-1.35	-1.325	-1.35	-1.348	-1.35	-1.327
39	4	7	Seed	-1.313	-1.352	-1.349	-1.349	-1.35	-1.312
40	4	8	Spacer	-1.348	-1.321	-1.35	-1.348	-1.35	-1.335
41	4	9	Seed	-1.317	-1.35	-1.35	-1.349	-1.351	-1.321
42	4	10	Spacer	-1.35	-1.321	-1.35	-1.349	-1.352	-1.317
43	5	1	Spacer	-1.349	-1.321	-1.35	-1.349	-1.35	-1.321
44	5	2	Spacer	-1.349	-1.322	-1.35	-1.348	-1.35	-1.332
45	5	3	Spacer	-1.35	-1.319	-1.35	-1.35	-1.35	-1.33
46	5	4	Spacer	-1.348	-1.322	-1.35	-1.35	-1.35	-1.349
47	5	5	Spacer	-1.348	-1.32	-1.349	-1.349	-1.352	-1.332
48	5	6	Spacer	-1.349	-1.327	-1.35	-1.348	-1.35	-1.332
49	5	7	Spacer	-1.348	-1.321	-1.35	-1.348	-1.35	-1.319
50	5	8	Spacer	-1.347	-1.318	-1.349	-1.35	-1.352	-1.319
51	5	9	Spacer	-1.348	-1.321	-1.35	-1.349	-1.351	-1.332
52	5	10	Seed	-1.32	-1.35	-1.35	-1.348	-1.349	-1.324
53	5	11	Spacer	-1.35	-1.321	-1.349	-1.349	-1.35	-1.321
54	5	12	Seed	-1.313	-1.35	-1.349	-1.349	-1.351	-1.329
55	5	13	Spacer	-1.347	-1.325	-1.35	-1.35	-1.35	-1.33
56	5	14	Seed	-1.319	-1.35	-1.35	-1.348	-1.35	-1.33
57	5	15	Spacer	-1.348	-1.321	-1.35	-1.35	-1.35	-1.323
58	5	16	Spacer	-1.348	-1.324	-1.349	-1.35	-1.347	-1.317
59	6	1	Seed	-1.318	-1.35	-1.349	-1.348	-1.35	-1.323

60	6	2	Spacer	-1.348	-1.321	-1.35	-1.35	-1.35	-1.331
61	6	3	Spacer	-1.349	-1.324	-1.349	-1.348	-1.349	-1.322
62	6	4	Spacer	-1.348	-1.35	-1.35	-1.35	-1.349	-1.35
63	6	5	Spacer	-1.348	-1.318	-1.349	-1.348	-1.349	-1.329
64	6	6	Spacer	-1.35	-1.321	-1.35	-1.35	-1.351	-1.329
65	6	7	Spacer	-1.348	-1.318	-1.35	-1.349	-1.35	-1.329
66	6	8	Seed	-1.314	-1.351	-1.35	-1.348	-1.35	-1.314
67	6	9	Spacer	-1.349	-1.321	-1.349	-1.348	-1.348	-1.33
68	6	10	Seed	-1.324	-1.35	-1.35	-1.349	-1.35	-1.31
69	7	1	Spacer	-1.35	-1.323	-1.349	-1.349	-1.351	-1.328
70	7	2	Spacer	-1.348	-1.321	-1.349	-1.35	-1.35	-1.316
71	7	3	Spacer	-1.348	-1.322	-1.349	-1.348	-1.35	-1.35
72	7	4	Spacer	-1.349	-1.324	-1.35	-1.349	-1.35	-1.321
73	7	5	Spacer	-1.349	-1.32	-1.35	-1.348	-1.35	-1.316
74	7	6	Seed	-1.314	-1.35	-1.35	-1.348	-1.349	-1.329
75	7	7	Spacer	-1.348	-1.321	-1.35	-1.348	-1.35	-1.327
76	7	8	Spacer	-1.35	-1.326	-1.349	-1.349	-1.353	-1.321
77	7	9	Seed	-1.319	-1.351	-1.35	-1.347	-1.35	-1.311
78	7	10	Seed	-1.315	-1.35	-1.35	-1.348	-1.35	-1.33
79	8	1	Seed	-1.318	-1.35	-1.35	-1.349	-1.35	-1.314
80	8	2	Spacer	-1.35	-1.324	-1.35	-1.349	-1.35	-1.319
81	8	3	Seed	-1.316	-1.35	-1.35	-1.346	-1.35	-1.33
82	8	4	Seed	-1.322	-1.35	-1.35	-1.349	-1.35	-1.319
83	8	5	Seed	-1.321	-1.35	-1.349	-1.348	-1.35	-1.312
84	8	6	Seed	-1.319	-1.35	-1.35	-1.348	-1.349	-1.315
85	8	7	Spacer	-1.35	-1.324	-1.35	-1.35	-1.353	-1.322
86	8	8	Seed	-1.316	-1.348	-1.35	-1.349	-1.349	-1.331
87	8	9	Seed	-1.321	-1.351	-1.35	-1.35	-1.348	-1.317
88	8	10	Seed	-1.321	-1.35	-1.349	-1.347	-1.35	-1.315
89	9	1	Spacer	-1.35	-1.325	-1.35	-1.348	-1.354	-1.316
90	9	2	Seed	-1.319	-1.35	-1.35	-1.35	-1.35	-1.311
91	9	3	Seed	-1.325	-1.35	-1.35	-1.35	-1.353	-1.318
92	9	4	Seed	-1.323	-1.35	-1.35	-1.348	-1.35	-1.323
93	9	5	Spacer	-1.35	-1.322	-1.35	-1.349	-1.349	-1.328
94	9	6	Spacer	-1.35	-1.326	-1.35	-1.35	-1.35	-1.334
95	9	7	Seed	-1.316	-1.35	-1.35	-1.349	-1.352	-1.33
96	9	8	Seed	-1.312	-1.35	-1.351	-1.349	-1.35	-1.332
97	9	9	Spacer	-1.348	-1.321	-1.351	-1.347	-1.35	-1.349
98	9	10	Seed	-1.348	-1.349	-1.349	-1.348	-1.35	-1.348
99	9	11	Seed	-1.316	-1.35	-1.35	-1.35	-1.349	-1.315
100	9	12	Seed	-1.311	-1.35	-1.35	-1.348	-1.349	-1.313
101	9	13	Spacer	-1.346	-1.32	-1.35	-1.347	-1.35	-1.33
102	10	1	Seed	-1.316	-1.35	-1.35	-1.346	-1.35	-1.315
103	10	2	Seed	-1.314	-1.351	-1.35	-1.348	-1.35	-1.311
104	10	3	Spacer	-1.347	-1.321	-1.349	-1.346	-1.349	-1.321

105	10	4	Seed	-1.314	-1.349	-1.349	-1.349	-1.35	-1.33
106	10	5	Spacer	-1.349	-1.318	-1.35	-1.346	-1.35	-1.317
107	10	6	Seed	-1.312	-1.349	-1.35	-1.348	-1.35	-1.325
108	10	7	Seed	-1.316	-1.351	-1.349	-1.347	-1.349	-1.32
109	10	8	Spacer	-1.348	-1.326	-1.35	-1.348	-1.351	-1.329
110	10	9	Spacer	-1.347	-1.319	-1.348	-1.346	-1.349	-1.329
111	10	10	Seed	-1.316	-1.349	-1.349	-1.348	-1.35	-1.32

Note. Trials with unsatisfactory results or errors have been highlighted above.

The following lists explanations for data omission of the highlighted values in *table 4.4.*

Run 23 – Air pressures within system too high causing seed element to bypass comparison light gate.

Run 25 – Air pressures within system too high causing seed element to bypass comparison light gate.

Run 34 – System failed to feed element once called by automated program.

Run 40 – Air pressures within system too high causing seed element to bypass comparison light gate.

Run 46 – Vacuum pressures within system too high causing seed element to be recaptured once released from the initial light gate area.

Run 62 – Only one seed element in line within system. Trailing element needed to prevent recaptured by previous vacuum line. Seed element unreleased from hand-off area.

Run 71 – Air pressures within system too high causing seed element to bypass comparison light gate.

Run 97 – Air pressures within system too high causing seed element to bypass comparison light gate.

Run 98 – Only one seed element in line within system. Trailing element needed to prevent recaptured by previous vacuum line. Seed element unreleased from hand-off area.

Single element type high speed trials.

The following *table 4.5* and *table 4.6* represent the raw data collected from trial runs concerning the automated loading of elements from a single hopper at higher speeds than other trials. Specifically, speeds between operations were set at 0.2 seconds between normal operations rather than the normal 0.4 seconds as in previous trials. In these trials, seed elements were loaded into only one of the two hoppers and the automated control system was programmed to call elements from the selected area. *Table 4.5* shows data collected through voltage loss across all light gates at the previously discussed two conditions using the automated system to load elements from only the seed element hopper loaded with seed elements. Errors within the loading process have been highlighted to show improper loads.

Table 4.5

Raw Voltage Loss Data Concerning Single Line Loading Trials with Higher Speed of Operations Utilizing Seed Elements and Spacer Channel

	Condition 1			Condition 2		
Run	Light Gate Seed	Light Gate Spacer	Light Gate Compare	Light Gate Seed	Light Gate Spacer	Light Gate Compare
1	-1.32	-1.352	-1.35	-1.348	-1.351	-1.313
2	-1.312	-1.35	-1.349	-1.346	-1.35	-1.33
3	-1.315	-1.35	-1.349	-1.348	-1.35	-1.321
4	-1.309	-1.318	-1.346	-1.344	-1.346	-1.298
5	-1.302	-1.345	-1.346	-1.348	-1.35	-1.33
6	-1.317	-1.348	-1.35	-1.347	-1.347	-1.35

7	-1.316	-1.347	-1.349	-1.348	-1.35	-1.329
8	-1.311	-1.351	-1.349	-1.347	-1.35	-1.311
9	-1.303	-1.346	-1.345	-1.344	-1.345	-1.299
10	-1.302	-1.346	-1.344	-1.344	-1.345	-1.306
11	-1.308	-1.346	-1.347	-1.343	-1.348	-1.321
12	-1.344	-1.347	-1.347	-1.344	-1.345	-1.346
13	-1.303	-1.346	-1.346	-1.344	-1.346	-1.31
14	-1.304	-1.346	-1.344	-1.343	-1.344	-1.311
15	-1.298	-1.345	-1.348	-1.344	-1.344	-1.31
16	-1.304	-1.346	-1.346	-1.344	-1.345	-1.31
17	-1.303	-1.345	-1.346	-1.344	-1.348	-1.322
18	-1.308	-1.309	-1.345	-1.344	-1.344	-1.323
19	-1.3	-1.348	-1.345	-1.346	-1.345	-1.305
20	-1.315	-1.348	-1.349	-1.347	-1.35	-1.316
21	-1.315	-1.35	-1.349	-1.347	-1.35	-1.319
22	-1.317	-1.35	-1.35	-1.347	-1.35	-1.324
23	-1.317	-1.348	-1.35	-1.346	-1.35	-1.315
24	-1.316	-1.35	-1.349	-1.348	-1.349	-1.33
25	-1.317	-1.349	-1.349	-1.347	-1.349	-1.32
26	-1.312	-1.35	-1.349	-1.349	-1.35	-1.313
27	-1.31	-1.349	-1.35	-1.348	-1.348	-1.318
28	-1.315	-1.35	-1.35	-1.348	-1.35	-1.328
29	-1.314	-1.349	-1.349	-1.347	-1.35	-1.331
30	-1.316	-1.351	-1.347	-1.347	-1.349	-1.319
31	-1.316	-1.35	-1.35	-1.347	-1.352	-1.33
32	-1.316	-1.35	-1.351	-1.348	-1.35	-1.327
33	-1.32	-1.348	-1.349	-1.348	-1.351	-1.329

Note. Trials with unsatisfactory results or errors have been highlighted above.

The following lists explanations for data omission of the highlighted values in *table 4.5*.

Run 4 – Seed elements loaded from both hoppers. Both elements successfully captured by comparison light gate.

Run 6 – Air pressures within system too high causing seed element to bypass comparison light gate.

Run 12 – System failed to feed element once called by automated program.

Run 18 – Seed elements loaded from both hoppers. Both elements successfully captured by comparison light gate.

Table 4.6 shows data collected through voltage loss across all light gates at the previously discussed two conditions using the automated system to load elements from only the spacer element hopper loaded with seed elements. Errors within the loading process have been highlighted to show improper loads.

Table 4.6

Raw Voltage Loss Data Concerning Single Line Loading Trials with Higher Speed of Operations Utilizing Seed Elements and Spacer Channel

Run	Condition 1			Condition 2		
	Light Gate Seed	Light Gate Spacer	Light Gate Compare	Light Gate Seed	Light Gate Spacer	Light Gate Compare
1	-1.345	-1.313	-1.35	-1.349	-1.35	-1.33
2	-1.347	-1.32	-1.35	-1.348	-1.35	-1.321
3	-1.344	-1.311	-1.346	-1.344	-1.345	-1.326
4	-1.344	-1.31	-1.345	-1.344	-1.345	-1.318
5	-1.343	-1.305	-1.345	-1.345	-1.345	-1.31
6	-1.344	-1.308	-1.344	-1.345	-1.345	-1.323
7	-1.344	-1.305	-1.345	-1.344	-1.345	-1.326
8	-1.344	-1.312	-1.346	-1.344	-1.349	-1.315
9	-1.344	-1.306	-1.344	-1.344	-1.345	-1.311
10	-1.344	-1.31	-1.347	-1.344	-1.348	-1.315
11	-1.344	-1.316	-1.347	-1.344	-1.345	-1.309
12	-1.344	-1.309	-1.345	-1.343	-1.346	-1.324
13	-1.344	-1.31	-1.345	-1.344	-1.346	-1.324
14	-1.344	-1.306	-1.347	-1.344	-1.346	-1.32
15	-1.344	-1.309	-1.344	-1.344	-1.345	-1.312
16	-1.344	-1.306	-1.345	-1.343	-1.346	-1.317
17	-1.344	-1.314	-1.345	-1.344	-1.345	-1.31
18	-1.344	-1.307	-1.345	-1.344	-1.346	-1.321
19	-1.344	-1.305	-1.348	-1.344	-1.345	-1.308
20	-1.343	-1.313	-1.346	-1.344	-1.346	-1.323
21	-1.344	-1.306	-1.346	-1.344	-1.347	-1.326
22	-1.344	-1.316	-1.347	-1.343	-1.346	-1.315
23	-1.344	-1.31	-1.345	-1.344	-1.347	-1.322
24	-1.343	-1.307	-1.345	-1.344	-1.347	-1.31

25	-1.344	-1.307	-1.346	-1.344	-1.346	-1.315
26	-1.344	-1.306	-1.346	-1.344	-1.348	-1.324
27	-1.344	-1.306	-1.345	-1.344	-1.346	-1.31
28	-1.344	-1.31	-1.346	-1.344	-1.345	-1.31
29	-1.344	-1.304	-1.347	-1.344	-1.348	-1.32
30	-1.344	-1.309	-1.345	-1.344	-1.346	-1.348
31	-1.344	-1.308	-1.346	-1.344	-1.345	-1.327
32	-1.344	-1.308	-1.347	-1.344	-1.346	-1.312
33	-1.344	-1.306	-1.346	-1.344	-1.346	-1.321
34	-1.343	-1.309	-1.347	-1.343	-1.345	-1.326
35	-1.344	-1.308	-1.345	-1.344	-1.347	-1.314
36	-1.344	-1.309	-1.345	-1.343	-1.345	-1.315
37	-1.345	-1.307	-1.348	-1.344	-1.346	-1.324
38	-1.344	-1.306	-1.344	-1.343	-1.345	-1.31
39	-1.344	-1.31	-1.348	-1.343	-1.347	-1.315
40	-1.344	-1.308	-1.347	-1.343	-1.344	-1.328
41	-1.344	-1.306	-1.345	-1.344	-1.346	-1.31
42	-1.344	-1.308	-1.347	-1.344	-1.345	-1.319
43	-1.344	-1.315	-1.345	-1.347	-1.35	-1.32
44	-1.348	-1.315	-1.349	-1.349	-1.35	-1.33
45	-1.349	-1.317	-1.35	-1.348	-1.35	-1.294
46	-1.349	-1.321	-1.35	-1.348	-1.349	-1.321
47	-1.347	-1.321	-1.349	-1.345	-1.35	-1.33
48	-1.349	-1.322	-1.349	-1.347	-1.35	-1.332
49	-1.348	-1.322	-1.349	-1.348	-1.349	-1.331
50	-1.349	-1.324	-1.349	-1.349	-1.35	-1.349
51	-1.35	-1.325	-1.349	-1.347	-1.352	-1.328

Note. Trials with unsatisfactory results or errors have been highlighted above.

The following lists explanations for data omission of the highlighted values in *table 4.6.*

Run 30 – Air pressures within system too high causing seed element to bypass comparison light gate.

Run 50 – Air pressures within system too high causing seed element to bypass comparison light gate.

4.3 Interpreted Light Gate Data Sets

The following interpreted data sets within this section represent correct loads gathered from trials executed using the automated non-mechanical element loading device. Errors within the automated loading of elements were removed from previously stated raw light gate data sets to remove possible error in data analysis. These edited light gate data sets were then subjected to interpretation to general statistical analysis and normal distribution curves. As many data sets consisted of low population sizes, translation of the recorded data sets into those of normal curves would allow for general visual interpretations representing a larger population. Within these edited data sets, presented in the previous section, there existed six individual data sets. These data sets related to both the light gates in which the data was recorded and the condition present during the automated loading process. The following results within this section are presented with respect to the overall data sets and have been partitioned as in the previous section. Within these separations, the general statistical analyses of the individual data set have been displayed first. General statistical analysis of the individual data sets has been followed by interpretation of these data sets to those of normal distribution values. Finally, these normal distribution values are subsequently followed by multiple graphs displaying these normal distribution curves.

Single element type normal distributions.

The following *tables 4.7* through *4.10* represent the general statistical analysis and interpretation to normal distribution values performed on both single element type trials. *Figures 4.1* through *4.4* represent normal distribution curves generated from the data sets.

Table 4.7 displays general statistical analysis values calculated from trials concerning seed elements loaded from only the seed type hopper utilizing only seed elements.

Table 4.7

General Statistical Analysis Performed on Edited Voltage Loss Data Concerning Single Line Loading Trials Utilizing Seed Elements and Seed Channel

	Condition 1			Condition 2		
Value	Light Gate Seed	Light Gate Spacer	Light Gate Compare	Light Gate Seed	Light Gate Spacer	Light Gate Compare
μ	1.318619	1.347286	1.346095	1.349048	1.347095	1.313667
σ	0.001857	0.001189	0.000995	0.00107	0.001546	0.005379
R	0.005	0.004	0.003	0.004	0.006	0.02
max	1.321	1.349	1.348	1.351	1.35	1.33
min	1.316	1.345	1.345	1.347	1.344	1.31
n	21	21	21	21	21	21

Note. μ = mean, σ = standard deviation, R = range, max = maximum value, min = minimum value, n = population.

Table 4.8 displays general statistical analysis values calculated from trials concerning seed elements loaded from only the spacer type hopper utilizing only seed elements.

Table 4.8

General Statistical Analysis Performed on Edited Voltage Loss Data Concerning Single Line Loading Trials Utilizing Seed Elements and Spacer Channel

	Condition 1			Condition 2		
Value	Light Gate Seed	Light Gate Spacer	Light Gate Compare	Light Gate Seed	Light Gate Spacer	Light Gate Compare
μ	1.349667	1.320600	1.345400	1.350200	1.348333	1.321600
σ	0.000617	0.001805	0.001502	0.001207	0.001345	0.010301
R	0.002	0.007	0.006	0.005	0.004	0.040
max	1.350	1.324	1.349	1.353	1.350	1.330
min	1.348	1.317	1.343	1.348	1.346	1.290
n	15	15	15	15	15	15

Note. μ = mean, σ = standard deviation, R = range, max = maximum value, min = minimum value, n = population.

Table 4.9 displays calculated values of normal distribution curves concerning all possible light gates and conditions from trials utilizing seed element loads from only the seed type hopper.

Table 4.9

Interpretation of Edited Voltage Loss Data to Normal Distribution Values Concerning Single Line Loading Trials Utilizing Seed Elements and Seed Channel

	Condition 1					
Scale	Light Gate Seed		Light Gate Spacer		Light Gate Compare	
±3 Stand. Dev.	Rescale	Norm. Dist.	Rescale	Norm. Dist.	Rescale	Norm. Dist.
-3	1.3130	2.3869	1.3437	3.7266	1.3431	4.4531
-2.7	1.3136	5.6124	1.3441	8.7627	1.3434	10.4709
-2.4	1.3142	12.0610	1.3444	18.8310	1.3437	22.5019
-2.1	1.3147	23.6881	1.3448	36.9847	1.3440	44.1945
-1.8	1.3153	42.5200	1.3451	66.3872	1.3443	79.3288

-1.5	1.3158	69.7540	1.3455	108.9081	1.3446	130.1388
-1.2	1.3164	104.5824	1.3459	163.2862	1.3449	195.1174
-0.9	1.3169	143.3049	1.3462	223.7444	1.3452	267.3614
-0.6	1.3175	179.4640	1.3466	280.2002	1.3455	334.8228
-0.3	1.3181	205.4032	1.3469	320.6995	1.3458	383.2170
0	1.3186	214.8575	1.3473	335.4606	1.3461	400.8557
0.3	1.3192	205.4032	1.3476	320.6995	1.3464	383.2170
0.6	1.3197	179.4640	1.3480	280.2002	1.3467	334.8228
0.9	1.3203	143.3049	1.3484	223.7444	1.3470	267.3614
1.2	1.3208	104.5824	1.3487	163.2862	1.3473	195.1174
1.5	1.3214	69.7540	1.3491	108.9081	1.3476	130.1388
1.8	1.3220	42.5200	1.3494	66.3872	1.3479	79.3288
2.1	1.3225	23.6881	1.3498	36.9847	1.3482	44.1945
2.4	1.3231	12.0610	1.3501	18.8310	1.3485	22.5019
2.7	1.3236	5.6124	1.3505	8.7627	1.3488	10.4709
3	1.3242	2.3869	1.3509	3.7266	1.3491	4.4531

Condition 2

Scale	Light Gate Seed		Light Gate Spacer		Light Gate Compare	
±3 Stand. Dev.	Rescale	Norm. Dist.	Rescale	Norm. Dist.	Rescale	Norm. Dist.
-3	1.3458	4.1370	1.3425	2.8664	1.2975	0.8239
-2.7	1.3462	9.7276	1.3429	6.7401	1.2991	1.9373
-2.4	1.3465	20.9047	1.3434	14.4844	1.3008	4.1633
-2.1	1.3468	41.0574	1.3438	28.4478	1.3024	8.1770
-1.8	1.3471	73.6977	1.3443	51.0635	1.3040	14.6776
-1.5	1.3474	120.9010	1.3448	83.7696	1.3056	24.0785
-1.2	1.3478	181.2672	1.3452	125.5960	1.3072	36.1010
-0.9	1.3481	248.3830	1.3457	172.0991	1.3088	49.4677
-0.6	1.3484	311.0557	1.3462	215.5236	1.3104	61.9495
-0.3	1.3487	356.0147	1.3466	246.6747	1.3121	70.9035
0	1.3490	372.4013	1.3471	258.0286	1.3137	74.1670
0.3	1.3494	356.0147	1.3476	246.6747	1.3153	70.9035
0.6	1.3497	311.0557	1.3480	215.5236	1.3169	61.9495
0.9	1.3500	248.3830	1.3485	172.0991	1.3185	49.4677
1.2	1.3503	181.2672	1.3490	125.5960	1.3201	36.1010
1.5	1.3507	120.9010	1.3494	83.7696	1.3217	24.0785
1.8	1.3510	73.6977	1.3499	51.0635	1.3233	14.6776
2.1	1.3513	41.0574	1.3503	28.4478	1.3250	8.1770
2.4	1.3516	20.9047	1.3508	14.4844	1.3266	4.1633
2.7	1.3519	9.7276	1.3513	6.7401	1.3282	1.9373
3	1.3523	4.1370	1.3517	2.8664	1.3298	0.8239

Table 4.10 displays calculated values of normal distribution curves concerning all possible light gates and conditions from trials utilizing spacer element loads from only the seed type hopper.

Table 4.10

Interpretation of Edited Voltage Loss Data to Normal Distribution Values Concerning Single Line Loading Trials Utilizing Seed Elements and Spacer Channel

	Condition 1					
Scale	Light Gate Seed		Light Gate Spacer		Light Gate Compare	
±3 Stand. Dev.	Rescale	Norm. Dist.	Rescale	Norm. Dist.	Rescale	Norm. Dist.
-3.000	1.34782	7.180415	1.315186	2.45565	1.340893	2.94989
-2.571	1.34808	23.69431	1.315959	8.103282	1.341537	9.73419
-2.143	1.34834	65.06839	1.316733	22.25292	1.342181	26.7317
-1.714	1.34861	148.7057	1.317506	50.85629	1.342824	61.0919
-1.286	1.34887	282.8245	1.31828	96.72394	1.343468	116.191
-0.857	1.34914	447.6494	1.319053	153.0929	1.344112	183.905
-0.429	1.3494	589.6449	1.319827	201.6543	1.344756	242.24
0.000	1.34967	646.3604	1.3206	221.0506	1.3454	265.54
0.429	1.34993	589.6449	1.321373	201.6543	1.346044	242.24
0.857	1.3502	447.6494	1.322147	153.0929	1.346688	183.905
1.286	1.35046	282.8245	1.32292	96.72394	1.347332	116.191
1.714	1.35073	148.7057	1.323694	50.85629	1.347976	61.0919
2.143	1.35099	65.06839	1.324467	22.25292	1.348619	26.7317
2.571	1.35125	23.69431	1.325241	8.103282	1.349263	9.73419
3.000	1.35152	7.180415	1.326014	2.45565	1.349907	2.94989

	Condition 2					
Scale	Light Gate Seed		Light Gate Spacer		Light Gate Compare	
±3 Stand. Dev.	Rescale	Norm. Dist.	Rescale	Norm. Dist.	Rescale	Norm. Dist.
-3.000	1.346579	3.671418	1.344298	3.2946	1.2907	0.430227
-2.571	1.347096	12.11514	1.344874	10.87169	1.29511	1.419686

-2.143	1.347613	33.27012	1.345451	29.85542	1.29953	3.898688
-1.714	1.348131	76.03473	1.346027	68.23087	1.30394	8.909968
-1.286	1.348648	144.611	1.346604	129.7688	1.30836	16.94593
-0.857	1.349165	228.8876	1.34718	205.3956	1.31277	26.82171
-0.429	1.349683	301.4913	1.347757	270.5476	1.31719	35.32962
0.000	1.3502	330.4905	1.348333	296.5705	1.3216	38.72783
0.429	1.350717	301.4913	1.34891	270.5476	1.32602	35.32962
0.857	1.351235	228.8876	1.349486	205.3956	1.33043	26.82171
1.286	1.351752	144.611	1.350063	129.7688	1.33484	16.94593
1.714	1.352269	76.03473	1.350639	68.23087	1.33926	8.909968
2.143	1.352787	33.27012	1.351216	29.85542	1.34367	3.898688
2.571	1.353304	12.11514	1.351792	10.87169	1.34809	1.419686
3.000	1.353821	3.671418	1.352369	3.2946	1.3525	0.430227

The following *Figures 4.1* and 4.*2* graphically display the calculated normal distribution values found in *table 4.9.* These graphs illustrate three normal distribution curves a piece with respect to both individual light gate and conditions.

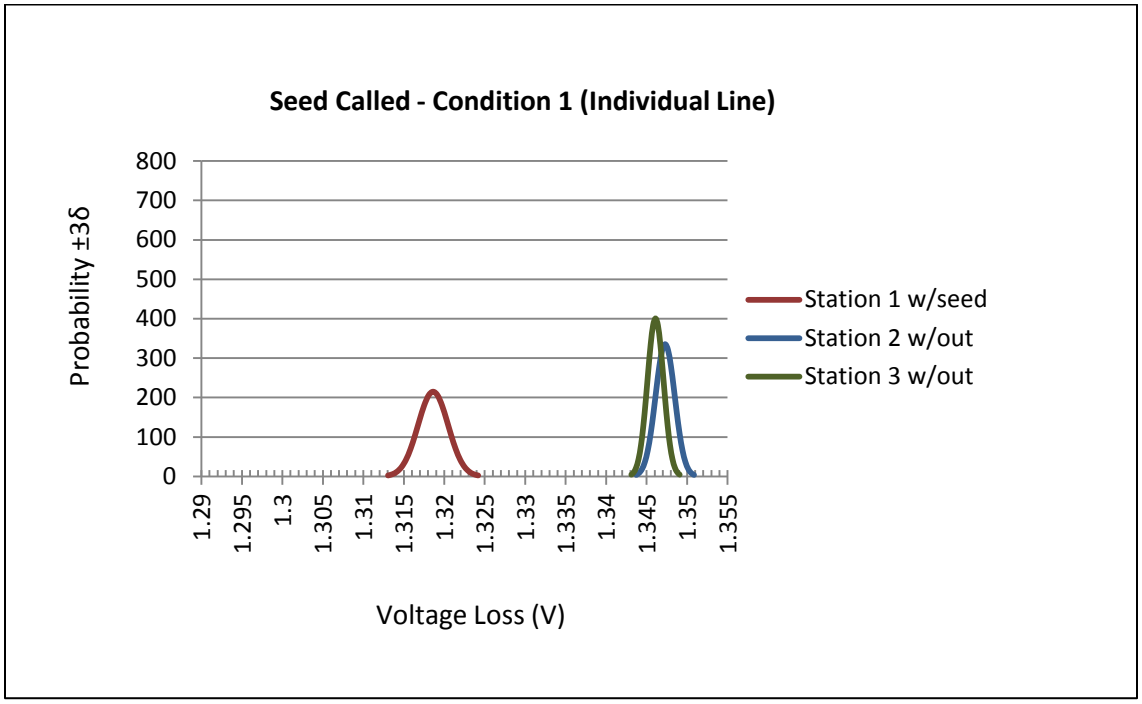

Figure 4.1: Normal distribution curves of Condition 1 with single line loading where element has been called (from seed hopper) and captured on the corresponding seed light gate area.

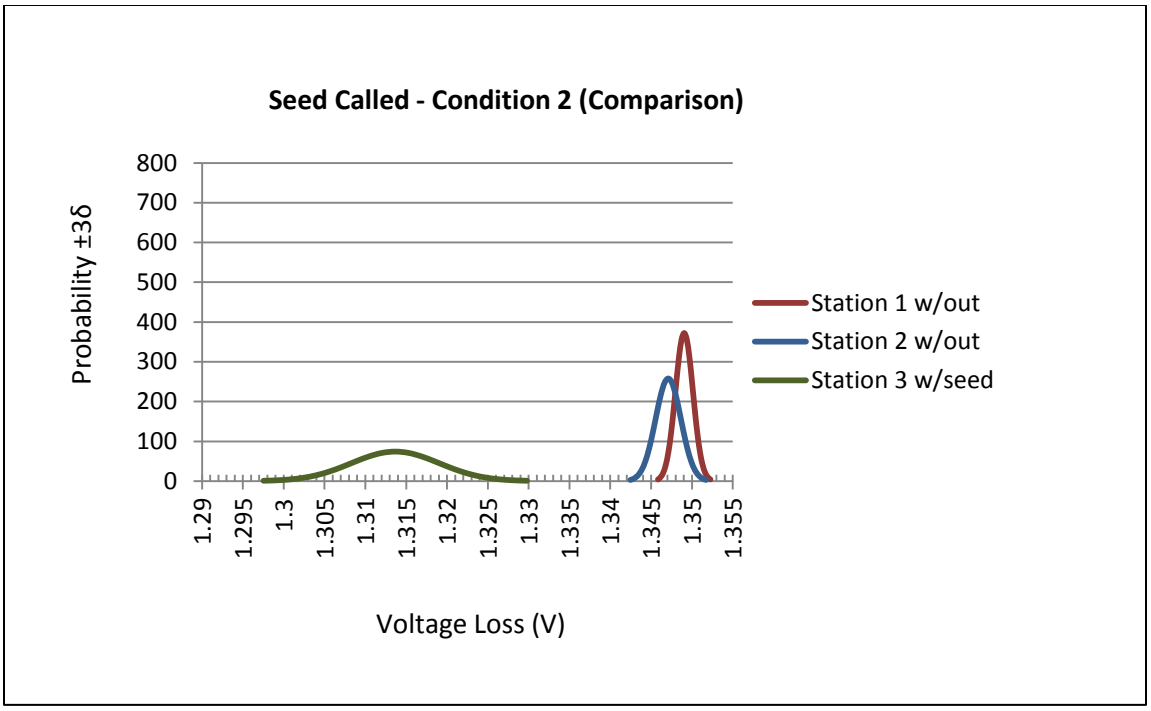

Figure 4.2: Normal distribution curves of Condition 2 with single line loading where element has been called (from seed hopper) and captured on the comparison light gate area.

The following *Figures 4.3* and *4.4* graphically display the calculated normal distribution values found in *table 4.10.* These graphs illustrate three normal distribution curves a piece with respect to both individual light gate and conditions.

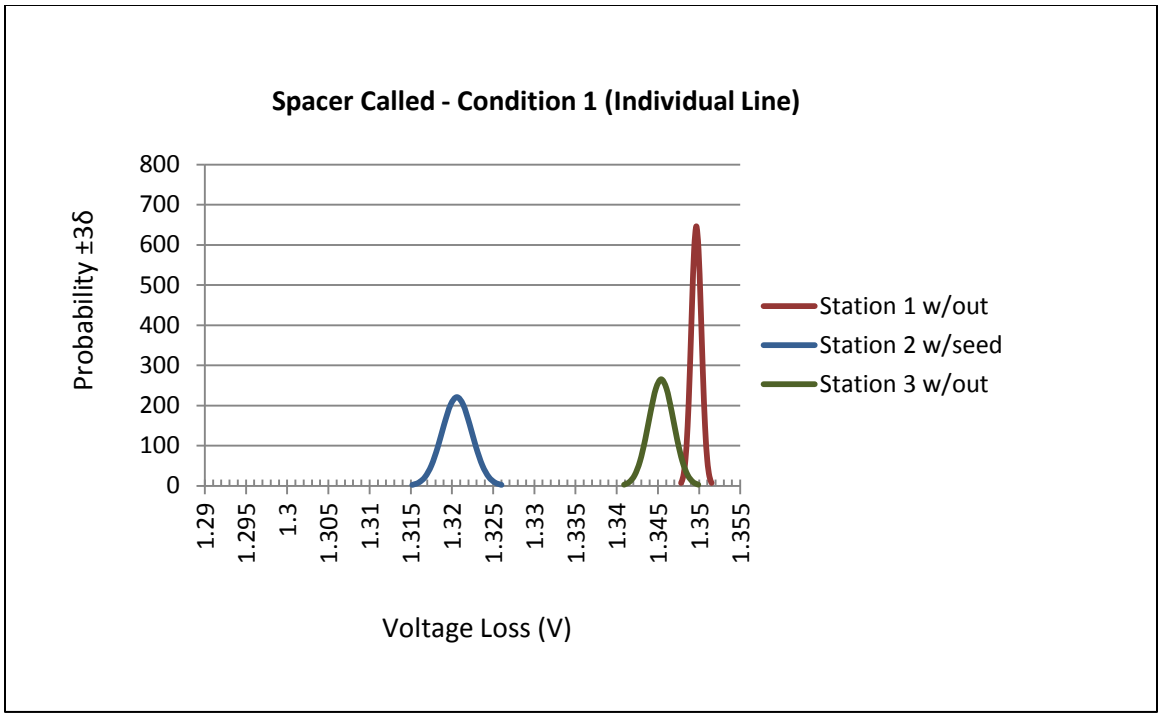

Figure 4.3: Normal distribution curves of Condition 1 with single line loading where element has been called (from spacer hopper) and captured on the corresponding spacer light gate area.

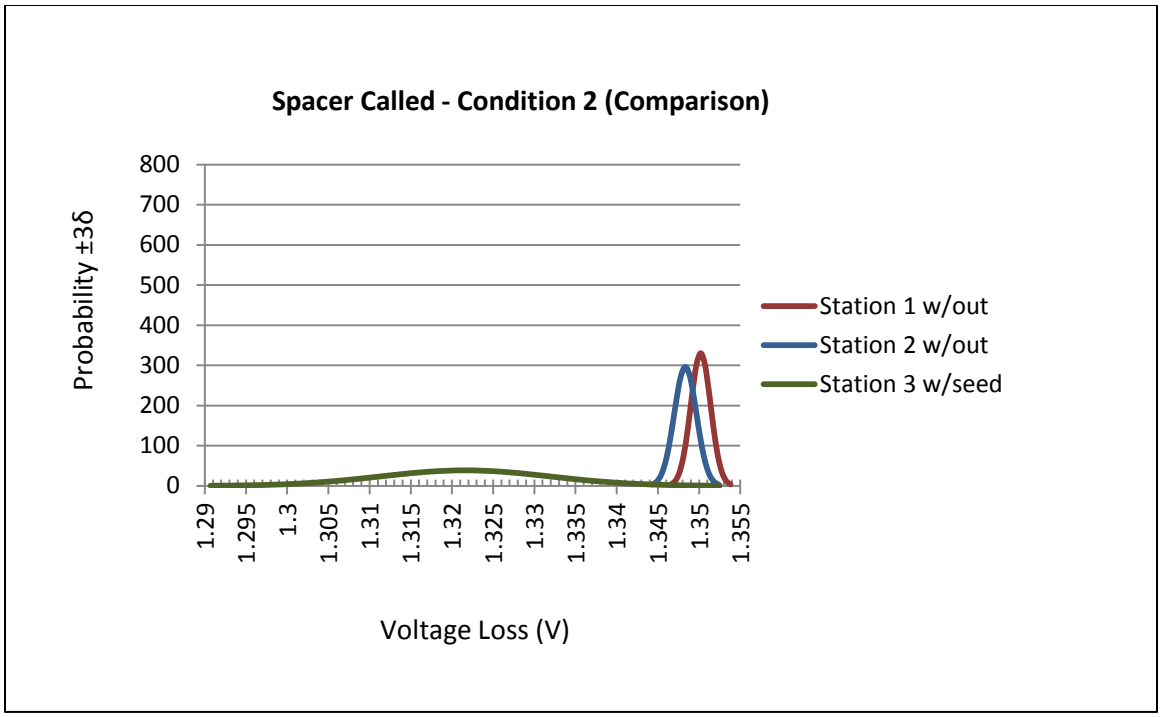

Figure 4.4: Normal distribution curves of Condition 2 with single line loading where element has been called (from spacer hopper) and captured on the comparison light gate area.

Random small scale dosimetry normal distributions.

The following *tables 4.11* through *4.14* represents the general statistical analysis and interpretation to normal distribution values performed on both single element type trials. *Figures 4.5* through *4.8* represent normal distribution curves generated from the data sets. *Table 4.7* displays general statistical analysis values calculated from trials concerning seed element loading using a small scale random dosimetry pattern utilizing only seed elements.

Table 4.11

General Statistical Analysis Performed on Edited Voltage Loss Data Concerning Random Small Scale Dosimetry Loading Trials Utilizing Seed Elements and Seed Channel

	Condition 1			Condition 2		
Value	Light Gate Seed	Light Gate Spacer	Light Gate Compare	Light Gate Seed	Light Gate Spacer	Light Gate Compare
μ	1.318538	1.346962	1.345385	1.348923	1.345885	1.317077
σ	0.002486	0.001587	0.000852	0.001055	0.001306	0.006764
R	0.012	0.006	0.003	0.004	0.006	0.021
max	1.326	1.350	1.347	1.350	1.350	1.329
min	1.314	1.344	1.344	1.346	1.344	1.308
n	26	26	26	26	26	26

Note. μ = mean, σ = standard deviation, R = range, max = maximum value, min = minimum value, n = population.

Table 4.12 displays general statistical analysis values calculated from trials concerning seed element loading using a small scale random dosimetry pattern utilizing only seed elements.

Table 4.12

General Statistical Analysis Performed on Edited Voltage Loss Data Concerning Random Small Scale Dosimetry Loading Trials Utilizing Seed Elements and Spacer Channel

	Condition 1			Condition 2		
Value	Light Gate Seed	Light Gate Spacer	Light Gate Compare	Light Gate Seed	Light Gate Spacer	Light Gate Compare
μ	1.349000	1.317130	1.345261	1.349391	1.346565	1.320000
σ	0.000953	0.001938	0.001010	0.001305	0.001441	0.006836
R	2.697	2.636	2.691	2.700	2.695	2.640
max	1.350	1.322	1.347	1.353	1.350	1.330

min	1.347	1.314	1.344	1.347	1.345	1.310
n	23	23	23	23	23	23

Note. μ = mean, σ = standard deviation, R = range, max = maximum value, min = minimum value, n = population.

Table 4.13 displays calculated values of normal distribution curves concerning all possible light gates and conditions from trials utilizing seed element loads with a randomized small scale dosimetry pattern and seed elements loaded into both hoppers.

Table 4.13

Interpretation of Edited Voltage Loss Data to Normal Distribution Values Concerning Random Small Scale Dosimetry Loading Trials Utilizing Seed Elements and Seed Channel

	Condition 1					
Scale	Light Gate Seed		Light Gate Spacer		Light Gate Compare	
±3 Stand. Dev.	Rescale	Norm. Dist.	Rescale	Norm. Dist.	Rescale	Norm. Dist.
-3	1.311082	1.782973	1.342201	2.792655	1.342828	5.200805
-2.75	1.311703	3.658423	1.342597	5.730155	1.343041	10.67136
-2.5	1.312324	7.051794	1.342994	11.04516	1.343254	20.56958
-2.25	1.312946	12.76915	1.343391	20.00021	1.343467	37.2467
-2	1.313567	21.72106	1.343788	34.0215	1.34368	63.35878
-1.75	1.314189	34.71015	1.344184	54.3662	1.343893	101.247
-1.5	1.31481	52.1061	1.344581	81.61333	1.344106	151.9898
-1.25	1.315431	73.48138	1.344978	115.0932	1.344319	214.34
-1	1.316053	97.34702	1.345375	152.4738	1.344532	283.9543
-0.75	1.316674	121.1503	1.345771	189.7567	1.344746	353.3869
-0.5	1.317296	141.6391	1.346168	221.848	1.344959	413.1511
-0.25	1.317917	155.5601	1.346565	243.6524	1.345172	453.7577
0	1.318538	160.4981	1.346962	251.3868	1.345385	468.1616
0.25	1.31916	155.5601	1.347358	243.6524	1.345598	453.7577
0.5	1.319781	141.6391	1.347755	221.848	1.345811	413.1511
0.75	1.320403	121.1503	1.348152	189.7567	1.346024	353.3869
1	1.321024	97.34702	1.348549	152.4738	1.346237	283.9543
1.25	1.321646	73.48138	1.348945	115.0932	1.34645	214.34

1.5	1.322267	52.1061	1.349342	81.61333	1.346663	151.9898
1.75	1.322888	34.71015	1.349739	54.3662	1.346876	101.247
2	1.32351	21.72106	1.350135	34.0215	1.347089	63.35878
2.25	1.324131	12.76915	1.350532	20.00021	1.347302	37.2467
2.5	1.324753	7.051794	1.350929	11.04516	1.347515	20.56958
2.75	1.325374	3.658423	1.351326	5.730155	1.347728	10.67136
3	1.325995	1.782973	1.351722	2.792655	1.347941	5.200805

Condition 2

Scale	Light Gate Seed		Light Gate Spacer		Light Gate Compare	
±3 Stand. Dev.	Rescale	Norm. Dist.	Rescale	Norm. Dist.	Rescale	Norm. Dist.
-3	1.345757	4.199255	1.341966	3.392937	1.296784	0.655196
-2.75	1.346021	8.616313	1.342293	6.961855	1.298475	1.344374
-2.5	1.346285	16.60838	1.342619	13.41933	1.300167	2.59135
-2.25	1.346548	30.07389	1.342946	24.29926	1.301858	4.692328
-2	1.346812	51.1574	1.343272	41.33444	1.303549	7.981919
-1.75	1.347076	81.7493	1.343599	66.05224	1.30524	12.75507
-1.5	1.34734	122.7202	1.343925	99.15616	1.306931	19.14763
-1.25	1.347604	173.0633	1.344252	139.8326	1.308622	27.00248
-1	1.347868	229.2716	1.344578	185.2481	1.310313	35.77248
-0.75	1.348132	285.3331	1.344905	230.545	1.312004	44.51957
-0.5	1.348395	333.5882	1.345232	269.5344	1.313695	52.04865
-0.25	1.348659	366.3749	1.345558	296.0256	1.315386	57.16426
0	1.348923	378.0049	1.345885	305.4225	1.317077	58.97884
0.25	1.349187	366.3749	1.346211	296.0256	1.318768	57.16426
0.5	1.349451	333.5882	1.346538	269.5344	1.320459	52.04865
0.75	1.349715	285.3331	1.346864	230.545	1.32215	44.51957
1	1.349978	229.2716	1.347191	185.2481	1.323841	35.77248
1.25	1.350242	173.0633	1.347517	139.8326	1.325532	27.00248
1.5	1.350506	122.7202	1.347844	99.15616	1.327223	19.14763
1.75	1.35077	81.7493	1.34817	66.05224	1.328914	12.75507
2	1.351034	51.1574	1.348497	41.33444	1.330605	7.981919
2.25	1.351298	30.07389	1.348824	24.29926	1.332296	4.692328
2.5	1.351562	16.60838	1.34915	13.41933	1.333987	2.59135
2.75	1.351825	8.616313	1.349477	6.961855	1.335678	1.344374
3	1.352089	4.199255	1.349803	3.392937	1.337369	0.655196

Table 4.14 displays calculated values of normal distribution curves concerning all possible light gates and conditions from trials utilizing spacer element loads with a randomized small scale dosimetry pattern and seed elements loaded into both hoppers.

Table 4.14

Interpretation of Edited Voltage Loss Data to Normal Distribution Values Concerning Random Small Scale Dosimetry Loading Trials Utilizing Seed Elements and Seed Channel

	Condition 1					
Scale	Light Gate Seed		Light Gate Spacer		Light Gate Compare	
±3 Stand. Dev.	Rescale	Norm. Dist.	Rescale	Norm. Dist.	Rescale	Norm. Dist.
-3	1.34614	4.648162	1.311317	2.287091	1.342231	4.388694
-2.75	1.346378	9.537409	1.311802	4.692805	1.342484	9.005015
-2.5	1.346616	18.38384	1.312286	9.045619	1.342736	17.35762
-2.25	1.346855	33.28883	1.31277	16.3795	1.342989	31.43059
-2	1.347093	56.6262	1.313255	27.86247	1.343241	53.46524
-1.75	1.347331	90.48842	1.313739	44.52409	1.343494	85.43721
-1.5	1.34757	135.8392	1.314224	66.83858	1.343746	128.2564
-1.25	1.347808	191.564	1.314708	94.25751	1.343999	180.8706
-1	1.348047	253.781	1.315193	124.8709	1.344251	239.6146
-0.75	1.348285	315.8356	1.315677	155.4044	1.344503	298.2052
-0.5	1.348523	369.2492	1.316162	181.6861	1.344756	348.6372
-0.25	1.348762	405.5409	1.316646	199.5431	1.345008	382.903
0	1.349	418.4142	1.31713	205.8773	1.345261	395.0576
0.25	1.349238	405.5409	1.317615	199.5431	1.345513	382.903
0.5	1.349477	369.2492	1.318099	181.6861	1.345766	348.6372
0.75	1.349715	315.8356	1.318584	155.4044	1.346018	298.2052
1	1.349953	253.781	1.319068	124.8709	1.346271	239.6146
1.25	1.350192	191.564	1.319553	94.25751	1.346523	180.8706
1.5	1.35043	135.8392	1.320037	66.83858	1.346776	128.2564
1.75	1.350669	90.48842	1.320522	44.52409	1.347028	85.43721
2	1.350907	56.6262	1.321006	27.86247	1.347281	53.46524
2.25	1.351145	33.28883	1.32149	16.3795	1.347533	31.43059
2.5	1.351384	18.38384	1.321975	9.045619	1.347785	17.35762

2.75	1.351622	9.537409	1.322459	4.692805	1.348038	9.005015
3	1.35186	4.648162	1.322944	2.287091	1.34829	4.388694

	Condition 2					
Scale	Light Gate Seed		Light Gate Spacer		Light Gate Compare	
±3 Stand. Dev.	Rescale	Norm. Dist.	Rescale	Norm. Dist.	Rescale	Norm. Dist.
-3	1.345476	3.395522	1.342244	3.076561	1.299493	0.648335
-2.75	1.345802	6.967158	1.342604	6.312693	1.301202	1.330298
-2.5	1.346128	13.42955	1.342964	12.16803	1.302911	2.564216
-2.25	1.346455	24.31777	1.343324	22.03346	1.30462	4.643195
-2	1.346781	41.36592	1.343684	37.48018	1.306329	7.898341
-1.75	1.347107	66.10256	1.344044	59.89316	1.308037	12.62151
-1.5	1.347433	99.23169	1.344404	89.91029	1.309746	18.94714
-1.25	1.34776	139.9391	1.344765	126.7938	1.311455	26.71974
-1	1.348086	185.3892	1.345125	167.9745	1.313164	35.39791
-0.75	1.348412	230.7206	1.345485	209.0477	1.314873	44.05341
-0.5	1.348739	269.7397	1.345845	244.4015	1.316582	51.50365
-0.25	1.349065	296.2511	1.346205	268.4225	1.318291	56.5657
0	1.349391	305.6551	1.346565	276.9432	1.32	58.36129
0.25	1.349718	296.2511	1.346925	268.4225	1.321709	56.5657
0.5	1.350044	269.7397	1.347285	244.4015	1.323418	51.50365
0.75	1.35037	230.7206	1.347646	209.0477	1.325127	44.05341
1	1.350697	185.3892	1.348006	167.9745	1.326836	35.39791
1.25	1.351023	139.9391	1.348366	126.7938	1.328545	26.71974
1.5	1.351349	99.23169	1.348726	89.91029	1.330254	18.94714
1.75	1.351675	66.10256	1.349086	59.89316	1.331963	12.62151
2	1.352002	41.36592	1.349446	37.48018	1.333671	7.898341
2.25	1.352328	24.31777	1.349806	22.03346	1.33538	4.643195
2.5	1.352654	13.42955	1.350167	12.16803	1.337089	2.564216
2.75	1.352981	6.967158	1.350527	6.312693	1.338798	1.330298
3	1.353307	3.395522	1.350887	3.076561	1.340507	0.648335

Figures 4.5 and *4.6* graphically display the calculated normal distribution values found in *table 4.13.* These graphs illustrate three normal distribution curves a piece with respect to both individual light gate and conditions.

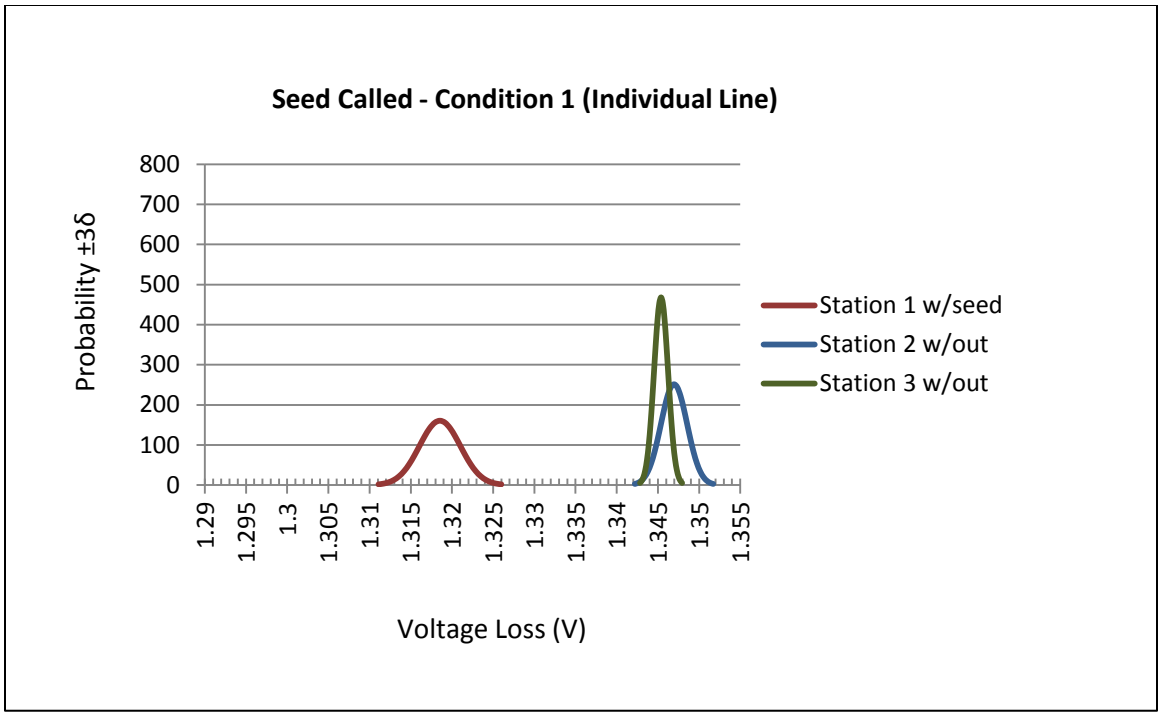

Figure 4.5: Normal distribution curves of Condition 1 with small scale dosimetry loading where element has been called (from seed hopper) and captured on the corresponding seed light gate area.

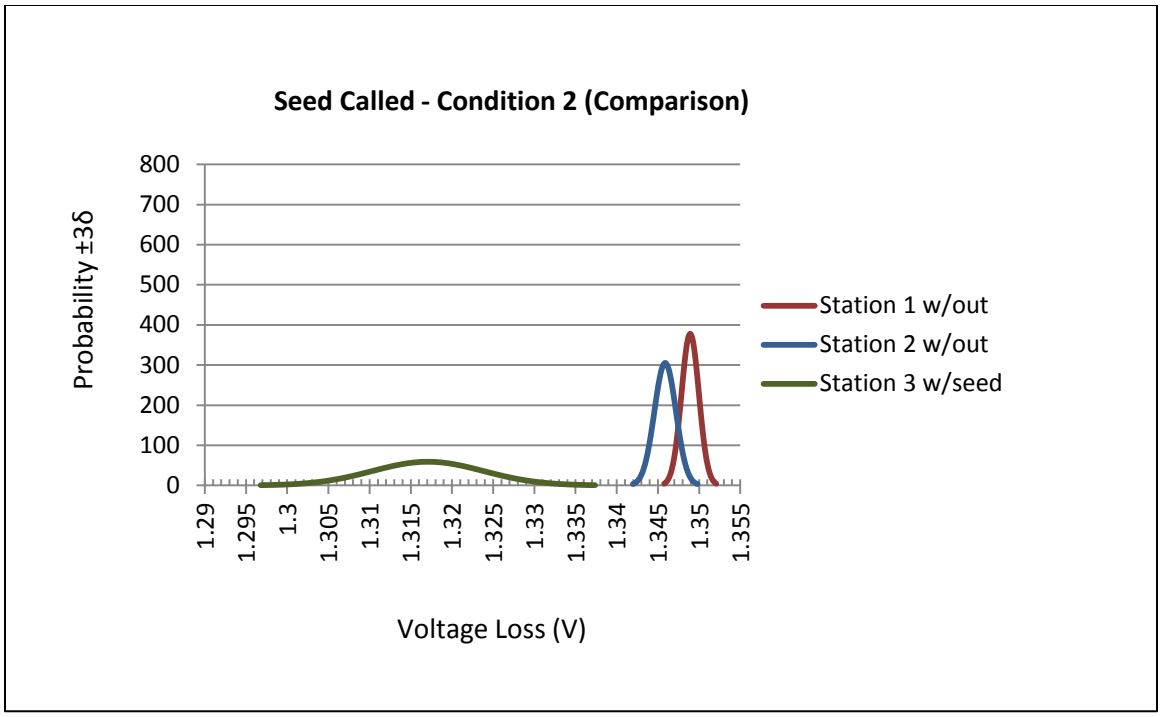

Figure 4.6: Normal distribution curves of Condition 2 with small scale dosimetry loading where element has been called (from seed hopper) and captured on the comparison light gate area.

Figure 4.7 and *figure 4.8* display graphically the calculated normal distribution values found in *table 4.14.* These graphs illustrate three normal distribution curves a piece with respect to both individual light gate and conditions.

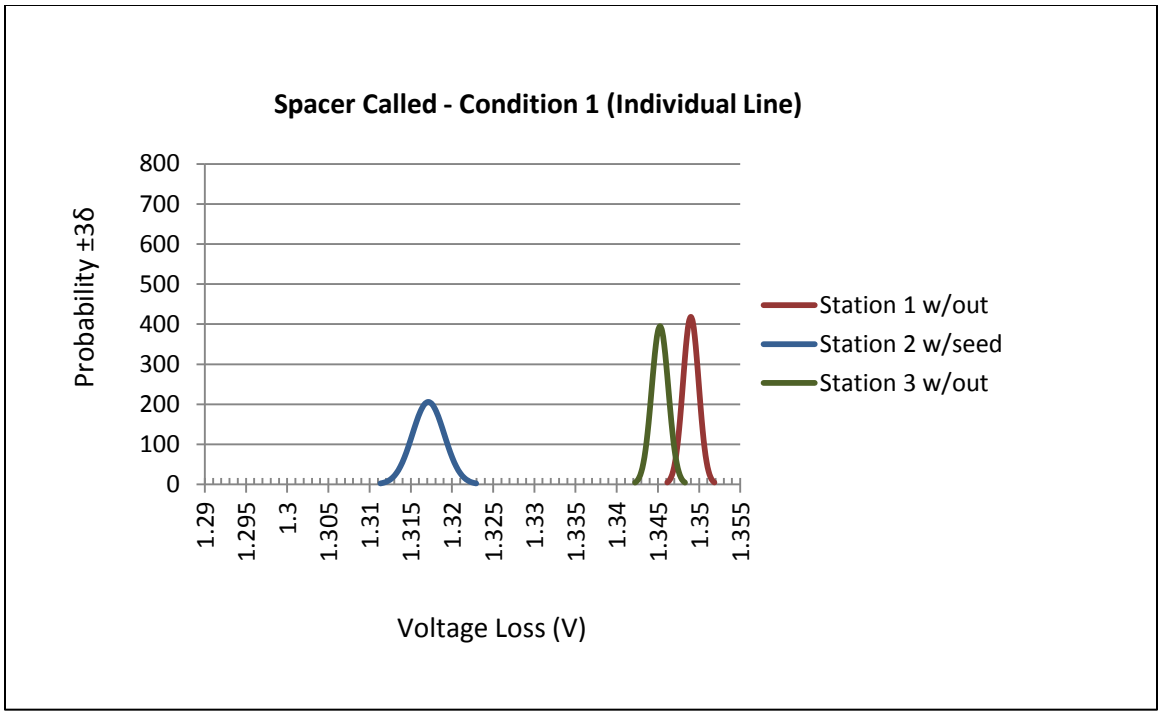

Figure 4.7: Normal distribution curves of Condition 1 with small scale dosimetry loading where element has been called (from spacer hopper) and captured on the corresponding spacer light gate area.

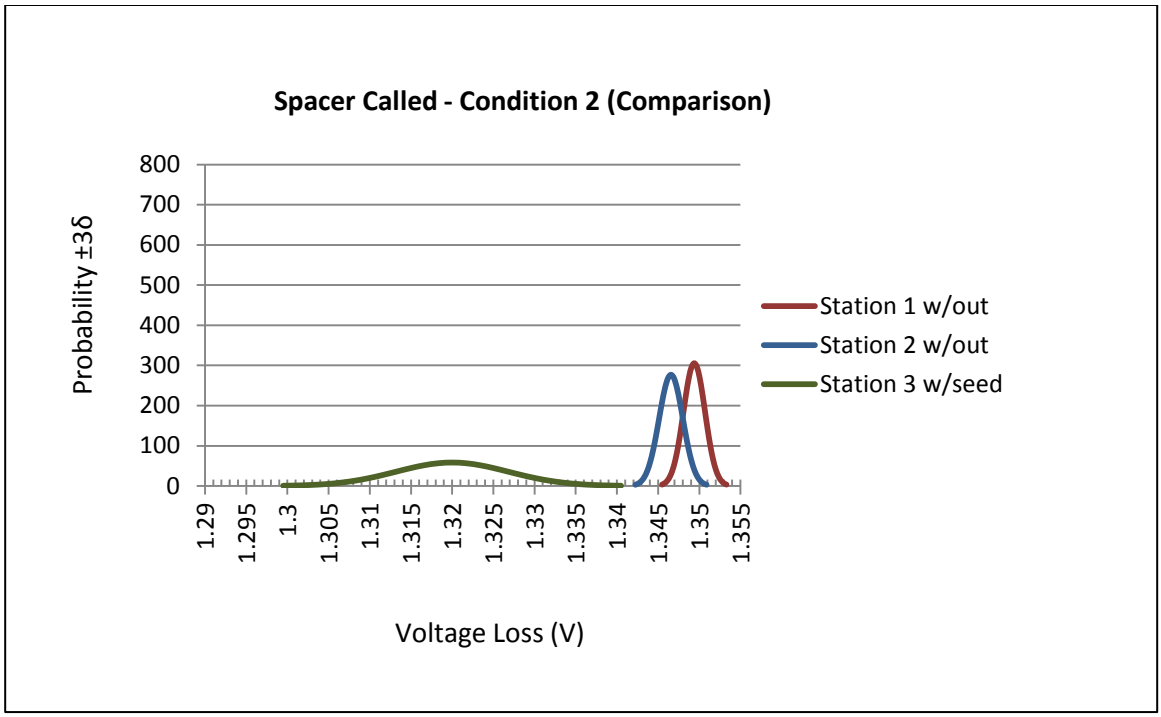

Figure 4.8: Normal distribution curves of Condition 2 with small scale dosimetry loading where element has been called (from spacer hopper) and captured on the comparison light gate area.

Random large scale dosimetry normal distributions.

The following *tables 4.15* through *4.18* represents the general statistical analysis and interpretation to normal distribution values performed on both single element type trials. *Figures 4.9* through *4.12* represent normal distribution curves generated from the data sets. *Table 4.15* displays general statistical analysis values calculated from trials concerning seed element loading using a large scale random dosimetry pattern utilizing only seed elements.

Table 4.15

General Statistical Analysis Performed on Edited Voltage Loss Data Concerning Random Large Scale Dosimetry Loading Trials Utilizing Seed Elements and Seed Channel

Value	Condition 1			Condition 2		
	Light Gate Seed	Light Gate Spacer	Light Gate Compare	Light Gate Seed	Light Gate Spacer	Light Gate Compare
μ	1.317842	1.350158	1.349789	1.348509	1.350105	1.321702
σ	0.003390	0.000862	0.000526	0.001037	0.000920	0.007322
R	0.015	0.005	0.002	0.004	0.005	0.023
max	1.326	1.353	1.351	1.350	1.353	1.333
min	1.311	1.348	1.349	1.346	1.348	1.310
n	57	57	57	57	57	57

Note. μ = mean, σ = standard deviation, R = range, max = maximum value, min = minimum value, n = population.

Table 4.16 displays general statistical analysis values calculated from trials concerning seed element loading using a large scale random dosimetry pattern utilizing only seed elements.

Table 4.16

General Statistical Analysis Performed on Edited Voltage Loss Data Concerning Random Large Scale Dosimetry Loading Trials Utilizing Seed Elements and Spacer Channel

	Condition 1			Condition 2		
Value	Light Gate Seed	Light Gate Spacer	Light Gate Compare	Light Gate Seed	Light Gate Spacer	Light Gate Compare
μ	1.348733	1.321867	1.349711	1.348689	1.350267	1.324622
σ	0.001053	0.002519	0.000549	0.001083	0.001250	0.006482
R	0.004	0.009	0.003	0.004	0.007	0.029
max	1.350	1.327	1.351	1.350	1.354	1.334
min	1.346	1.318	1.348	1.346	1.347	1.305
n	45	45	45	45	45	45

Note. μ = mean, σ = standard deviation, R = range, max = maximum value, min = minimum value, n = population.

Table 4.17 displays calculated values of normal distribution curves concerning all possible light gates and conditions from trials utilizing spacer element loads with a randomized large scale dosimetry pattern and seed elements loaded into both hoppers.

Table 4.17

Interpretation of Edited Voltage Loss Data to Normal Distribution Values Concerning Random Large Scale Dosimetry Loading Trials Utilizing Seed Elements and Spacer Channel

	Condition 1					
Scale	Light Gate Seed		Light Gate Spacer		Light Gate Compare	
±3 Stand. Dev.	Rescale	Norm. Dist.	Rescale	Norm. Dist.	Rescale	Norm. Dist.
-3.000	1.307672	1.307308	1.347573	5.143304	1.348213	8.431057
-2.893	1.308035	1.792586	1.347665	7.052516	1.348269	11.56069
-2.786	1.308398	2.429944	1.347758	9.560056	1.348325	15.67113
-2.679	1.308762	3.25632	1.34785	12.81124	1.348381	21.00057
-2.571	1.309125	4.313923	1.347942	16.97214	1.348438	27.82124
-2.464	1.309488	5.649789	1.348034	22.2278	1.348494	36.43647
-2.357	1.309851	7.314868	1.348127	28.77867	1.34855	47.17485
-2.250	1.310214	9.362574	1.348219	36.83489	1.348607	60.38086
-2.143	1.310578	11.84673	1.348311	46.60823	1.348663	76.40161
-2.036	1.310941	14.81891	1.348404	58.30159	1.348719	95.5697
-1.929	1.311304	18.32519	1.348496	72.09623	1.348776	118.1823
-1.821	1.311667	22.40243	1.348588	88.13719	1.348832	144.4771
-1.714	1.312031	27.07423	1.348681	106.5173	1.348888	174.6064
-1.607	1.312394	32.34683	1.348773	127.2612	1.348945	208.6103
-1.500	1.312757	38.20515	1.348865	150.3094	1.349001	246.3916
-1.393	1.31312	44.60941	1.348958	175.5055	1.349057	287.6938
-1.286	1.313483	51.49268	1.34905	202.5861	1.349114	332.0852
-1.179	1.313847	58.75962	1.349142	231.1762	1.34917	378.951
-1.071	1.31421	66.28679	1.349235	260.7901	1.349226	427.495
-0.964	1.314573	73.92468	1.349327	290.8397	1.349283	476.7531
-0.857	1.314936	81.50165	1.349419	320.6495	1.349339	525.6183
-0.750	1.3153	88.82963	1.349512	349.4797	1.349395	572.8777
-0.643	1.315663	95.71142	1.349604	376.5546	1.349452	617.2595
-0.536	1.316026	101.9493	1.349696	401.096	1.349508	657.4885
-0.429	1.316389	107.3542	1.349789	422.3604	1.349564	692.3457
-0.321	1.316752	111.7553	1.349881	439.6757	1.349621	720.7296
-0.214	1.317116	115.0091	1.349973	452.4768	1.349677	741.7135
-0.107	1.317479	117.0066	1.350066	460.3356	1.349733	754.5959
0.000	1.317842	117.6801	1.350158	462.9854	1.349789	758.9396
0.107	1.318205	117.0066	1.35025	460.3356	1.349846	754.5959
0.214	1.318569	115.0091	1.350343	452.4768	1.349902	741.7135

0.321	1.318932	111.7553	1.350435	439.6757	1.349958	720.7296
0.429	1.319295	107.3542	1.350527	422.3604	1.350015	692.3457
0.536	1.319658	101.9493	1.35062	401.096	1.350071	657.4885
0.643	1.320021	95.71142	1.350712	376.5546	1.350127	617.2595
0.750	1.320385	88.82963	1.350804	349.4797	1.350184	572.8777
0.857	1.320748	81.50165	1.350896	320.6495	1.35024	525.6183
0.964	1.321111	73.92468	1.350989	290.8397	1.350296	476.7531
1.071	1.321474	66.28679	1.351081	260.7901	1.350353	427.495
1.179	1.321838	58.75962	1.351173	231.1762	1.350409	378.951
1.286	1.322201	51.49268	1.351266	202.5861	1.350465	332.0852
1.393	1.322564	44.60941	1.351358	175.5055	1.350522	287.6938
1.500	1.322927	38.20515	1.35145	150.3094	1.350578	246.3916
1.607	1.32329	32.34683	1.351543	127.2612	1.350634	208.6103
1.714	1.323654	27.07423	1.351635	106.5173	1.350691	174.6064
1.821	1.324017	22.40243	1.351727	88.13719	1.350747	144.4771
1.929	1.32438	18.32519	1.35182	72.09623	1.350803	118.1823
2.036	1.324743	14.81891	1.351912	58.30159	1.35086	95.5697
2.143	1.325107	11.84673	1.352004	46.60823	1.350916	76.40161
2.250	1.32547	9.362574	1.352097	36.83489	1.350972	60.38086
2.357	1.325833	7.314868	1.352189	28.77867	1.351029	47.17485
2.464	1.326196	5.649789	1.352281	22.2278	1.351085	36.43647
2.571	1.326559	4.313923	1.352374	16.97214	1.351141	27.82124
2.679	1.326923	3.25632	1.352466	12.81124	1.351197	21.00057
2.786	1.327286	2.429944	1.352558	9.560056	1.351254	15.67113
2.893	1.327649	1.792586	1.352651	7.052516	1.35131	11.56069
3.000	1.328012	1.307308	1.352743	5.143304	1.351366	8.431057

	Condition 2					
Scale	Light Gate Seed		Light Gate Spacer		Light Gate Compare	
±3 Stand. Dev.	Rescale	Norm. Dist.	Rescale	Norm. Dist.	Rescale	Norm. Dist.
-3.000	1.345397	4.272836	1.347346	4.818751	1.299737	0.605311
-2.893	1.345508	5.858927	1.347445	6.607487	1.300521	0.830005
-2.786	1.345619	7.942084	1.347543	8.956797	1.301306	1.125115
-2.679	1.345731	10.64303	1.347642	12.00283	1.30209	1.507744
-2.571	1.345842	14.09972	1.34774	15.90116	1.302875	1.997437
-2.464	1.345953	18.4659	1.347839	20.82518	1.303659	2.615971
-2.357	1.346064	23.90808	1.347937	26.96267	1.304444	3.386937
-2.250	1.346175	30.60085	1.348036	34.51054	1.305228	4.335068
-2.143	1.346286	38.72012	1.348134	43.66716	1.306013	5.485284

-2.036	1.346397	48.43445	1.348233	54.62264	1.306797	6.861465
-1.929	1.346508	59.89445	1.348332	67.54681	1.307582	8.484945
-1.821	1.34662	73.22059	1.34843	82.57555	1.308366	10.37279
-1.714	1.346731	88.49004	1.348529	99.79588	1.30915	12.53594
-1.607	1.346842	105.7231	1.348627	119.2307	1.309935	14.97726
-1.500	1.346953	124.8706	1.348726	140.8245	1.310719	17.68978
-1.393	1.347064	145.8024	1.348824	164.4307	1.311504	20.65509
-1.286	1.347175	168.2998	1.348923	189.8025	1.312288	23.84219
-1.179	1.347286	192.0513	1.349021	216.5885	1.313073	27.20694
-1.071	1.347397	216.6532	1.34912	244.3337	1.313857	30.69217
-0.964	1.347509	241.6171	1.349218	272.4871	1.314642	34.22868
-0.857	1.34762	266.3818	1.349317	300.4159	1.315426	37.73697
-0.750	1.347731	290.3328	1.349415	327.4269	1.316211	41.12998
-0.643	1.347842	312.8254	1.349514	352.7932	1.316995	44.31639
-0.536	1.347953	333.2133	1.349613	375.786	1.317779	47.20465
-0.429	1.348064	350.8788	1.349711	395.7086	1.318564	49.70724
-0.321	1.348175	365.2637	1.34981	411.9313	1.319348	51.74507
-0.214	1.348287	375.8983	1.349908	423.9246	1.320133	53.25161
-0.107	1.348398	382.427	1.350007	431.2875	1.320917	54.17651
0.000	1.348509	384.6284	1.350105	433.7701	1.321702	54.48837
0.107	1.34862	382.427	1.350204	431.2875	1.322486	54.17651
0.214	1.348731	375.8983	1.350302	423.9246	1.323271	53.25161
0.321	1.348842	365.2637	1.350401	411.9313	1.324055	51.74507
0.429	1.348953	350.8788	1.350499	395.7086	1.32484	49.70724
0.536	1.349064	333.2133	1.350598	375.786	1.325624	47.20465
0.643	1.349176	312.8254	1.350697	352.7932	1.326409	44.31639
0.750	1.349287	290.3328	1.350795	327.4269	1.327193	41.12998
0.857	1.349398	266.3818	1.350894	300.4159	1.327977	37.73697
0.964	1.349509	241.6171	1.350992	272.4871	1.328762	34.22868
1.071	1.34962	216.6532	1.351091	244.3337	1.329546	30.69217
1.179	1.349731	192.0513	1.351189	216.5885	1.330331	27.20694
1.286	1.349842	168.2998	1.351288	189.8025	1.331115	23.84219
1.393	1.349953	145.8024	1.351386	164.4307	1.3319	20.65509
1.500	1.350065	124.8706	1.351485	140.8245	1.332684	17.68978
1.607	1.350176	105.7231	1.351583	119.2307	1.333469	14.97726
1.714	1.350287	88.49004	1.351682	99.79588	1.334253	12.53594
1.821	1.350398	73.22059	1.35178	82.57555	1.335038	10.37279
1.929	1.350509	59.89445	1.351879	67.54681	1.335822	8.484945
2.036	1.35062	48.43445	1.351978	54.62264	1.336606	6.861465
2.143	1.350731	38.72012	1.352076	43.66716	1.337391	5.485284
2.250	1.350843	30.60085	1.352175	34.51054	1.338175	4.335068
2.357	1.350954	23.90808	1.352273	26.96267	1.33896	3.386937
2.464	1.351065	18.4659	1.352372	20.82518	1.339744	2.615971
2.571	1.351176	14.09972	1.35247	15.90116	1.340529	1.997437
2.679	1.351287	10.64303	1.352569	12.00283	1.341313	1.507744

2.786	1.351398	7.942084	1.352667	8.956797	1.342098	1.125115
2.893	1.351509	5.858927	1.352766	6.607487	1.342882	0.830005
3.000	1.35162	4.272836	1.352864	4.818751	1.343667	0.605311

Table 4.18 displays calculated values of normal distribution curves concerning all possible light gates and conditions from trials utilizing spacer element loads with a randomized small scale dosimetry pattern and seed elements loaded into both hoppers.

Table 4.18

Interpretation of Edited Voltage Loss Data to Normal Distribution Values Concerning Random Small Scale Dosimetry Loading Trials Utilizing Seed Elements and Seed Channel

	Condition 1					
Scale	Light Gate Seed		Light Gate Spacer		Light Gate Compare	
±3 Stand. Dev.	Rescale	Norm. Dist.	Rescale	Norm. Dist.	Rescale	Norm. Dist.
-3.000	1.345574	4.208248	1.31431	1.759355	1.348065	8.077824
-2.893	1.345687	5.770364	1.31458	2.412434	1.348124	11.07634
-2.786	1.3458	7.822032	1.314849	3.270181	1.348183	15.01456
-2.679	1.345912	10.48215	1.315119	4.382305	1.348242	20.12072
-2.571	1.346025	13.88659	1.315389	5.805611	1.3483	26.65562
-2.464	1.346138	18.18677	1.315659	7.603399	1.348359	34.9099
-2.357	1.346251	23.54669	1.315929	9.844236	1.348418	45.19838
-2.250	1.346364	30.13829	1.316199	12.60001	1.348477	57.8511
-2.143	1.346477	38.13483	1.316469	15.94315	1.348535	73.20064
-2.036	1.346589	47.70232	1.316739	19.94306	1.348594	91.56565
-1.929	1.346702	58.98909	1.317009	24.66175	1.348653	113.2308
-1.821	1.346815	72.1138	1.317278	30.14884	1.348712	138.424
-1.714	1.346928	87.15243	1.317548	36.43608	1.348771	167.291
-1.607	1.347041	104.125	1.317818	43.53187	1.348829	199.8702
-1.500	1.347154	122.983	1.318088	51.4159	1.348888	236.0686
-1.393	1.347266	143.5985	1.318358	60.03465	1.348947	275.6404
-1.286	1.347379	165.7558	1.318628	69.29805	1.349006	318.1719

-1.179	1.347492	189.1483	1.318898	79.07779	1.349064	363.0742
-1.071	1.347605	213.3783	1.319168	89.20774	1.349123	409.5844
-0.964	1.347718	237.9648	1.319438	99.48669	1.349182	456.7787
-0.857	1.347831	262.3552	1.319708	109.6837	1.349241	503.5966
-0.750	1.347943	285.9441	1.319977	119.5455	1.3493	548.876
-0.643	1.348056	308.0967	1.320247	128.8069	1.349358	591.3984
-0.536	1.348169	328.1765	1.320517	137.2018	1.349417	629.9419
-0.429	1.348282	345.575	1.320787	144.4756	1.349476	663.3387
-0.321	1.348395	359.7424	1.321057	150.3986	1.349535	690.5334
-0.214	1.348508	370.2162	1.321327	154.7774	1.349594	710.6381
-0.107	1.34862	376.6463	1.321597	157.4657	1.349652	722.9808
0.000	1.348733	378.8144	1.321867	158.3721	1.349711	727.1425
0.107	1.348846	376.6463	1.322137	157.4657	1.34977	722.9808
0.214	1.348959	370.2162	1.322406	154.7774	1.349829	710.6381
0.321	1.349072	359.7424	1.322676	150.3986	1.349887	690.5334
0.429	1.349185	345.575	1.322946	144.4756	1.349946	663.3387
0.536	1.349298	328.1765	1.323216	137.2018	1.350005	629.9419
0.643	1.34941	308.0967	1.323486	128.8069	1.350064	591.3984
0.750	1.349523	285.9441	1.323756	119.5455	1.350123	548.876
0.857	1.349636	262.3552	1.324026	109.6837	1.350181	503.5966
0.964	1.349749	237.9648	1.324296	99.48669	1.35024	456.7787
1.071	1.349862	213.3783	1.324566	89.20774	1.350299	409.5844
1.179	1.349975	189.1483	1.324836	79.07779	1.350358	363.0742
1.286	1.350087	165.7558	1.325105	69.29805	1.350417	318.1719
1.393	1.3502	143.5985	1.325375	60.03465	1.350475	275.6404
1.500	1.350313	122.983	1.325645	51.4159	1.350534	236.0686
1.607	1.350426	104.125	1.325915	43.53187	1.350593	199.8702
1.714	1.350539	87.15243	1.326185	36.43608	1.350652	167.291
1.821	1.350652	72.1138	1.326455	30.14884	1.35071	138.424
1.929	1.350764	58.98909	1.326725	24.66175	1.350769	113.2308
2.036	1.350877	47.70232	1.326995	19.94306	1.350828	91.56565
2.143	1.35099	38.13483	1.327265	15.94315	1.350887	73.20064
2.250	1.351103	30.13829	1.327534	12.60001	1.350946	57.8511
2.357	1.351216	23.54669	1.327804	9.844236	1.351004	45.19838
2.464	1.351329	18.18677	1.328074	7.603399	1.351063	34.9099
2.571	1.351441	13.88659	1.328344	5.805611	1.351122	26.65562
2.679	1.351554	10.48215	1.328614	4.382305	1.351181	20.12072
2.786	1.351667	7.822032	1.328884	3.270181	1.351239	15.01456
2.893	1.35178	5.770364	1.329154	2.412434	1.351298	11.07634
3.000	1.351893	4.208248	1.329424	1.759355	1.351357	8.077824

Condition 2

Scale	Light Gate Seed		Light Gate Spacer		Light Gate Compare	
±3 Stand. Dev.	Rescale	Norm. Dist.	Rescale	Norm. Dist.	Rescale	Norm. Dist.
-3.000	1.345439	4.090717	1.346515	3.54419	1.305177	0.683742
-2.893	1.345555	5.609205	1.346649	4.859806	1.305871	0.93755
-2.786	1.345671	7.603573	1.346783	6.587722	1.306566	1.270898
-2.679	1.345787	10.1894	1.346917	8.828077	1.30726	1.703105
-2.571	1.345903	13.49876	1.347051	11.6953	1.307955	2.256248
-2.464	1.346019	17.67884	1.347185	15.31691	1.308649	2.954926
-2.357	1.346135	22.88906	1.347319	19.83104	1.309344	3.825788
-2.250	1.346251	29.29656	1.347453	25.38249	1.310038	4.896769
-2.143	1.346367	37.06977	1.347587	32.11719	1.310733	6.196021
-2.036	1.346483	46.37006	1.347721	40.17494	1.311427	7.750515
-1.929	1.346599	57.3416	1.347855	49.68066	1.312122	9.584352
-1.821	1.346716	70.09975	1.347989	60.7343	1.312816	11.71681
-1.714	1.346832	84.71837	1.348123	73.39985	1.313511	14.16024
-1.607	1.346948	101.2169	1.348257	87.69419	1.314205	16.91789
-1.500	1.347064	119.5483	1.348391	103.5764	1.3149	19.98188
-1.393	1.34718	139.5879	1.348525	120.9387	1.315594	23.3314
-1.286	1.347296	161.1265	1.348659	139.5997	1.316289	26.93146
-1.179	1.347412	183.8656	1.348793	159.3008	1.316983	30.73218
-1.071	1.347528	207.4189	1.348927	179.7074	1.317677	34.669
-0.964	1.347644	231.3188	1.349061	200.4142	1.318372	38.66374
-0.857	1.34776	255.028	1.349195	220.9558	1.319066	42.62661
-0.750	1.347876	277.9581	1.349329	240.8224	1.319761	46.45925
-0.643	1.347992	299.492	1.349463	259.4793	1.320455	50.05853
-0.536	1.348109	319.0109	1.349597	276.3905	1.32115	53.32103
-0.429	1.348225	335.9235	1.349731	291.0436	1.321844	56.14788
-0.321	1.348341	349.6953	1.349865	302.9754	1.322539	58.44975
-0.214	1.348457	359.8766	1.349999	311.7964	1.323233	60.1515
-0.107	1.348573	366.1271	1.350133	317.2119	1.323928	61.19625
0.000	1.348689	368.2346	1.350267	319.0378	1.324622	61.54851
0.107	1.348805	366.1271	1.350401	317.2119	1.325317	61.19625
0.214	1.348921	359.8766	1.350535	311.7964	1.326011	60.1515
0.321	1.349037	349.6953	1.350669	302.9754	1.326706	58.44975
0.429	1.349153	335.9235	1.350803	291.0436	1.3274	56.14788
0.536	1.349269	319.0109	1.350937	276.3905	1.328095	53.32103
0.643	1.349385	299.492	1.351071	259.4793	1.328789	50.05853
0.750	1.349501	277.9581	1.351205	240.8224	1.329484	46.45925
0.857	1.349618	255.028	1.351338	220.9558	1.330178	42.62661
0.964	1.349734	231.3188	1.351472	200.4142	1.330872	38.66374

1.071	1.34985	207.4189	1.351606	179.7074	1.331567	34.669
1.179	1.349966	183.8656	1.35174	159.3008	1.332261	30.73218
1.286	1.350082	161.1265	1.351874	139.5997	1.332956	26.93146
1.393	1.350198	139.5879	1.352008	120.9387	1.33365	23.3314
1.500	1.350314	119.5483	1.352142	103.5764	1.334345	19.98188
1.607	1.35043	101.2169	1.352276	87.69419	1.335039	16.91789
1.714	1.350546	84.71837	1.35241	73.39985	1.335734	14.16024
1.821	1.350662	70.09975	1.352544	60.7343	1.336428	11.71681
1.929	1.350778	57.3416	1.352678	49.68066	1.337123	9.584352
2.036	1.350894	46.37006	1.352812	40.17494	1.337817	7.750515
2.143	1.35101	37.06977	1.352946	32.11719	1.338512	6.196021
2.250	1.351127	29.29656	1.35308	25.38249	1.339206	4.896769
2.357	1.351243	22.88906	1.353214	19.83104	1.339901	3.825788
2.464	1.351359	17.67884	1.353348	15.31691	1.340595	2.954926
2.571	1.351475	13.49876	1.353482	11.6953	1.34129	2.256248
2.679	1.351591	10.1894	1.353616	8.828077	1.341984	1.703105
2.786	1.351707	7.603573	1.35375	6.587722	1.342679	1.270898
2.893	1.351823	5.609205	1.353884	4.859806	1.343373	0.93755
3.000	1.351939	4.090717	1.354018	3.54419	1.344067	0.683742

Figures 4.9 and *4.10* graphically display the calculated normal distribution values found in *table 4.17.* These graphs illustrate three normal distribution curves a piece with respect to both individual light gate and conditions.

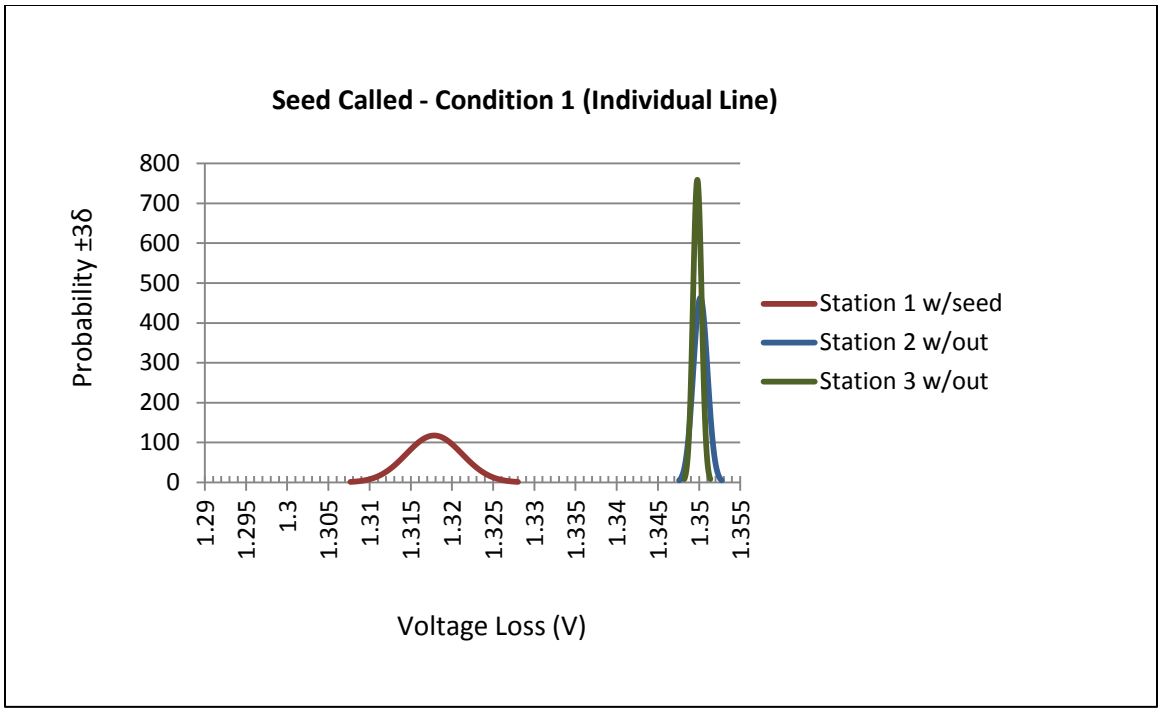

Figure 4.9: Normal distribution curves of Condition 1 with large scale dosimetry loading where element has been called (from seed hopper) and captured on the corresponding seed light gate area.

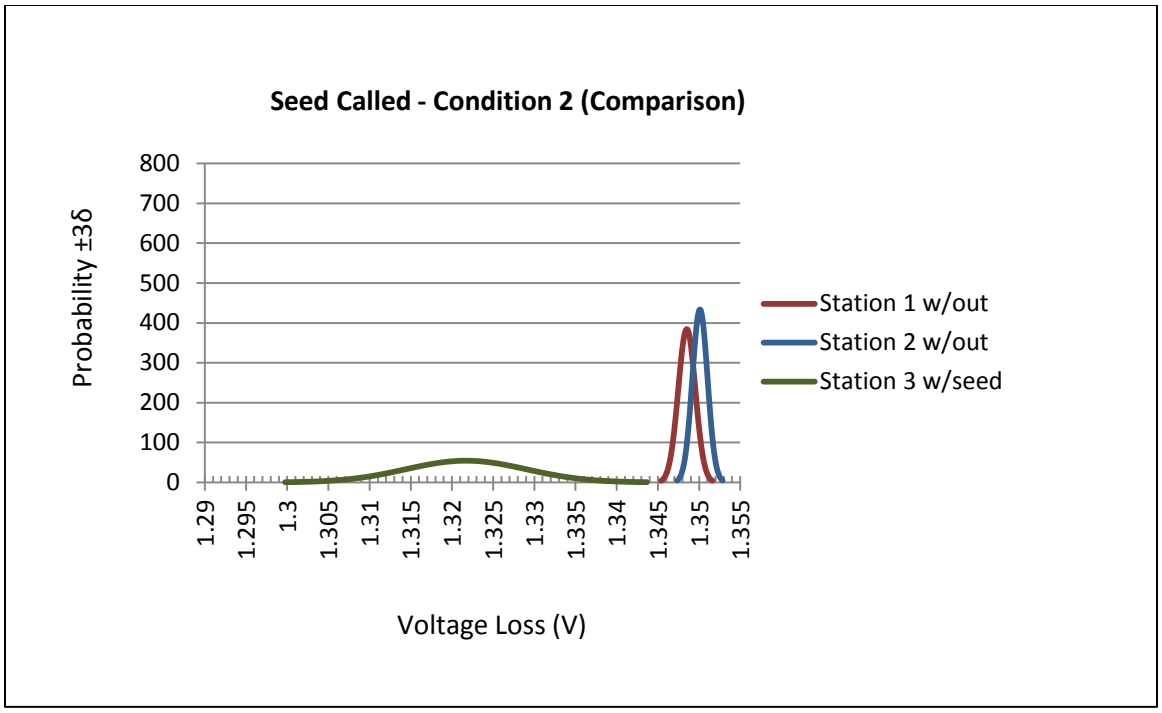

Figure 4.10: Normal distribution curves of Condition 2 with large scale dosimetry loading where element has been called (from seed hopper) and captured on the comparison light gate area.

Figure 4.11 and *figure 4.12* display graphically the calculated normal distribution values found in *table 4.18.* These graphs illustrate three normal distribution curves a piece with respect to both individual light gate and conditions.

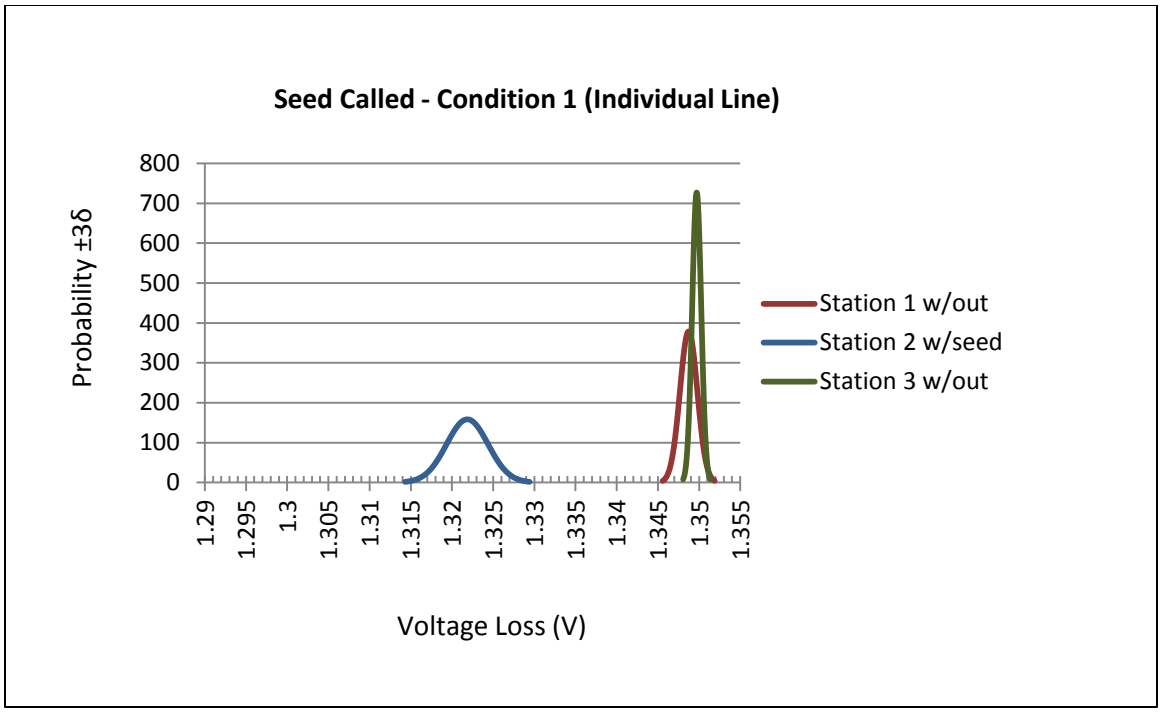

Figure 4.11: Normal distribution curves of Condition 1 with large scale dosimetry loading where element has been called (from spacer hopper) and captured on the corresponding spacer light gate area.

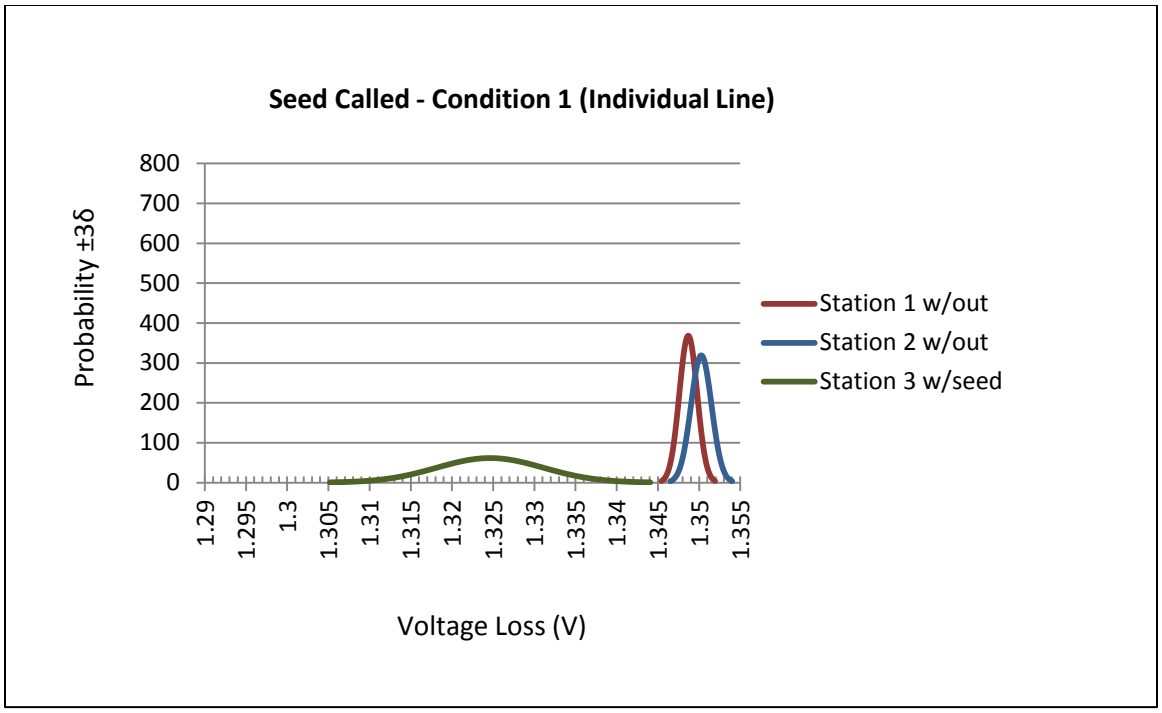

Figure 4.12: Normal distribution curves of Condition 2 with large scale dosimetry loading where element has been called (from spacer hopper) and captured on the comparison light gate area.

High speed single element type normal distributions.

The following *tables 4.19* through *4.22* represent the general statistical analysis and interpretation to normal distribution values performed on both high speed single element type trials. *Figures 4.13* through *4.16* represent normal distribution curves generated from the data sets. *Table 4.19* displays general statistical analysis values calculated from trials concerning seed elements loaded at higher than normal speeds from only the seed type hopper utilizing only seed elements.

Table 4.19

General Statistical Analysis Performed on Edited Voltage Loss Data Concerning High Speed Single Line Loading Trials Utilizing Seed Elements and Seed Channel

	Condition 1			Condition 2		
Value	Light Gate Seed	Light Gate Spacer	Light Gate Compare	Light Gate Seed	Light Gate Spacer	Light Gate Compare
μ	1.310931	1.348310	1.348068	1.346379	1.348586	1.318862
σ	0.006605	0.002089	0.001998	0.001801	0.002322	0.008963
R	0.022	0.007	0.007	0.006	0.008	0.032
max	1.320	1.352	1.351	1.349	1.352	1.331
min	1.298	1.345	1.344	1.343	1.344	1.299
n	29	29	29	29	29	29

Note. μ = mean, σ = standard deviation, R = range, max = maximum value, min = minimum value, n = population.

Table 4.20 displays general statistical analysis values calculated from trials concerning seed elements loaded at higher than normal speeds from only the spacer type hopper utilizing only seed elements.

Table 4.20

General Statistical Analysis Performed on Edited Voltage Loss Data Concerning High Speed Single Line Loading Trials Utilizing Seed Elements and Spacer Channel

	Condition 1			Condition 2		
Value	Light Gate Seed	Light Gate Spacer	Light Gate Compare	Light Gate Seed	Light Gate Spacer	Light Gate Compare
μ	1.344673	1.310571	1.346469	1.344612	1.346735	1.318816
σ	0.001737	0.005339	0.001769	0.001669	0.001966	0.007849
R	0.007	0.021	0.006	0.006	0.008	0.038
max	1.350	1.325	1.350	1.349	1.352	1.332
min	1.343	1.304	1.344	1.343	1.344	1.294
n	49	49	49	49	49	49

Note. μ = mean, σ = standard deviation, R = range, max = maximum value, min = minimum value, n = population.

Table 4.21 displays calculated values of normal distribution curves concerning all possible light gates and conditions from trials utilizing seed element loads from only the seed type hopper at higher than normal speeds.

Table 4.21

Interpretation of Edited Voltage Loss Data to Normal Distribution Values Concerning Single Line Loading Trials Utilizing Seed Elements and Seed Channel at Higher Than Normal Speeds

	Condition 1					
Scale	Light Gate Seed		Light Gate Spacer		Light Gate Compare	
±3 Stand. Dev.	Rescale	Norm. Dist.	Rescale	Norm. Dist.	Rescale	Norm. Dist.
-3	1.291113	0.670892	1.342043	2.121368	1.342073	2.21729
-2.8	1.292435	1.198239	1.342461	3.788845	1.342472	3.960165
-2.6	1.293756	2.056187	1.342879	6.501684	1.342872	6.79567
-2.4	1.295077	3.390079	1.343296	10.71947	1.343272	11.20417
-2.2	1.296398	5.370137	1.343714	16.98043	1.343672	17.74823
-2	1.297719	8.173142	1.344132	25.84356	1.344071	27.01212
-1.8	1.29904	11.95146	1.34455	37.79063	1.344471	39.49941
-1.6	1.300362	16.79117	1.344968	53.09386	1.344871	55.4946
-1.4	1.301683	22.66571	1.345386	71.66921	1.345271	74.90987
-1.2	1.303004	29.39585	1.345803	92.94996	1.34567	97.15287
-1	1.304325	36.62948	1.346221	115.8228	1.34607	121.0599
-0.8	1.305646	43.85345	1.346639	138.665	1.34647	144.935
-0.6	1.306967	50.44347	1.347057	159.5028	1.34687	166.715
-0.4	1.308289	55.74866	1.347475	176.2778	1.347269	184.2486
-0.2	1.30961	59.19596	1.347893	187.1782	1.347669	195.6419
0	1.310931	60.3918	1.34831	190.9595	1.348069	199.5941
0.2	1.312252	59.19596	1.348728	187.1782	1.348469	195.6419
0.4	1.313573	55.74866	1.349146	176.2778	1.348868	184.2486
0.6	1.314895	50.44347	1.349564	159.5028	1.349268	166.715
0.8	1.316216	43.85345	1.349982	138.665	1.349668	144.935

1	1.317537	36.62948	1.350399	115.8228	1.350068	121.0599
1.2	1.318858	29.39585	1.350817	92.94996	1.350467	97.15287
1.4	1.320179	22.66571	1.351235	71.66921	1.350867	74.90987
1.6	1.3215	16.79117	1.351653	53.09386	1.351267	55.4946
1.8	1.322822	11.95146	1.352071	37.79063	1.351667	39.49941
2	1.324143	8.173142	1.352489	25.84356	1.352067	27.01212
2.2	1.325464	5.370137	1.352906	16.98043	1.352466	17.74823
2.4	1.326785	3.390079	1.353324	10.71947	1.352866	11.20417
2.6	1.328106	2.056187	1.353742	6.501684	1.353266	6.79567
2.8	1.329428	1.198239	1.35416	3.788845	1.353666	3.960165
3	1.330749	0.670892	1.354578	2.121368	1.354065	2.21729

Condition 2

Scale	Light Gate Seed		Light Gate Spacer		Light Gate Compare	
±3 Stand. Dev.	Rescale	Norm. Dist.	Rescale	Norm. Dist.	Rescale	Norm. Dist.
-3	1.340976	2.460679	1.341619	1.908209	1.291973	0.494454
-2.8	1.341336	4.394868	1.342083	3.408134	1.293765	0.883114
-2.6	1.341697	7.541623	1.342548	5.848381	1.295558	1.515429
-2.4	1.342057	12.43404	1.343012	9.642351	1.297351	2.498521
-2.2	1.342417	19.69643	1.343477	15.2742	1.299143	3.957842
-2	1.342777	29.97721	1.343941	23.24674	1.300936	6.023683
-1.8	1.343137	43.83521	1.344406	33.99335	1.302728	8.808339
-1.6	1.343498	61.58618	1.34487	47.75888	1.304521	12.37525
-1.4	1.343858	83.13265	1.345335	64.46774	1.306314	16.70485
-1.2	1.344218	107.8172	1.345799	83.61015	1.308106	21.66502
-1	1.344578	134.3485	1.346264	104.1847	1.309899	26.99627
-0.8	1.344938	160.8444	1.346728	124.7317	1.311692	32.32041
-0.6	1.345299	185.0151	1.347193	143.4756	1.313484	37.17732
-0.4	1.345659	204.4733	1.347657	158.565	1.315277	41.08729
-0.2	1.346019	217.1172	1.348122	168.3702	1.317069	43.62799
0	1.346379	221.5033	1.348586	171.7715	1.318862	44.50933
0.2	1.34674	217.1172	1.349051	168.3702	1.320655	43.62799
0.4	1.3471	204.4733	1.349515	158.565	1.322447	41.08729
0.6	1.34746	185.0151	1.34998	143.4756	1.32424	37.17732
0.8	1.34782	160.8444	1.350444	124.7317	1.326033	32.32041
1	1.34818	134.3485	1.350909	104.1847	1.327825	26.99627
1.2	1.348541	107.8172	1.351373	83.61015	1.329618	21.66502
1.4	1.348901	83.13265	1.351838	64.46774	1.33141	16.70485
1.6	1.349261	61.58618	1.352302	47.75888	1.333203	12.37525

1.8	1.349621	43.83521	1.352767	33.99335	1.334996	8.808339
2	1.349981	29.97721	1.353231	23.24674	1.336788	6.023683
2.2	1.350342	19.69643	1.353696	15.2742	1.338581	3.957842
2.4	1.350702	12.43404	1.35416	9.642351	1.340374	2.498521
2.6	1.351062	7.541623	1.354625	5.848381	1.342166	1.515429
2.8	1.351422	4.394868	1.355089	3.408134	1.343959	0.883114
3	1.351783	2.460679	1.355554	1.908209	1.345751	0.494454

Table 4.22 displays calculated values of normal distribution curves concerning all possible light gates and conditions from trials utilizing seed element loads from only the seed type hopper at higher than normal speeds.

Table 4.22

Interpretation of Edited Voltage Loss Data to Normal Distribution Values Concerning Single Line Loading Trials Utilizing Seed Elements and Spacer Channel at Higher Than Normal Speeds

	Condition 1					
Scale	Light Gate Seed		Light Gate Spacer		Light Gate Compare	
±3 Stand. Dev.	Rescale	Norm. Dist.	Rescale	Norm. Dist.	Rescale	Norm. Dist.
-3	1.339463	2.551867	1.294556	0.830161	1.341162	2.505328
-2.8	1.339811	4.557732	1.295624	1.4827	1.341516	4.474613
-2.6	1.340158	7.821099	1.296691	2.544323	1.34187	7.678466
-2.4	1.340505	12.89481	1.297759	4.19488	1.342224	12.65965
-2.2	1.340853	20.42634	1.298827	6.645	1.342578	20.05382
-2	1.3412	31.0881	1.299894	10.11343	1.342931	30.52115
-1.8	1.341547	45.45965	1.300962	14.78872	1.343285	44.6306
-1.6	1.341895	63.86842	1.30203	20.77738	1.343639	62.70366
-1.4	1.342242	86.21335	1.303097	28.04652	1.343993	84.64109
-1.2	1.342589	111.8127	1.304165	36.37438	1.344347	109.7736
-1	1.342937	139.3272	1.305233	45.32527	1.3447	136.7863
-0.8	1.343284	166.8049	1.306301	54.2642	1.345054	163.7629
-0.6	1.343631	191.8713	1.307368	62.41869	1.345408	188.3722

-0.4	1.343979	212.0506	1.308436	68.98332	1.345762	208.1835
-0.2	1.344326	225.1631	1.309504	73.24901	1.346116	221.0568
0	1.344673	229.7117	1.310571	74.72874	1.346469	225.5225
0.2	1.345021	225.1631	1.311639	73.24901	1.346823	221.0568
0.4	1.345368	212.0506	1.312707	68.98332	1.347177	208.1835
0.6	1.345715	191.8713	1.313775	62.41869	1.347531	188.3722
0.8	1.346063	166.8049	1.314842	54.2642	1.347885	163.7629
1	1.34641	139.3272	1.31591	45.32527	1.348238	136.7863
1.2	1.346758	111.8127	1.316978	36.37438	1.348592	109.7736
1.4	1.347105	86.21335	1.318045	28.04652	1.348946	84.64109
1.6	1.347452	63.86842	1.319113	20.77738	1.3493	62.70366
1.8	1.3478	45.45965	1.320181	14.78872	1.349654	44.6306
2	1.348147	31.0881	1.321249	10.11343	1.350007	30.52115
2.2	1.348494	20.42634	1.322316	6.645	1.350361	20.05382
2.4	1.348842	12.89481	1.323384	4.19488	1.350715	12.65965
2.6	1.349189	7.821099	1.324452	2.544323	1.351069	7.678466
2.8	1.349536	4.557732	1.325519	1.4827	1.351423	4.474613
3	1.349884	2.551867	1.326587	0.830161	1.351776	2.505328

Condition 2

Scale	Light Gate Seed		Light Gate Spacer		Light Gate Compare	
±3 Stand. Dev.	Rescale	Norm. Dist.	Rescale	Norm. Dist.	Rescale	Norm. Dist.
-3	1.339607	2.656129	1.340836	2.254103	1.295268	0.564618
-2.8	1.33994	4.743949	1.34123	4.025915	1.296838	1.008429
-2.6	1.340274	8.140649	1.341623	6.908498	1.298408	1.73047
-2.4	1.340608	13.42166	1.342016	11.39019	1.299978	2.853064
-2.2	1.340941	21.2609	1.342409	18.0429	1.301548	4.519464
-2	1.341275	32.35828	1.342802	27.4606	1.303118	6.87845
-1.8	1.341609	47.31701	1.343196	40.15521	1.304688	10.05825
-1.6	1.341943	66.47792	1.343589	56.41597	1.306257	14.13132
-1.4	1.342276	89.73581	1.343982	76.1536	1.307827	19.07528
-1.2	1.34261	116.3811	1.344375	98.76589	1.309397	24.73931
-1	1.342944	145.0197	1.344769	123.0699	1.310967	30.82707
-0.8	1.343277	173.6202	1.345162	147.3414	1.312537	36.90671
-0.6	1.343611	199.7107	1.345555	169.4829	1.314107	42.45282
-0.4	1.343945	220.7145	1.345948	187.3076	1.315677	46.91762
-0.2	1.344279	234.3627	1.346341	198.8901	1.317246	49.81885
0	1.344612	239.0971	1.346735	202.9079	1.318816	50.82525
0.2	1.344946	234.3627	1.347128	198.8901	1.320386	49.81885

0.4	1.34528	220.7145	1.347521	187.3076	1.321956	46.91762
0.6	1.345613	199.7107	1.347914	169.4829	1.323526	42.45282
0.8	1.345947	173.6202	1.348308	147.3414	1.325096	36.90671
1	1.346281	145.0197	1.348701	123.0699	1.326666	30.82707
1.2	1.346614	116.3811	1.349094	98.76589	1.328235	24.73931
1.4	1.346948	89.73581	1.349487	76.1536	1.329805	19.07528
1.6	1.347282	66.47792	1.34988	56.41597	1.331375	14.13132
1.8	1.347616	47.31701	1.350274	40.15521	1.332945	10.05825
2	1.347949	32.35828	1.350667	27.4606	1.334515	6.87845
2.2	1.348283	21.2609	1.35106	18.0429	1.336085	4.519464
2.4	1.348617	13.42166	1.351453	11.39019	1.337655	2.853064
2.6	1.34895	8.140649	1.351847	6.908498	1.339224	1.73047
2.8	1.349284	4.743949	1.35224	4.025915	1.340794	1.008429
3	1.349618	2.656129	1.352633	2.254103	1.342364	0.564618

The following *Figures 4.13* and 4*.14* graphically display the calculated normal distribution values found in *table 4.21*. These graphs illustrate three normal distribution curves a piece with respect to both individual light gate and conditions.

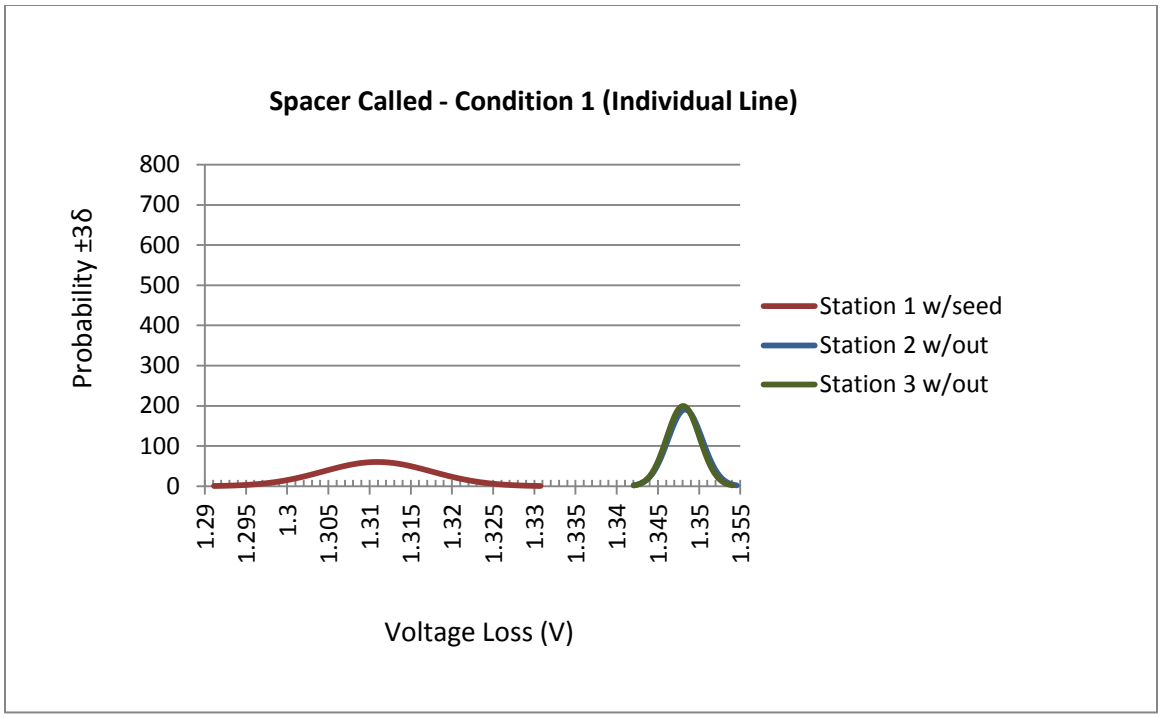

Figure 4.13: Normal distribution curves of Condition 1 with single line loading where element has been called (from seed hopper) and captured on the corresponding seed light gate area.

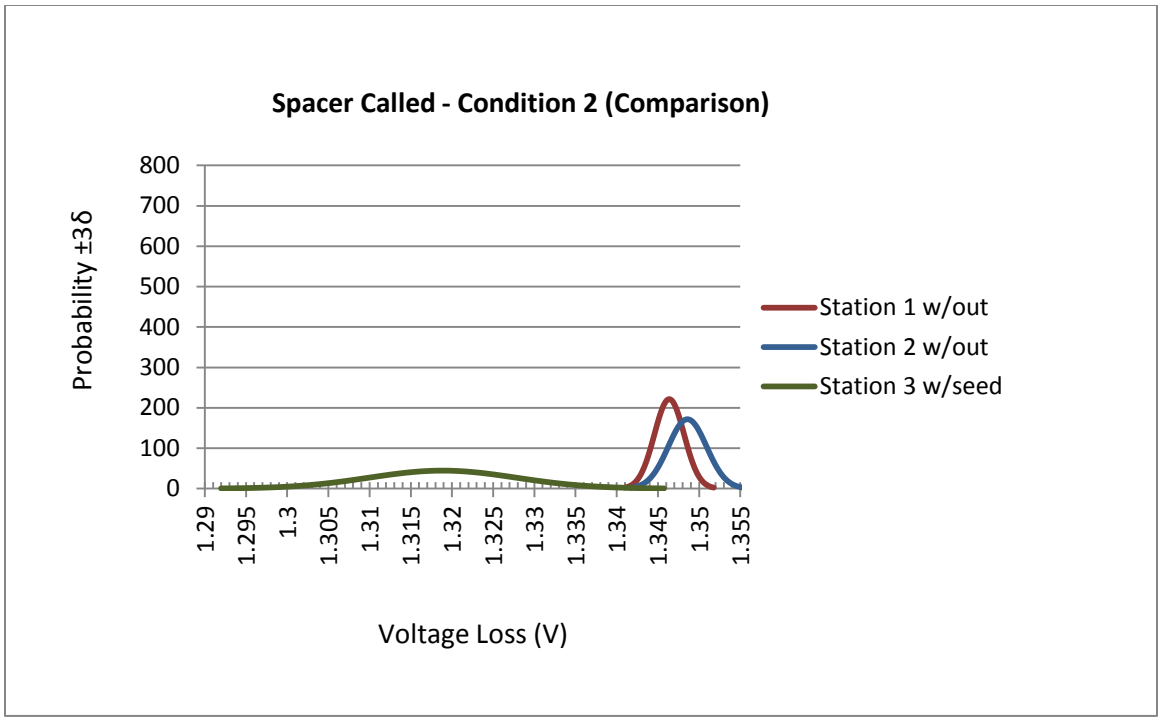

Figure 4.14: Normal distribution curves of Condition 2 with single line loading where element has been called (from seed hopper) and captured on the comparison light gate area.

The following *Figures 4.15* and *4.16* graphically display the calculated normal distribution values found in *table 4.22.* These graphs illustrate three normal distribution curves a piece with respect to both individual light gate and conditions.

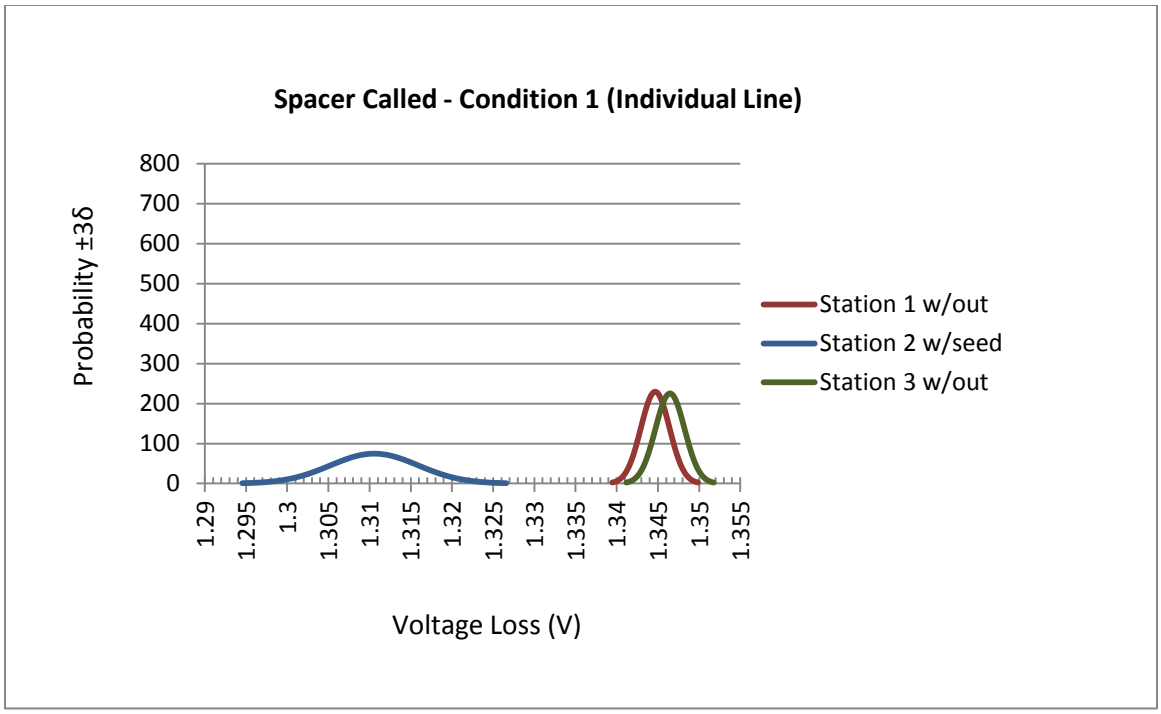

Figure 4.15: Normal distribution curves of Condition 1 with single line loading where element has been called (from spacer hopper) and captured on the corresponding spacer light gate area.

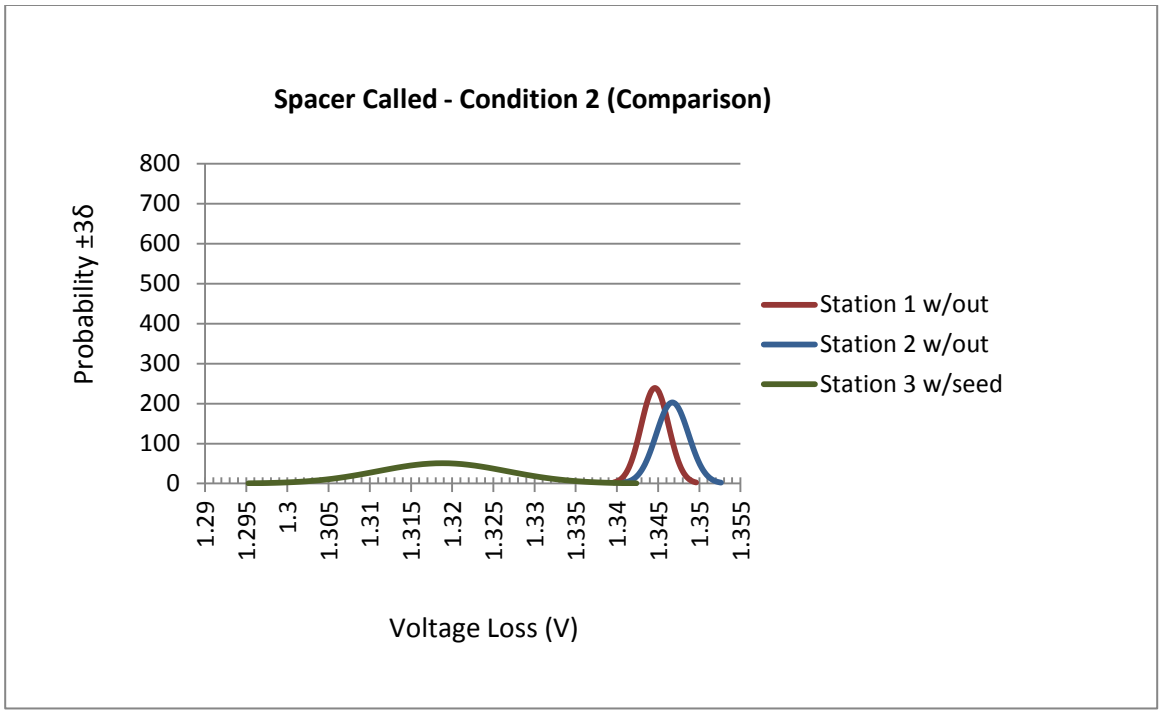

Figure 4.16: Normal distribution curves of Condition 2 with single line loading where element has been called (from spacer hopper) and captured on the comparison light gate area.

Combined normal distributions.

Following the completion of all data sets to that of normal distribution curves, an overall graph was created illustrating all trial runs in relation to element presence. This multiple line graph shows (red) all normal distributions derived from data sets in which an element was captured while also showing (blue) all normal distributions derived from data sets in which an element was not present in *figure 4.17.*

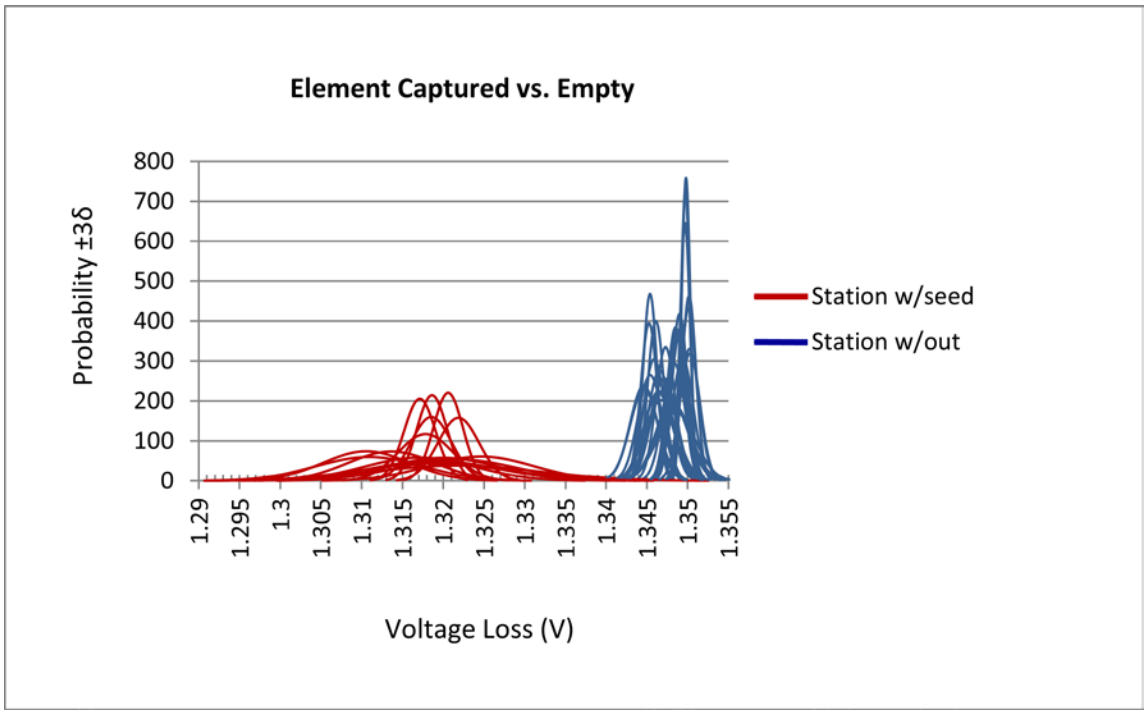

Figure 4.17: Normal distribution curves of all Conditions and trials with respect to element capture.

It should be noted that while all light gates were normalized to an empty condition voltage loss of around -1.35v, conditions and factors have not been accounted for.

4.4 Performed Two-Sample t Tests

To determine if a change of status had occurred, seed element present or not present, at any light gate during the initial testing trials, statistical analysis using multiple two-sample t tests was performed using the recorded data sets. As with the interpretation of the recorded data to that of normal distribution curves, raw data sets found in *tables 4.1* through *4.4* were edited to remove known errors during the automated loading process. Following the removal of these errors, the edited data sets were subjected to separation based upon light gates in which the values were recorded from. For each trial, three data sets were obtained with each consisting of both a condition 1 and condition 2.

These conditions were then compared using the two-sample t test method. The following table 4.23 shows resulting p values from the performed two-sample t tests.

Table 4.22

P-Values Resulting From the Performed Two-Sample t Tests

Trial	Element Called	Resulting p-values		
		Seed Gate	Spacer Gate	Compare Gate
Single Line Loading	Seed	0.000	0.675	0.000
	Spacer	0.143	0.000	0.000
Random Dosimetry (Small)	Seed	0.000	0.010	0.000
	Spacer	0.253	0.000	0.000
Random Dosimetry (Large)	Seed	0.000	0.753	0.000
	Spacer	0.844	0.000	0.000
Single Line High Speed Loading	Seed	0.000	0.636	0.000
	Spacer	0.859	0.000	0.000

Note. Trials with unsatisfactory results or errors have been highlighted above.

CHAPTER 5: ANALYSIS AND CONCLUSIONS

The following Chapter V Analysis and Conclusions provides interpretations and conclusions by the researcher based on the presented results in Chapter IV. Discussions regarding the current work and possible direction of future works will also be included within this chapter. Opinions of the researcher within this chapter are based on both gathered information and educated speculations.

5.1 Discussion of Results

In Chapter IV, results from both observations and initial testing have been displayed. In this chapter, various information regarding observations, general data set interpretation, and statistical testing was presented. While it should be noted that testing regarding the constructed device has been performed in an exploratory nature, all testing has been conducted in the intentions of allowing an unbiased "glimpse" into the feasibility and general working of the constructed system and design choices as they relate to the non-mechanical loading of brachytherapy elements. The following discussion of results section has been segmented to give attention to the various results gathered from the performed testing trials.

General operation and workings of device.

The automation of brachytherapy element loading process using non-mechanical interactions was achieved using the constructed system. It was observed that seed elements were readily introduced into the system from both hoppers during operation of the system. However, far too many errors occurred during the initial testing phase of the constructed system. While most of these errors were attributed to seed elements

bypassing the third comparison light gate, an error which did not affect the resulting load, other more critical errors were also observed. Critical errors within the system were seen as those resulting in a load of the brachytherapy needle incorrect with that of the predefined dosimetry plan. These critical errors can then be broken down again into fatally critical errors, in which, the automated program was unable to detect an error within the loading process. Within the trials conducted the following table represents non-critical loads, the following *table 5.1* expresses both the number and severity of all errors observed during the initial testing phase.

Table 5.1

Error Values and Severity within Initial Testing Trials

Trial	Element Called	# of Elements	Type of Error		
			Errors	Critical Errors	Fatally Critical Errors
Single Line Loading	Seed	24	3	0	0
	Spacer	21	4	0	0
Random Dosimetry (Small)	Seed	28	2	0	0
	Spacer	29	6	1	1
Random Dosimetry (Large)	Seed	60	3	0	0
	Spacer	51	6	1	0
Single Line High Speed Loading	Seed	33	4	2	0
	Spacer	51	2	0	0

Note. Fatally critical errors that were undetected by the automated system have been highlighted above.

Within normal operations of the constructed system, only one fatally critical error was observed. This fatally critical error occurred during the small scale random dosimetry trial on run 38. Within this run a spacer was called for by the automated program. Once called by the program, the automated sequence began and an attempt was made to load a single seed element from the spacer reservoir hopper. During this loading attempt two seed elements were allowed to pass into the remainder of the system through the "hand-off" method. These seed elements traveled to, and were detected by, the spacer light gate area. At this area, the automated program was unable to recognize the second element and declared the presence of only one seed element. Following this initial spacer light gate reading, both elements were released and allowed to continue travel through the system. Sequentially, both elements were then captured by the comparison light gate area and underwent the second inspection. This second comparison by the automated system was unable to recognize the trailing element of the pair and concluded that a correct load had been established. Once released from the comparison light gate area both elements traveled into the brachytherapy needle resulting in the loading of an extra element violating the dosimetry plan. Providing the constructed system had performed such a fatally critical load within the prostate brachytherapy procedure, all elements preceding the error, including the secondary element loaded during the error, would be incorrect changing the applied radiation locations within the prostate. A fatally critical error, such as the one previously described, could be discovered and corrected through the use of a visual comparison by the end user or subsequent secondary comparison through the automated process.

Normal distributions.

The normal distribution graphs displayed in *figures 4.1* through *4.16 show* a clear similarity across all trials under repeated conditions. This similarity refers to both the shape and location of the distributions. Normal distributions calculated from data sets in which an element was captured showed separation from the remaining two data sets in which nothing was present. This was to be expected as an element present at a light gate would decrease the voltage loss across the circuit. This separation of normal distribution curves was consistent through all trials showing a clear separation between voltage losses attributed to element presence.

Shape of the normal distributions calculated from the light gates tended to show a direct correlation to both the presence of an element and the location of the light gate within the constructed system. In instances were no element was present within the light gate, the normal distribution tended to show a low standard deviation resulting in a tight distribution. This tight distribution inferred that all values recorded when no seed was present fell within a small range of values. This was expected as values within an empty light gate we subjected to no change. Differing from the tight distributions found with empty light gates, those light gates containing a seed element showed far wider distributions. These wider distributions inferred that the recorded values fell within a range larger than the previously described empty light gate distributions. This was also an expected result as the position of the captured seed element naturally varied in location within the light gates. This variation in position within the light gates resulted in more or less light passing through the gate thus changing the voltage loss across that circuit.

In all cases, data sets recorded with a seed element present at the light gate were found to posses wide distributions with large standard deviations, especially within the high speed single element loading trial. However, when comparing normal distributions calculated with a seed present between condition 1 and condition 2, a difference can be readily seen. This difference concerns the range of values within the data sets. Distributions with a seed captured at condition 1(seed or spacer light gate) were consistently narrower than those at condition 2 (comparison light gate). This translated to a higher range of values within the condition 2 or comparison light gate distributions. With a higher range of values recorded from the secondary comparison light gate within the system, it can be inferred that seed element capture was less precise at this light gate. These large distributions at the comparison light gate data sets showed that capture of a seed element as it traveled through the system was less consistent at this lower position. This was also observed through the error values within the raw data sets. Out of the recorded thirty errors within all results, seventeen errors were attributed to failure of the comparison light gate to capture the seed element as it was released from either of the first light gates. Based on this information, it can be said that elements travelling past this comparison light gate were traveling at a speed too high for the vacuum line to properly capture them. This lack of proper vacuum capture caused the elements to vary highly in their captured position within the comparison light gate which in turn affected the resulting normal distributions and the many recorded errors. Normal distributions also saw a widening effect when time between operations was reduced. Again this was an expected outcome as higher speeds would naturally tend to decrease accuracy of element captures.

Another observation made regarding the wide distributions, especially those generated from the comparison light gate with a seed present, regarded the crossing of distributions. Evident within *figure 4.4, figure 4.14, and figure 4.16* the normal distribution generated from the comparison light gate within condition 2 seems to slightly cross with the remaining two normal distributions. This was a concerning issue as values falling within this overlapping area would be indiscernible as to the presence of a captured element. As threshold values were applied within the automated system to discern the presence of an element at any light gate, any overlapping of values was seen as detrimental to the systems element loading capabilities. However, while the overlapping of these distributions was observed, no recorded values within the distributions crossed one another. To better illustrate this, *figure 5.1* shows an additional normal distribution graph calculated from all values within the large scale random dosimetry trial. In these figures, data from the large scale random dosimetry trial were grouped together based on the presence of a seed element. In the first *figure 5.1,* the normal distributions can be seen. The distributions within this graph show the same characteristics as all other normal distribution graphs with a wide distribution across seed element captures and a narrow distribution where no element was present. While these distributions do not show a tendency to cross one another, a comparison graph in the form of a box and whisker plot has been provided as contrast in *figure 5.2.*

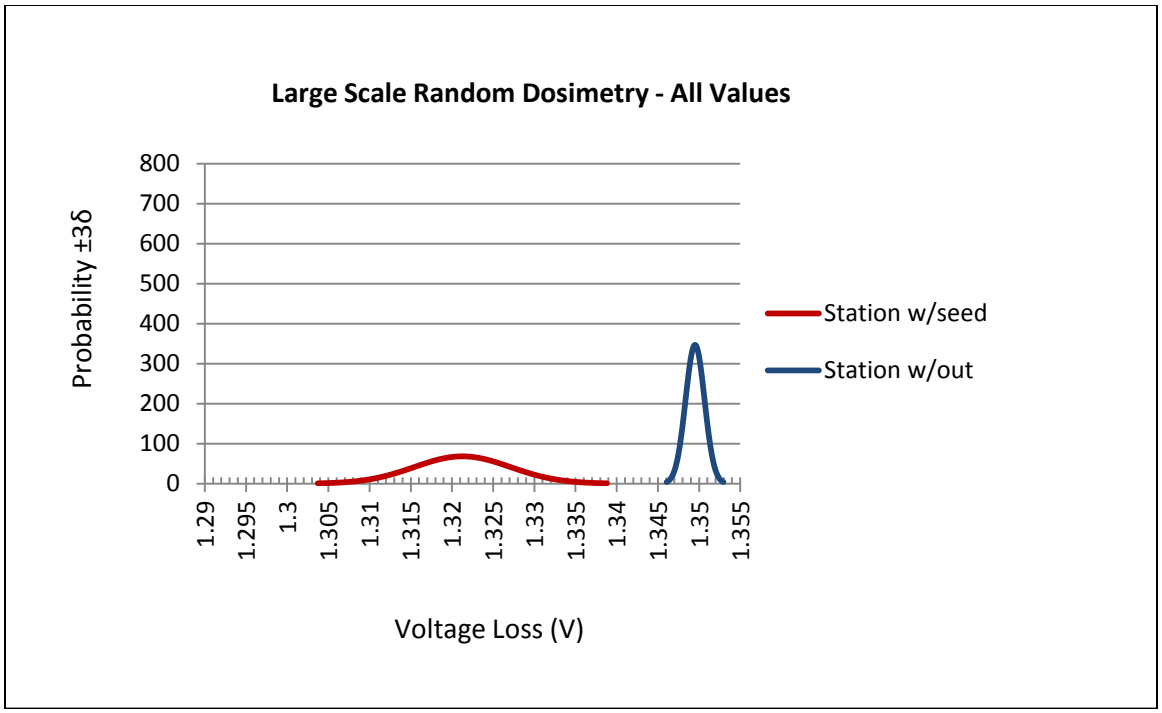

Figure 5.1: Combined normal distribution curves of large scale random dosimetry trial with respect to element capture.

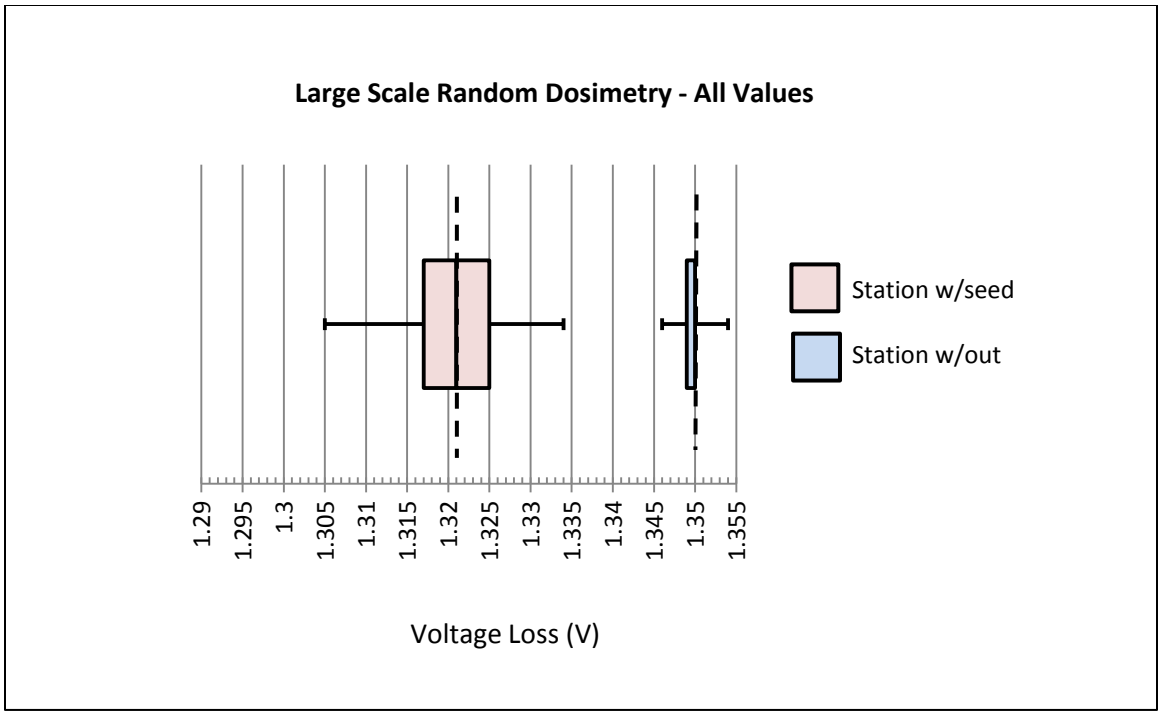

Figure 5.2: Box and whisker plot of all recorded values within the large scale random dosimetry trial.

In comparison of the graphs in *figures 5.1* and *5.2* the space between the two data sets becomes more apparent as the maximum and minimum values of each data set has been displayed within the box and whisker plot. This difference between the seed captured and empty data sets become even more extreme if attention is paid to the upper and lower quartiles of each data set within the box and whisker plot.

Two-sample t tests.

Within the performed two-sample t tests, all resulting p values showed expected significance with an α value of 0.05 save one. It was expected that all compared means would show significance if the presence of a seed within the specified light gate had changed from condition 1 to condition 2 and those with no seed in either condition would show insignificance. The only p value to contradict the expected outcomes was attributed

to the small scale dosimetry trial in which a seed element was called for by the automated system. In this capacity, the spacer light gate experienced no change in condition. However, the p value contradicted this statement as a resulting α value of 0.010 falling below the selected α value of 0.05 was found for the performed two-sample t test. In this interpretation, the spacer light gate means were statistically different from each other. This difference, while statistically significant, still possessed a relatively low p value when compared to other statistically significant values which all resulted in 0.000. This issue could be resolved through the use of a higher confidence interval with an α of around 0.01 or lower. With a lower α value, the associated p value in this situation would have remained insignificant inferring the selected means were not statistically different from one another allowing for the expected outcomes. With the p values from the two-sample t tests stated with an α value of 0.01, the claim can be made that the presence of a seed element within any light gate statistically changes the resulting mean.

5.2 Conclusions

Within the scope of the presented work, a system has been successfully developed and tested to allow for the automated non-mechanical loading of brachytherapy elements utilizing loose elements and the method of pre-loaded brachytherapy needle applicators. Through the use of pilot testing and full scale development, a design was conceived that utilized mainly the factors of vacuum and air pressures in the manipulation and sorting of loose elements according to a preset dosimetry plan. Within this design, the use of the "hand-off" method of introducing only one element at a time to the system from the hoppers was not without issue. Mainly, errors attributed to the "hand-off" method were due to the connection of the air lines on both single element channels and the reliance on

vacuum pressures alone. With the current connection method, all air lines connecting to the spacer element channel were split and also connected to the seed element channel. This setup was utilized with the assumption that independent vacuum lines would disallow release from the “hand-off” area, even with air lines on both single element channels activating during every load. This provided a savings as to the amount of components required on the on the pneumatics, but introduced air pressures in unneeded areas. This extra air pressure on elements intended to be kept stationary through vacuum pressures was detrimental and required lower than intended air pressures as to not overcome the necessary vacuum lines. Multiple errors were attributed to this lack of air pressures at the single element channels in which a secondary, or trailing, element failed to be loaded. This caused the single seed element within the “hand-off” area to not be released.

The constructed system has been able to successfully load and verify this dosimetry plan with only one critically fatal error, which can easily be remedied. Design changes, including the addition of a secondary comparison light gate to detect the presence of any trailing elements and the reduction of element speed at the comparison light gate, would improve the overall functionality of the device ensuring the occurrence of any loading error would be detected by the automated control system. The verification method within the constructed system using light to determine the presence of elements as they pass through the system was found to be a valid method of detection based on both normal distributions and two-sample t tests performed with initial testing data. These light gates also posses the possible application in discern element type as well within the system based on pilot test observations. While still possessing a multitude of

improvable areas, the proposed method of non-mechanical element loading has shown great promise in future implementation within the medical brachytherapy community.

5.3 Recommendations and Future Works

There exist numerous paths in which the presented work could be expanded within future works. The system constructed within this work only represents an exploration into the design concept of using non-mechanical methods in the loading of brachytherapy elements. As such, many of the design decisions and assumed variables should be fully investigated and explored. Paramount in these is the full empirical testing of the device constructed within this work. Extensive testing is needed to both validate and confirm the results and conclusions made within this work. While control of such factors as vacuum, air pressure, and voltage was present, these factors were only optimized based on observations of the researcher. It is unknown if these factors were correctly calibrated to allow for optimum loading conditions. Unidentified relationships and factors could be present within the constructed system and remain an unexplored possibility. Testing concerning these control factors should be performed with both the current system and with auxiliary instrumentation. Additionally, further testing using the current system should also include multiple large-scale random dosimetry trials to truly indicate any potential problems not found within the current work and simulate an actual brachytherapy procedure.

Regarding the design of the main body pieces post initial testing, slight design changes could be made within subsequent prototypes. Exploration of the concept of vibration, especially as it relates to element travel and vacuum interaction, could improve or worsen functions within the system. The introduction of vibration to the system was

explored within the pilot testing, and to a lesser extent within the full scale construction, but was never utilized during the presented initial testing. Initially it was assumed that vibration would play a pivotal role in the loading of non-mechanical loading of brachytherapy elements, and it yet still may. But observations found from the performed iterations seemed to show a tendency for vibration to play a secondary or even background role to that of vacuum and air pressures. However this should not bias future experimentations as design decisions could have resulted in a system in which vibration had little observed affect. Combined in this is the fact that no large scale vibration was introduced to the loading process, rather only small vibration motors were employed. This choice of vibration size within this work could have dampened the impact of vibration further. Future small and large scale testing should be performed on the interaction imparted from vibration to the loading of elements.

As the currently constructed system is by nature a prototype, the refinement of the device would be necessary for any manufacturing capacity. As the end goal in performing this research was to the allow for the production of such a loading system for its use in both cancer treatment and specialty facilities, future work should concentrate on both the production and manufacturing aspects of future systems. Of these product refinements, the end product should be consolidated resulting in a single unit. It is expected that such a system would need a small size envelope to become more readily usable when placed in an emergency or clean room within a particular facility. This differs from the current system in that a large testing stand was thought necessary due to the unidentified nature of the components needed to complete the set tasks of this work. Other features unable to be implemented in the current system could also be placed in this new system, paramount

of these being the addition of hoppers able to prohibit the passage of elements into the main body. This would prevent an issue found within the current system that forces the emptying of both hopper sections using the loading program, a time consuming process. Additionally, the use of the NI DAQ and LabVIEW™ software would need to be replaced with that of a standalone and custom controller with the capabilities of the current setup.

In short, the presented work has only scratched the surface of the possible directions available in the loading of brachytherapy elements through non-mechanical means. The use of automated processes to improve medical procedures will only increase in the coming years. Even in the specific area covered within this work, only a one of the possible solutions has been attempted.

BIBLIOGRAPHY

Jemal, A. Siegel, R., Ward, E., Hao, Y., Xu, J., and Thun, M. J. (2009). Cancer statistics, 2009. *CA Cancer J Clin, 59,* 225-249.

Naitoh, J., Zeiner, R. L., Dekernion, J. B. (1998, April) Diagnosis and treatment of prostate cancer. *American Family Physician*, Retrieved from http://www.aafp.org/afp/980401ap/naitoh.html

Wirth, M. P., Hakenberg, O. W. (1999). Brachytherapy for prostate cancer. *Int J Radiation Oncology Biology Physics 63,* 87-91.

R. Helmig, T. Mitchell, and B. Lu, personal communication, March 2010.

Crook, J. M., Raymond, Y., Salhani, D., Yang, H., Esche, B. (1995). Prostate motion during standard radiotherapy as assessed by fiducial markers. *Radiotherapy and Oncology, 37,* 35-42.

T. Mitchell, personal communication, Jan. 2011.

R. Helmig, personal communication, May 2010.

Zhang, Y. D., Podder, T. K., Ng, W. S., Sherman, J., Misic, V., Fuller, D., Messing, E. M., … Yu. Y. (2006, October). *Semi-automated needling and seed delivery device for prostate brachytherapy.* Paper presented at IEEE/RSJ International Conference on Intelligent Robots and Systems, Beijing, China.

R. Helmig, personal communication, Aug 2009.

Glasser, O. (1931). First roentgen evidences. *Radiology, 17,* 789-791.

Orton, C. G. (1995). Uses of therapeutic x-rays in medicine. *Health Physics*, *69*(5), 662-676.

Bostwick, D. G., Crawford, E. D., Higano, C. S., Roach, M. (2005). *American cancer society's complete guide to prostate cancer*. Atlanta, GA: American Cancer Society.

Wallner, K., Merrick, G., Blasko, J. C., and Dattoli, M. J. (2008). *Prostate Brachytherapy Made Complicated. (Rev. 3)* Seattle, WA: SmartMedicine Press.

Simon, H. B., & Laing, K. S. (2008, September). Treating prostate cancer, part V: radiation therapy. *Harvard Men's Health Watch, 13*(2), 1-4.

Potters, L., Morgenstern, C., Calugaru, E., Fearn, P., Jassal, A., Presser, J., and Mullen, E. (2005). 12-year outcomes following permanent prostate brachytherapy in patients with clinically localized prostate cancer. *The Journal of Urology, 173*(5), 1562-1566.

Pasteau, O., and Degrais, P. (1913). De L'emploi du radium dans le traitement des cancers de la prostate. *The Journal of Urology, 4,* 341-346.

Flocks, R. H., Kerr, H. D., Elkins, H. B., and Culp, D. (1952). Treatment of carcinoma of the prostate by interstitial radiation with radio-active gold (Au 198): a preliminary report. *Journal of Urology, 68*(2), 510-522.

Ash, D., Bottomley, D. M., Carey, B. M. (1998). Review prostate brachytherapy. *Prostate Cancer and Prostatic Diseases, 1*, 185-188.

Whitmore, W. F., Hilaris, B., Grabstald, H. (1972). Retropubic implantation to iodine 125 in the treatment of prostatic cancer. *Journal of Urology, 108*(6), 918-920

Aronowitz, J.N (2002). Benjamin Barringer: originator of the transperineal prostate implant. Urology 2002 *60(4), 731-734*.

Holm, H. H., and Gammelgaard, J. (1981). Ultrasonically guided precise needle placement in the prostate and the seminal vesicles. *The Journal of Urology, 125*(3), 385-387.

Ellis, W. J. (2002). Prostate brachytherapy. *Cancer and Metastasis Reviews, 21,* 125-129.

Yu, Y., Anderson, L. L., Li, Z., Mellenberg, D. E., Nath, R., Schell, M. C., Waterman, F. M., Wu, A., Blasko, J. C. (1999). Permanent prostate seed implant brachytherapy: Report of the American Association of Physicists in Medical Task Group No. 64. *Medical Physics 26(10), 2054*-2076.

Lucas, J. N. (Ed.). (2004). Trends *in Prostate Cancer Research (Rev. 7)*. Hauppauge, NY: Nova Biomedical Books.

Hammer, J., Hawliczek, R., Kárcher, H., and Riccabona, M. (1989). A new spacing material for interstitial implantation of radioactive seeds. *Int J Radiation Oncology Biology Physics, 16,* 259-260.

Dicker, A. P., Merrick, G. S., Waterman, F. M., Valicenti, R. K., and Gomella, L. G. (2005). *Basic and Advanced Techniques in Prostate Brachytherapy.* Oxfordshire, England: Taylor & Francis.

Wallner, K., Ellis, W., Russell, K., et al. (1999). Use of TRUS to predict pubic arch interference of prostate brachytherapy. *Int. J Radiation Oncology Biology Physics, 43,* 583-585.

Davis, B. J., Pisansky, T. M., Wilson, T. M., Rothenberg, H. J., Pacelli, A., Hillman, D. W., …and Bostwick, D. G. (1999). The radial distance of extraprostatic extenstion of prostate carcinoma. *Cancer, 85,* 2630-2637.

Beard, C. J., Kijewski, P., Bussiére, M., Gelman, R., Gladstone, D., Shaffer, K., …Coleman, C. N. (1996). Analysis of prostate and seminal vesicle motion: implications for treatment planning. *Int J Radiation Oncology Biology Physics, 34*(2), 451-458.

Schild, S. E., Casale, H. E., Bellefontaine, L. P. (1993). Movements of the prostate due to rectal and bladder distension: implications for radiotherapy. *Medical Dosimetry, 18*(1), 13-18.

R. Helmig, personal communication, Sept. 2009.

Mercereau, S. F., Jacobs, C. (2004). *U.S. Patent No. 6450937 B1*. Washington, DC: U.S. Patent and Trademark Office.

Prestidge, B. R., Prete, J. J., Buchholz, T. A., et al. (1998) *A survey of current clinical practice of permanent prostate brachytherapy in the United States. Int. J Radiation Oncology Biology Physics, 40,* 461-465.

.

Whitmore, W. F., Barzell, W. E., and Wilson, R. F. (2000). *U.S. Patent No. 6,036,632.* Washington, DC: U.S. Patent and Trademark Office.

Mick, F. W., and Zabrouski, K. (1999). *U.S. Patent No. 5,860,909.* Washington, DC: U.S. Patent and Trademark Office.

DeGinder, W. L., and Mistry, V. D. (1978) Novel and inexpensive system for interstitial I^{125} seed implants. *Int J Radiation Oncology Biology Physics, 4,* 745-747.

Ellard, T. R. (2003). *U.S. Patent No. 6,582,354 B2.* Washington, DC: U.S. Patent and Trademark Office.

Green, T. C., Boucher, R. P, Belman, Y. (2004). *U.S. Patent No. 2004/0162458 A1.* Washington, DC: U.S. Patent and Trademark Office.

Shi, X., (2000). *U.S. Patent No. 6,113,529.* Washington, DC: U.S. Patent and Trademark Office.

Kan, W. C., (1999). *U.S. Patent No. 5,906,574.* Washington, DC: U.S. Patent and Trademark Office.

R. Helmig, personal communication, Sept. 2010.

Kalas, D., Bossi, D., Cutrer, L. M. (2003). *U.S. Patent No. 2003/0045769 A1*. Washington, DC: U.S. Patent and Trademark Office.

White, J. C., Carr, S. N. (2005). *U.S. Patent No. 2005/0267319 A1*. Washington, DC: U.S. Patent and Trademark Office.

REFERENCES

Correct Products (2008). Vacuum Pick-Up Tools. Retrieved from: http://www.correctproducts.com

Emory Healthcare (2010). Interstitial Radiation or Seeds (Brachytherapy). Retrieved from: http://www.emoryhealthcare.org/urology/img/brachytherapyseeds.jpg

Australasian Brachytherapy Group (2008). Frequently Asked Question. Retrieved from: http://www.abg.org.au/General/BrachytherapyFAQs.asp

Prostate UK (2010). Radiotherapy. Retrieved from: http://www.prostateuk.org/prca/prcatreatinradio.htm

IZI Medical Products (2010). Radiation Therapy. Retrieved from: http://izimed.com/radiation_therapy.shtml

Appendix A

Reference Photographs

Additional MTA Photographs

Photos of unsuccessful MTAs exploring the uses of an additive rapid prototype approach with a focus on the “hand-off” area and various atmospheric vent designs.

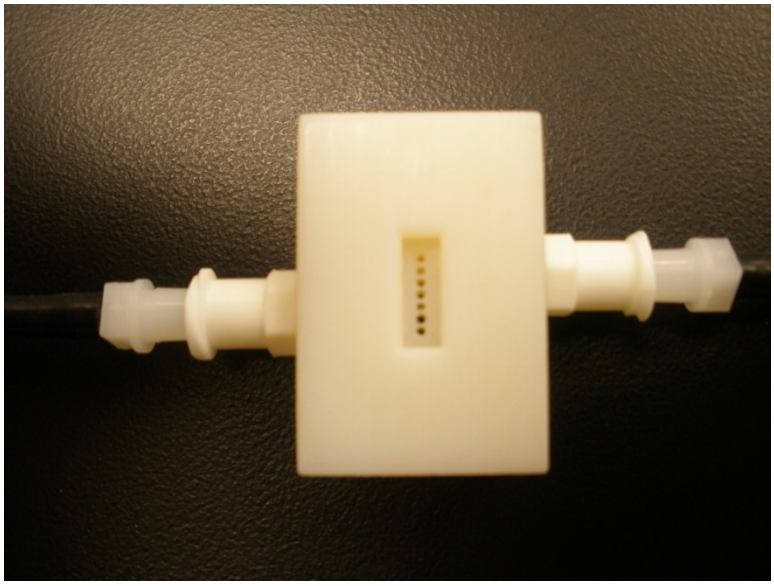

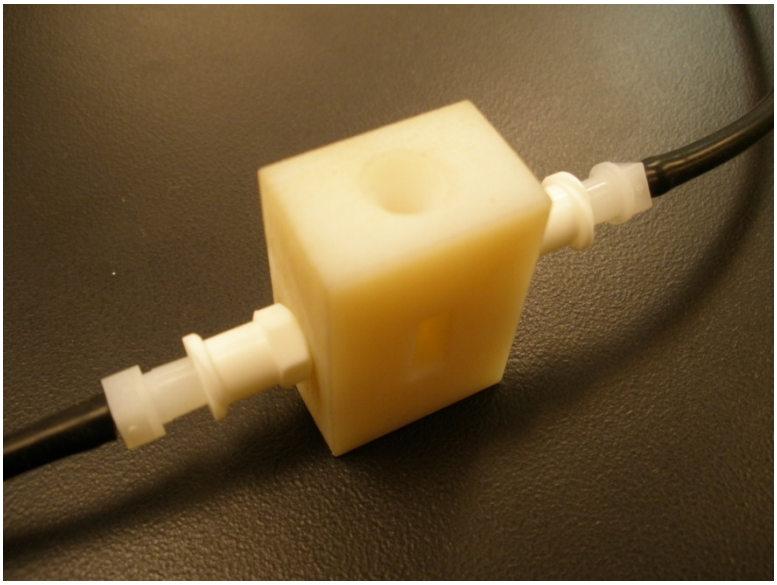

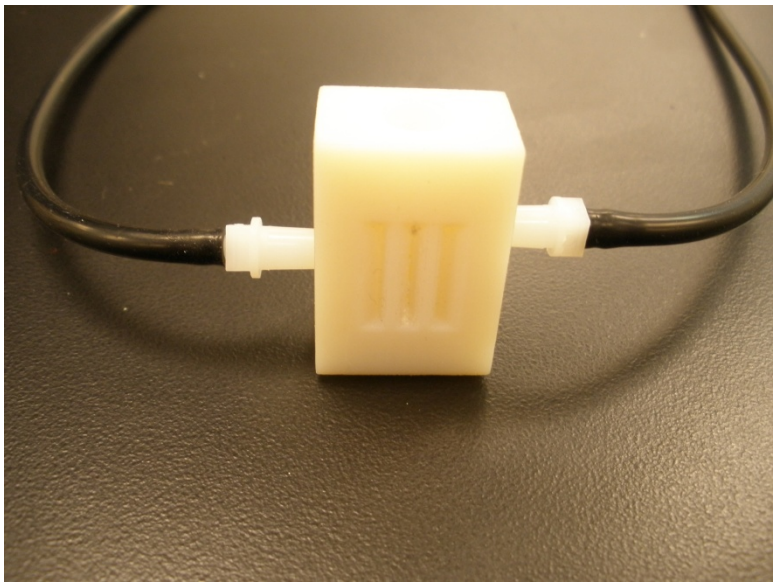

Additional Photos of acrylic MTAs fabricated using subtractive CNC machining.

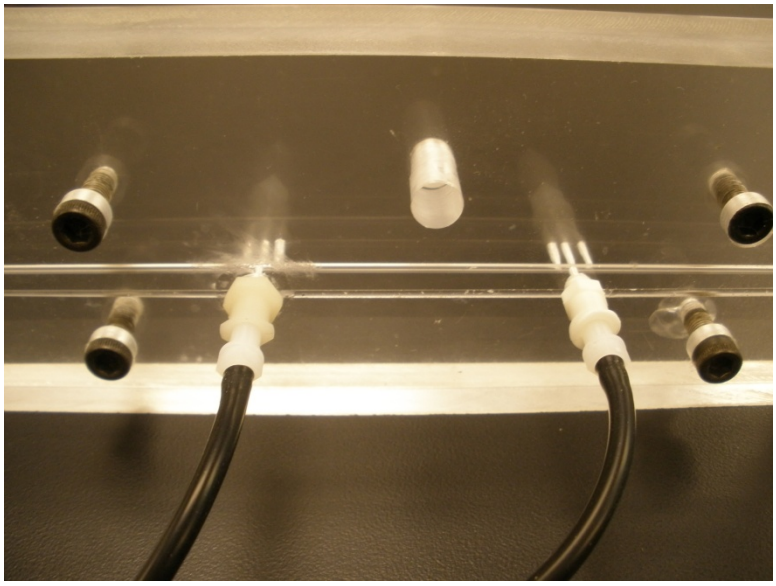

Initial Full Scale Device Construction

Photo of the straight “pre-stacked” hoppers magazines. Shown with air inlets quick disconnects.

Photo of initial setup including entire full scale system with initial main body sections and attached computer running automated loading program.

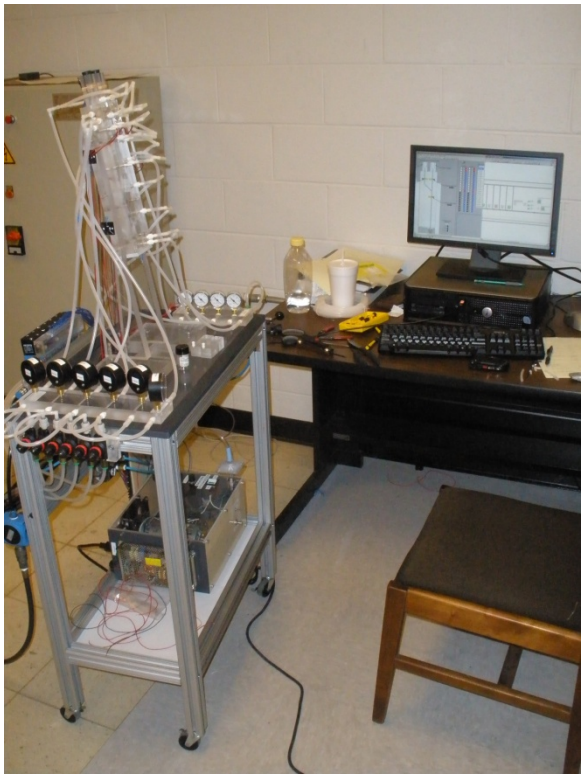

Photo of initial main body sections attached to full scale system.

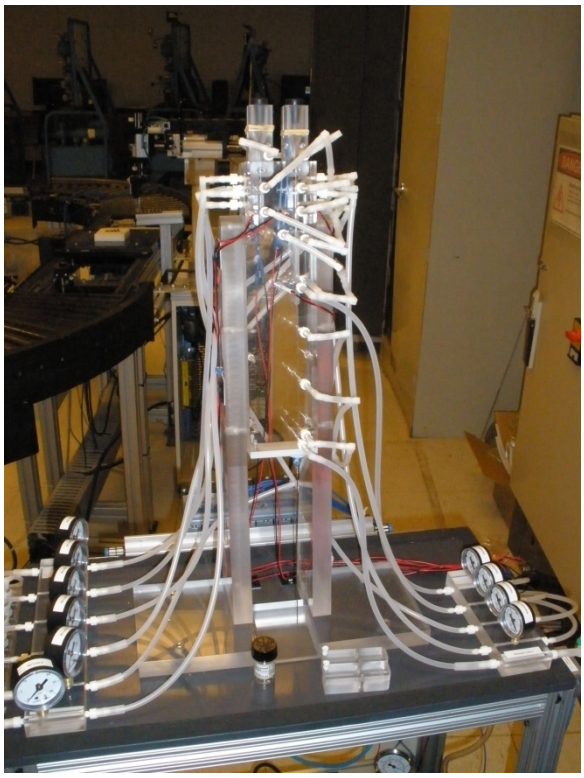

Photo of upper section of initial acrylic main body and connected funnel hoppers connected into full scale system.

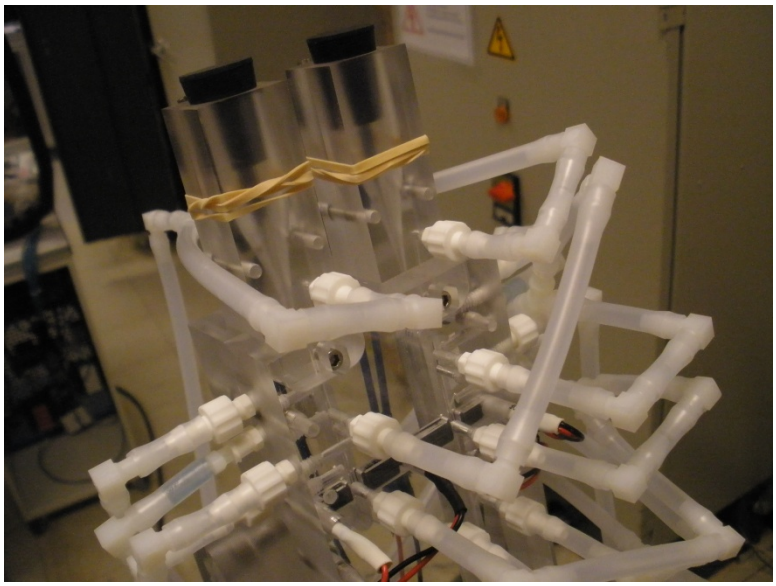

Photo of “hand-off” area within initial acrylic main body connected to full scale system.

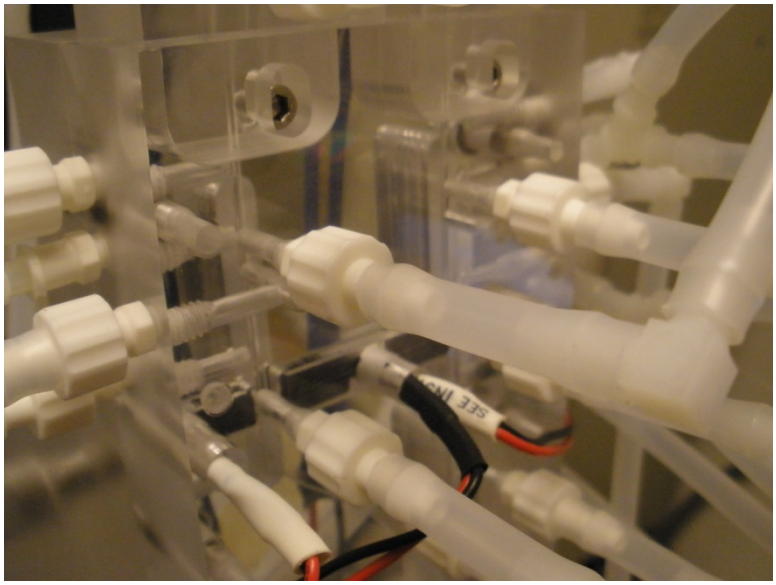

Control and Testing Stand

Photo of air volume reducers and subsequent air pressure (PSI) gauge array.

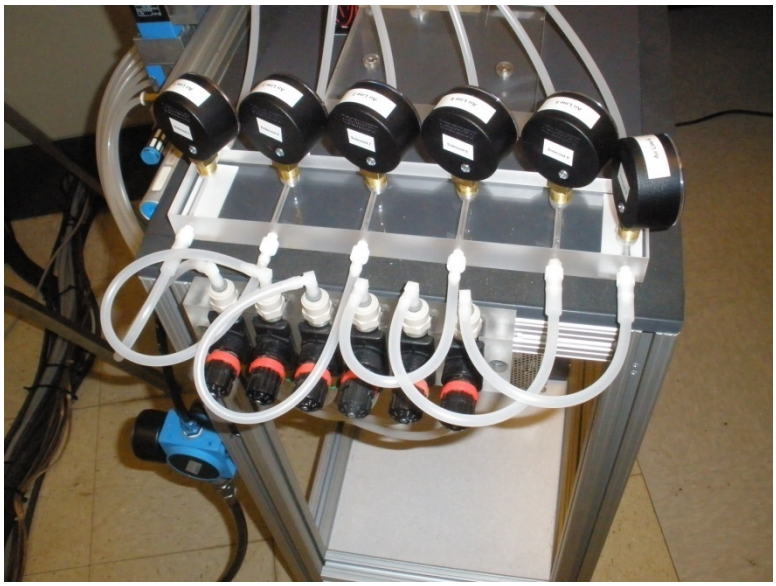

Photo of vacuum (inHg) gauge array including manual “release to needle” actuator. Photo also includes light gate voltage adjustment area.

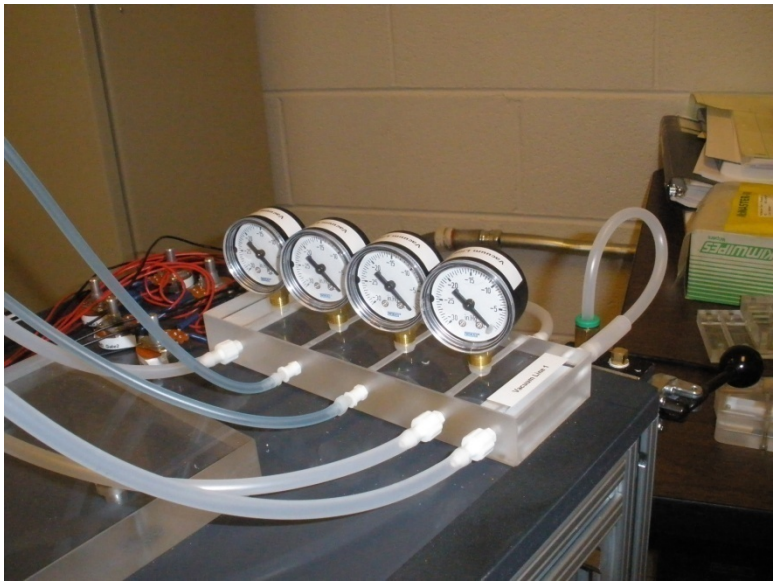

Photo of air pressure (PSI) gauge array.

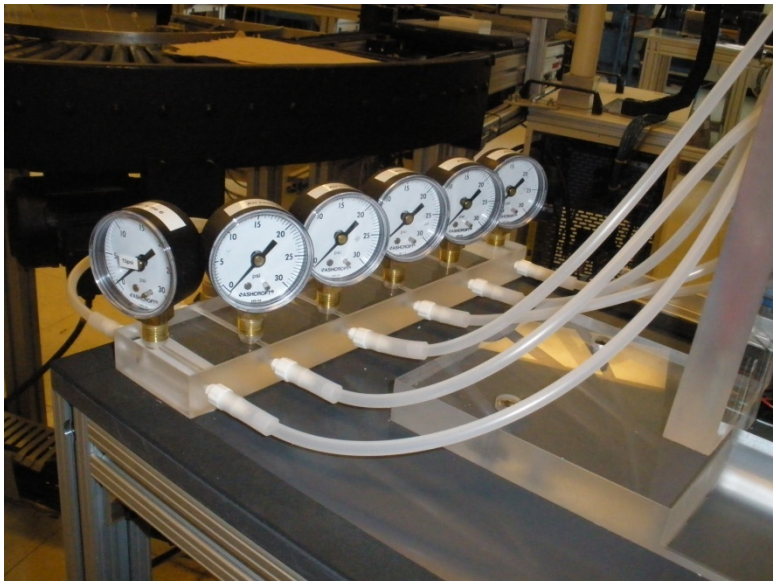

Photo of electrical component box.

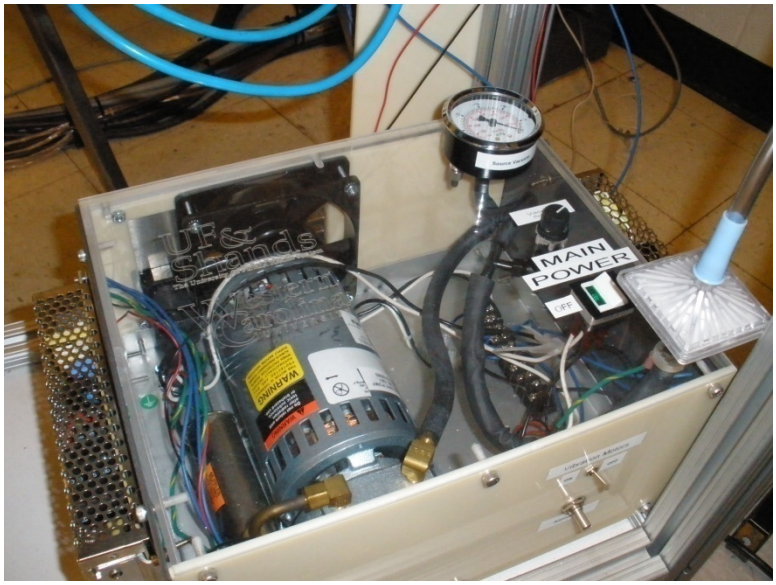

Photo of air piloted solenoid valves and vacuum line splitter.

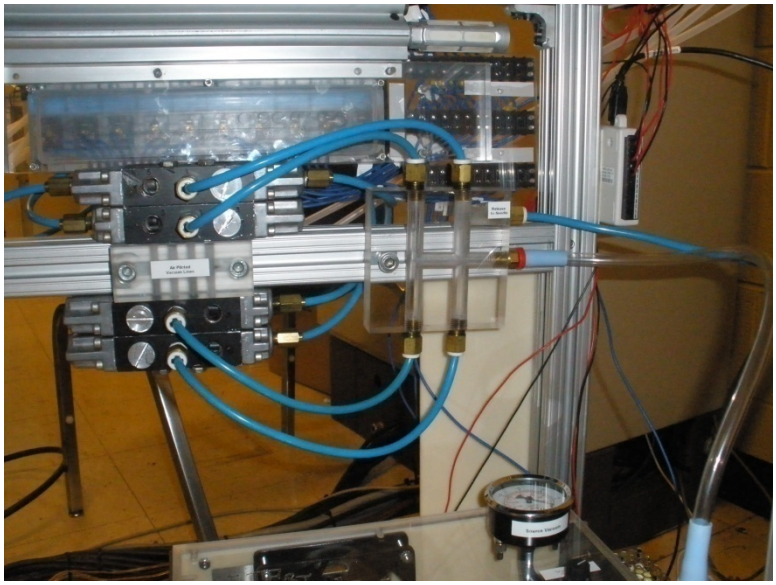

Photo of manual ‘release to needle’ actuator and DAQ device.

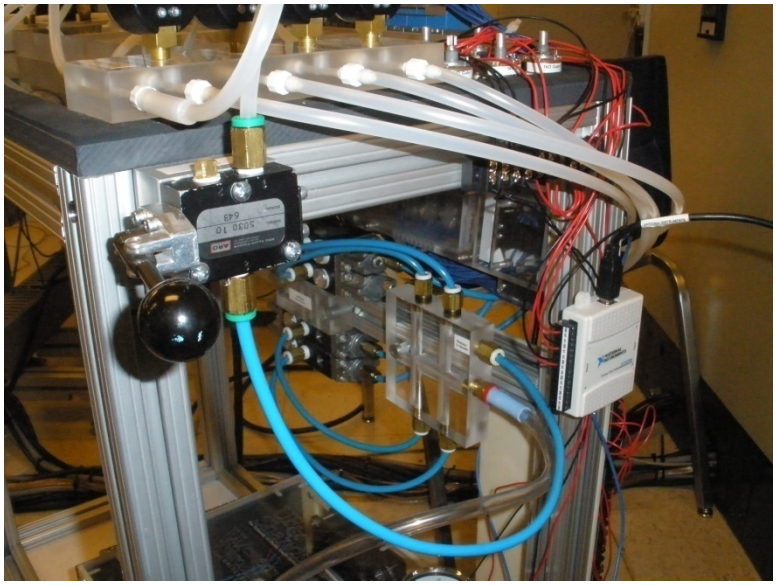

Secondary Full Scale Device Construction:

Photo of seed elements exiting acrylic main body through needle connection plate.

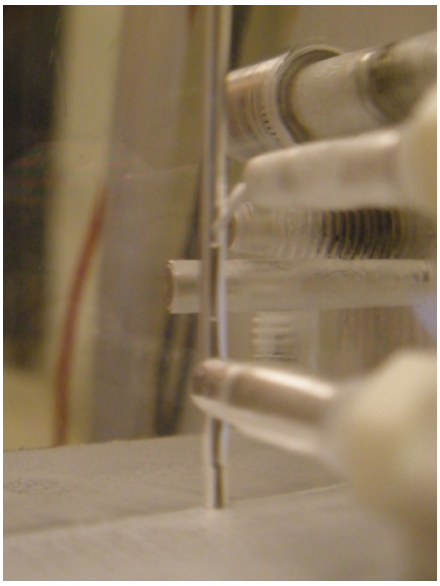

Light gate with seed element captured.

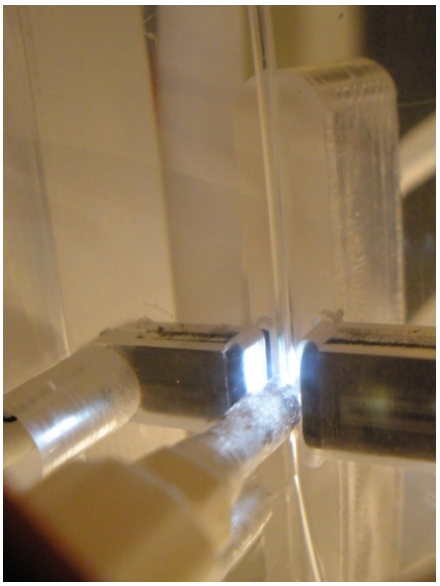

Photos of secondary acrylic main body section attached within the full scale system.

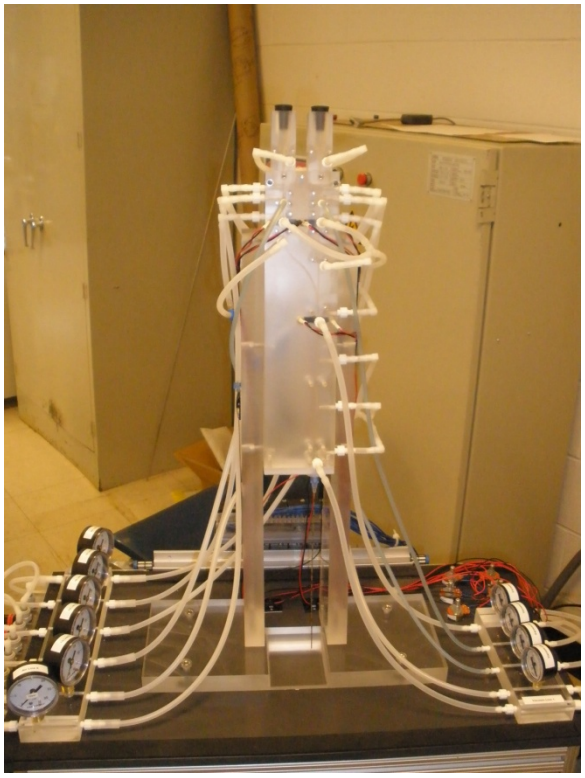

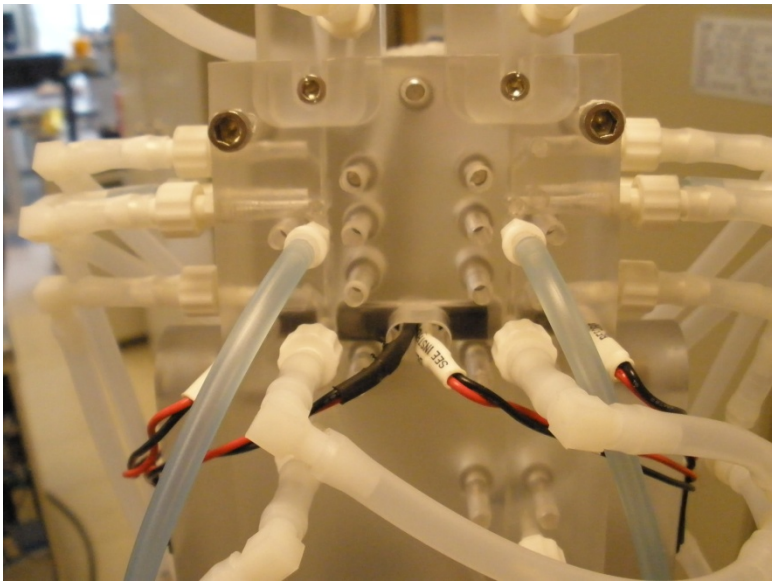

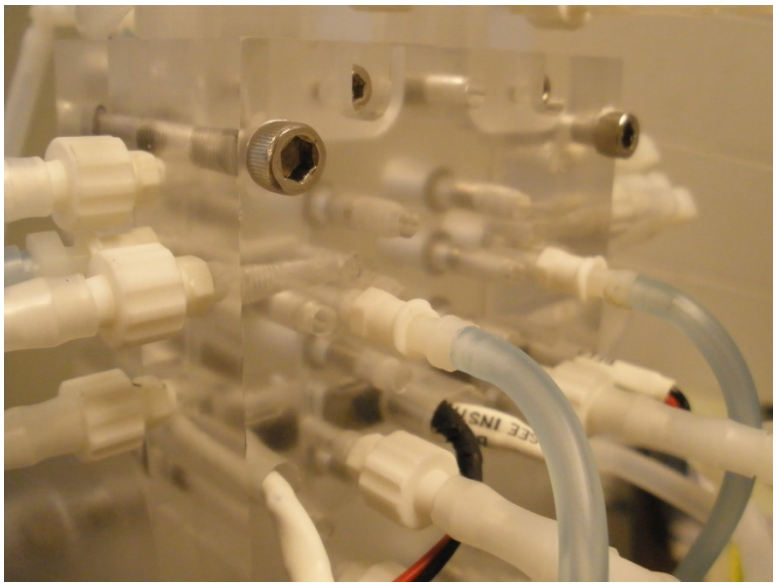

Appendix B

System Schematics

NI DAQ Wiring Diagram:

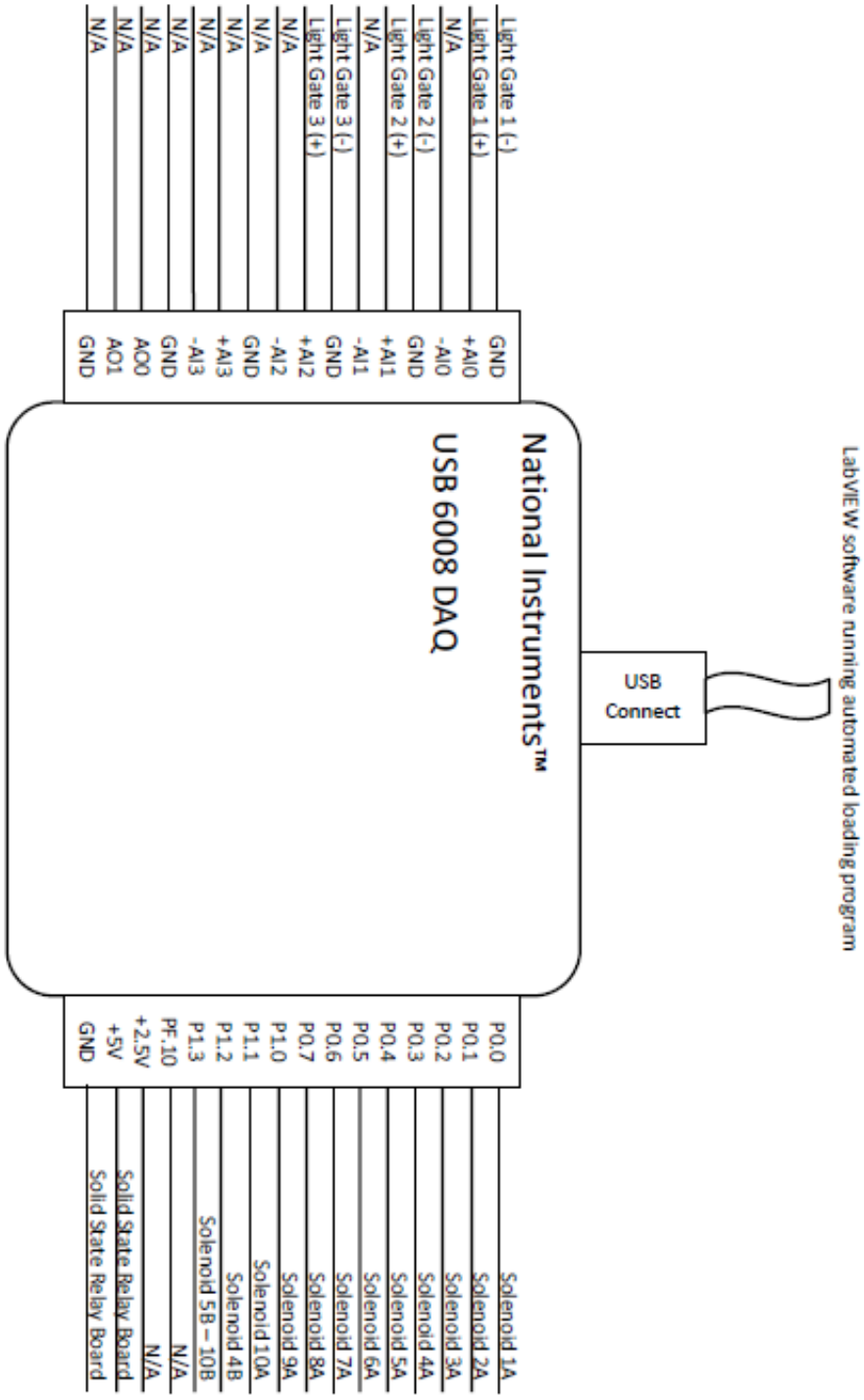

Full Scale System Pneumatic Diagram:

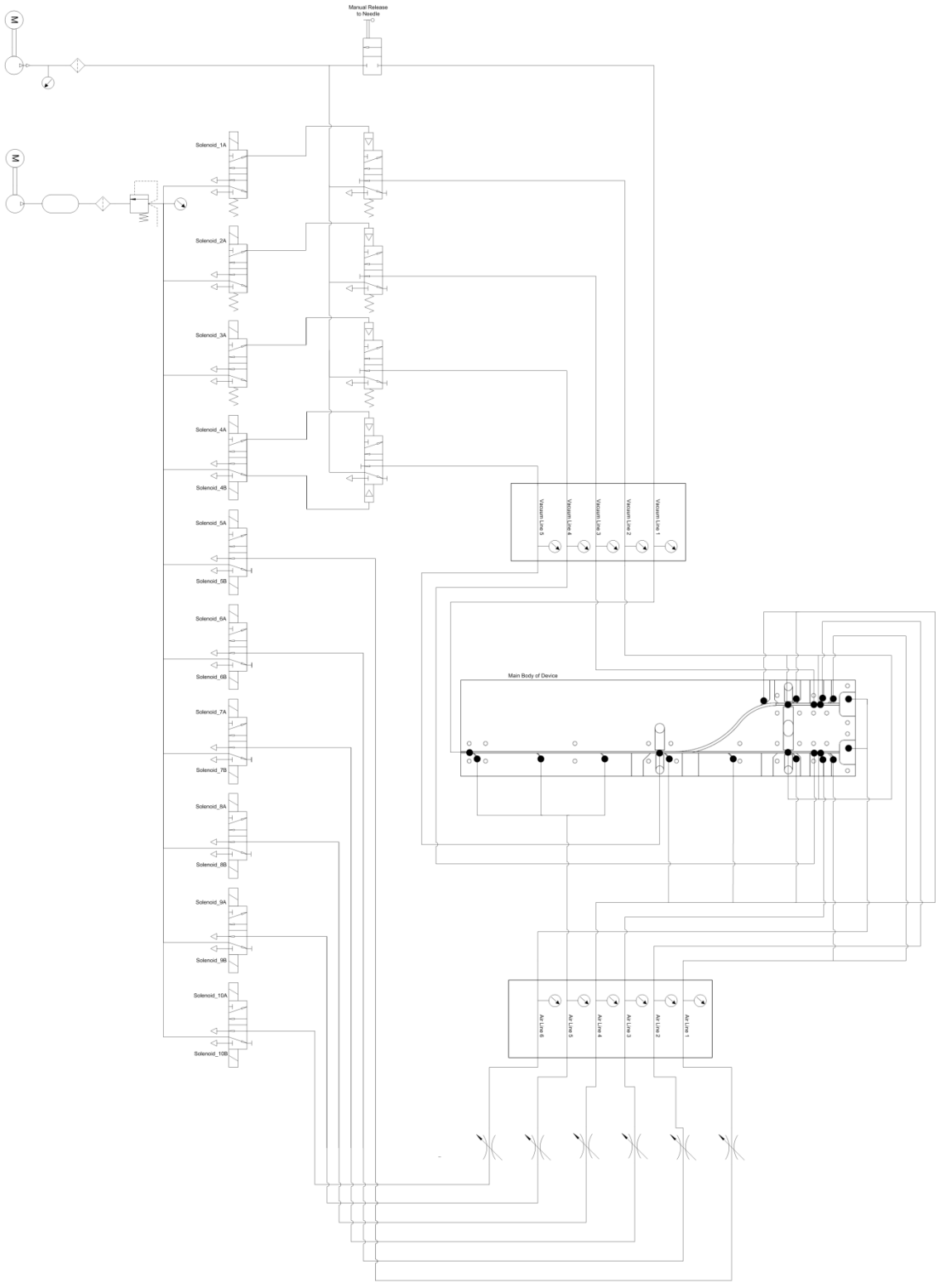

Testing Stand Electrical Wiring Diagrams:

General Wiring Diagram (Main Electrical Housing)

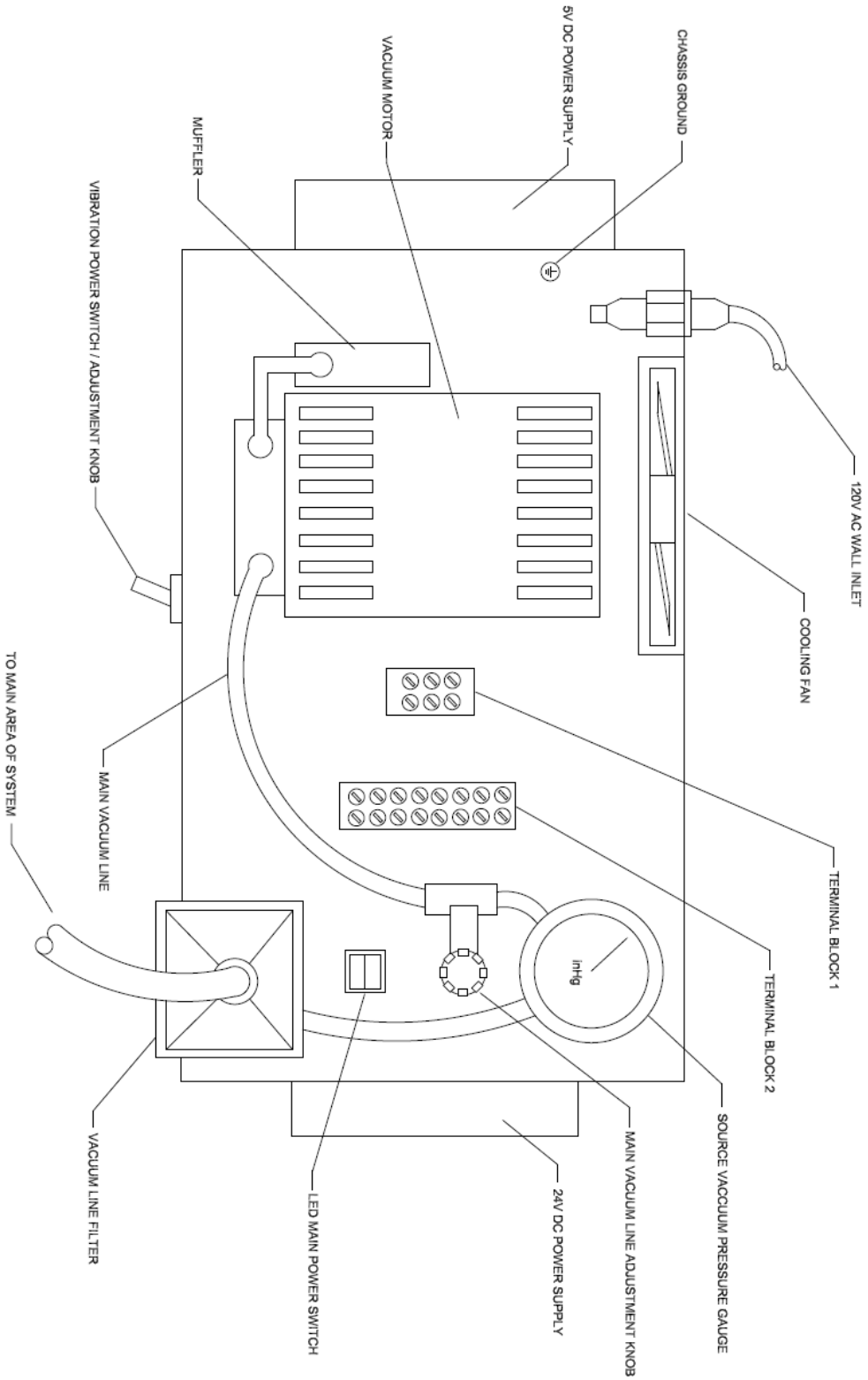

Main Wiring Diagram (Main Electrical Housing)

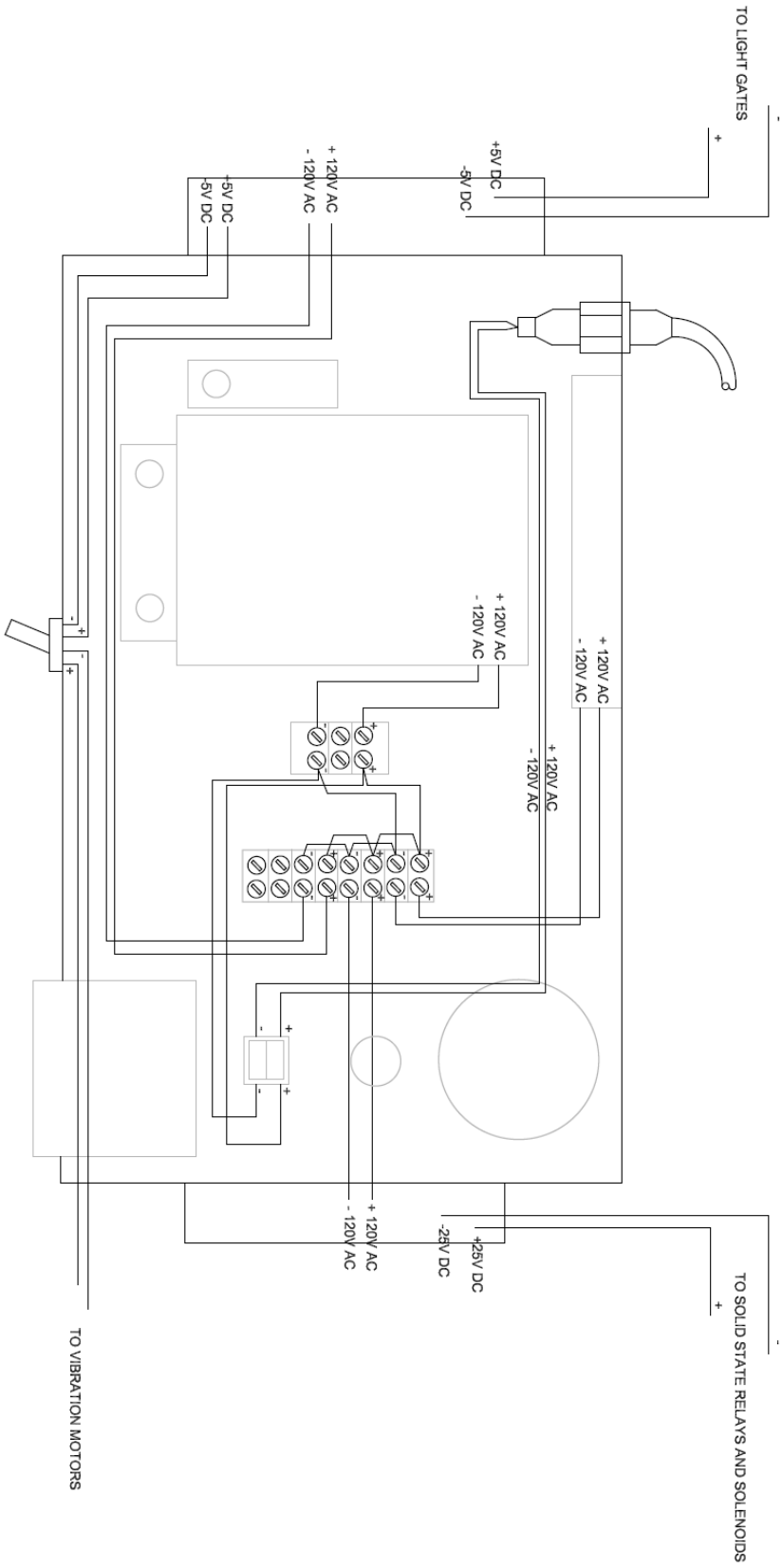

Wiring Diagram of Chassis Grounds (Main Electrical Housing)

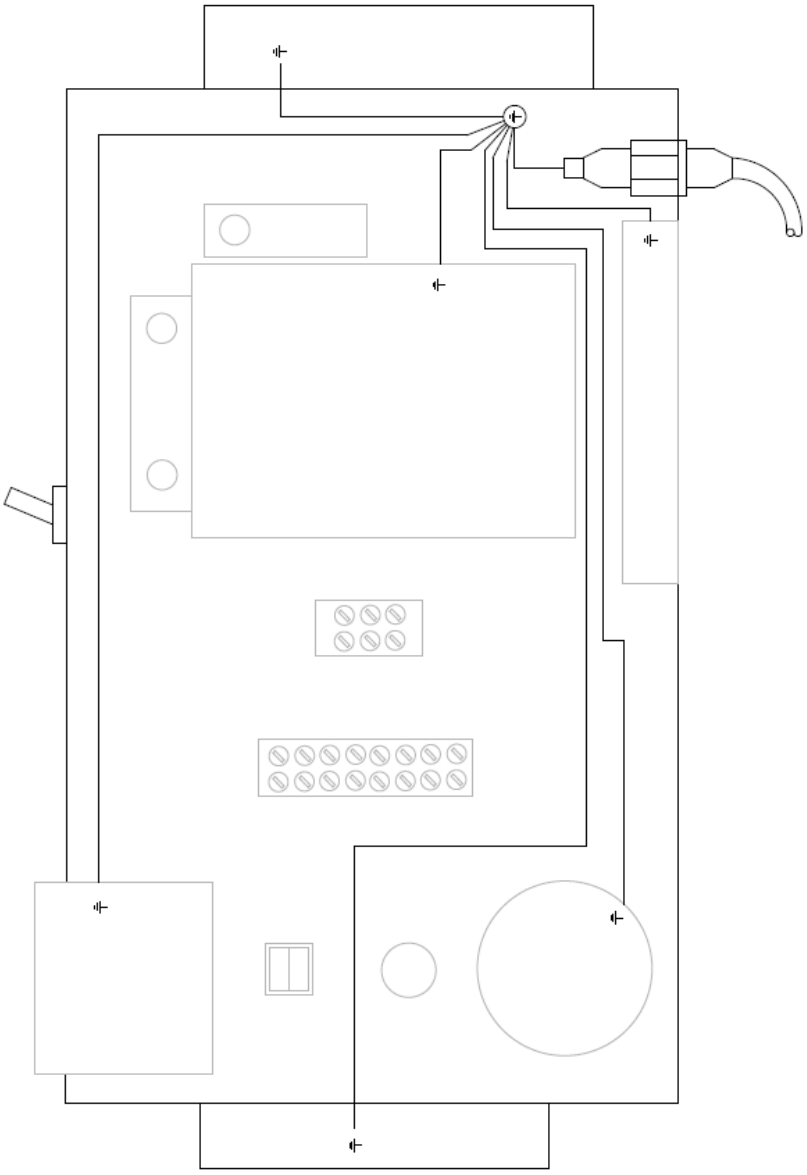

Wiring Diagram of Solid State Relay Board